University of Sussex

Phenomenology and Naturalness in Gauge Extensions of the MSSM after the Higgs discovery

THESIS

Author:
Agamemnon Sfondilis

Supervisor:
Dr. Sebastian Jäger

Submitted for the degree of Doctor of Philosophy
University of Sussex
September 2015

Declaration

I hereby declare that this thesis has not been and will not be submitted in whole or in part to another University for the award of any other degree. I have read and understood the definition of 'Plagiarism' as set out in the Examination and Assessment Handbook for Postgraduate Students under item 7. This dissertation is my own work, except where explicitly stated.

Signature:

Agamemnon Sfondilis

UNIVERSITY OF SUSSEX

Agamemnon Sfondilis, Doctor of Philosophy

My Thesis Report

Phenomenology and Naturalness in Gauge Extensions of the MSSM after the Higgs discovery

Abstract

Supersymmetry remains one of the most favourable candidates for physics beyond the standard model (BSM) due to the solution it provides to the little hierarchy problem as well as the prediction of a Dark matter candidate and other theoretical caveats of the standard model. The minimal supersymmetric standard model despite its success, faces the well known μ problem and the need for large radiative corrections in light of the Higgs discovery which destabilizes the weak scale. Our project addresses this problem in the MSSM and studies the possibility of having a natural theory of singlet extensions of the MSSM with an additional $U(1)'$ gauge group. In a bottom-up approach we have considered a phenomenological version of the gauge extensions of the MSSM (pUMSSM) with generic charges which obey the relations of gauge invariance of the Yukawa terms in the superpotential and perturbativity bounds. Furthermore, we construct a model independent way to impose constraints on the mixing angle from the W mass measurement.

We show a strong dependence of the lightest CP-even Higgs boson mass in different models of pUMSSM, on the Higgsino mass μ_{eff} and we identify regions of the parameter space in which the Higgs mass is enhanced at tree level by heavy Higgsinos. Furthermore, we analyse the squark sector and find interesting scenarios with heavy third generation squarks with masses directed by large $U(1)'$ D-term contributions. Using the program `SARAH` and its interface with `SPheno`, which allow for the calculation of the Higgs mass at the two-loop level in BSM scenarios, we improve the quality and the validity of our results in light of the Higgs discovery. We investigate the role of the gaugino masses M_1, M_2, M_1' in affecting the fine-tuning at one-loop in the MSSM and in different models of the pUMSSM.

A study of the fine tuning measure in MSSM is presented, moreover constraints from collider searches using the program `Fastlim` are imposed and all points of the parameter scans are being tested. We explore regions of the parameter space in which the natural MSSM scenario is not yet ruled out by currently available searches. We proceed to investigate the fine tuning in scenarios of the pUMSSM with different charge assignments, with light and heavy Z' bosons, and identify interesting regions with low fine tuning. We impose constraints from collider searches on supersymmetric particles using `Fastlim` and find models which can evade current and future searches at the LHC.

Acknowledgements

I wish to thank my supervisor Dr. Sebastian Jäger for his help and support throughout my PhD. I would also wish to express my gratitude to Dr. Daniel Litim, Prof. Peter Coles and the School of Mathematical and Physical Sciences for offering me a postgraduate studentship for the last sixteen months of my PhD. Special thanks to Prof. Mark Hindmarsh, Prof. Antonella De Santo, Prof. Xavier Calmet and Dr. Stephan Huber for their valuable advice.

Since September 2010, when I first arrived in the UK to start my MSc in theoretical particle physics at Sussex university, I have been embraced by all the faculty and staff members at the Physics Department, something that has played a major role in my success despite all the hurdles I have encountered over these years. I will never forget my physics and non-physics discussions with Dr. Sebastian Jäger, my friends and office mates Andrew Granger, Jan Schröder, Barry Dillon, Edouard Marchais, my fellow PhD students Glauber Carvalho Dorsch, Chris Harman, Tugba Buyukbese, Djuna Croon, Wissarut Ketaiam, Raul Cuesta and of course our post-docs Ken Mimasu and Jose No. I would also like to thank a very good friend, Dr. Jorge Martin Camalich for his invaluable advice and our great discussions in my early years as a PhD student.

On a more personal level I would like to express my greatest gratitude to my beloved father, Andreas, my mother, Sonia and my sister Claire for their unconditional love and support. I owe them everything and there are no words to express this in a few lines. Furthermore a big thanks to my uncle Dr. Ioannis V. Constantopoulos and my aunt Elina Sfondylis for their advice and moral support when I needed it the most. My uncle Ioannis is one of the people in my life I have been admiring since I was a child for his unbelievably sharp mind, his knowledge and his achievements. He is admittedly the person who has influenced the most my educational choices in an indirect way. Like father, like son, Dr. Vassilis Constantopoulos has also been a great inspiration for his professional achievements in his field. I wish to thank him for his valuable advice and his help.

Lastly, I need not to forget my great inspiration and the person who “indoctrinated”

me into the secrets of Nature, my great teacher Panos Giannaropoulos. Panos was the person who made me fall in love with Physics when I was in high school and decided to become a physicist. He is one of the best teachers I have ever known in my life and he has helped numerous students to achieve their goals. In difficult times, my mind would travel back in time and recall his words, this would help me go through the various obstacles and focus entirely on my goal. I wish people could remember me the same way I remember Panos and have the same positive impact on their lives ....

Agamemnon Sfondilis

"*A good deal of my research work in physics has consisted in not setting out to solve some particular problem, but simply examining mathematical quantities of a kind that physicists use and trying to fit them together in an interesting way, regardless of any application that the work may have. It is simply a search for pretty mathematics. It may turn out later that the work does have an application. Then one has good luck.*"

P.A.M. Dirac

Dedication

I dedicate this work to my beloved daughter Ariadne,

> " I want you to know that your thought dominates my mind and my heart, and gives me the strength to carry on. I thank God for bringing you into my life. I love you so much . . . "

Your Father

Contents

List of Tables

List of Figures

Chapter 1

Introduction

Supersymmetric models provide an intriguing and elegant solution to many problems of the Standard Model (SM) exhibiting new rich phenomenology at the TeV scale. Experimental analyses from the CMS and ATLAS collaboration [1, 2] show no sign of the new particles predicted by supersymmetric theories and put constraints on the parameter space of these theories. Most of these searches have been focusing on the study of the Minimal Supersymmetric Standard Model (MSSM). Certain theoretical as well as phenomenological arguments enforce the necessity for studying extentions of the MSSM. In this chapter we will briefly discuss some of the motivations of supersymmetry and the solution it provides to the hierarchy problem. Then we will introduce the MSSM and we will motivate the need to go beyond this minimal scenario. In the next chapter we will focus on introducing the main concepts of supersymmetric models and build the Lagrangian for the $U(1)'$ extension of the MSSM and derive useful relations.

1.1 What is Supersymmetry?

The SM has been proven experimentally to be very successful so far but it seems unable to give answers to some fundamental problems.

- SUSY cancels the quadratic divergencies to the Higgs squared mass m_H^2, solving the hierarchy problem in a natural way without the need of fine tuning our parameters.
- SUSY accomodates the unification of the gauge couplings at the GUT (Grand Unified Theory) scale $M_{GUT} \sim 10^{16}$ GeV. Unlike the SM it contains the right particle content in order to ensure this unification.
- Supersymmetric GUT models predict larger unification scales. (There is a better

chance to explain proton lifetime).

- The large top Yukawa coupling inferred by the large measured mass of the top quark drives the squared mass m_H^2 of the Higgs boson to run negative at the EW scale thereby dynamically breaking electroweak symmetry while helping the Higgs obtain a vacuum expectation value (vev).

- In the SM the quartic self coupling of the Higgs λ (Higgs potential $V = m_H^2|H|^2 + \lambda|H|^4$) is arbitrary but in the SUSY models the Higgs quartic coupling is totally fixed. In the MSSM for example $\lambda = \frac{g_1^2+g_2^2}{8}$.

- In the MSSM at least one Higgs scalar - the lightest CP-even state has to be light $m_{h^0} \lesssim 135$ GeV.

- SUSY allows more Higgses and sparticles with masses at the TeV scale that can be detected at the LHC.

- Allows for possible dark matter candidates.

- Gauged SUSY is a Supergravity Theory.

1.1.1 The Hierarchy problem

The masses of the SM particles are proportional to the vev of the Higgs field $\langle H \rangle$ which in turn depends on the quadratic scalar mass of the Higgs boson

$$\langle H \rangle = \sqrt{\frac{-m_H^2}{2\lambda}} \quad . \tag{1.1}$$

The problem arises from the fact that the squared mass m_H^2 of the Higgs boson receives quadratic corrections with respect to the ultraviolet (UV) cutoff scale Λ_{UV} from loop diagrams involving heavy particles. The largest contribution is given by the top-quark loop. But let us make this more clear by making some simple loop calculations [59, 124]. Consider the scalar-fermion-fermion coupling term in the SM Lagrangian of the form

$$\mathcal{L}_{\bar{f}f\phi} = -\lambda_f \bar{f} f \phi \quad , \tag{1.2}$$

where λ_f is the Yukawa coupling and $\phi = \frac{1}{\sqrt{2}}(h^0 + \upsilon)$. The Higgs mass m_{h_0} receives radiative corrections from fermion loop diagrams

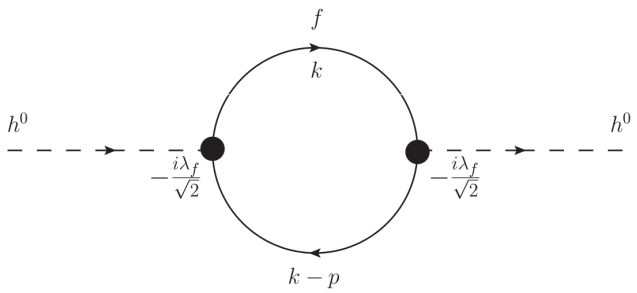

The divergent loop integral will look like this

$$-\left(-\frac{i\lambda_f}{\sqrt{2}}\right)^2 \int \frac{d^4k}{(2\pi)^4} Tr\left[\frac{i}{\not{k}-m}\cdot\frac{i}{(\not{k}-\not{p})-m}\right] \quad . \tag{1.3}$$

By counting the powers of momenta $4-2=2$ it clear that the integral diverges quadratically. Since we are interested to see the degree of divergence of the integral we can set the external momenta equal to zero i.e. $p^\mu = 0$.

$$-\frac{\lambda_f^2}{2}\int \frac{d^4k}{(2\pi)^4} Tr\ \left[\frac{1}{(\not{k}-m)\cdot(\not{k}-m)}\right] \quad , \tag{1.4}$$

this integral can be simplified more

$$\begin{aligned}
&(-)\frac{\lambda_f^2}{2}\int \frac{d^4k}{(2\pi)^4} Tr\left[\frac{(\not{k}+m)(\not{k}+m)}{(k^2-m^2)^2}\right] \\
&= (-)\frac{\lambda_f^2}{2}\int \frac{d^4k}{(2\pi)^4}\frac{Tr[k^2\mathbf{1}_4 + m^2\mathbf{1}_4 + 2\not{k}m]}{(k^2-m^2)^2} \\
&= -2\lambda_f^2\int \frac{d^4k}{(2\pi)^4}\cdot\frac{k^2+m^2}{(k^2-m^2)^2} \quad ,
\end{aligned} \tag{1.5}$$

where we used the fact that $Tr[\gamma^\mu]=0$ and also $Tr[\mathbf{1}_4]=4$ in the last step. Now in order to evaluate this integral we perform a rotation of the time axis by setting $k_0 \to ik_{0_E}$ and we resort to the Euclidean space defined as $k^2 = -k_E^2$. Using the fact that $d^4k = id^4k_E$ the loop integral becomes

$$\begin{aligned}
I &= -2\lambda_f^2\int \frac{id^4k_E}{(2\pi)^4}\cdot\frac{-k_E^2+m^2}{(-k_E^2-m^2)^2} \\
&= -2i\lambda_f^2\int \frac{d^4k_E}{(2\pi)^4}\cdot\frac{k_E^2-m^2}{(k_E^2+m^2)^2} \quad .
\end{aligned} \tag{1.6}$$

The advantage now is that having eliminated this minus sign introduced by the Minkowski metric we can perform the momentum integration in 4-dimensional spherical coordinates since in this case the integration measure is

$$d^4k = k_E^3\ dk_E\ d\Omega_4 \quad , \tag{1.7}$$

where $d\Omega_4$ is the element of surface area of the 4-dimensional unit sphere. In general $\int d\Omega_d = \frac{2\pi^{\frac{d}{2}}}{\Gamma(\frac{d}{2})}$ in d-dimensions, so for $d=4$ dimensions $\int d\Omega_d = 2\pi^2$ and the integral

becomes

$$\begin{aligned} I &= \frac{2i\lambda_f^2}{(2\pi)^4} \cdot 2\pi^2 \int dk_E \; k_E^3 \frac{k_E^2 - m^2}{(k_E^2 + m^2)^2} \\ &= \frac{2i\lambda_f^2}{8\pi^2} \int dk_E^2 \; k_E^2 \frac{k_E^2 - m^2}{(k_E^2 + m^2)^2} \quad , \end{aligned} \tag{1.8}$$

where we used $dk_E^2 = 2k_E dk_E$ in the last step. This integral is clearly still quadratically divergent and in order to regularize it we have to introduce a UV cut off momentum Λ which we are going to take it that goes to infinity at the end of the calculation $\Lambda \to \infty$. Now we change variables and set $x = k_E^2 + m^2 \Rightarrow dx = d(k_E^2)$ and we get

$$\begin{aligned} I &= \frac{i\lambda_f^2}{8\pi^2} \int_{m^2}^{\Lambda^2+m^2} dx \frac{(x - m^2)(x - 2m^2)}{x^2} \\ &= \frac{i\lambda_f^2}{8\pi^2} \int_{m^2}^{\Lambda^2+m^2} dx \left\{ 1 - \frac{3m^2}{x} - \frac{2m^4}{x^2} \right\} \\ &= \frac{i\lambda_f^2}{8\pi^2} \left\{ \Lambda^2 - 3m^2 ln \left(\frac{\Lambda^2 + m^2}{m^2} \right) - 2m^2 \frac{\Lambda^2}{\Lambda^2 + m^2} \right\} \\ &= i\delta m_{h^0}^2 \quad , \end{aligned} \tag{1.9}$$

the first term diverges quadratically when $\Lambda \to \infty$ and the second term diverges logarithmically. Thus we have shown that

$$\delta m_{h^0}^2 \sim \kappa \Lambda^2 \quad . \tag{1.10}$$

The corrected squared mass of the Higgs scalar depends on the UV cut-off scale Λ

$$m_{h^0}^2 = 2\upsilon^2 \lambda + \kappa \Lambda^2 \quad , \tag{1.11}$$

where $\upsilon = \langle H \rangle \approx 174$ GeV.

- if $\Lambda \sim M_W$ then m_{h^0} is of the order $\mathcal{O}(M_W)$ and the SM corrections then pose no problem.
- but if we go to a higher scale much larger than the EW scale $\Lambda \gg M_W$ then the Higgs mass follows this scale $m_{h^0} \sim \Lambda \gg M_W$.

In order to avoid the Higgs mass from becoming too large we have to fine tune the parameter κ

$$\begin{aligned} \text{if} \quad \Lambda \sim M_P \Longrightarrow \qquad \kappa &\sim \frac{M_W^2}{M_P^2} \sim 10^{-34} \quad , \\ \text{if} \quad \Lambda \sim M_{GUT} \Longrightarrow \qquad \kappa &\sim \frac{M_W^2}{M_{GUT}^2} \sim 10^{-26} \quad . \end{aligned} \tag{1.12}$$

1.1.2 SUSY gives an elegant solution to the hierarchy problem

The naturalness criterion attributes this quadratic divergence of the Higgs mass to the lack of a symmetry that would protect the mass from diverging. Supersymmetry (SUSY) provides such a symmetry between fermions and bosons by ensuring that each supermultiplet contains the same number of fermionic and bosonic degrees of freedom (dof) i.e. every known SM particle has its own superpartner with a spin that differs by 1/2 unit. Every Weyl spinor has 2 fermionic dof due to the two possible spin states. In order to equate these fermionic dof with bosonic dof we need to associate 2 real scalar fields (1 bosonic dof each) to every Weyl spinor (left-handed or right-handed). The simplest way to do this is by accommodating these dof into a complex scalar field. Introduce two complex scalar felds $\tilde{f}_L$ as the superpartner of the left-handed Weyl spinor f_L and $\tilde{f}_R$ as the superpartner of f_R and assume that these scalar fields have the following coupling to the Higgs field

$$\begin{aligned}\mathcal{L}_{\tilde{f}\tilde{f}\phi} = &-\frac{\lambda_{\tilde{f}}}{2}(h^0)^2\big(|\tilde{f}_L|^2+|\tilde{f}_R|^2\big) - h^0\big(\mu_L|\tilde{f}_L|^2+\mu_R|\tilde{f}_R|^2\big)\\ &- m_L^2|\tilde{f}_L|^2 - m_R^2|\tilde{f}_R|^2 \ .\end{aligned} \tag{1.13}$$

The contributions via the quartic and trilinear couplings of the superpartners to the Higgs field h^0 are depicted below

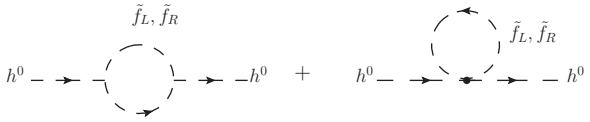

Following the same steps as before we can write down the loop contributions from the quartic and trilinear couplings separately

for the quartic coupling contribution (right diagram) we have

$$\begin{aligned}i\delta m_{h^0}^2\big|_4 &= -i\lambda\int\frac{d^4k}{(2\pi)^4}\left[\frac{i}{k^2-m_L^2}+\frac{i}{k^2-m_R^2}\right] = \ldots =\\ &= -i\frac{\lambda_{\tilde{f}}}{16\pi^2}\Big\{2\Lambda^2 - m_L^2\ ln\left(\frac{\Lambda^2+m_L^2}{m_L^2}\right) - m_R^2\ ln\left(\frac{\Lambda^2+m_R^2}{m_R^2}\right)\Big\} \quad ,\end{aligned} \tag{1.14}$$

for the trilinear coupling contribution (left diagram) we have

$$\begin{aligned}i\delta m_{h^0}^2\big|_3 &= \int\frac{d^4k}{(2\pi)^4}\left\{\frac{(-i\mu_L)^2}{(k^2-m_L^2)^2}+\frac{(-i\mu_R)^2}{(k^2-m_R^2)^2}\right\} = \ldots =\\ &= -\frac{i}{16\pi^2}\Big[\mu_L^2\cdot ln\left(\frac{\Lambda^2+m_L^2}{m_L^2}\right)+\mu_R^2\cdot ln\left(\frac{\Lambda^2+m_R^2}{m_R^2}\right)\\ &\quad -\frac{\Lambda^2}{\Lambda^2+m_L^2}-\frac{\Lambda^2}{\Lambda^2+m_R^2}\Big] \quad .\end{aligned} \tag{1.15}$$

Note the minus sign difference between eq.(1.9) and eqs.(1.15,1.14) due to the fermion loop in the first case. Eqs.(1.9,1.14) are responsible for the quadratic divergence of the Higgs squared mass

$$\begin{aligned} -i\delta m_{h^0}^2 = & \frac{i\lambda_f^2}{8\pi^2}\Big\{\Lambda^2 + \dots \text{ logarithmic terms}\Big\} \\ & - \frac{i\lambda_{\tilde{f}}}{16\pi^2}\Big\{2\Lambda^2 + \dots \text{ logarithmic terms}\Big\} \\ & - i\delta m_{h^0}^2\big|_3 \quad . \end{aligned} \tag{1.16}$$

- from eq.(1.16) it is obvious that if $\lambda_f^2 = \lambda_{\tilde{f}}$ then the quadratic divergencies vanish. Note that if it was not for that minus sign difference from the bosonic states this cancellation would not happen.
- furthermore if $m_L^2 = m_R^2 = m^2$ and also $\mu_L^2 = \mu_R^2 = 2\lambda_{\tilde{f}} m^2$ then also the logarithmic divergencies vanish.

1.2 The MSSM

The superpotential of the MSSM reads [124]

$$\begin{aligned} W_{MSSM} &= \bar{u}^i y_{u_{ij}} Q_\alpha^{Tj} \epsilon^{\alpha\beta} H_{u_\beta} + \bar{d}^i y_{d_{ij}} Q_\alpha^{Tj} \epsilon^{\alpha\beta} H_{d_\beta} + \bar{e}^i y_{e_{ij}} L_\alpha^{Tj} \epsilon^{\alpha\beta} H_{d_\beta} \\ &+ \mu H_{u_\alpha}^T \epsilon^{\alpha\beta} H_{d_\beta} \quad , \end{aligned} \tag{1.17}$$

where $Q, L, \bar{u}, \bar{d}, \bar{e}, H_u, H_d$ are the chiral superfields of the theory. The term $\mu H_u H_d$ represents the supersymmetric version of the Higgs boson mass $m_{h^0}^2|H|^2$ in the SM. The dimensionless Yukawa matrices have dimension three in the family space and they give masses to the quarks and leptons after electroweak symmetry breaking takes place. They also determine the Cabibbo-Kobayashi-Maskawa (CKM) mixing angles of the fermions. A difference one notices immediately from (1.17), compared to the SM is that there are two Higgs H_u,H_d doublets giving masses to the up and down-type quarks, respectively. This is because the superpotantial is an analytic function of the fields ϕ_i but not the conjugate fields ϕ_i^*. This means that unlike the SM we cannot construct a new Higgs doublet with opposite hypercharge by complex conjugation in order to give masses to the down-type quarks because this term is not allowed in the superpotential. The particle content of the MSSM is given in Tables 1.1, 1.2 from Ref.[124]. The MSSM as we mentioned in the introduction has many successes. The theory predicts gauge coupling unification at the

Names		spin 0	spin 1/2	$SU(3)_C$, $SU(2)_L$, $U(1)_Y$
squarks, quarks	Q	$(\widetilde{u}_L \;\; \widetilde{d}_L)$	$(u_L \;\; d_L)$	$(\mathbf{3}, \mathbf{2}, \frac{1}{6})$
(×3 families)	$\overline{u}$	$\widetilde{u}^*_R$	$u^\dagger_R$	$(\overline{\mathbf{3}}, \mathbf{1}, -\frac{2}{3})$
	$\overline{d}$	$\widetilde{d}^*_R$	$d^\dagger_R$	$(\overline{\mathbf{3}}, \mathbf{1}, \frac{1}{3})$
sleptons, leptons	L	$(\widetilde{\nu} \;\; \widetilde{e}_L)$	$(\nu \;\; e_L)$	$(\mathbf{1}, \mathbf{2}, -\frac{1}{2})$
(×3 families)	$\overline{e}$	$\widetilde{e}^*_R$	$e^\dagger_R$	$(\mathbf{1}, \mathbf{1}, 1)$
Higgs, Higgsinos	H_u	$(H^+_u \;\; H^0_u)$	$(\widetilde{H}^+_u \;\; \widetilde{H}^0_u)$	$(\mathbf{1}, \mathbf{2}, +\frac{1}{2})$
	H_d	$(H^0_d \;\; H^-_d)$	$(\widetilde{H}^0_d \;\; \widetilde{H}^-_d)$	$(\mathbf{1}, \mathbf{2}, -\frac{1}{2})$

Table 1.1: Chiral supermultiplets in the MSSM. The spin-0 fields are complex scalars, and the spin-1/2 fields are left-handed two-component Weyl fermions [124].

Names	spin 1/2	spin 1	$SU(3)_C$, $SU(2)_L$, $U(1)_Y$
gluino, gluon	$\widetilde{g}$	g	$(\mathbf{8}, \mathbf{1}, 0)$
winos, W bosons	$\widetilde{W}^\pm \;\; \widetilde{W}^0$	$W^\pm \;\; W^0$	$(\mathbf{1}, \mathbf{3}, 0)$
bino, B boson	$\widetilde{B}^0$	B^0	$(\mathbf{1}, \mathbf{1}, 0)$

Table 1.2: Gauge supermultiplets in the MSSM [124].

GUT scale and has a restricted Higgs sector with an upper bound on the lightest Higgs mass around $m_{h^0_1} \lesssim 135$ GeV. Furthermore, it predicts a dark matter candidate. On the other hand it has its own pitfalls, stemming from well established theoretical questions and phenomenological facts. The superpotential eq.(1.17) contains the so called "$\mu-$term" where μ is a dimensionful parameter. The dimensionful parameter μ gives the Higgsino mass terms and the Higgs squared mass terms in the scalar potential V_{scalar} of the theory

$$-\mathcal{L}_{\tilde{H}} = \mu(\widetilde{H}^+_u \widetilde{H}^-_d - \widetilde{H}^0_u \widetilde{H}^0_d) + c.c. \quad , \tag{1.18}$$

$$-\mathcal{L}_{\text{Higgs mass}} = |\mu|^2 \Big(|H^0_u|^2 + |H^+_u|^2 + |H^0_d|^2 + |H^-_d|^2 \Big). \tag{1.19}$$

The second equation is non-negative with a minimum at $H^0_u = H^0_d = 0$. In order to achieve electroweak symmetry breaking one has to add a soft supersymmetry breaking squared mass term for the Higgs scalars $\mathcal{L}_{soft} \supset m^2_{H_d}, m^2_{H_u}$. The Higgs scalar potential consists of supersymmetry respecting $|\mu|^2$ terms and soft supersymmetry breaking terms $m^2_{H_d}, m^2_{H_u}$ that provide us the needed negative contributions in order to break SUSY radiatively. The problem lies in the fact that these terms have a totally different origin, yet they have to be of the same order $(10^2 - 10^3)$ GeV in order for the Higgs to obtain a vev at the electroweak

(EW) scale $\langle H \rangle = 174$ GeV. The reason why these two terms have to be of the order of m_{soft} while μ is a supersymmetry respecting dimensionful parameter it is unknown and thus leads to a tuning of this parameter without any sound theoretical argument to do so. This problem manifests itself also through the equation that exhibits the stability of the electroweak scale in the MSSM. At the minimum of the potential one can find that the mass of the Z boson is given by (in the large $\tan\beta$ limit)

$$\frac{M_Z^2}{2} = -m_{H_u}^2 - |\mu|^2 \quad , \tag{1.20}$$

already at tree level the soft parameter $m_{H_u}^2$ and the dimensionful μ parameter are much larger than the weak scale so that a cancellation is needed for the equation to hold. The first term on the right hand side (rhs) of eq.(1.20) is also very sensitive to radiative corrections and at one-loop as we will see the beta function of $m_{H_u}^2$ depends on the soft supersymmetry breaking masses of the top squarks m_{Q_3}, m_{T^c} and the trilinear coupling A_t which induces mixing in the stop sector. The stop masses also control the radiative corrections to the lightest Higgs mass. An approximate equation which gives the 1-loop correction to the lightest CP-even Higgs mass in the MSSM with only the effect of the stops in the loop is given by [56]:

$$m_{h_0}^2 = M_Z^2 \cos 2\beta^2 + \frac{3g_2^2}{8\pi^2}\frac{m_t^4}{M_W^2}\left[\ln\frac{m_{\tilde{t}_1}m_{\tilde{t}_2}}{m_t^2} + \frac{X_t^2}{m_{\tilde{t}_1}m_{\tilde{t}_2}}\left(1 - \frac{X_t^2}{12 m_{\tilde{t}_1}m_{\tilde{t}_2}}\right)\right] \quad , \tag{1.21}$$

where $X_t = A_t - \mu\cot\beta$ and one can make the approximation $M_{\text{SUSY}}^2 \equiv m_{\tilde{t}_1}m_{\tilde{t}_2} \approx m_{Q_3}m_{T^c}$. Due to the fact that the observed Higgs mass is close to the upper bound in the MSSM, large radiative corrections are needed to achieve $m_{h_1^0} \sim 125$ GeV. This means that the stops have to be relatively heavy with large mixing X_t which in turn will cause large radiative corrections to the soft mass $m_{H_u}^2$ entering eq.(1.20). Larger corrections will enhance the imbalance between the two terms in eq.(1.20) and thus induce more fine tuning in order to stabilize the weak scale.

Chapter 2

U(1) extensions of the MSSM

As we have seen earlier the MSSM suffers from the so-called "μ-problem" [145, 146, 124]. The μ parameter is the only dimensionful supersymmerty preserving parameter in the superpotential of the minimal supersymmetric model and it has to be of the order of the electroweak scale $\mathcal{O}(M_W)$ as the supersymmetry breaking paramaters m_{soft} in order to stabilize the electroweak scale. An intuitive solution to this fundamental problem of the MSSM can be provided by adding an extra singlet chiral field [146, 145] to the superpotential in the following manner

$$\begin{aligned} W_{UMSSM} &= \bar{u}^i y_{u_{ij}} Q_\alpha^{T^j} \epsilon^{\alpha\beta} H_{u_\beta} + \bar{d}^i y_{d_{ij}} Q_\alpha^{T^j} \epsilon^{\alpha\beta} H_{d_\beta} + \bar{e}^i y_{e_{ij}} L_\alpha^{T^j} \epsilon^{\alpha\beta} H_{d_\beta} \\ &+ \lambda S H_{u_\alpha}^T \epsilon^{\alpha\beta} H_{d_\beta} \quad , \end{aligned} \tag{2.1}$$

where $i, j = 1, 2, 3$ are as before the generation indices and $\alpha, \beta = 1, 2$ the $SU(2)$ doublet indices. The new chiral supermultiplet contains a spin zero singlet particle S and a spin 1/2 particle $\tilde{S}$ called the "singlino". The singlet field acquires a vacuum expectation value $\langle S \rangle$ that breaks an additional $U(1)'$ local abelian gauge symmetry at some higher scale. The extra $U(1)$ gauge group can result from the breaking of larger groups like $SO(10)$ or $SU(5)$ in the context of GUTs and also from string inspired theories. In a bottom-up approach it can be thought of as a solution to the domain wall problem arising in the next-to-minimal supesymmetric standard model (NMSSM) [123, 134]. In the latter case the superpotential is invariant under a continuous global Peccei-Quinn (PQ) symmetry which has to be broken explicitly rather than spontaneously to avoid the emergence of a massless axion that is not realised in nature. This is achieved in the NMSSM by the addition of a cubic self-coupling term $1/3\kappa S^3$ which on the other hand respects the $\mathcal{Z}_3$ discrete symmetry leading to domain-wall problems after the singlet acquires a vev. In both scenarios the μ term present in the MSSM superpotential has been replaced by the

trilinear term $\lambda S H_u H_d$ which generates the μ term effectively after electroweak symmetry breaking takes place. In the context of UMSSM the massless Goldstone boson is eaten by the new Z' gauge boson and no explicit breaking of the symmetry is needed thus making the theory free from problems that can spoil the observed cosmic microwave background radiation.

2.1 Particle Content of UMSSM

Vector supermultiplets

The symmetry group under which the supersymmetric Langrangian is invariant, as we have discussed earlier, will be the same as in the MSSM extended by one extra $U(1)'$ abelian gauge group, i.e.

$$G = SU(3)_c \otimes SU(2)_L \otimes U(1)_Y \otimes U(1)' \quad . \tag{2.2}$$

It is already known from the SM and its minimal supersymmetric extension that the color group has 8 generators T^a $(a = 1, \ldots, 8)$, which are 3×3 traceless unitary matrices obeying the anticommutation relation

$$[T^a, T^b] = i f^{abc} T^c \tag{2.3}$$

where f_{abc} are the real structure constants of the symmetry group. In order for the Lagrangian to be invariant under the non-abelian local transformations one introduces 8 vector gluon fields A^a_μ which transform according to

$$A^{a\prime}_\mu = A^a_\mu + \partial_\mu \epsilon^a + g f^{abc} A^b_\mu \epsilon^c \quad , \tag{2.4}$$

where $\epsilon^a(x)$ are the 8 infinitesimal gauge transformation parameters and $g \equiv g_3$ is the gauge coupling of the strong interaction in this case. In the adjoint representation where $(T^a)_{bc} = -i f^{abc}$ the transformation of the gluon fields becomes

$$\delta A^{a\prime}_\mu = \partial_\mu \epsilon^a - i g (T^b)_{ac} A^b_\mu \epsilon^c \quad , \tag{2.5}$$

and this defines the form of the covariant derivative in the adjoint representation of the group:

$$D_\mu = \partial_\mu - i g T^b A^b_\mu \quad . \tag{2.6}$$

When one supersymmetrizes the theory the vector supermultiplet will contain along the bosonic degrees of freedom the corresponding fermionic dofs, which in this case are the

gluinos

$$SU(3)_c \to V_3 = (\tilde{G}^b, G^b_\mu) \ , \qquad b = 1 \dots 8 \ . \tag{2.7}$$

Similarly the $SU(2)_L$ group has 3 generators τ^i $(i = 1, 2, 3)$ which have to satisfy (2.3). In the fundamental representation the structure constants are just the totally anticommuting Levi-Civita tensor $f^{abc} = \epsilon^{abc}$ and the generators are just half the Pauli matrices

$$\tau^i = \frac{1}{2}\sigma^i \ , \qquad i = 1, 2, 3 \ . \tag{2.8}$$

The vector supermultiplet will contain the three gauge boson eigenstate fields W^a_μ and the corresponding gaugino fields $\tilde{W}^a_\mu$

$$SU(2)_L \to V_2 = (\tilde{W}^i, W^i_\mu) \ , \qquad i = 1, 2, 3 \ . \tag{2.9}$$

The $U(1)_Y$ and the extra $U(1)'$ abelian gauge groups have one dimensional generators which correspond to the weak hypercharge Y in the first case and to the extra $U(1)'$ hypercharge Q_i in the latter. The two $U(1)$ supermultiplets will now contain

$$U(1)_Y \to (\tilde{B}, B_\mu) \tag{2.10}$$

$$U(1)' \to (\tilde{B}', B'_\mu) \tag{2.11}$$

the covariant derivative for the full theory can now be written for convenience as

$$D_\mu = \partial_\mu - ig_1 B_\mu Y - ig_2 \sum_{i=1}^{3} W^i_\mu \tau^i - ig_3 \sum_{b=1}^{8} G^b_\mu T^b - ig'_1 B'_\mu Q \ . \tag{2.12}$$

The Lagrangian density for a gauge supermultiplet is given by

$$\mathcal{L}_{gauge} = -\frac{1}{4} F^a_{\mu\nu} F^{\mu\nu,a} + i\lambda^{a\dagger} \bar{\sigma}^\mu D_\mu \lambda^a + \frac{1}{2} D^a D^a \quad , \tag{2.13}$$

where the covariant field strength tensor $F^a_{\mu\nu}$ is given by

$$F^a_{\mu\nu} = \partial_\mu A^a_\nu - \partial A^a_\mu + g f^{abc} A^b_\mu A^c_\nu \quad , \tag{2.14}$$

where there is an implicit sum over all the field strength tensors corresponding to every gauge group of the theory (2.2) with $a = 1, \dots, 8$ for $SU(3)_c$ and $a \equiv i = 1, 2, 3$ for $SU(2)_L$. The second term corresponds to the interaction Lagrangian of the gauge sector to the gauginos λ^a

$$a = 1, \dots, 8 \qquad \lambda^a \equiv \tilde{G}^a \tag{2.15}$$

$$a = 1, 2, 3 \qquad \lambda^a \equiv \tilde{W}^a \tag{2.16}$$

$$a = 1 \qquad \lambda \equiv \tilde{B} \tag{2.17}$$

$$a = 1 \qquad \lambda \equiv \tilde{B}' \tag{2.18}$$

the last term corresponds to the real bosonic auxiliary field D^a which we have to add to the Lagrangian in order for supersymmetry to close off-shell. These are not the only terms which are allowed by the symmetries of the Lagrangian and renormalizability. We have to include terms which correspond the gaugino-fermion-scalar coupling (plus the hermitian conjugate) and also the coupling of the auxiliary bosonic field D^a to the scalar fields of the theory. These additional gauge terms are,

$$\mathcal{L}_{+gauge} = -\sqrt{2}g(\phi_i^\star T^a \psi_i)\lambda^a + h.c. - D^a D^a \quad , \tag{2.19}$$

where $D^a = -g(\phi_i^* T^a \phi_i)$ and again there is an implicit sum over the number of chiral supermultiplets i and a the adjoint representation of every gauge group. The coefficients of these terms are determined by supersymmetry (it is easy to show this by using the superfield formalism.) Adding (2.20) plus (2.19) we finally get to the general expression

$$\boxed{\mathcal{L}_{gauge} = -\frac{1}{4}F^a_{\mu\nu}F^{\mu\nu,a} + i\lambda^{a\dagger}\bar{\sigma}^\mu D_\mu \lambda^a - \frac{1}{2}D^a D^a + (-\sqrt{2}g(\phi_i^\star T^a \psi_i)\lambda^a + h.c.)} \tag{2.20}$$

the third term $1/2 D^a D^a$ corresponds to the D-term contribution to the scalar potential $V(\phi, \phi^*)$ of the theory. It is obvious that in the UMSSM the extra $U(1)'$ gauge group will provide extra contributions to this term and thus modify as we will see the squared mass matrices of the sfermions with respect to the minimal supersymmetric scenario. Additional D-terms will also be present at tree level in the Higgs sector which will boost up the mass of the lightest Higgs boson.

Chiral supermultiplets

The chiral supermultiplets $\Phi_i \equiv (\phi_i, \psi_i)$ where ϕ_i are the complex scalar fields and ψ_i are the Weyl fermionic fields of left-handed helicity. Since every fermionic dof has two helicity states

$$\psi_D = \begin{pmatrix} \psi_L \\ \\ \psi_R \end{pmatrix} \equiv \begin{pmatrix} \psi_a \\ \\ \psi^{\dagger\dot{a}} \end{pmatrix} \quad , \tag{2.21}$$

one chiral supermultiplet is needed to accommodate the fermionic dofs coming from each helicity state. Note that if we want to define the supermuliplets rigorously according to the superfield formalism we have to include the scalar complex auxiliary field F_i to every supermultiplet in order to match the fermionic and bosonic dof off-shell[1]. Since

[1] Off-shell the two helicity states correspond to 2 complex fermionic fields i.e. 4 real fermionic dofs while the scalar complex field ϕ still has two bosonic dofs.

Supermultiplet	$SU(3)_c \otimes SU(2)_L \otimes U(1)_Y \otimes U(1)'$
$Q_i \equiv (\tilde{Q}_i, Q_i)$	$(3, 2, \frac{1}{6}, Q_{q_i})$
$\bar{u}_i \equiv (\tilde{u}_R^*, \tilde{u}_R^\dagger)$	$(3, 1, -\frac{2}{3}, Q_{\bar{u}_i})$
$\bar{d}_i \equiv (\tilde{d}_R^*, \tilde{d}_R^\dagger)$	$(3, 1, \frac{1}{3}, Q_{\bar{d}_i})$
$L_i \equiv (\tilde{L}_i, L_i)$	$(1, 2, -\frac{1}{2}, Q_{L_i})$
$\bar{e}_i \equiv (\tilde{e}_R^*, \tilde{e}_R^\dagger)$	$(1, 1, 1, Q_{\bar{e}_i})$
$H_u \equiv (H_u, \tilde{H}_u)$	$(1, 2, +\frac{1}{2}, Q_{H_u})$
$H_d \equiv (H_d, \tilde{H}_d)$	$(1, 2, -\frac{1}{2}, Q_{H_d})$
$S \equiv (S, \tilde{S})$	$(1, 1, 1, Q_s)$

Table 2.1: The table shows the chiral supermultiplets in the UMSSM and the quantum numbers under the corresponding gauge group. Note that in this minimal $U(1)$ extension of the MSSM the only extra chiral supermultiplet involves the gauge singlet S and the fermionic superpartner which is called "singlino". The index $i = 1, 2, 3$ runs over the 3 generations of quarks and leptons.

supersymmetry transformations commute with the transformations under the gauge group G of the theory (2.2), all the particles that belong to the same supermultiplet have the same quantum numbers. This allows to parametrize chiral supermultiplets further according to their transformation properties under the weak isospin $SU(2)_L$ gauge group. The chiral supermultiplets for the UMSSM are given in Table 2.1. The quark and lepton doublets under the $SU(2)_L$ as well as the two Higgs doublets are given in Table 2.2.

The chiral Lagrangian will contain the kinetic terms for the fermionic and bosonic components of the various supermultiplets, the F-term scalar potential $V_F(\phi^*, \phi)$ plus the Lagrangian term responsible for the non-gauge chiral interactions $\mathcal{L}_{int}$

$$\boxed{\mathcal{L}_{chiral} = -D^\mu \phi^{*i} D_\mu \phi_i + i\psi_i^\dagger \bar{\sigma}^\mu \partial_\mu \psi_i - V_F(\phi, \phi^*) + \mathcal{L}_{int}}\,, \tag{2.22}$$

where the F-term scalar potential is determined by the superpotential of the theory (2.30) since

$$V_F(\phi^*, \phi) = F^{*i} F_i = (-W^i)(-W_i^*) = \left| \frac{\partial W}{\partial \phi_i} \right|^2 , \tag{2.23}$$

$SU(2)_L$ doublets	
$Q_i = \begin{pmatrix} u_{L_i} \\ d_{L_i} \end{pmatrix}$	$\tilde{Q}_i = \begin{pmatrix} \tilde{u}_{L_i} \\ \tilde{d}_{L_i} \end{pmatrix}$
$L_i = \begin{pmatrix} \nu_{e_{L_i}} \\ e_{L_i} \end{pmatrix}$	$\tilde{L}_i = \begin{pmatrix} \tilde{\nu}_{e_{L_i}} \\ \tilde{e}_{L_i} \end{pmatrix}$
$H_u = \begin{pmatrix} H_u^+ \\ H_u^0 \end{pmatrix}$	$\tilde{H}_u = \begin{pmatrix} \tilde{H}_u^+ \\ \tilde{H}_u^0 \end{pmatrix}$
$H_d = \begin{pmatrix} H_d^0 \\ H_d^- \end{pmatrix}$	$\tilde{H}_d = \begin{pmatrix} \tilde{H}_d^0 \\ \tilde{H}_d^- \end{pmatrix}$

Table 2.2: Weak iso-doublets. The iso-doublets are constructed in a way such that $T_3 = (1/2, -1/2)$ and the electric charges are given by the convention $Q_{em} = T_3 + Y$.

and the interaction Lagrangian is strictly constrained by supersymmetry and the condition of renormalizability to be as known

$$\begin{aligned} \mathcal{L}_{int} &= -\frac{1}{2} W^{ij} \psi_i \psi_j + h.c \\ &= -\frac{1}{2} \left(\frac{\partial^2 W}{\partial \phi_i \partial \phi_j} \right) \psi_i \psi_j + h.c. \quad , \end{aligned} \tag{2.24}$$

where W is the superpotential describing the theory which has the generic form

$$W = \frac{1}{2} M^{ij} \phi_i \phi_j + \frac{1}{6} y^{ijk} \phi_i \phi_j \phi_k + L^i \phi_i \quad , \tag{2.25}$$

where y^{ijk} are the 3×3 Yukawa coupling matrices, M^{ij} are symmetric fermion mass matrices and $L^i \phi_i$ is a linear term which is allowed in the presence of a gauge singlet field ϕ.

By adding up all the terms eq.(2.20),(2.22),(2.24) for the full supersymmetric Lag-

rangian we obtain finally

$$\begin{aligned}\mathcal{L}_{susy} = &-\frac{1}{4}F^a_{\mu\nu}F^{\mu\nu,a} + i\lambda^{a\dagger}\bar{\sigma}^\mu D_\mu\lambda^a + \Big(-\sqrt{2}g(\phi_i^\star T^a\psi_i)\lambda^a + h.c\Big) \\ &- D^\mu\phi^{*i}D_\mu\phi_i + i\psi_i^\dagger\bar{\sigma}^\mu\partial_\mu\psi_i - \underbrace{\left(V_F(\phi,\phi^*) + \frac{1}{2}D^aD^a\right)}_{=V(\phi,\phi^*)} \\ &- \frac{1}{2}\left(\frac{\partial^2 W}{\partial\phi_i\partial\phi_j}\right)\psi_i\psi_j + h.c. \\ &+ \mathcal{L}_{soft}\ ,\end{aligned} \tag{2.26}$$

where i (not to be confused with the generation index) runs over the number of the chiral supermultiplets. In the UMSSM we have $5 \times 3 = 15$ supermultiplets for the SM fermions and the corresponding supersymmetric bosonic dofs plus two Higgs and one singlet supermultiplet, in total $i_{max} = 18$ (see Tab. 2.1). We avoid to write the sum explicitly for reasons of simplicity and clarity. The term in the last line corresponds to the Lagrangian term which breaks supersymmetry explicitly and creates the mass splitting between the components of the same supermultiplet. Before supersymmetry is broken the Weyl fermion and the complex scalar field belonging to the same supermultiplet satisfy the same wave equation with exactly the same squared-mass matrix and so the two field have degenerate masses. In the next subsection we give the prescription for the soft supersymmetric Lagrangian and we write down the $\mathcal{L}_{soft}$ for UMSSM.

The Soft Supersymmetry breaking Lagrangian

The most generic soft supersymmetric Lagrangian term one can write is given by

$$\mathcal{L}_{soft} = -\left(\frac{1}{2}M_a\lambda^a\lambda^a + \frac{1}{6}a^{ijk}\phi_i\phi_j\phi_k + \frac{1}{2}b^{ij}\phi_i\phi_j + t^i\phi_i\right) + c.c. - \phi_i^* m^2_{\phi,ij}\phi_j\ , \tag{2.27}$$

where M^a are the gaugino masses, $m^2_{\phi,ij}$ are the scalar soft squared masses, b^{ij}, a^{ijk} are the bilinear and trilinear soft couplings, respectively. Note that the above Lagrangian term does not contain dimensionless couplings and in that sense it is considered as "soft". All the couplings have a positive mass dimension in order to preserve the relationships between the dimensionless couplings which eliminate the quadratic divergences in all orders of perturbation theory after the breaking of supersymmetry. If we were to include dimensionless couplings this property would be spoiled and the initial motivation for supersymmetry would not be meaningful any more. As mentioned previously the superpartners belonging to the same supermultiplet have the same mass if supersymmetry remains unbroken. One would expect that the Lagrangian has to be invariant under supersymmetric transformations but the vacuum should break this symmetry spontaneously in a way similar to

the SM. Note that the first and the third term of eq.(2.27) are the scalar masses for the gaugino fermions and the scalar quarks, leptons and Higgs doublets. The second trilinear in the scalar fields term has the same form as the Yukawa terms in the superpotential. The gaugino masses receive no other contribution from any other Lagrangian term as we can clearly deduce by looking at eq.(2.26). The situation is different, as we implied previously, for the squarks and sleptons of the theory. The bilinear and the trilinear mass term will give contributions to the sfermion squared mass matrix creating the mass splitting between the components of a supermultiplet after one switches on the symmetry breaking mechanism. The details of this spontaneously breaking mechanism are yet to be found, leading to an "effective" parametrization which introduces a variety of new couplings and soft parameters which make the model more complicated than in the Standard Model. The soft breaking Lagrangian in the UMSSM thus will be given by

$$\begin{aligned}
\mathcal{L}_{soft} &= -\frac{1}{2}M_1\tilde{B}\tilde{B} - \frac{1}{2}M_2\tilde{W}\tilde{W} - \frac{1}{2}M_3\tilde{g}\tilde{g} + c.c \\
&- \Big(\bar{u}^i A_{u_{ij}} y_{u_{ij}} Q^{T^j}\epsilon H_u - \bar{d}^i A_{d_{ij}} y_{d_{ij}} Q^{T^j}\epsilon H_d - \bar{e}^i A_{e_{ij}} y_{e_{ij}} L^{T^j}\epsilon H_d \\
&+ b(H_u^T\epsilon H_d) + c.c\Big) \\
&- Q^{\dagger^i} m^2_{Q_{ij}} Q^j - L^{\dagger^i} m^2_{L_{ij}} L^j - \bar{u}^{*^i} m^2_{\bar{u}_{ij}} \bar{u}^j - \bar{d}^{*^i} m^2_{\bar{d}_{ij}} \bar{d}^j - \bar{e}^{*^i} m^2_{\bar{e}_{ij}} \bar{e}^j \\
&- m^2_{H_u}|H_u|^2 - m^2_{H_d}|H_d|^2 - m_s^2|S|^2 \quad , \qquad (2.28)
\end{aligned}$$

where $b = A_s\mu_{eff} = A_s\lambda S$ is the corresponding $B\mu$ soft term in the MSSM but due to the presence of the extra gauge singlet has been transformed into a trilinear soft term with parameter A_s in the UMSSM. A_{ij} are the soft supersymmetry breaking trilinear couplings and y_{ij} are the Yukawa matrices. Their product gives the soft supersymmetry breaking trilinear matrices defined as

$$a_{ij} = A_{ij}y_{ij} \quad . \qquad (2.29)$$

In the relationship for $\mathcal{L}_{soft}$ eq.(2.31) we have supressed the indices a, b for the fundamental representation of the $SU(2)_L$ group. The soft masses m^2_{ij} are 3×3 matrices in generation space and can contain off-diagonal mixings which can affect low energy constraints from experiments involving flavour changing neutral currents (FCNC) and CP-violating effects. Since these studies are not in the scope of our current project in order to keep the model safe from these effects we assume that the soft masses are diagonal and do not impose any mixing. For the same reason in order to avoid any additional mixing coming from the soft trilinear "Yukawa" induced terms we assume that the "Yukawa" matrices are all diagonal. Since only the third generation quarks and leptons have $\mathcal{O}(1)$ Yukawa couplings this implies

that only the third generation quarks and leptons can have large trilinear scalar couplings. With these assumptions we can the rewrite a simplified version of the superpotential (2.30) and the soft supersymmetry breaking Lagrangian (2.31). Suppressing the generation i, j and the $SU(2)$ indices we have

$$W_{UMSSM} = \bar{u} y_u Q^T \epsilon H_u + \bar{d} y_d Q^T \epsilon H_d + \bar{e} y_e L^T \epsilon H_d + \lambda S H_u^T \epsilon H_d \quad , \tag{2.30}$$

and

$$\begin{aligned} \mathcal{L}_{soft} &= -\frac{1}{2} M_1 \tilde{B}\tilde{B} - \frac{1}{2} M_2 \tilde{W}\tilde{W} - \frac{1}{2} M_3 \tilde{g}\tilde{g} + c.c \\ &- \left(\bar{u} A_u y_u Q^T \epsilon H_u - \bar{d} A_d y_d Q^T \epsilon H_d - \bar{e} A_e y_e L^T \epsilon H_d + b(H_u^T \epsilon H_d) + c.c \right) \\ &- Q^\dagger m_Q^2 \mathbb{1}_3 Q - L^\dagger m_L^2 \mathbb{1}_3 L - m_{\bar{u}}^2 \mathbb{1}_3 |\bar{u}|^2 - m_{\bar{d}}^2 \mathbb{1}_3 |\bar{d}|^2 - m_{\bar{e}}^2 \mathbb{1}_3 |\bar{e}|^2 \\ &- m_{H_u}^2 |H_u|^2 - m_{H_d}^2 |H_d|^2 - m_s^2 |S|^2 \quad . \end{aligned} \tag{2.31}$$

The identity matrix $\mathbb{1}_3$ is there to remind the reader that the soft masses are diagonal matrices in the generation space.

The Scalar Potential

As we have seen in the previous sections the full scalar potential of a given supersymmetric model can be decomposed into the potential coming from the F-terms V_F, the D-terms V_D and the soft supersymmetry breaking terms V_{soft}

$$V_{scalar} = V_F + V_D + V_{soft} \quad . \tag{2.32}$$

The F-term scalar potential V_F. The F-term contribution to the scalar potential is given by eq.(2.23). To calculate the derivatives we first expand the superpotential eq.(2.30) by inserting the chiral superfields

$$\begin{aligned} W &= \bar{u} y_u (u_L H_u^0 - d_L H_u^+) + \bar{d} y_d (d_L H_d^0 - u_L H_d^-) + \bar{e} y_e (e_L H_d^0 - \nu_L H_d^-) \\ &+ \lambda S (H_u^+ H_d^- - H_u^0 H_d^0) \; . \end{aligned} \tag{2.33}$$

Calculating the derivatives of the superpotential with respect to all the fields of the theory $\phi_i = (\bar{u}, \bar{d}, \bar{e}, u_L, d_L, \nu_L, e_L, H_u^0, H_d^0, H_u^+, H_d^-, S)$ we have

$$\begin{aligned} V_F &= \sum_i^{12} \left| \frac{\partial W}{\partial \phi_i} \right|^2 = \\ &= |y_d (d_L H_d^0 - u_L H_d^-)|^2 + |y_e \bar{e} H_d^0|^2 + |y_e \bar{e} H_d^-|^2 + |y_u (u_L H_u^0 - d_L H_u^+)|^2 \\ &+ y_d \bar{d} H_d^- - y_u \bar{u} H_u^0|^2 + |y_d \bar{d} H_d^0 - y_u \bar{u} H_u^+|^2 + |\lambda (H_d^- H_u^+ - H_d^0 H_u^0)|^2 \\ &+ |y_u \bar{u} u_L - \lambda S H_d^0|^2 + |y_u \bar{u} d_L - \lambda S H_d^-|^2 + |y_e (e_L H_d^0 - \nu_L H_d^-)|^2 \\ &+ |y_d \bar{d} d_L + y_e \bar{e} e_L - \lambda S H_u^0|^2 + |y_d \bar{d} u_L + y_e \bar{e} \nu_L - \lambda S H_u^+|^2 \quad , \end{aligned} \tag{2.34}$$

where we introduce here the notation $\bar{u} \equiv \tilde{u}_R^*$.

The D-term scalar potential. The D-term contributions to the scalar potential according to eq.(2.26) is given by

$$\begin{aligned} V_D = \frac{1}{2} D^a D^a &= \frac{1}{2} \sum_{a,i,j} g_a^2 (\phi_i^* T^a \phi_i)(\phi_j^* T^a \phi_j) \\ &= V_{SU(2)} + V_{U(1)} + V_{U(1)'} \quad , \end{aligned} \tag{2.35}$$

where the summation over the gauge groups $SU(2)_L, U(1)_Y, U(1)'$ is decomposed into three terms to be calculated separately. The $SU(2)$ D-term contribution will involve only the chiral superfields $\phi_i = (Q, L, H_u, H_d)$ which transform under the $SU(2)$ fundamental representation so we can write

$$\begin{aligned} V_{SU(2)} &= \frac{1}{2} \sum_{i,j} g_2^2 (\phi_i^\dagger \frac{\sigma^a}{2} \phi_i)(\phi_j^\dagger \frac{\sigma^a}{2} \phi_j) = \frac{1}{8} \sum_{i,j} g_2^2 \Big[(\phi_i^\dagger)_{1k} \sigma^a_{kl} (\phi_i)_{l1} \Big] \Big[(\phi_j^\dagger)_{1r} \sigma^a_{rt} (\phi_j)_{t1} \Big] \\ &= \frac{1}{8} \sum_{i,j} g_2^2 \Big[(\phi_i^\dagger)_{1k} (\phi_i)_{l1} \Big] \Big[(\phi_j^\dagger)_{1r} (\phi_j)_{t1} \Big] \cdot (\sigma^a_{kl} \sigma^a_{rt}) \\ &= \frac{1}{8} \sum_{i,j} g_2^2 \Big[(\phi_i^\dagger)_{1k} (\phi_i)_{l1} \Big] \Big[(\phi_j^\dagger)_{1r} (\phi_j)_{t1} \Big] \cdot (2\delta_{kt}\delta_{lr} - \delta_{kl}\delta_{rt}) \\ &= \frac{1}{8} g_2^2 \sum_{i,j} \Big[2 (\phi_i^\dagger)_{1k} (\phi_j)_{k1} (\phi_j^\dagger)_{1l} (\phi_i)_{l1} - (\phi_i^\dagger)_{1l} (\phi_i)_{l1} (\phi_j^\dagger)_{1r} (\phi_j)_{r1} \Big] \\ &= \frac{1}{8} g_2^2 \sum_{i,j} \Big[2 (\phi_i^\dagger \phi_j)(\phi_i^\dagger \phi_j)^\dagger - (\phi_i^\dagger \phi_i)(\phi_j^\dagger \phi_j) \Big] \quad , \\ V_{SU(2)} &= \frac{1}{8} g_2^2 \sum_{i,j} \Big[2 |\phi_i^\dagger \phi_j|^2 - |\phi_i|^2 |\phi_j|^2 \Big] \quad . \end{aligned} \tag{2.36}$$

By inserting the weak isodoublets into the above equation we will have

$$\begin{aligned} V_{SU(2)} &= \frac{1}{8} g_2^2 \Big\{ |Q|^4 + |L|^4 + |H_u|^4 + |H_d|^4 - 2|H_d|^2 |H_u|^2 + 4|H_d^\dagger H_u|^2 - 2|H_d|^2 |L|^2 \\ &+ 4|L^\dagger H_d|^2 - 2|H_d|^2 |Q|^2 + 4|Q^\dagger H_d|^2 - 2|H_u|^2 |L|^2 + 4|L^\dagger H_u|^2 - 2|H_u|^2 |Q|^2 \\ &+ 4|Q^\dagger H_u|^2 - 2|L|^2 |Q|^2 + 4|Q^\dagger L|^2 \Big\} \quad . \end{aligned} \tag{2.37}$$

Note that the $SU(2)$ D-terms are the same as in the minimal model since the doublet content remains the same. Similarly the $U(1)$ D-term contribution to the scalar potential will be

$$\begin{aligned} V_{U(1)} &= \frac{1}{2} g_1^2 \sum_{i,j} (\phi_i^* Y_i \phi_i)(\phi_j^* Y_j \phi_j) = \frac{1}{2} g_1^2 \left(\sum_i \phi_i^* Y_i \phi_i \right)^2 \\ &= \frac{1}{2} g_1^2 \left(\sum_i Y_i |\phi_i|^2 \right)^2 \quad , \end{aligned} \tag{2.38}$$

where Y_i is the hypercharge of the chiral superfield i. By inserting in the above equation all the chiral superfields which are charged under the $U(1)$ group we will have

$$\begin{aligned} V_{U(1)} &= \frac{1}{2}g_1^2\Big\{Y_Q(Q^\dagger Q)+Y_L(L^\dagger L)+Y_{H_u}(H_u^\dagger H_u)+Y_{H_d}(H_d^\dagger H_d) \\ &+ Y_{\bar{u}}|\bar{u}|^2+Y_{\bar{d}}|\bar{d}|^2+Y_{\bar{e}}|\bar{e}|^2\Big\}^2 . \end{aligned} \tag{2.39}$$

As in the case of $SU(2)$ the $U(1)$ D-terms are the same as in the MSSM. Finally the contribution from the extra $U(1)'$ gauge group will have the same form as in eq.(2.39) with the replacement $Y_i \to Q_i$ for the $U(1)'$ extra charges. In this case there will be one additional term in the sum from the chiral superfield S which is charged under the extra $U(1)'$ gauge group. Therefore we will have

$$\begin{aligned} V_{U(1)'} &= \frac{1}{2}g_1'^2\left(\sum_i Q_{\phi_i}|\phi_i|^2\right)^2 \\ &= \frac{1}{2}g_1'^2\Big\{Q_q(Q^\dagger Q)+Q_L(L^\dagger L)+Q_{H_u}(H_u^\dagger H_u)+Q_{H_d}(H_d^\dagger H_d) \\ &+ Q_{\bar{u}}|\bar{u}|^2+Q_{\bar{d}}|\bar{d}|^2+Q_{\bar{e}}|\bar{e}|^2+Q_s|S|^2\Big\}^2 . \end{aligned} \tag{2.40}$$

Note that in all the final equations above we have suppressed the generation index and an implicit sum over the three families of squarks and sleptons should be considered.

The soft term scalar potential. The soft breaking supersymmetric Lagrangian as we have seen earlier is given by eq.(2.27) so that the the scalar potential coming from the soft terms can be written as

$$\begin{aligned} V_{soft} &= -\mathcal{L}_{soft} = \frac{1}{2}M_1\tilde{B}\tilde{B}+\frac{1}{2}M_2\tilde{W}\tilde{W}+\frac{1}{2}M_3\tilde{g}\tilde{g}+c.c \\ &+ \Big(\bar{u}A_u y_u Q^T\epsilon H_u-\bar{d}A_d y_d Q^T\epsilon H_d-\bar{e}A_e y_e L^T\epsilon H_d+b(H_u^T\epsilon H_d)+c.c\Big) \\ &+ Q^\dagger m_Q^2\mathbb{1}_3 Q+L^\dagger m_L^2\mathbb{1}_3 L+m_{\bar{u}}^2\mathbb{1}_3|\bar{u}|^2+m_{\bar{d}}^2\mathbb{1}_3|\bar{d}|^2-m_{\bar{e}}^2\mathbb{1}_3|\bar{e}|^2 \\ &+ m_{H_u}^2|H_u|^2+m_{H_d}^2|H_d|^2+m_s^2|S|^2 . \end{aligned} \tag{2.41}$$

2.2 The Gauge Sector

In this section we will calculate the tree-level expressions for the gauge bosons in the $U(1)$ extensions of the MSSM. As we will analyse below the extra gauge eigenstate B'_μ associated with the extra gauge group mixes with the other two gauge eigenstates B_μ, W_μ^3 to form a massless photon and two intermediate gauge eigenstates Z_μ, Z'_μ which mix in order to give the mass eigenstates Z_1, Z_2, which correspond to the weak neutral gauge boson Z present in the SM and a new neutral gauge boson often called Z'. Notice that here Z, Z', in our

notation, do not correspond to the mass eigenstates of these two bosons but they represent intermediate gauge eigenstates which are superpositions of the eigenstates (B_μ, B'_μ, W^3_μ). This amounts merely to a change of basis from (B_μ, B'_μ, W^3_μ) to (A_μ, Z_μ, B'_μ), where now A_μ is diagonal with respect to $Z_\mu, B'_\mu \equiv Z'_\mu$ and can be identified as the massless photon since electromagnetism remains unbroken. The two remaining states $B'_\mu \equiv Z'_\mu, B_\mu$ mix with each other to form the mass eigenstates of the two neutral gauge bosons. Since there is no extra charged component the tree-level mass expression for the W boson remains unchanged in the UMSSM. Let's proceed with the calculation of these tree-level expressions.

The information for the gauge boson masses resides in the Lagrangian part of the covariant derivative acting on the Higgs bosons $(D^\mu\phi)^\dagger D_\mu\phi$ (see eq.(2.26)) where ϕ_i are the two Higgs doublets and the scalar component of the singlet field S which are charged under $SU(2)_L, U(1), U(1)'$ and $U(1)'$ respectively. The operator D_μ when acting upon the $SU(2)$ doublets reads

$$D_\mu\phi_i = \Big(- ig_1 B_\mu Y_i \cdot \mathbf{1_2} - ig_2 \sum_{a=1}^{3} W^a_\mu T^a_i - ig'_1 B'_\mu Q_i \cdot \mathbf{1_2} \Big)\phi_i \ , \tag{2.42}$$

$$D_\mu S = (-ig'_1 B'_\mu Q_i) S \ , \tag{2.43}$$

where we keep only the relevant part for the calculation of the gauge boson masses, that is why we have ignored the kinetic part coming from the derivative ∂_μ. The sum over all Higgs doublets and singlets will then be

$$(D^\mu\phi)^\dagger D_\mu\phi = |D^\mu H_u|^2 + |D^\mu H_d|^2 + |D^\mu S|^2 \ , \tag{2.44}$$

which takes the matrix form

$$\begin{aligned}(D^\mu\phi)^\dagger (D_\mu\phi) = \quad & \left| \begin{pmatrix} -iB_\mu \frac{g_1}{2} - iB'_\mu g'_1 Q_{H_u} - \frac{g_2}{2} W^3_\mu & -g_2 \left(\frac{W^1_\mu - iW^2_\mu}{2} \right) \\ -g_2 \left(\frac{W^1_\mu + iW^2_\mu}{2} \right) & -iB_\mu \frac{g_1}{2} - iB'_\mu g'_1 Q_{H_u} + \frac{g_2}{2} W^3_\mu \end{pmatrix} \begin{pmatrix} H^+_u \\ H^0_u \end{pmatrix} \right|^2 + \\ & \left| \begin{pmatrix} +iB_\mu \frac{g_1}{2} - iB'_\mu g'_1 Q_{H_d} - \frac{g_2}{2} W^3_\mu & -g_2 \left(\frac{W^1_\mu - iW^2_\mu}{2} \right) \\ -g_2 \left(\frac{W^1_\mu + iW^2_\mu}{2} \right) & +iB_\mu \frac{g_1}{2} - iB'_\mu g'_1 Q_{H_d} + \frac{g_2}{2} W^3_\mu \end{pmatrix} \begin{pmatrix} H^0_d \\ H^-_d \end{pmatrix} \right|^2 + \\ & | - iB'_\mu g'_1 Q_s S|^2 \ . \end{aligned} \tag{2.45}$$

After electroweak symmetry breaking takes place and the Higgs fields receive vevs the

above equation becomes

$$(D^\mu\phi)^\dagger(D_\mu\phi) = \left|\frac{v_u}{\sqrt{2}}\begin{pmatrix} -g_2\left(\frac{W^1_\mu - iW^2_\mu}{2}\right) \\ -iB_\mu\frac{g_1}{2} - iB'_\mu g'_1 Q_{H_u} + i\frac{g_2}{2}W^3_\mu \end{pmatrix}\right|^2 +$$

$$\left|\frac{v_d}{\sqrt{2}}\begin{pmatrix} +iB_\mu\frac{g_1}{2} - iB'_\mu g'_1 Q_{H_d} - i\frac{g_2}{2}W^3_\mu \\ -g_2\left(\frac{W^1_\mu + iW^2_\mu}{2}\right) \end{pmatrix}\right|^2 +$$

$$|-iB'_\mu g'_1 Q_s\frac{v_s}{\sqrt{2}}|^2 \ . \tag{2.46}$$

Now using the above form it is easy to see how the gauge eigenstates mix with each other and derive the squared mass matrices for the gauge bosons. For the W bosons in the basis (W^1_μ, W^2_μ) the mass terms reads

$$\begin{pmatrix} W^\mu_1 & W^\mu_2 \end{pmatrix}\begin{pmatrix} \frac{g_2^2}{8}(v_u^2+v_d^2) & 0 \\ 0 & \frac{g_2^2}{8}(v_u^2+v_d^2) \end{pmatrix}\begin{pmatrix} W^1_\mu \\ W^2_\mu \end{pmatrix} = \frac{1}{2}\cdot\underbrace{\frac{g_2^2}{4}v^2}_{=M_W^2}\Big((W^1_\mu)^2 + (W^2_\mu)^2\Big), \tag{2.47}$$

and thus predicting the mass of the W boson as in the SM (and MSSM) to be $M_W^2 = g_2^2v^2/4$. In the case of the neutral gauge bosons we can now see clearly that the extra gauge eigenstate B'_μ associated with the $U(1)'$ group mixes with the B_μ and W^3_μ to form a 3×3 non-diagonal matrix in the basis (W^3_μ, B_μ, B'_μ). The 3×3 matrix can be read off easily from eq.(2.46)

$$M^2_{W-B-B'} = \begin{pmatrix} W^3_\mu & B_\mu & B'_\mu \end{pmatrix}\cdot\frac{v_u^2+v_d^2}{8}\begin{pmatrix} g_2^2 & -g_1g_2 & 2g'_1g_2\frac{(v_d^2Q_{H_d}-v_u^2Q_{H_u})}{v_u^2+v_d^2} \\ -g_1g_2 & g_1^2 & -2g'_1g_1\frac{(v_d^2Q_{H_d}-v_u^2Q_{H_u})}{v_u^2+v_d^2} \\ 2g'_1g_2\frac{(v_d^2Q_{H_d}-v_u^2Q_{H_u})}{v_u^2+v_d^2} & -2g'_1g_1\frac{(v_d^2Q_{H_d}-v_u^2Q_{H_u})}{v_u^2+v_d^2} & 4{g'_1}^2\frac{Q^2_{H_d}v_d^2+Q^2_{H_u}v_u^2+Q_s^2v_s^2}{v^2} \end{pmatrix}\begin{pmatrix} W^3_\mu \\ B_\mu \\ B'_\mu \end{pmatrix}, \tag{2.48}$$

the determinant of the 3×3 non-diagonal matrix in eq.(2.46) is zero meaning that the matrix has a zero eigenvalue which can be identified as the photon since electromagnetism remains unbroken. The eigenvector corresponding to the zero eigenvalue is given by

$$A_\mu = W^3_\mu\frac{g_1}{\sqrt{g_1^2+g_2^2}} + B_\mu\frac{g_2}{\sqrt{g_1^2+g_2^2}} \tag{2.49}$$

$$\equiv s_W W^3_\mu + c_W B_\mu \ , \tag{2.50}$$

and as we see it is the same expression that gives the photon A_μ in the SM in terms of the the gauge eigenstates W^3_μ, B_μ and the Weinberg angle θ_W, where the sine and the cosine

of the Weinberg angle are defined as

$$\sin\theta_W \equiv s_W = \frac{g_1}{\sqrt{g_1^2+g_2^2}} \qquad \cos\theta_W \equiv c_W \frac{g_2}{\sqrt{g_1^2+g_2^2}} \ . \tag{2.51}$$

Note the the upper left 2×2 matrix corresponds to the mixing matrix between the states (W_μ^3, B_μ) which in the SM after we diagonalize it by rotating the fields using a special orthogonal transformation, we get two mass eigenstates one with zero eigenvalue which corresponds to the photon and a second one with squared mass $1/4 g_z^2 v^2$ that corresponds to the neutral Z boson, i.e.

$$\begin{pmatrix} W_\mu^3 & B_\mu \end{pmatrix} \cdot \tfrac{v_u^2+v_d^2}{8} \begin{pmatrix} g_2^2 & -g_1 g_2 \\ -g_1 g_2 & g_1^2 \end{pmatrix} \begin{pmatrix} W_\mu^3 \\ B_\mu \end{pmatrix} = \boxed{\mathbf{0}} A_\mu A^\mu + \frac{1}{2}\cdot \boxed{\frac{1}{4} g_z^2 v^2} Z_\mu Z^\mu \tag{2.52}$$

where A_μ is given by eq.(2.49) and Z_μ is given by the rotated mass eigenstate

$$Z_\mu = c_W W_\mu^3 - s_W B_\mu \ , \tag{2.53}$$

we can use the same trick here in the case of the presence of the extra $U(1)'$ symmetry. By introducing the intermediate gauge eigenstate Z_μ given by eq.(2.53), A_μ given by eq.(2.49) and setting $B'_\mu \equiv Z'_\mu$ we essentially rotate the fields $(W_\mu^3, B_\mu, B\mu')$ into a new basis (A_μ, Z_μ, Z'_μ)

$$\begin{pmatrix} A_\mu \\ Z_\mu \\ Z'_\mu \end{pmatrix} = \begin{pmatrix} s_W & c_W & 0 \\ c_W & -s_W & 0 \\ 0 & 0 & 1 \end{pmatrix} \begin{pmatrix} W_\mu^3 \\ B_\mu \\ B'_\mu \end{pmatrix} \ . \tag{2.54}$$

The advantage is that in this new basis Z_μ will only mix with the gauge eigenstate Z'_μ to give the mass eigenstates of the two neutral gauge bosons Z_1, Z_2 after diagonalizing the mixing matrix. Using the rotated fields eq.(2.54) we can rewrite the 3×3 mixing matrix in eq.(2.46) as follows

$$M_{Z-Z'-A_\mu} = \frac{1}{2}\begin{pmatrix} A_\mu & Z_\mu & Z'_\mu \end{pmatrix} \cdot \begin{pmatrix} 0 & 0 & 0 \\ 0 & \frac{1}{4}(g_1^2+g_2^2)v^2 & \frac{1}{2}g'_1\sqrt{g_1^2+g_2^2}(Q_{H_d}v_d^2 - Q_{H_u}v_u^2) \\ 0 & \frac{1}{2}g'_1\sqrt{g_1^2+g_2^2}(Q_{H_d}v_d^2 - Q_{H_u}v_u^2) & g_1'^2(Q_{H_d}^2 v_d^2 + Q_{H_u}^2 v_u^2 + Q_s^2 v_s^2) \end{pmatrix} \begin{pmatrix} A_\mu \\ Z_\mu \\ Z'_\mu \end{pmatrix} \tag{2.55}$$

$$= \boxed{0} A_\mu A^\mu + \frac{1}{2}\begin{pmatrix} Z_\mu & Z'_\mu \end{pmatrix} \mathcal{M}^2_{Z-Z'} \begin{pmatrix} Z_\mu \\ Z'_\mu \end{pmatrix} \ , \tag{2.56}$$

where $M^2_{Z-Z'}$ is the 2×2 real symmetric matrix which corresponds to the squared $Z-Z'$ mass mixing matrix

$$M^2_{Z-Z'} = \begin{pmatrix} M^2_Z & \Delta^2_Z \\ \Delta^2_Z & M^2_{Z'} \end{pmatrix} \ , \tag{2.57}$$

with the diagonal elements given by

$$M^2_Z = \frac{1}{4} g_z^2 v^2 \ , \qquad M^2_{Z'} = g_1'^2 (Q^2_{H_d} v_d^2 + Q^2_{H_u} v_u^2 + Q_s^2 v_s^2) \ , \tag{2.58}$$

and the off-diagonal mixing term given by

$$\Delta^2_Z = \frac{1}{2} g_1' g_z (Q_{H_d} v_d^2 - Q_{H_u} v_u^2) \ , \tag{2.59}$$

one can diagonalize the $Z-Z'$ squared mass mixing matrix by doing an orthogonal transformation $O(\theta')$ such that the gauge eigenstates (Z_μ, Z'_μ) are being rotated into the mass eigenstates $(Z_{1,\mu}, Z_{2,\mu})$

$$\frac{1}{2}\begin{pmatrix} Z_\mu \\ Z'_\mu \end{pmatrix}^T \mathcal{M}^2_{Z-Z'} \begin{pmatrix} Z_\mu \\ Z'_\mu \end{pmatrix} = \frac{1}{2}\begin{pmatrix} Z_{1\mu} \\ Z_{2\mu} \end{pmatrix}^T \underbrace{O^T \mathcal{M}^2_{Z-Z'} O}_{=M^2_{diag}(M^2_{Z_1}, M^2_{Z_2})} \begin{pmatrix} Z_{1\mu} \\ Z_{2\mu} \end{pmatrix} \tag{2.60}$$

$$= \frac{1}{2} M^2_{Z_1} Z_{1\mu} Z_1^\mu + \frac{1}{2} M^2_{Z_2} Z_{2\mu} Z_2^\mu \ , \tag{2.61}$$

where $M^2_{Z_1}, M^2_{Z_2}$ are the squared mass eigenvalues of the mixing matrix $\mathcal{M}^2_{Z-Z'}$

$$M^2_{Z_1,Z_2} = \frac{1}{2}\left(M^2_Z + M^2_{Z'} \mp \sqrt{(M^2_Z - M^2_{Z'})^2 + 4\,\Delta^4_Z} \right) \ , \tag{2.62}$$

the mass eigenstates can be rotated back to the gauge eigenstates as follows

$$\begin{pmatrix} Z_{1\mu} \\ Z_{2\mu} \end{pmatrix} = \underbrace{\begin{pmatrix} \cos\theta' & -\sin\theta' \\ \sin\theta' & \cos\theta' \end{pmatrix}}_{=O^T} \begin{pmatrix} Z_\mu \\ Z'_\mu \end{pmatrix} \ , \tag{2.63}$$

and the mixing angle θ' [2] is then defined as

$$\tan 2\theta' = \frac{2\Delta^2_Z}{M^2_{Z'} - M^2_Z} = \frac{g_1' g_z (Q_{H_d} v_d^2 - Q_{H_u} v_u^2)}{M^2_{Z'} - M^2_Z} \ , \tag{2.64}$$

[2] Note that the orthogonal matrix which rotates the gauge eigenstates into the mass eigenstates is ambiguous up to a minus sign in the off-diagonal element. Had we chosen the minus sign differently this would be equivalent make a change of variables $\theta' \to -\theta'$ and this would in turn yield the tangent of the mixing angle to be multiplied by a minus sign in this case.

by using now eq.(2.54) and eq.(2.63) we can write down the orthogonal matrix that diagonalizes the 3×3 matrix in eq.(2.48) and express the mass eigenstate basis $(A_\mu, Z_{1\mu}, Z_{2\mu})$ in terms of the initial gauge eigenstate basis $(W_{3\mu}, B_\mu, B'_\mu)$

$$\begin{pmatrix} A_\mu \\ Z_{1\mu} \\ Z_{2\mu} \end{pmatrix} = \underbrace{\begin{pmatrix} s_W & c_W & 0 \\ c_{\theta'} c_W & -c_{\theta'} s_W & -s_{\theta'} \\ s_{\theta'} c_W & -s_{\theta'} s_W & c_{\theta'} \end{pmatrix}}_{\mathcal{O}_T} \begin{pmatrix} W_{3\mu} \\ B_\mu \\ B'_\mu \end{pmatrix} . \tag{2.65}$$

2.3 The Higgs Sector

In this section our main goal to reproduce the mass matrices for the Higgs boson and calculate the 1-loop contributions to the CP-even Higgs bosons using the Weinberg-Coleman effective potential. The presence of the SM gauge singlet that mixes with the MSSM Higgs doublets modifies the Higgs sector in the extensions of the MSSM. Having computed the full scalar potential of the theory in the previous section by explicitly calculating the F, D and soft term contributions it is easy to construct the Higgs scalar potential and then rederive the tree-level mass matrices for the Higgs bosons. From the various contributions to the scalar potential eq.(2.23),(2.38),(2.39),(2.40) we keep only the terms containing the Higgs doublets H_u, H_d and the SM gauge singlet S. The Higgs scalar potential after simplifying the various terms can be written in the following form

$$\begin{aligned} V_{Higgs} &= |\lambda H_u^T \epsilon H_d|^2 + |\lambda S|^2 (|H_u|^2 + |H_d|^2) + \frac{1}{8}(g_1^2 + g_2^2)\left(|H_u|^2 - |H_d|^2\right)^2 + \frac{1}{2} g_2^2 |H_d^\dagger H_u|^2 \\ &+ \frac{1}{2} g_1'^2 \left(Q_{H_u}|H_u|^2 + Q_{H_d}|H_d|^2 + Q_s|S|^2\right)^2 \\ &+ \lambda S A_s H_u^T \epsilon H_d + h.c \\ &+ m_{H_u}^2 |H_u|^2 + m_{H_d}^2 |H_d|^2 + m_s^2 |S|^2 \ . \end{aligned} \tag{2.66}$$

Since we have broken supersymmetry explicitly by inserting the soft supersymmetry breaking terms in the potential, we now have to make sure that electroweak symmetry is broken spontaneously down to electromagnetism at the minimum of the potential and give masses to the SM bosons and fermions. By doing that we have to remind ourselves to be cautious with directions of the fields that can drive the Higgs potential to negative values since in any supersymmetric theory the potential has to be positive definite. Since color and charge remain unbroken we must take the vacuum expectation value of all fields which have non zero charge and color to be zero. This means that only the components of the Higgs doublets with zero charge H_u^0, H_d^0 are allowed to receive vevs as well as the singlet

S. Using gauge invariance we can rotate one of the Higgs field, let's choose H_u to have a vanishing zero vev of the positive charged component $\langle H_u^+ \rangle = 0$ at the minimum of the potential

$$\langle H_u \rangle = \frac{1}{\sqrt{2}} \begin{pmatrix} 0 \\ \\ v_u \end{pmatrix} \ , \tag{2.67}$$

in order for the potential to have an extremum the derivatives of the potential with respect to the the Higgs fields and the singlet have to be zero. Asking the derivative $\partial V/\partial H_d^- = 0$ to be zero we can easily see that this implies that also $H_d^{-*} = 0 = H_d^-$. So we can safely set $H_u^+ = H_d^- = 0$ in eq.(2.66) at the minimum of the potential without loss of generality. The Higgs potential then simplifies containing only the components of the Higgs fields with zero charges that are allowed to get vev's

$$\begin{aligned} V_{Higgs} &= |\lambda H_d^0 H_u^0|^2 + |\lambda S|^2(|H_u^0|^2 + |H_d^0|^2) + \frac{1}{8}(g_1^2 + g_2^2)\left(|H_u^0|^2 - |H_d^0|^2\right)^2 \\ &+ \frac{1}{2}g_1'^2\left(Q_{H_u}|H_u^0|^2 + Q_{H_d}|H_d^0|^2 + Q_s|S|^2\right)^2 \\ &- \lambda S A_s H_u^0 H_d^0 + h.c \\ &+ m_{H_u}^2|H_u^0|^2 + m_{H_d}^2|H_d^0|^2 + m_s^2|S|^2 \ . \end{aligned} \tag{2.68}$$

We can then rewrite the above relationship in a way that resembles the MSSM scalar potential, so that we can identify any differences in our analyses. We get

$$\begin{aligned} V_{Higgs} &= (|\mu_{eff}|^2 + m_{H_u}^2)|H_u^0|^2 + (|\mu_{eff}|^2 + m_{H_d}^2)|H_d^0|^2 - (bH_u^0 H_d^0 + h.c) \\ &+ \frac{1}{8}(g_1^2 + g_2^2)\left(|H_u|^2 - |H_d|^2\right)^2 + \frac{1}{2}g_1'^2\left(Q_{H_u}|H_u|^2 + Q_{H_d}|H_d|^2 + Q_s|S|^2\right)^2 \\ &+ m_s^2|S|^2 \ , \end{aligned} \tag{2.69}$$

where we have set $\mu_{eff} = \lambda\langle S \rangle$ before electroweak symmetry breaking for that reason. The last two terms are the extra terms not present in the minimal theory. The third term in the first line depends on the phases of the fields and we can always make a redefinition of the Higgs fields so that we can choose $b \geq 0$. If for example $b < 0$ we can write it as a complex phase $b = e^{i\pi}|b|$ and then absorb this phase into one of the two fields H_u^0, H_d^0. For the potential to have a minimum $H_u^0 H_d^0 = e^{i(\phi_u + \phi_d)}|H_u^0 H_d^0|$ has to be real and positive which means that the phases have to be opposite $\phi_u = -\phi_d$. This means that since the hypercharges of the two Higgs doublets are opposite we can use gauge invariance to make a $U(1)_Y$ gauge transformation in order to always choose both H_u^0, H_d^0 to be real and positive without loss of generality. Choosing b, H_u^0, H_d^0 simultaneously real and positive means that the combined transformation of charge conjugation and parity (CP) cannot

be violated in the Higgs sector. Thus we can assign eigenvalues of CP to the Higgs mass eigenstates. Let's consider for now the simplest case of the MSSM, i.e. we consider for a minute the expression for the Higgs potential above (2.69) without the last two terms coming from the $U(1)'$ D-terms and the scalar soft term and we simplify the notation by setting $H_u^0 = x, H_u^0 = y$, and defining the coefficients of each term accordingly as seen below

$$V_{Higgs} = a_1 x^2 + a_2 y^2 - 2bxy + a_3 \left(x^2 - y^2\right)^2 , \tag{2.70}$$

the Higgs potential in the MSSM involves quadratic and quartic powers of the two neutral Higgs fields. For large values of either one of the Higgs fields for example if we move in the direction of large $x \to \infty$ or $y \to \infty$ keeping the other field constant the quartic term in eq.(2.70) will dominate and thus the potential will grow to large positive values. The problem arises when the quartic term vanishes. This happens when $x = y$ or equivalently $H_u^0 = H_d^0$. Moving along this direction $x = y$ (D-flat direction) to infinity does not ensure that the potential is still bounded from below. The above equation becomes a parabola

$$V_{Higgs} = (a_1 + a_2 - 2b)x^2 , \tag{2.71}$$

which has a minimum when the coefficient of the quadratic term becomes positive. And this translates into the following condition

$$\boxed{2|\mu|^2 + m_{H_u}^2 + m_{H_d}^2 > 2b} . \tag{2.72}$$

A second condition comes from the requirement that the origin should not be a stable minimum of the potential otherwise electroweak symmetry will not be broken spontaneously. Having that in mind we have to force the origin of the potential $x = y = 0$ to be a saddle point i.e. we have to require that the 2-dimensional Hessian matrix has a negative determinant

$$\begin{vmatrix} \frac{\partial^2 V}{\partial x^2} & \frac{\partial^2 V}{\partial x \partial y} \\ \frac{\partial^2 V}{\partial x \partial y} & \frac{\partial^2 V}{\partial y^2} \end{vmatrix} = 4a_1 a_2 - 4b^2 < 0 \Rightarrow \boxed{(|\mu|^2 + m_{H_u}^2)(|\mu|^2 + m_{H_d}^2) < b^2} . \tag{2.73}$$

The previous two relationships (2.72),(2.73) are necessary in order to have a minimum that is not the origin and that the potential is bounded from below, as required by supersymmetry. Now in the general case (MSSM) where the vacua are non zero one can easily retrieve the tadpole conditions which minimize the scalar potential by requiring

$$\frac{\partial V}{\partial \phi_i}\Big|_{\phi_i = v_i}^{\min} = 0 , \qquad \text{where } i = u, d , \tag{2.74}$$

and thus one finds

$$m_{H_u}^2 = -|\mu|^2 + b\cot\beta + \frac{M_Z^2}{2}\cos 2\beta \ , \tag{2.75}$$

$$m_{H_d}^2 = -|\mu|^2 + b\tan\beta - \frac{M_Z^2}{2}\cos 2\beta \ , \tag{2.76}$$

where $M_Z = 1/2 g_z v$ as in (2.58). One can re-write these two equations as follows

$$\sin 2\beta = \frac{2b}{m_{H_u}^2 + m_{H_d}^2 + 2|\mu|^2} \ , \tag{2.77}$$

$$\frac{M_Z^2}{2} = \frac{m_{H_d}^2 - m_{H_u}^2\tan^2\beta}{\tan^2\beta - 1} - |\mu|^2 \ , \tag{2.78}$$

where the last equation (2.78) represents the stability of the electroweak scale in the MSSM. In the case of UMSSM the study of the vaccum stability becomes more involved and exceeds the scope of this discussion. Like before one expands the Higgs and singlet fields around the minimum in terms of the real scalar fields ϕ_d, ϕ_u, ϕ_s and parametrizes the imaginary part, which corresponds to the Goldstone modes, using the real fields χ_d, χ_u, χ_s

$$H_u = \begin{pmatrix} H_u^+ \\ \frac{1}{\sqrt{2}}(v_u + \phi_u + i\chi_u) \end{pmatrix}, \quad H_d = \begin{pmatrix} \frac{1}{\sqrt{2}}(v_d + \phi_d + i\chi_d) \\ H_d^- \end{pmatrix}, \quad S = \frac{1}{\sqrt{2}}(v_s + \phi_s + i\chi_s). \tag{2.79}$$

At the minimum of the potential the Higgs doublets and the singlet field will obtain non-zero vevs and the vacua of the fields will be

$$\langle H_u\rangle = \frac{1}{\sqrt{2}}\begin{pmatrix} 0 \\ v_u \end{pmatrix}, \quad \langle H_d\rangle = \frac{1}{\sqrt{2}}\begin{pmatrix} v_d \\ 0 \end{pmatrix}, \quad \langle S\rangle = \frac{1}{\sqrt{2}}v_s, \tag{2.80}$$

one can calculate the minimization conditions using the prescription of (2.74) with $i = u, d, s$

$$\begin{aligned} \frac{\partial V_{Higgs}}{\partial \phi_d}\Big|_{\min} &= 0 \Rightarrow \\ m_{H_d}^2 &= -\frac{v_d^2}{2}\left(\frac{g_z^2}{4} + g_1'^2 Q_{H_d}^2\right) + \frac{v_u^2}{2}\left(\frac{g_z^2}{4} - g_1'^2 Q_{H_u} Q_{H_d} - |\lambda|^2\right) \\ &- \frac{v_s^2}{2}\left(|\lambda|^2 + g_1'^2 Q_{H_d} Q_s\right) + \frac{v_s v_u}{v_d 2\sqrt{2}}(A_s\lambda + A_s^*\lambda^*) \ , \end{aligned} \tag{2.81}$$

$$\begin{aligned} \frac{\partial V_{Higgs}}{\partial \phi_u}\Big|_{\min} &= 0 \Rightarrow \\ m_{H_u}^2 &= -\frac{v_d^2}{2}\left(\frac{g_z^2}{4} - g_1'^2 Q_{H_u} Q_{H_d} - |\lambda|^2\right) - \frac{v_u^2}{2}\left(\frac{g_z^2}{4} + g_1'^2 Q_{H_u}^2\right) \\ &- \frac{v_s^2}{2}\left(|\lambda|^2 + g_1'^2 Q_{H_u} Q_s\right) + \frac{v_s v_d}{v_u 2\sqrt{2}}(A_s\lambda + A_s^*\lambda^*) \ , \end{aligned} \tag{2.82}$$

$$\begin{aligned}\frac{\partial V_{Higgs}}{\partial \phi_s}\Big|_{\min} &= 0 \Rightarrow \\ m_S^2 &= -\frac{v_d^2}{2}\Big(|\lambda|^2 + g_1'^2 Q_{H_d} Q_s\Big) - \frac{v_u^2}{2}\Big(|\lambda|^2 + g_1'^2 Q_{H_u} Q_s\Big) \\ &- \frac{v_s^2}{2} q_1'^2 Q_s^2 + \frac{v_d v_u}{v_s 2\sqrt{2}}(A_s\lambda + A_s^*\lambda^*) \ . \end{aligned} \tag{2.83}$$

In the calculation of the minimization conditions we have preserved the possibility of λ, A_s being complex numbers but we have to stress here that in our calculations throughout this project we have assumed that λ, A_s are real numbers. In that case the tadpole conditions simplify further. In addition, we have explicitly written the extra gauge coupling and have not absorbed it yet into the charges of the extra U(1) symmetry. This has been done deliberately so that it easier for someone to compare these calculations with the literature. In order to find the tree-level matrix of the CP-even Higgs scalars we need to write this part of the scalar potential in the form

$$V_{\text{CP-even}}^{\text{Higgs}} = \frac{1}{2}\begin{pmatrix}\phi_d & \phi_u & \phi_s\end{pmatrix} M^2_{\text{CP-even}} \begin{pmatrix}\phi_d \\ \phi_u \\ \phi_s\end{pmatrix} = \frac{1}{2}\Phi_i^T \Big(M^2_{\text{CP-even}}\Big)_{ij}\Phi_j \ . \tag{2.84}$$

The mass squared matrix is then obtained by taking the second derivative of the Higgs potential with respect to the scalar fields $\phi_i, i = d, u, s$ at the minimum of the potential where the tadpole conditions hold

$$\Big(M^2_{\text{CP-even}}\Big)_{ij} = \frac{\partial V_{\text{Higgs}}}{\partial\phi_i \partial\phi_j}\Big|_{\min} \ . \tag{2.85}$$

After substituting the minimization conditions (2.81),(2.82),(2.83) and simplifying our results the 3×3 symmetrical squared matrix looks like this

$$\Big(M^2_{\text{CP-even}}\Big)_{ij} =$$

$$\begin{pmatrix} \left[\frac{g_z^2}{4} + Q_{H_d}^2 g_1'^2\right] v_d^2 + \frac{\lambda A_s}{\sqrt{2}}\frac{v_u v_s}{v_d} & -\left[\frac{g_z^2}{4} - \lambda^2 - Q_{H_d}Q_{H_u} g_1'^2\right] v_d v_u - \frac{\lambda A_s}{\sqrt{2}} v_s & \left[\lambda^2 + Q_{H_d} Q_s g_1'^2\right] v_d v_s - \frac{\lambda A_s}{\sqrt{2}} v_u \\ -\left[\frac{g_z^2}{4} - \lambda^2 - Q_{H_d}Q_{H_u} g_1'^2\right] v_d v_u - \frac{\lambda A_s}{\sqrt{2}} v_s & \left[\frac{g_z^2}{4} + Q_{H_u}^2 g_1'^2\right] v_u^2 + \frac{\lambda A_s}{\sqrt{2}}\frac{v_d v_s}{v_u} & \left[\lambda^2 + Q_{H_u} Q_s g_1'^2\right] v_u v_s - \frac{\lambda A_s}{\sqrt{2}} v_d \\ \left[\lambda^2 + Q_{H_d} Q_s g_1'^2\right] v_d v_s - \frac{\lambda A_s}{\sqrt{2}} v_u & \left[\lambda^2 + Q_{H_u} Q_s g_1'^2\right] v_u v_s - \frac{\lambda A_s}{\sqrt{2}} v_d & Q_s^2 g_1'^2 v_s^2 + \frac{\lambda A_s}{\sqrt{2}}\frac{v_d v_u}{v_s} \end{pmatrix} . \tag{2.86}$$

The three gauge eigenstates of the Higgs fields H_d, H_u, S are thus mixing with each other to form the three neutral physical mass eigenstates which are denoted in ascending mass order h_1^0, H_2^0, H_3^0. The 3×3 orthogonal matrix R_{ij} which rotates the field gauge eigenstate basis $\Phi = (H_d^0\ H_u^0\ S)^T$ into the mass eigenstate basis $H = (h_1^0\ H_2^0\ H_3^0)^T$ and diagonalizes the Higgs squared mass matrix $M^2_{\text{CP-even}}$ will have to satisfy the following matrix relation

$$\mathbf{R}^T\mathbf{M}^2_{\text{CP-even}}\mathbf{R} = \mathbf{diag}(m^2_{h_1^0}\ m^2_{H_2^0}\ m^2_{H_3^0}) \tag{2.87}$$

and thus we will have

$$\begin{aligned}\mathbf{\Phi}^T\mathbf{M}^2_{\text{CP-even}}\mathbf{\Phi} &= (\mathbf{RH})^T\mathbf{M}^2_{\text{CP-even}}(\mathbf{RH}) = \mathbf{H}^T\underbrace{\left(\mathbf{R}^T\mathbf{M}^2_{\text{CP-even}}\mathbf{R}\right)}_{\mathbf{diag}(m^2_{h_1^0}\ m^2_{H_2^0}\ m^2_{H_3^0})}\mathbf{H}\\ \Rightarrow \mathcal{L}^{\text{Higgs}}_{\text{CP-even}} &= -\frac{1}{2}\mathbf{H}^T\mathcal{M}^2_{\text{diag}}\mathbf{H}\ ,\end{aligned} \tag{2.88}$$

where the two different basis are connected by the relations

$$\Phi_i = \sum_j R_{ij}H_j\ , \tag{2.89}$$

where $i = d, u, s$ and $j = 1, 2, 3$ for the equation on the left and the other way around for the equation on the right. Eq.(2.89) relates the mass eigenstates to the gauge eigenstates and the squared absolute values of the coefficients $|R_{ji}|^2$ gives the j-th admixture of the i-th Higgs mass eigenstate. For example the component $|R_{u1}|^2$ shows the H_u^0 mixing of the lightest CP-even Higgs boson h_1^0 and so on.

CP-odd Higgs boson and Neutral Goldstone boson. Having expanded the Higgs scalar potential (2.68) using the parametrization (2.79) we can read off the tree-level squared mass matrix for the CP-odd Higgs fields from the bilinear terms in the expansion

$$V^{\text{Higgs}}_{\text{CP-odd}} = \frac{1}{2}\begin{pmatrix}\chi_d & \chi_u & \chi_s\end{pmatrix}M^2_{\text{CP-odd}}\begin{pmatrix}\chi_d\\ \chi_u\\ \chi_s\end{pmatrix} = \frac{1}{2}\mathcal{X}_i^T\left(M^2_{\text{CP-odd}}\right)_{ij}\mathcal{X}_j\ , \tag{2.90}$$

where the fields χ_i are the imaginary parts of the Higgs and singlet fields representing the neutral gauge eigenstates of the Goldstone bosons present in the theory. The column matrix $\mathcal{X} = (\chi_d\ \chi_u\ \chi_s)^T$ represents the gauge eigenstate basis of the fields. By taking the second derivatives of the Higgs potential with respect to the $\mathcal{X}_i$ fields we obtain the tree-level expression for the CP-odd Higgs squared matrix after plugging in the minimization

conditions and simplifying the relations

$$\left(M^2_{\text{CP-odd}}\right)_{ij} = \frac{\partial V_{\text{Higgs}}}{\partial\chi_i\partial\chi_j}\Big|_{\text{min}} =$$

$$= \frac{\lambda A_s}{\sqrt{2}}\begin{pmatrix} \frac{v_u v_s}{v_d} & v_s & v_u \\ v_s & \frac{v_d v_s}{v_u} & v_d \\ v_u & v_d & \frac{v_d v_u}{v_s} \end{pmatrix} , \tag{2.91}$$

which can also be written as

$$\left(M^2_{\text{CP-odd}}\right)_{ij} = \underbrace{\mu_{eff} A_s}_{B\mu}\begin{pmatrix} \frac{v_u}{v_d} & 1 & \frac{v_u}{v_s} \\ 1 & \frac{v_d}{v_u} & \frac{v_d}{v_s} \\ \frac{v_u}{v_s} & \frac{v_d}{v_s} & \frac{v_d v_u}{v_s^2} \end{pmatrix} , \tag{2.92}$$

where we have set $\mu_{eff} = \lambda A_s$. In this form is easy to see that the top left 2×2 matrix is merely the CP-odd squared mass matrix in the MSSM. The CP-odd squared mass matrix has two zero mass eigenvalues which correspond to the mass eigenstates of the two neutral Goldstone bosons $G^0_{1,2}$ that are eaten by the Z, Z' bosons giving them their masses. The third non-zero eigenvalue corresponds to the tree-level mass of the CP-odd pseudo-scalar Higgs boson A^0 in pUMSSM which reads

$$M^2_{A^0} = \underbrace{\frac{2A_s\mu_{eff}}{\sin 2\beta}}_{\text{MSSM}} + \underbrace{\frac{\lambda A_s}{\sqrt{2}}\frac{v_d v_u}{v_s}}_{\text{extra term}} \qquad \text{and} \qquad m_{G^0_{1,2}} = 0 \ . \tag{2.93}$$

Note that since in the MSSM we have essentially $A_s \to B$, the first term in (2.93) corresponds to the tree-level mass of the CP-odd Higgs boson in the MSSM, and the second term is just the extra term present in the extended model under study here. Rotating the fields from the gauge eigenstate basis $\mathcal{X} = (\chi_d\ \chi_u\ \chi_s)^T$ to the mass eigenstate basis $\mathbf{X} = (G^0_1\ G^0_2\ A^0)^T$ through an orthogonal matrix $\mathcal{O}_{ij}$ such that

$$\mathcal{O}^T\mathbf{M}^2_{\text{CP-even}}\mathcal{O} = \mathbf{diag}(m^2_{G^0_1}\ \ m^2_{G^0_2}\ \ m^2_{A^0}) \ , \tag{2.94}$$

will transform the part of the scalar potential V_{Higgs} for the CP-odd Higgs mass in diagonal form providing the physical states

$$V^{\text{CP-odd}}_{\text{Higgs}} = \frac{1}{2}\begin{pmatrix} G^0_1 & G^0_2 & A^0 \end{pmatrix}\begin{pmatrix} \mathbf{0} & & \\ & \mathbf{0} & \\ & & m^2_A \end{pmatrix}\begin{pmatrix} G^0_1 \\ G^0_2 \\ A^0 \end{pmatrix} , \tag{2.95}$$

the physical states are linked to the gauge eigenstates through the rotation matrices $\mathbf{X} = \mathcal{O}^T\mathcal{X}$ or equivalently $X_i = \sum_j \mathcal{O}_{ji}\mathcal{X}_j$, thus the composition of the CP-odd Higgs boson is given by

$$\begin{aligned} A^0 = \sum_j \mathcal{O}_{j3}\mathcal{X}_j &= \mathcal{O}_{13}\mathcal{X}_1 + \mathcal{O}_{23}\mathcal{X}_2 + \mathcal{O}_{33}\mathcal{X}_3 \\ &= \kappa\left(\frac{v_s}{v_d}\chi_d + \frac{v_s}{v_u}\chi_u + \chi_s\right) , \end{aligned} \tag{2.96}$$

where $\kappa = 1/\sqrt{1 + (v_s/v_d)^2 + (v_s/v_u)^2}$ is a normalization factor. In the unitary gauge the Goldstone fields are considered to be zero $G^0_{1,2} = 0$. Due to the fact that the coupling of the Higgs boson A^0 to the fermionic matter involves the matrix γ_5 which does not preserve parity, it is also referred as pseudo-scalar Higgs boson.

Charged Higgs bosons and Charged Goldstones. Following the same procedure for the charged Higgs mass matrix we obtain

$$V_{\pm}^{\text{Higgs}} = \left(H_d^{-^*}\ H_u^+\right) \begin{pmatrix} \frac{v_u^2(g_2^2-2\lambda^2)}{4} + \frac{1}{\sqrt{2}}\lambda A_s\frac{v_s v_u}{v_d} & -\frac{v_d v_u(g_2^2-2\lambda^2)}{4} - \frac{1}{\sqrt{2}}A_s\lambda v_s \\ -\frac{v_d v_u(g_2^2-2\lambda^2)}{4} - \frac{1}{\sqrt{2}}A_s\lambda v_s & \frac{v_d^2(g_2^2-2\lambda^2)}{4} + \frac{1}{\sqrt{2}}\lambda A_s\frac{v_s v_d}{v_u} \end{pmatrix} \begin{pmatrix} H_d^- \\ H_u^{+^*} \end{pmatrix} . \tag{2.97}$$

Diagonalizing the charged-Higgs mass matrix by first computing its eigenvalues we see that we end up with one massless state (and the conjugate state) which corresponds to the charged Goldstone modes $G^{\pm}$ which are "eaten" by the charged $W^{\pm}$ bosons to form their mass and another massive state $H^{\pm}$ and its conjugate state which constitute the sector of the charged Higgs scalars

$$\begin{aligned} \left(M^{(0)}_{H^{\pm}}\right)^2 &= \frac{1}{4}g_2^2(v_d^2+v_u^2) + \frac{\lambda v_s A_s(v_d^2+v_u^2)}{\sqrt{2}v_d v_u} - \frac{1}{2}(v_d^2+v_u^2)\lambda^2 \\ &= \frac{1}{4}g_2^2 v^2 + \frac{\lambda v_s A_s}{\sqrt{2}\sin\beta\cos\beta} - \frac{1}{2}v^2\lambda^2 \\ &= \frac{1}{4}g_2^2 v^2 + \frac{\sqrt{2}\lambda v_s A_s}{\sin 2\beta} - \frac{1}{2}v^2\lambda^2 . \end{aligned} \tag{2.98}$$

Here the first term is just the tree-level W boson mass while the second term corresponds to the relation for the tree-level mass of the CP-odd Higgs boson in the MSSM scenario as

we have seen in the previous paragraph (2.93)

$$\left(M_{A^0}^{MSSM}\right)^2 = \frac{\lambda v_s A_s}{\sqrt{2}\sin 2\beta/2}$$

$$= \frac{2A_s\mu_{eff}}{\sin 2\beta} \ , \tag{2.99}$$

so one can write the mass eigenvalues for the charged Higgs in the following form

$$\boxed{\left(M_{H^\pm}^{(0)}\right)^2 = \underbrace{M_W^2 + \left(M_{A^0}^{MSSM}\right)^2}_{MSSM} - \frac{1}{2}v^2\lambda^2} \ . \tag{2.100}$$

Again in this form it is easy to notice that the sum of the first two terms represents the squared mass of the charged-Higgs scalars in the MSSM. The extra term present in the UMSSM has a negative contribution to the square of the charged-Higgs mass thus resulting in lighter mass eigenstates at tree-level compared to the MSSM counterpart. Finding the eigenvectors corresponding to each eigenvalue we can diagonalize the squared matrix so that

$$\mathbf{R}_{H^\pm}^T \mathbf{M}_\pm^{\mathbf{0}\,2} \mathbf{R}_{H^\pm} = \mathbf{diag}(m_{G^\pm}^2 \ , \ m_{H^\pm}^2) \ , \tag{2.101}$$

the rotation matrix is constructed so that every column corresponds to one of the eigenvectors, in the basis $H_u^\pm, H_d^\pm$ we have

$$\mathbf{R}_{H^\pm} = \begin{pmatrix} -\frac{v_d}{v_u\sqrt{1+(v_d/v_u)^2}} & \frac{v_u}{v_d\sqrt{1+(v_u/v_d)^2}} \\ \frac{1}{\sqrt{1+(v_d/v_u)^2}} & \frac{1}{\sqrt{1+(v_u/v_d)^2}} \end{pmatrix}$$

$$= \begin{pmatrix} -\cos\beta & \sin\beta \\ \sin\beta & \cos\beta \end{pmatrix} \ , \tag{2.102}$$

where we have used the fact that $v^2 = v_u^2 + v_d^2$ and $v_u = v\sin\beta$, $v_d = v\cos\beta$. The mass eigenstates $\mathbf{S_m} = (G^\pm \quad H^\pm)^T$ can then be related to the gauge eigenstate basis $\mathbf{S_g} = (H_d^- \quad H_u^-)^T$ using the rotation matrix $\mathbf{R}_{H^\pm}$

$$\mathbf{S_m} = \mathbf{R}_{H^\pm}^T \mathbf{S_g}$$

$$\Rightarrow \begin{pmatrix} G^\pm \\ H^\pm \end{pmatrix} = \begin{pmatrix} -\cos\beta & \sin\beta \\ \sin\beta & \cos\beta \end{pmatrix} \begin{pmatrix} H_d^\pm \\ H_u^\pm \end{pmatrix} \ , \tag{2.103}$$

from which we get the mixing of the physical particles with respect to un-physical gauge eigenstates

$$G^{\pm} = -\cos\beta H_d^{\pm} + \sin\beta H_u^{\pm} \ , \tag{2.104}$$

$$H^{\pm} = \sin\beta H_d^{\pm} + \cos\beta H_u^{\pm} \ . \tag{2.105}$$

Note that although in the case of the charged-Higgs bosons we have an additional term in the diagonal elements of the squared mass matrix, stemming from the extra F-term contribution (λ-term in the superpotential) present in the UMSSM (we have a similar case in the NMSSM as well) the mixing of the particles is MSSM-like. The gauge singlet S has no charged component and doesn't mix with the other two charged states $H_u^{\pm}, H_d^{\pm}$ present in the MSSM and therefore the rotation matrix is identical to that in the MSSM.

2.4 The Squark Sector

Let us gather here all tRhe squark mass terms from the scalar potential and construct the mass matrix for the up and down type squarks. The mass terms for the squarks originate from various terms of the Lagrangian density. We have contributions from the F-terms which arise from the superpotential of the theory, from the D-terms, the soft trilinear coupling A-terms and of course from the explicit soft mass terms in the soft part of the scalar potential. One can write the Lagrangian density which contains the squark mass terms for the **up-type** squarks in the following way

$$\mathcal{L}_{\tilde{u}} = \mathcal{L}_{\tilde{u}_L^*\tilde{u}_L} + \mathcal{L}_{\tilde{u}_R^*\tilde{u}_R} + \mathcal{L}_{\tilde{u}_L^*\tilde{u}_R} + \mathcal{L}_{\tilde{u}_R^*\tilde{u}_L} \ , \tag{2.106}$$

where the various terms can be calculated by taking the second derivative of the squark scalar potential with respect to the corresponding squark fields $-\mathcal{L}_{\phi_i^*\phi_j} = \partial V/\partial\phi_i^*\partial\phi_j$. For instance

$$\begin{aligned}
\mathcal{L}_{\tilde{u}_L^*\tilde{u}_L} &= \tilde{u}_L^*\Big\{ -\Big(|H_d^0|^2 - |H_u^0|^2\Big)\left(\frac{g_2^2}{4} - \frac{g_1^2}{12}\right) \\
&- g_1'^2\Big(Q_{H_d}|H_d^0|^2 + Q_{H_u}|H_u^0|^2 + Q_s|S|^2\Big)Q_{Q_i} \\
&- |y_u|^2|H_u^0|^2 - m_{Q_i}^2\Big\}\tilde{u}_L \ .
\end{aligned} \tag{2.107}$$

Similarly we have for the other diagonal term $\tilde{u}_R^*\tilde{u}_R$

$$\begin{aligned}
\mathcal{L}_{\tilde{u}_R^*\tilde{u}_R} &= \tilde{u}_R^*\Big\{ -g_1^2\left(\frac{|H_d^0|^2}{3} - \frac{|H_u^0|^2}{3}\right) \\
&- g_1'^2\Big(Q_{H_d}|H_d^0|^2 + Q_{H_u}|H_u^0|^2 + Q_s|S|^2\Big)Q_{\tilde{u}_i} \\
&- |y_u|^2|H_u^0|^2 - m_{\tilde{u}_i}^2\Big\}\tilde{u}_R \ ,
\end{aligned} \tag{2.108}$$

for the left-handed and right-handed mixing which will give as in the end the off-diagonal terms of the matrix we have

$$\mathcal{L}_{\tilde{u}_L^*\tilde{u}_R} = \tilde{u}_L^*\Big(y_u^*\lambda S H_d^0 - y_u^* H_u^{0\,*} A_u^*\Big)\tilde{u}_R \ , \tag{2.109}$$

and its complex conjugate

$$\mathcal{L}_{\tilde{u}_R^*\tilde{u}_L} = \tilde{u}_R^*\Big(y_u\lambda S^* H_d^{0^*} - y_u H_u A_u\Big)\tilde{u}_L \ . \tag{2.110}$$

After electroweak symmetry breaking the Higgs and singlet fields obtain vevs and the squared-mass matrix for the squark gauge eigenstate fields can be written as

$$\begin{aligned} -\mathcal{L}_{\tilde{u}} &= \begin{pmatrix}\tilde{u}_L^* & \tilde{u}_R^*\end{pmatrix}\begin{pmatrix}\mathcal{M}^2_{\tilde{u}_L^*\tilde{u}_L} & \mathcal{M}^2_{\tilde{u}_L^*\tilde{u}_R} \\ \mathcal{M}^2_{\tilde{u}_R^*\tilde{u}_L} & \mathcal{M}^2_{\tilde{u}_R^*\tilde{u}_R}\end{pmatrix}\begin{pmatrix}\tilde{u}_L \\ \tilde{u}_R\end{pmatrix} \\ &= \tilde{u}_i^\dagger\Big(\mathcal{M}^2_{\tilde{u}}\Big)_{ij}\tilde{u}_j \ , \end{aligned} \tag{2.111}$$

where the elements of the squared-mass matrix are given by eq.(2.109) at the minimum of the potential

$$\mathcal{M}^2_{\tilde{u}_L^*\tilde{u}_L} = m^2_{Q_i} + m_u^2 + \Delta_{\tilde{u}_L} + \Delta_{Q_{i_{U(1)'}}} \ , \tag{2.112}$$

$$\mathcal{M}^2_{\tilde{u}_R^*\tilde{u}_R} = m^2_{\tilde{u}_i} + m_u^2 + \Delta_{\tilde{u}_R} + \Delta_{\bar{u}_{i_{U(1)'}}} \ , \tag{2.113}$$

$$\mathcal{M}^2_{\tilde{u}_L^*\tilde{u}_R} = \frac{y_u^* v_u}{\sqrt{2}}\left(A_u^* - \mu_{eff}\cot\beta\right) = \left(\mathcal{M}^2_{\tilde{u}_R^*\tilde{u}_L}\right)^* \ , \tag{2.114}$$

$i = 1,2,3$ is the family index and we have denoted as $\Delta_{\tilde{u}_L}$ and $\Delta_{Q_{i_{U(1)'}}}$ the D-term contributions coming from the $U(1)+SU(2)_L$ and the extra $U(1)'$ gauge group respectively. One has

$$\Delta_{\tilde{u}_L} = \frac{v_d^2 - v_u^2}{24}\Big(3g_2^2 - g_1^2\Big) = \left(\frac{1}{2} - \frac{2}{3}s_W^2\right)M_Z^2\cos(2\beta) \ , \tag{2.115}$$

$$\Delta_{\tilde{u}_R} = g_1^2\left(\frac{v_d^2}{6} - \frac{v_u^2}{6}\right) = \frac{2}{3}s_W^2 M_Z^2\cos(2\beta) \ . \tag{2.116}$$

For the second equalities in the equations above we have used the fact that $M_Z^2 = (g_1^2 + g_2^2)v^2/4$ and that the Weinberg angle can be written as $s_W^2 = g_1^2/(g_1^2+g_2^2)$. The $U(1)'$ D-terms are

$$\Delta_{Q_{i_{U(1)'}}} = \frac{g_1'^2}{2}\Big(Q_{H_d}v_d^2 + Q_{H_u}v_u^2 + Q_s v_s^2\Big)Q_{Q_i} \ , \tag{2.117}$$

$$\Delta_{\bar{u}_{i_{U(1)'}}} = \frac{g_1'^2}{2}\Big(Q_{H_d}v_d^2 + Q_{H_u}v_u^2 + Q_s v_s^2\Big)Q_{\bar{u}_i} \ . \tag{2.118}$$

The mass terms $m_u = y_u v_u/\sqrt{2}$ [3] are just the masses of the corresponding SM partners belonging to the same chiral supermultiplet. The squared-mass matrix for the up-type squarks has to be diagonalized by a unitary matrix $(R^{\tilde{u}})^\dagger = (R^{\tilde{u}})^{-1}$ (or orthogonal if $\mathcal{M}^2_{\tilde{u}}$ is real) in order to form the physical mass eigenstates

$$\tilde{u}_i^m = R^{\tilde{u}}_{ij}\tilde{u}_j \Longleftrightarrow \tilde{u}_i = (R^{\tilde{u}\,\dagger})_{ij}\tilde{u}_j^m \ , \tag{2.119}$$

and thus the Lagrangian mass term can be written in a diagonal form

$$\mathcal{L}_{\tilde{u}} = -\tilde{u}_i^\dagger \Big(\mathcal{M}^2_{\tilde{u}}\Big)_{ij}\tilde{u}_j = -\tilde{u}_i^m \underbrace{\Big[R^{\tilde{u}}\Big(\mathcal{M}^2_{\tilde{u}}\Big)_{ij}R^{\tilde{u}\,\dagger}\Big]_{ii}}_{\mathrm{diag}(m^2_{\tilde{u}_1},m^2_{\tilde{u}_2})}\tilde{u}_i^m \ , \tag{2.120}$$

$i = 1, 2$ for the two mass eigenstates. The diagonalized matrix is given by the unitary transformation

$$R^{\tilde{u}}\mathcal{M}^2_{\tilde{u}}R^{\tilde{u}\,\dagger} = \mathcal{M}^{\mathrm{m}^2}_{\tilde{u}} \equiv \mathrm{diag}(m^2_{\tilde{u}_1}, m^2_{\tilde{u}_2}) \ . \tag{2.121}$$

Now the Lagrangian for the **down-type** squarks $\tilde{d}_i$ (i is the family index) in the same manner is found to be

$$\begin{aligned}
\mathcal{L}_{\tilde{b}} &= \mathcal{L}_{\tilde{b}^*_L\tilde{b}_L} + \mathcal{L}_{\tilde{b}^*_R\tilde{b}_R} + \mathcal{L}_{\tilde{b}^*_L\tilde{b}_R} + \mathcal{L}_{\tilde{b}^*_R\tilde{b}_L} \\
&= \tilde{d}^*_L\Big\{g_2^2\left(\frac{1}{4}|H_d^0|^2 - \frac{1}{4}|H_u^0|^2\right) + \frac{g_1^2}{12}\Big(|H_d^0|^2 - |H_u^0|^2\Big) \\
&- g_1'^2\Big(Q_{H_u}|H_d^0|^2 + Q_{H_u}|H_u^0|^2 + Q_s|S|^2\Big)Q_{Q_i} - |y_d|^2|H_d^0|^2 - m^2_{Q_i}\Big\}\tilde{d}_L \\
&+ \tilde{d}^*_R\Big\{\frac{g_1^2}{6}(|H_d^0|^2 - |H_u^0|^2) - g_1'^2\Big(Q_{H_u}|H_d^0|^2 + Q_{H_u}|H_u^0|^2 + Q_s|S|^2\Big)Q_{\tilde{d}_i} \\
&- |y_d|^2|H_d^0|^2 - m^2_{\tilde{d}_i}\Big\}\tilde{d}_R + \ldots \\
&+ \tilde{d}^*_L\Big\{y_d^*\lambda S H_u^0 - y_d^* A_d^* H_d^{0\,*}\Big\}\tilde{d}_R + \mathrm{h.c.} \quad .
\end{aligned} \tag{2.122}$$

The hermitian matrix for the down-type squarks has the form

$$\begin{aligned}
-\mathcal{L}_{\tilde{d}} &= \begin{pmatrix}\tilde{d}^*_L & \tilde{d}^*_R\end{pmatrix}\begin{pmatrix}\mathcal{M}^2_{\tilde{d}^*_L\tilde{d}_L} & \mathcal{M}^2_{\tilde{d}^*_L\tilde{d}_R} \\ \mathcal{M}^2_{\tilde{d}^*_R\tilde{d}_L} & \mathcal{M}^2_{\tilde{d}^*_R\tilde{d}_R}\end{pmatrix}\begin{pmatrix}\tilde{d}_L \\ \tilde{d}_R\end{pmatrix} \\
&= \tilde{d}_i^\dagger\Big(\mathcal{M}^2_{\tilde{d}}\Big)_{ij}\tilde{d}_j = \tilde{d}_i^{m\,\dagger}\Big(\mathcal{M}^{m^2}_{\tilde{d}}\Big)_{ii}\tilde{d}_i^m \ .
\end{aligned} \tag{2.123}$$

The elements of the mass matrix squared are given by

$$\mathcal{M}^2_{\tilde{d}^*_L\tilde{d}_L} = m^2_{Q_i} + m^2_d + \Delta_{\tilde{d}_L} + \Delta_{Q_{i_{U(1)'}}} \ , \tag{2.124}$$

[3] Here we have assumed real Yukawa couplings.

$$\mathcal{M}^2_{\tilde{d}^*_R\tilde{d}_R} = m^2_{\tilde{d}_i} + m^2_d + \Delta_{\tilde{d}_R} + \Delta_{\bar{d}_{i_{U(1)'}}} \ , \tag{2.125}$$

$$\mathcal{M}^2_{\tilde{d}^*_L\tilde{d}_R} = \frac{y^*_d v_d}{\sqrt{2}}\left(A^*_d - \mu_{eff}\tan\beta\right) = (\mathcal{M}^2_{\tilde{d}^*_R\tilde{d}_L})^* \ , \tag{2.126}$$

where the D-term contributions to the diagonal terms are given by

$$\Delta_{\tilde{d}_L} = -\left(\frac{g_2^2}{4} + \frac{g_1^2}{12}\right)\left(\frac{v_d^2}{2} - \frac{v_u^2}{2}\right) = \left(-\frac{1}{2} + \frac{1}{3}s^2_W\right) M^2_Z\cos(2\beta) \ , \tag{2.127}$$

$$\Delta_{\tilde{d}_R} = -\frac{g_1^2}{6}\left(\frac{v_d^2}{2} - \frac{v_u^2}{2}\right) = -\frac{1}{3}s^2_W M^2_Z\cos(2\beta) \ , \tag{2.128}$$

$$\Delta_{\bar{d}_{i_{U(1)'}}} = \frac{g_1'^2}{2}\Big(Q_{H_d}v_d^2 + Q_{H_u}v_u^2 + Q_s v_s^2\Big)Q_{\bar{d}_i} \ . \tag{2.129}$$

Here the mass terms $m_d = y_d v_d/\sqrt{2}$ are just the masses of the corresponding down-type quarks. The unitary transformation which brings the squared mass matrix of the down-type squarks into a diagonal form is defined as

$$R^{\tilde{d}}\mathcal{M}^2_{\tilde{d}}R^{\tilde{d}\,\dagger} = \mathcal{M}^{2}_{\tilde{d}} \equiv \mathrm{diag}(m^2_{\tilde{d}_1}, m^2_{\tilde{d}_2}) \ , \tag{2.130}$$

and one can revert from the mass eigenstates $\tilde{d}^m_i$ to the chiral eigenstates $\tilde{d}_i$ through the unitary rotation matrix $R^{\tilde{d}}$

$$\tilde{d}_i = \left(R^{\tilde{d}\,\dagger}\right)_{ij}\tilde{d}^m_j \equiv \left(R^{\tilde{d}\,*}\right)_{ji}\tilde{d}^m_j \ . \tag{2.131}$$

2.5 The Slepton Sector

The supersymmetric Lagrangian density containing the slepton mass terms is given by

$$\begin{aligned}
\mathcal{L}_{\tilde{e}} &= \tilde{e}^*_L\Big\{g_2^2\left(\frac{|H^0_d|^2}{4} - \frac{|H^0_u|^2}{4}\right) - g_1^2\left(\frac{|H^0_d|^2}{4} - \frac{|H^0_u|^2}{4}\right) \\
&- g_1'^2\Big(Q_{H_d}|H^0_d|^2 + Q_{H_u}|H^0_u|^2 + Q_s|S|^2\Big)Q_{L_i} \\
&- |y_e|^2|H^0_d|^2 - m^2_{L_i}\Big\}\tilde{e}_L + \\
&+ \tilde{e}^*_R\Big\{\frac{g_1^2}{2}\Big(|H^0_d|^2 + |H^0_u|^2\Big) - g_1'^2\Big(Q_{H_d}|H^0_d|^2 + Q_{H_u}|H^0_u|^2 + Q_s|S|^2\Big)Q_{\bar{e}_i} \\
&- |y_e|^2|H^0_d|^2 - m^2_{\bar{e}_i}\Big\}\tilde{e}_R \\
&+ \tilde{e}^*_L\Big\{y^*_e\lambda S H^0_u - y^*_e A^*_e H^0_d\Big\}\tilde{e}_R + \text{h.c.} \quad .
\end{aligned} \tag{2.132}$$

The squared mass matrix is hence given by

$$
\begin{aligned}
-\mathcal{L}_{\tilde{e}} &= \begin{pmatrix} \tilde{e}_L^* & \tilde{e}_R^* \end{pmatrix} \begin{pmatrix} \mathcal{M}^2_{\tilde{e}_L^*\tilde{e}_L} & \mathcal{M}^2_{\tilde{e}_L^*\tilde{e}_R} \\ \\ \mathcal{M}^2_{\tilde{e}_R^*\tilde{e}_L} & \mathcal{M}^2_{\tilde{e}_R^*\tilde{e}_R} \end{pmatrix} \begin{pmatrix} \tilde{e}_L \\ \\ \tilde{e}_R \end{pmatrix} \\
&= \tilde{e}_i^{\,\dagger} \Big(\mathcal{M}^2_{\tilde{e}} \Big)_{ij} \tilde{e}_j = \tilde{e}_i^{m\,\dagger} \Big(\mathcal{M}^{m^2}_{\tilde{e}} \Big)_{ii} \tilde{e}_i^m \quad . \qquad (2.133)
\end{aligned}
$$

The matrix elements can be written in a similar way with the down-type squarks

$$
\begin{aligned}
\mathcal{M}^2_{\tilde{e}_L^*\tilde{e}_L} &= m^2_{L_i} + m_e^2 + \Delta_{\tilde{e}_L} + \Delta_{L_{i_{U(1)'}}} \ , \qquad (2.134) \\
\mathcal{M}^2_{\tilde{e}_R^*\tilde{e}_R} &= m^2_{\bar{e}_i} + m_e^2 + \Delta_{\tilde{e}_R} + \Delta_{\bar{e}_{i_{U(1)'}}} \ , \qquad (2.135) \\
\mathcal{M}^2_{\tilde{e}_L^*\tilde{e}_R} &= \frac{y_e^* v_d}{\sqrt{2}} \left(A_e^* - \mu_{eff} \tan\beta \right) = (\mathcal{M}^2_{\tilde{e}_R^*\tilde{e}_L})^* \ . \qquad (2.136)
\end{aligned}
$$

The D-term contributions to the diagonal elements of the squared-slepton matrix are given below

$$
\begin{aligned}
\Delta_{\tilde{e}_L} &= -\frac{1}{8}(v_d^2 - v_u^2)(g_2^2 - g_1^1) = \Big(-\frac{1}{2} + s_W^2 \Big) M_Z^2 \cos(2\beta) \ , \qquad (2.137) \\
\Delta_{\tilde{e}_R} &= -\frac{g_1^2}{4}(v_d^2 + v_u^2) = -s_W^2 M_Z^2 \cos(2\beta) \ , \qquad (2.138) \\
\Delta_{L_{i_{U(1)'}}} &= \frac{g_1'^2}{2} \Big(Q_{H_d} v_d^2 + Q_{H_u} v_u^2 + Q_s v_s^2 \Big) Q_{L_i} \ , \qquad (2.139) \\
\Delta_{\bar{e}_{i_{U(1)'}}} &= \frac{g_1'^2}{2} \Big(Q_{H_d} v_d^2 + Q_{H_u} v_u^2 + Q_s v_s^2 \Big) Q_{\bar{e}_i} \ , \qquad (2.140)
\end{aligned}
$$

and $m_e = y_e v_d/\sqrt{2}$ are the masses of the SM leptons. To get the mass eigenstates we have to rotate the chiral eigenstate fields $\tilde{e}_i$ with a unitary rotation matrix $R^{\tilde{e}}$

$$
\tilde{e}_i = \Big(R^{\tilde{e}\,\dagger} \Big)_{ij} \tilde{e}_j^m \equiv \Big(R^{\tilde{e}\,*} \Big)_{ji} \tilde{e}_j^m \ , \qquad (2.141)
$$

so that the diagonal matrix is given by the unitary transformation

$$
R^{\tilde{e}} \mathcal{M}^2_{\tilde{e}} R^{\tilde{e}\,\dagger} = \mathcal{M}^{\mathrm{m}^2}_{\tilde{e}} \equiv \mathrm{diag}(m^2_{\tilde{e}_1}, m^2_{\tilde{e}_2}) \ . \qquad (2.142)
$$

2.6 Neutralino Sector

The mass term in the Lagrangian of the theory for the neutralinos reads

$$
\begin{aligned}
\mathcal{L}^{\mathrm{mass}}_{\tilde{\chi}_i^0} &= -\frac{1}{2} \mathbf{X}^{g^T}_{\tilde{\chi}_i^0} \ \mathcal{M}_{\tilde{\chi}_i^0} \ \mathbf{X}^{g}_{\tilde{\chi}_i^0} + \mathrm{h.c.} \\
&= -\frac{1}{2} \mathbf{X}^{m^T}_{\tilde{\chi}_i^0} \ \mathbf{diag}(m_{\tilde{\chi}_1^0}, m_{\tilde{\chi}_2^0}, \ldots, m_{\tilde{\chi}_6^0}) \ \mathbf{X}^{m}_{\tilde{\chi}_i^0} \qquad (2.143)
\end{aligned}
$$

the 4 neutral gaugino gauge eigenstates present in the MSSM $\tilde{B}, \tilde{W}^3, \tilde{H}_d^0, \tilde{H}_u^0$ now mix with the two extra states $\tilde{S}, \tilde{M}_1'$ emerging in the $U(1)'$ extended models to form a 6×6 complex symmetric matrix which after diagonalization will give six neutral gaugino mass eigenstates $\mathbf{X}^m_{\tilde{\chi}_i^0} = (\tilde{\chi}_1^0, \tilde{\chi}_2^0, \tilde{\chi}_3^0, \tilde{\chi}_4^0, \tilde{\chi}_6^0)$ placed in ascending mass order. In the gauge eigenstate field basis $\mathbf{X}^g_{\tilde{\chi}_i^0} = (\tilde{B}, \tilde{W}^3, \tilde{H}_d{}^0, \tilde{H}_u{}^0, \tilde{S}, \tilde{B}')$ the matrix takes the form

$$M^{6\times 6}_{\tilde{\chi}^0} = \begin{pmatrix} M_1 & 0 & -\frac{1}{2}g_1 v_d & \frac{1}{2}g_1 v_u & 0 & 0 \\ 0 & M_2 & \frac{1}{2}g_2 v_d & -\frac{1}{2}g_2 v_u & 0 & 0 \\ -\frac{1}{2}g_1 v_d & \frac{1}{2}g_2 v_d & 0 & -\mu_{\text{eff}} & -\frac{\lambda v_u}{\sqrt{2}} & \tilde{Q}_{H_d} v_d \\ \frac{1}{2}g_1 v_u & -\frac{1}{2}g_2 v_u & -\mu_{\text{eff}} & 0 & -\frac{\lambda v_d}{\sqrt{2}} & \tilde{Q}_{H_u} v_u \\ 0 & 0 & -\frac{\lambda v_u}{\sqrt{2}} & -\frac{\lambda v_d}{\sqrt{2}} & 0 & \tilde{Q}_s v_s \\ 0 & 0 & \tilde{Q}_{H_d} v_d & \tilde{Q}_{H_u} v_u & \tilde{Q}_s v_s & M_1' \end{pmatrix} , \tag{2.144}$$

where we have set $\tilde{Q}_i = g_1' Q_i$. The top left 4×4 block of matrix contains the neutralino mass matrix of the MSSM. The two extra neutralino states present in the UMSSM model are contained in the 2×2 matrix residing in the bottom right corner of the neutralino matrix. In order to diagonalize the complex symmetric neutralino mas matrix (2.144) and to obtain the physical masses one has to find unitary matrix $V^\dagger = V^{-1}$ which rotates the gauge eigenstate basis such that

$$V^T \, \mathcal{M}_{\tilde{\chi}_i^0} \, V = \mathbf{diag}(|m_1|, |m_2|, \ldots, |m_6|) \ , \tag{2.145}$$

where $m_{\tilde{\chi}_i} = |m_i|$. If $V = \mathcal{N}^\dagger$ then we have

$$\mathcal{N}^* \, \mathcal{M}_{\tilde{\chi}_i^0} \, \mathcal{N}^\dagger = \mathbf{diag}(|m_1|, |m_2|, \ldots, |m_6|) \ . \tag{2.146}$$

Now the question is how do we construct this matrix $\mathcal{N}$. First of all the neutralino mass matrix is complex and what we know is, how to diagonalize a real symmetric matrix by finding an orthogonal similarity transformation. Therefore instead of diagonalizing the complex symmetric matrix $\mathcal{M}_{\tilde{\chi}^0}$ we will diagonalize the hermitian matrix $\mathcal{M}^\dagger_{\tilde{\chi}^0}\mathcal{M}_{\tilde{\chi}^0}$ which has real eigenvalues. Thus we are looking for a unitary matrix $U^\dagger = U^{-1}$ such that

$$U^\dagger \mathcal{M}^\dagger_{\tilde{\chi}^0} \mathcal{M}_{\tilde{\chi}^0} U = \mathbf{diag}(m_1^2, m_2^2, \ldots, m_6^2) \ , \tag{2.147}$$

where m_i are called the singular values of the neutralino symmetric matrix. The matrix U diagonalizes also the neutralino matrix

$$U^* \; \mathcal{M}_{\tilde{\chi}_i^0} \; U^\dagger = \mathbf{diag}(\pm|m_1|, \pm|m_2|, \ldots, \pm|m_6|) \; . \tag{2.148}$$

Note that in the right-hand side the diagonal matrix will possibly have entries with different phases. Since we want all the physical masses to have positive values $m_{\tilde{\chi}_i} = |m_i| > 0$ we will have to absorb these phases into the rotation matrix U. We can re-write the above equation as follows by factoring out the phases

$$U^* \; \mathcal{M}_{\tilde{\chi}_i^0} \; U^\dagger = \underbrace{\begin{pmatrix} e^{i\phi_1} & & & \\ & e^{i\phi_2} & & \\ & & \ddots & \\ & & & e^{i\phi_6} \end{pmatrix}}_{(P^*)^2} \mathbf{diag}(|m_1|, |m_2|, \ldots, |m_6|) \; , \tag{2.149}$$

where we define as $(P^*)^2 = \mathbf{diag}(e^{i\phi_1}, \ldots, e^{i\phi_6})$ the diagonal matrix with entries the phases $\phi_i = 0$ or π of the neutralinos. Note that the complex conjugate of this matrix P^2 is essentially the inverse matrix for which $(P^*)^2 \; P^2 = I$, thus we will have

$$\begin{aligned} P^2 U^* \; \mathcal{M}_{\tilde{\chi}_i^0} \; U^\dagger &= \mathbf{diag}(|m_1|, |m_2|, \ldots, |m_6|) \Rightarrow \\ (PU^*) \; \mathcal{M}_{\tilde{\chi}^0} \; (PU^*)^T &= \mathbf{diag}(|m_1|, |m_2|, \ldots, |m_6|) \Rightarrow \\ \mathcal{N}^* \; \mathcal{M}_{\tilde{\chi}^0} \; \mathcal{N}^\dagger &= \mathbf{diag}(|m_1|, |m_2|, \ldots, |m_6|) \; , \end{aligned} \tag{2.150}$$

where we identify the complex matrix to be $\mathcal{N} = P^* U$ and $P^* = \mathbf{diag}(e^{i\phi_1/2}, \ldots, e^{i\phi_6/2})$. Reversing (2.150) solving with respect to the neutralino matrix $\mathcal{M}_{\tilde{\chi}^0}$ we have

$$\mathcal{M}_{\tilde{\chi}^0} = \mathcal{N}^T \mathbf{diag}(|m_1|, |m_2|, \ldots, |m_6|) \mathcal{N} \; , \tag{2.151}$$

where we have used the fact that $\mathcal{N}^T \mathcal{N}^* = \mathbb{1}$. Plugging this equation into the first line of (2.143) we have

$$\begin{aligned} \mathcal{L}_{\tilde{\chi}_i^0}^{\text{mass}} &= -\frac{1}{2} \mathbf{X}_{\tilde{\chi}_i^0}^{g^T} \; \mathcal{M}_{\tilde{\chi}_i^0} \; \mathbf{X}_{\tilde{\chi}_i^0}^{g} + \text{h.c.} \\ &= -\frac{1}{2} \mathbf{X}_{\tilde{\chi}_i^0}^{g^T} \; \mathcal{N}^T \mathbf{diag}(|m_1|, |m_2|, \ldots, |m_6|) \mathcal{N} \; \mathbf{X}_{\tilde{\chi}_i^0}^{g} + h.c \\ &= -\frac{1}{2} \Big(\mathcal{N} \; \mathbf{X}_{\tilde{\chi}_i^0}^{g} \Big)^T \mathbf{diag}(|m_1|, |m_2|, \ldots, |m_6|) \Big(\mathcal{N} \; \mathbf{X}_{\tilde{\chi}_i^0}^{g} \Big) + h.c \\ &= -\frac{1}{2} \mathbf{X}_{\tilde{\chi}_i^0}^{m^T} \; \mathbf{diag}(m_{\tilde{\chi}_1^0}, m_{\tilde{\chi}_2^0}, \ldots, m_{\tilde{\chi}_6^0}) \; \mathbf{X}_{\tilde{\chi}_i^0}^{m} \; , \end{aligned} \tag{2.152}$$

where we identify the relation which rotates the gauge eigenstate basis $\mathbf{X}^{g}_{\tilde{\chi}^0}$ to the mass eigenstate $\mathbf{X}^{m}_{\tilde{\chi}^0}$

$$(X^{m}_{\tilde{\chi}^0})_i = \sum_j \mathcal{N}_{ij}(X^{g}_{\tilde{\chi}^0})_j \ . \tag{2.153}$$

The physical meaning of the rotation matrix $\mathcal{N}$ is that it determines the couplings of the neutralinos to the other particles. The components of the unitary matrix $\mathcal{N}_{ij}$ give us information about the composition of the mass eigenstates $m_{\tilde{\chi}^0_i}$ with respect to the gauge eigenstates consisting of the gauginos of the theory $\mathbf{X}^{g}_{\tilde{\chi}^0_i} = (\tilde{B}, \tilde{W}^3, \tilde{H}^0_d, \tilde{H}^0_u, \tilde{S}, \tilde{B}')$. More precisely, the coefficient $|\mathcal{N}_{ij}|^2$ gives the mixing of the i-th neutralino mass eigenstate with the j-th gauge eigenstate. For example the singlino component of the lightest neutralino $\tilde{\chi}^0_1$ will be given by the absolute value squared of the coefficient $|N_{15}|^2$,

$$\tilde{\chi}^0_1 = \mathcal{N}_{11}\tilde{B} + \mathcal{N}_{12}\tilde{W}^3 + \mathcal{N}_{13}\tilde{H}^0_d + \mathcal{N}_{14}\tilde{H}^0_u + \mathcal{N}_{15}\tilde{S} + \mathcal{N}_{16}\tilde{B}' \ . \tag{2.154}$$

Note that $\sum_j |\mathcal{N}_{ij}|^2 = 1$. It is interesting to investigate the extra neutralino sector present in the UMSSM, consisted of the $\tilde{B}', \tilde{S}$. The 2×2 bottom left matrix in (2.144) exhibits some interesting properties [75, 93, 25, 38] in the cases where (i) $|\tilde{Q}_s|v_s \gg M'_1$ and (ii) $M'_1 \gg |\tilde{Q}_s|v_s$. The two dimensional real symmetric matrix reads

$$\mathcal{M}_2 = \begin{pmatrix} 0 & \tilde{Q}_s v_s \\ \tilde{Q}_s v_s & M'_1 \end{pmatrix} \ . \tag{2.155}$$

This matrix has two eigenvalues which can easily be found to be [4]

$$m_{5,6} = \frac{1}{2}\Big(M'_1 \pm \sqrt{{M'_1}^2 + 4(\tilde{Q}_s v_s)^2}\Big) \ . \tag{2.156}$$

Now let's look at the two different scenarios in more detail:

(i) $|\tilde{Q}_s|v_s \gg M'_1$

In this case the eigenvalues of (2.156) simplify giving two degenerate neutralinos which have maximal mixing due to the large off-diagonal elements of the 2×2 matrix,

$$m_5 = -|\tilde{Q}_s|v_s \quad , \quad m_6 = +|\tilde{Q}_s|v_s \ . \tag{2.157}$$

Notice from (2.58) that since $M_{Z'} \approx |\tilde{Q}_s|v_s$ in the large v_s limit, the two neutralinos $\tilde{S}, \tilde{B}'$ will be approximately degenerate with the heaviest Z' boson. If the value of the singlet vev v_s is very large compared to the other parameters of the matrix the two states will

[4] The subscripts 5,6 do not correspond to mass ordering here. They are simply used to denote the extra sector in the UMSSM with two additional neutralino states.

decouple from the other MSSM-like states.

(ii) $M_1' \gg |\tilde{Q}_s| v_s$.

When the mass of the $\tilde{B}'$ is very heavy compared to the off-diagonal element of the matrix $\mathcal{M}_2$ the eigenvalues can be written in the form

$$m_{5,6} = \frac{M_1'}{2}\left[1 \pm \sqrt{1+4\left(\frac{\tilde{Q}_s v_s}{M_1'}\right)^2}\right] \tag{2.158}$$

$$\simeq \frac{M_1'}{2}\left[1 \pm \left(1+\frac{4}{2}\left(\frac{\tilde{Q}_s v_s}{M_1'}\right)^2\right)\right] , \tag{2.159}$$

so we get

$$\boxed{m_6 \simeq M_1' + \frac{(\tilde{Q}_s v_s)^2}{M_1'} \ , \quad m_5 \simeq -\frac{(\tilde{Q}_s v_s)^2}{M_1'}} \ . \tag{2.160}$$

and thus in this limit we obtain two mass eigenstates from which, m_5 becomes very light and can possibly play the role of the lightest supersymmetric particle (LSP) and account for the observed relic density in the universe and the other one, m_6 becomes very heavy and decouples from the other neutralinos. The extra neutralino sector exhibits a see-saw like mechanism, the two states decouple with zero mixing since the off-diagonal elements are very small compared to the difference of the two diagonal terms. Therefore the lightest neutralino is mostly singlino, whereas the heaviest of the two is mostly bino primed. In Figure 2.1 we have plotted the six physical neutralino states after diagonalizing the real symmetric 6×6 matrix $\mathcal{M}_{\tilde{\chi}^0}$ in eq.(2.144). The masses of the $\tilde{B}, \tilde{W}^0$ are taken to be $M_1 = 200$ GeV and $M_2 = 600$ GeV, resulting in one bino-like state $m_1 \equiv m_{\tilde{B}} \approx 200$ GeV and one mostly wino mass eigenstate $m_4 \equiv m_{\tilde{W}^0} \approx 600$ GeV respectively (at $M_1' = 0$). The mass of the extra neutral gauge boson Z' is taken to be relatively light $M_{Z'} \simeq |\tilde{Q}_s| v_s = 900$ GeV whereas the effective μ_{eff} parameter is set to $\mu_{eff} = 500$ GeV, resulting in two heavy, almost degenerate $\tilde{H}$ Higgsino states (blue and green lines $M_1' = 0$), with $m_{3,4} = m_{\tilde{H}} \approx \mu_{eff}$. The charges are considered as free parameters following the lines of our future discussion in Chapter 3, and we set their values to be $\tilde{Q}_{H_d} = 0.24$, $\tilde{Q}_s = -0.3$, $\tilde{Q}_{H_u} = 0.06$. At the limit where the bino primed mass vanishes $M_1' = 0$, the two extra neutralino states, consisted of a maximal mixture of $\tilde{S}, \tilde{B}'$ gauge eigenstates, have, at tree-level, almost degenerate masses $m_{5,6} \approx M_{Z'}$ which are given approximately by the tree-level mass of the extra neutral gauge boson Z'. Note in Fig. 2.2 that the singlino $\tilde{S}$ and bino primed $\tilde{B}'$ component of the 5-th mass eigenstate is $|N_{55}|^2 = |N_{56}|^2 = 0.5$ which implies maximal mixing in the extra gaugino sector as discussed earlier in this section. As the bino primed mass M_1' increases the mixing between the two states is reduced and their mass

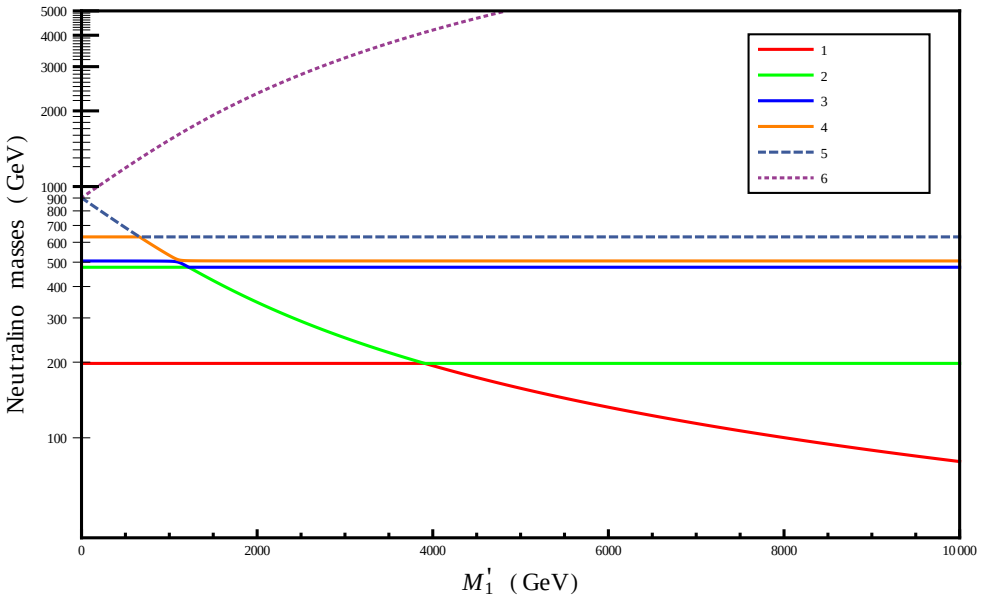

Figure 2.1: Logarithmic plot of the six neutralino mass eigenstates $m_{\tilde{\chi}_i^0}$, $i = 1, 2, \ldots 6$ as a function of the $\tilde{B}'$ gaugino mass parameter. Each mass eigenstate corresponds to a different coloured line. One should study this plot in conjunction with the following plots in this section in order to understand the various transitions of each mass eigenstate with respect to its gauge eigenstate composition. For more details see text.

splitting increases (Fig. 2.1). The see-saw like mechanism is switched on, creating one mass eigenstate which is mostly singlino $\tilde{S}$ and another one which is mostly $\tilde{B}'$. The singlino's mass is reducing gradually as we increase the bino primed mass and for $M_1' \simeq 4$ TeV it crosses the mostly bino state, becoming the lightest neutralino state $\tilde{\chi}_1^0$ (Fig. 2.5b). It is interesting to see the plots which show the gauge eigenstate components $|N_{ij}|^2$ for each physical neutralino state $\tilde{\chi}_i^0$.

In Fig. 2.3 we have plotted the singlino $\tilde{S}$ and $\tilde{B}'$ components of the heaviest neutralino state $\tilde{\chi}_6^0$. Increasing M_1' raises the bino primed component of the heaviest neutralino which decouples from all the other MSSM-like states. When $M_1' > 4$ TeV the mass of $\tilde{\chi}_6^0$ becomes heavier than $m_{\tilde{\chi}_6^0} > 3$ TeV and the bino primed component $|N_{66}|^2$ is more than 90% with a very small singlino $\tilde{S}$ admixture $|N_{65}|^2$ of the order of 10%. In the following Figures 2.4, 2.5 we plot the gauge eigenstate components of the remaining four lighter mass eigenstates $\tilde{\chi}_1^0$ (Fig. 2.5b), $\tilde{\chi}_2^0$ (Fig. 2.5a), $\tilde{\chi}_3^0$ (Fig. 2.4b), $\tilde{\chi}_4^0$ (Fig. 2.4a) as a function of M_1'. Let us have a look at the Figure 2.4a. For very small $\tilde{B}'$ mass the 4-th heaviest state $\tilde{\chi}_4^0$ is wino like $\tilde{W}^0$ (green line) with an admixture around 80%. There is a small Higgsino mixing $\sim 15\%$ since the effective Higgsino mass parameter is quite heavy $\mu_{eff} = 500$ GeV. Increasing M_1' makes the singlino eigenstate lighter and thus increases the singlino component of $\tilde{\chi}_4^0$ for 650 GeV $< M_1' <$ 1 TeV.

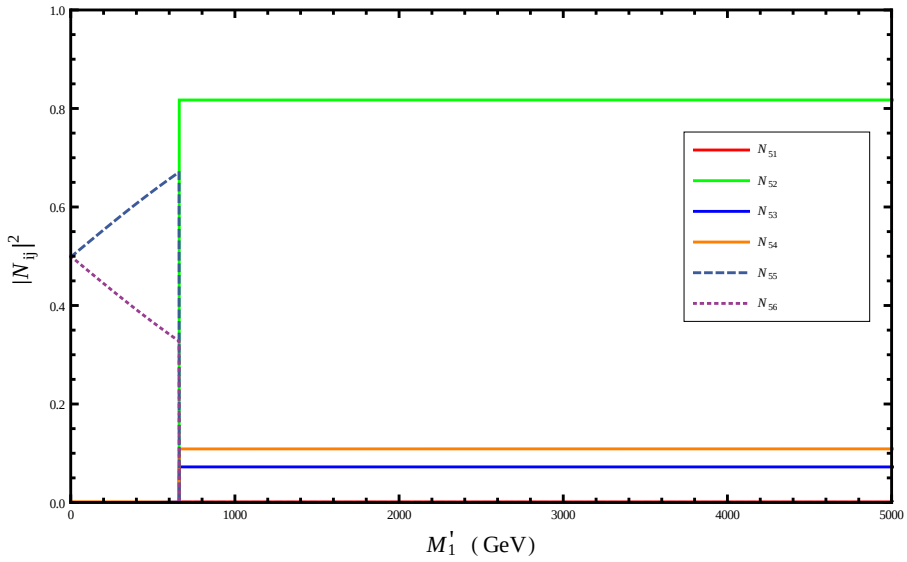

Figure 2.2: Gauge eigenstate decomposition of the 5-th neutralino in Fig. 2.1. At $M_1' = 0$ the neutralino $\tilde{\chi}_5^0$ is an equal mixture of $\tilde{S}$ and $\tilde{B}'$. While M_1' increases the singlino component increases to $|N_{55}|^2 \approx 0.68$ and then it drops suddenly to zero. At around $M_1' \sim 650$ GeV the $\tilde{\chi}_5^0$ changes identity and becomes mostly wino $\tilde{W}^0$. See also the crossing at this point with the 4-th mass eigenstate which is wino-like, in Fig. 2.1. The wino mixing $|N_{52}|^2$ is around 80% and remains the same since it is not affected by a further change in M_1'.

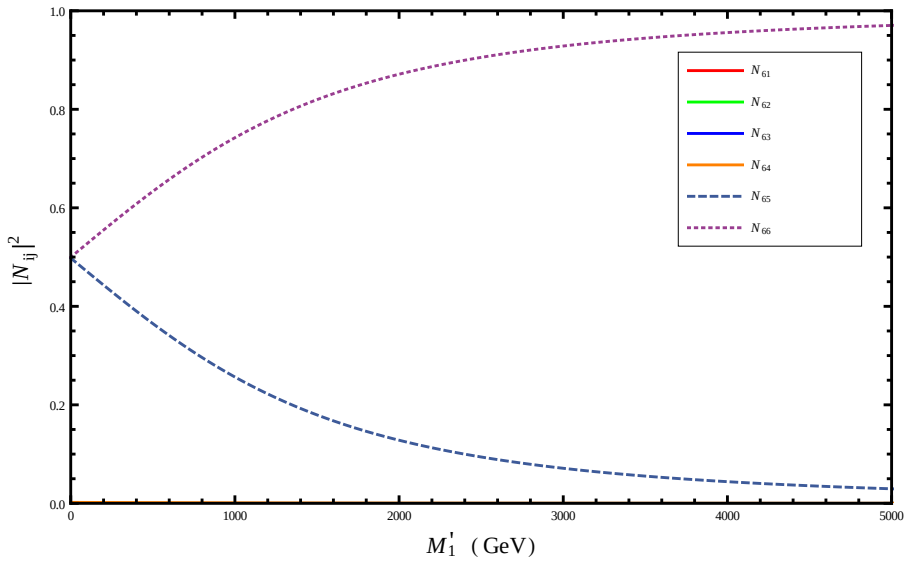

Figure 2.3: Gauge eigenstate components of the 6-th heaviest neutralino $\tilde{\chi}_6^0$ as a function of increasing bino primed mass parameter M_1'. The heaviest neutralino $m_{\tilde{\chi}_6^0}$ is an equal mixture of singlino $|N_{55}|^2 \approx 0.5$ and bino primed $|N_{56}|^2 \approx 0.5$ mass eigenstates. As M_1' mass increases $\tilde{\chi}_6^0$ becomes mostly $\tilde{B}'$. At $M_1' \sim 5$ TeV the bino primed component is $|N_{56}|^2 \approx 90\%$. Note that this state is decoupled from the other MSSM-like states.

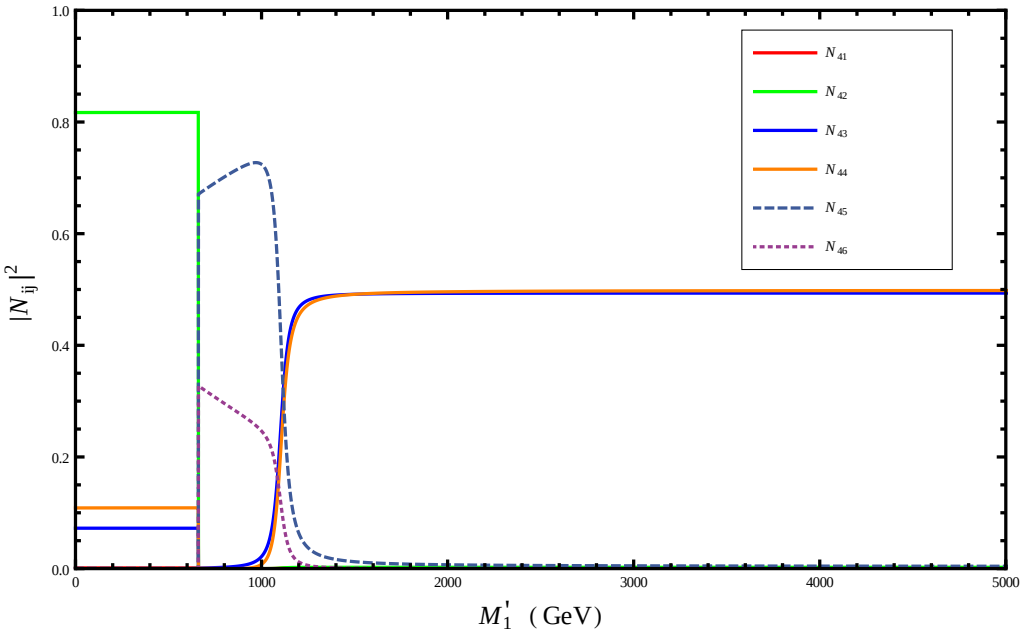

(a) Composition of $\tilde{\chi}_4^0$

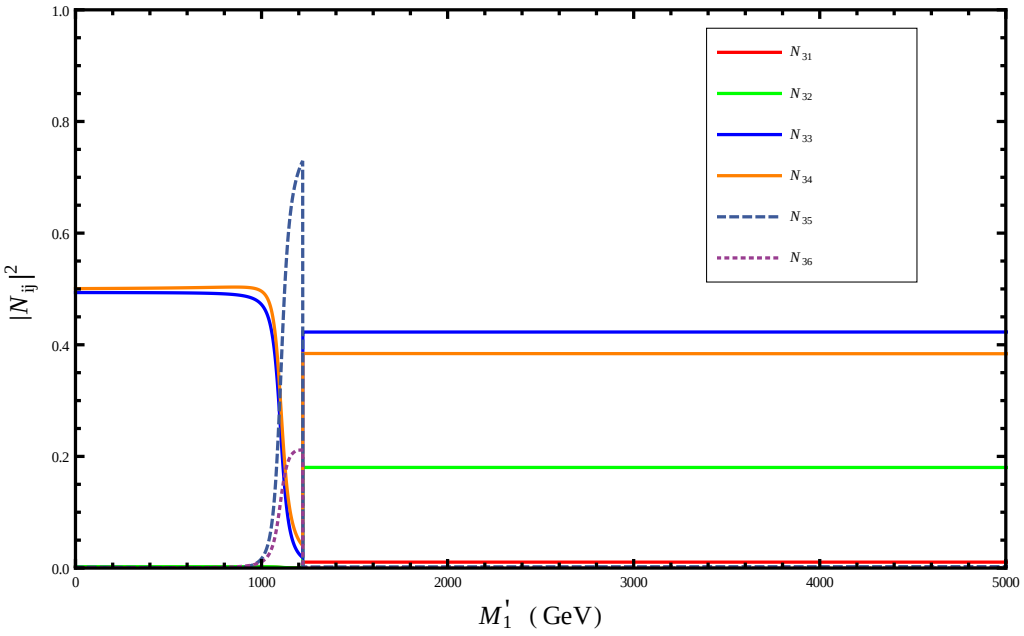

(b) Composition of $\tilde{\chi}_3^0$

Figure 2.4: Gauge eigenstate components $|N_{ij}|^2$ of the 4-th (Fig. 2.4a) and 3-rd (Fig. 2.4b) lightest neutralino as a function of M_1'. The singlino $\tilde{S}$ and bino primed $\tilde{B}'$ components are shown in blue and purple dashed lines. The $\tilde{\chi}_4^0$ physical state has a singlino component around 70% for $M_1' \simeq 1$ TeV. Increasing M_1' makes singlino even lighter and $\tilde{\chi}_4^0$ becomes Higgsino like state.

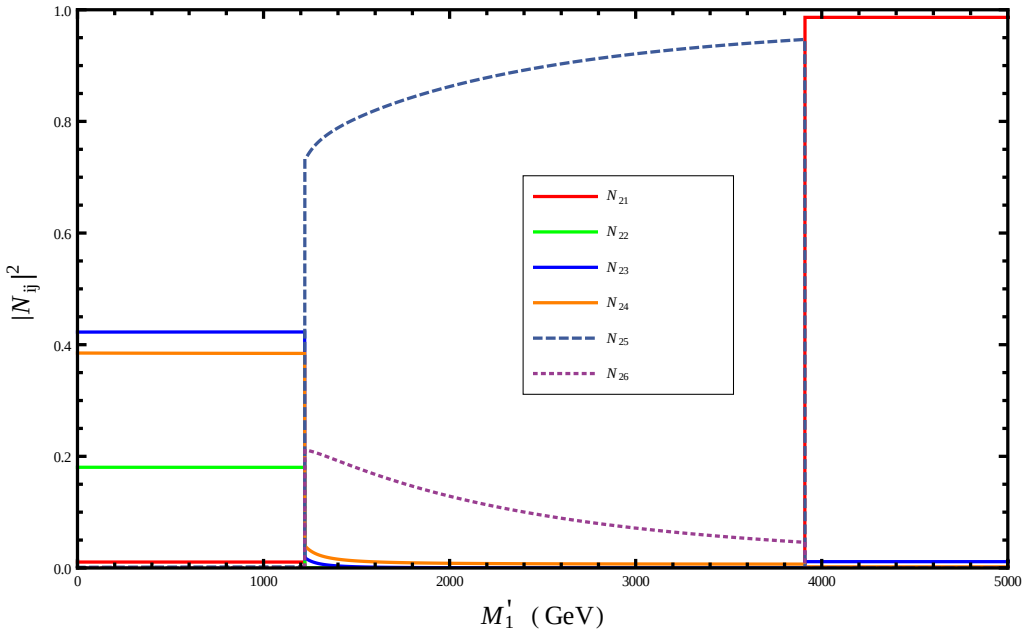

(a) Composition of $\tilde{\chi}_2^0$

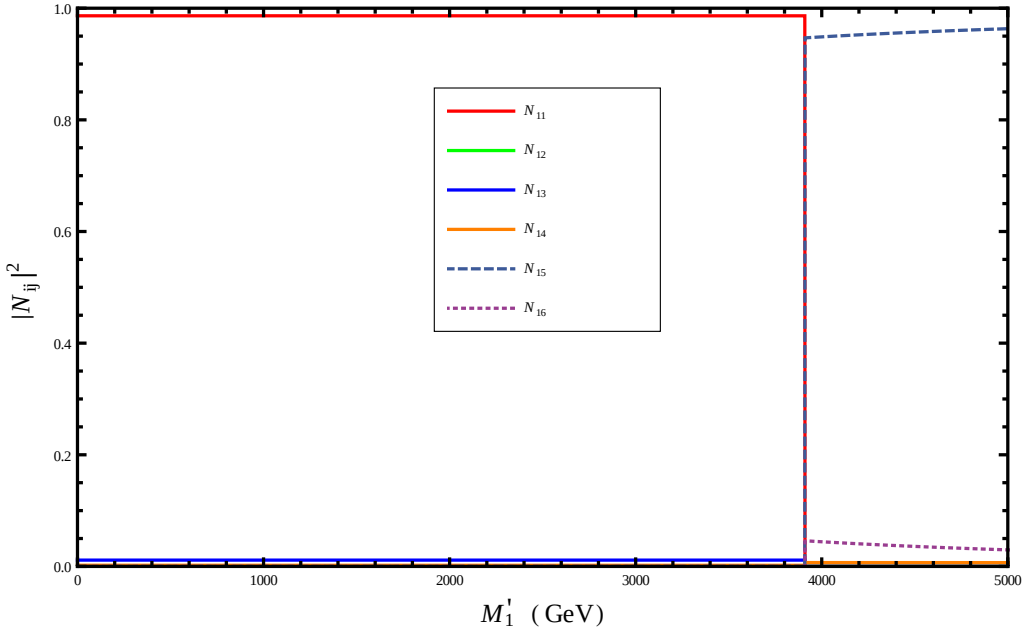

(b) Composition of $\tilde{\chi}_1^0$

Figure 2.5: Gauge eigenstate component $|N_{ij}|^2$ of the 2-nd lightest $\tilde{\chi}_2^0$ (Fig. 2.5a) and lightest neutralino $\tilde{\chi}_1^0$ (Fig. 2.5b). The lightest neutralino becomes mostly singlino for $M_1' > 4$ TeV with $|N_{15}|^2 > 90\%$. There is also a small mixing with the very heavy $\tilde{B}'$ gauge eigenstate. At this point the singlino has zero mixing with the MSSM-like states.

Increasing further the bino primed mass reduces further the singlino mass and the neutralino $\tilde{\chi}_4^0$ has an equal admixture of $\tilde{H}_u, \tilde{H}_d$ states. The 3-rd heaviest neutralino $\tilde{\chi}_3^0$ (Fig. 2.4b) starts off as a mixture of the two $\tilde{H}_u, \tilde{H}_d$ states with $|N_{33}|^2 = |N_{34}|^2 \approx 50\%$. For heavy bino primed mass M_1' the total Higgsino component of $\tilde{\chi}_3^0$ reduces to $|N_{33}|^2 + |N_{34}| \approx 80\%$ and obtains a mixing of the order of $|N_{32}|^2 \approx 20\%$ with the wino $\tilde{W}^0$ gauge eigenstate. The second lightest neutralino $\tilde{\chi}_2^0$ (Fig. 2.5a) for small M_1' is composed of Higgsino and Wino gauge eigenstates $\tilde{H}, \tilde{W}^0$. For $M_1' > 1.2$ TeV the singlino $\tilde{S}$ component increases gradually until $M_1' \approx 4$ TeV where it becomes purely bino-like state $|N_{21}|^2 = 100\%$. In the last Fig. 2.5b we plot the various transitions of the lightest neutralino $\tilde{\chi}_1^0$ from being a purely bino-like state to becoming a singlino mixture $|N_{15}|^2 \approx 95\%$ (for $M_1' = 5$ TeV) with a small bino primed component $|N_{16}|^2 \approx 5\%$. In Fig. 2.6 we plot the masses of the

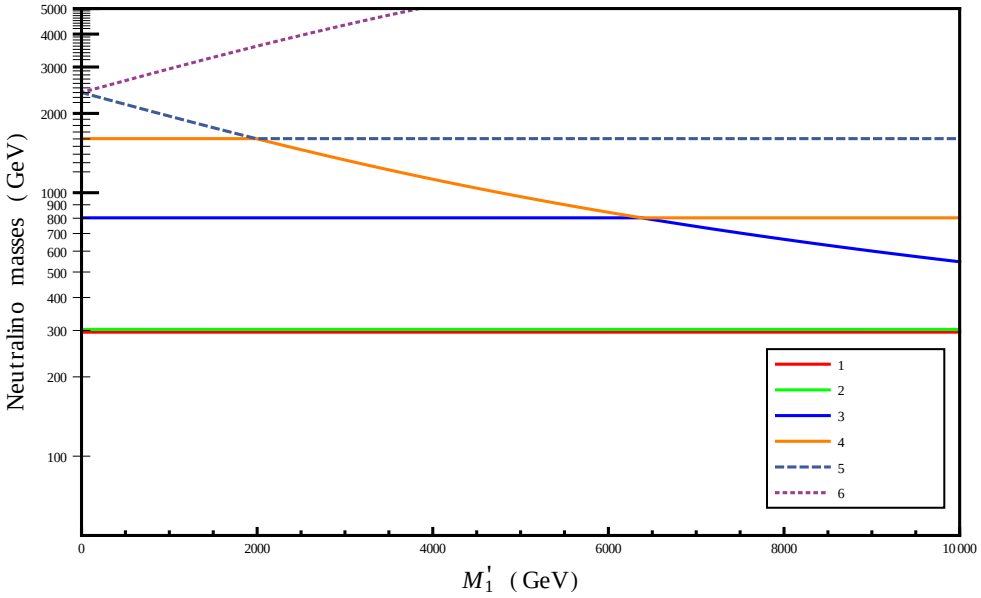

Figure 2.6: Logarithmic plot of the six neutralino masses as a function of M_1' for heavier Z' boson $M_{Z'} \simeq 2.4$ TeV and larger values of the $U(1)'$ charges $\tilde{Q}_s = -0.6$, $\tilde{Q}_{H_u} = 0.3$, $\tilde{Q}_{H_d} = 0.3$. The Bino and Wino mass are taken to be $M_1 = 0.8$ TeV and $M_2 = 1.6$ TeV respectively. The singlino $\tilde{S}$ and the $\tilde{B}'$ states at $M_1' = 0$ have the same mass with the heavy Z'. The singlino becomes the third lightest mass eigenstate for $M_1' > 6.5$ TeV. For $M_1' \simeq 10$ TeV the singlino mass is around $m_{\tilde{S}} \equiv m_3 \approx 500$ GeV. The lightest states are the two almost degenerate Higgsino like states with masses $m_{\tilde{H}} = m_{1,2} \approx \mu_{eff} = 300$ GeV. The heavy $\tilde{B}'$ state becomes rapidly heavy, for $M_1' \sim 4$ TeV we have $m_{\tilde{\chi}_6^0} \sim 5$ TeV.

six physical neutralino states $m_{\tilde{\chi}_i^0}$ while varying the bino primed mass and using different parameter values from Fig. 2.1 (see figure for details).

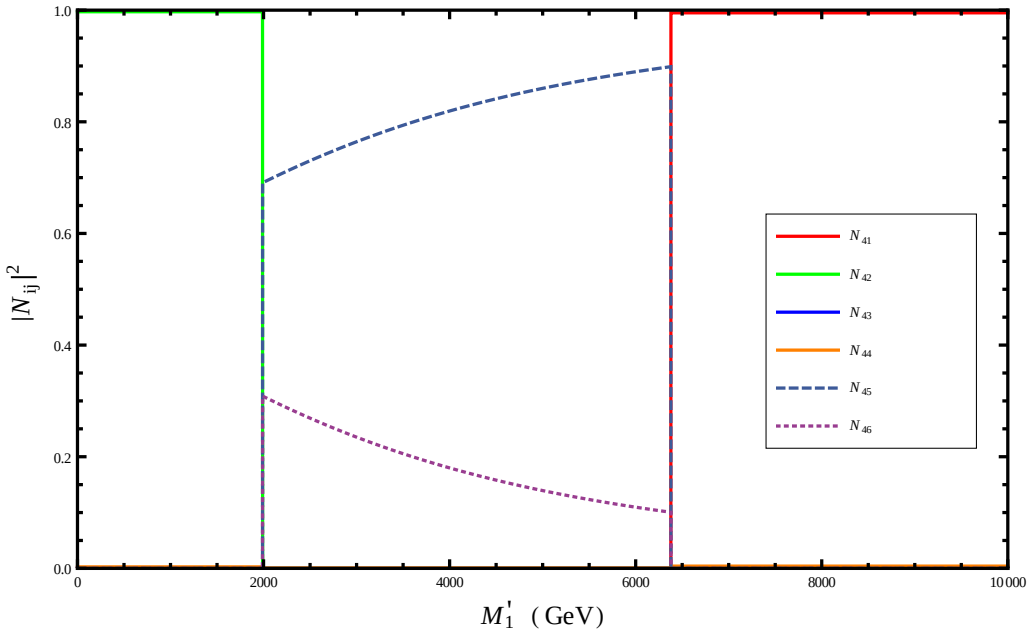

(a) Composition of $\tilde{\chi}_4^0$

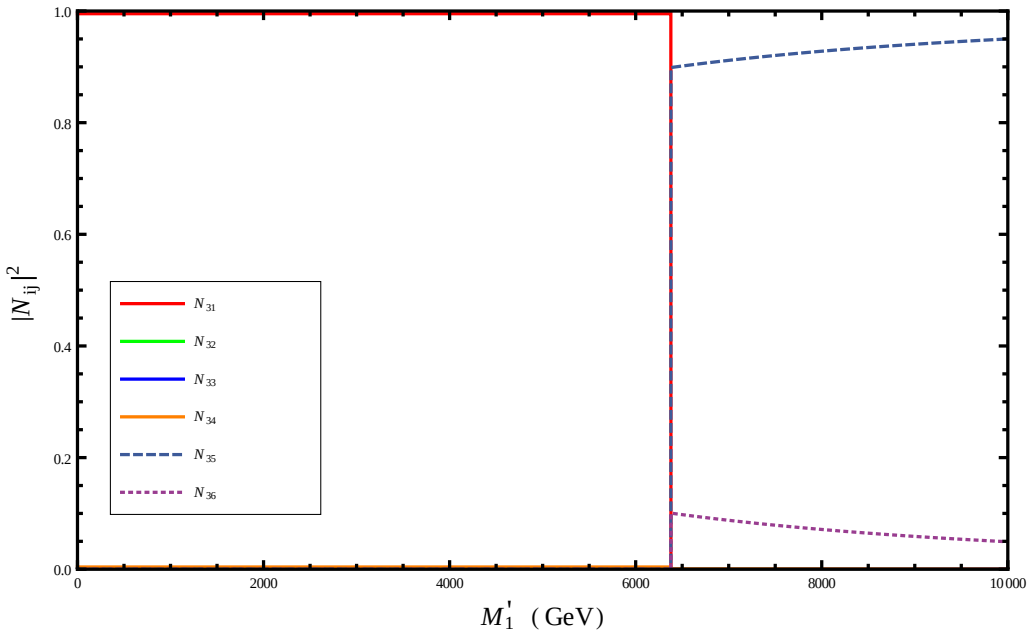

(b) Composition of $\tilde{\chi}_3^0$

Figure 2.7: Gauge eigenstate components $|N_{ij}|^2$ of the 4-th (Fig. 2.7a) and 3rd (Fig. 2.7b) lightest neutralino as a function of M_1'. The mass eigenstates correspond to those of the plot in Fig. 2.6.

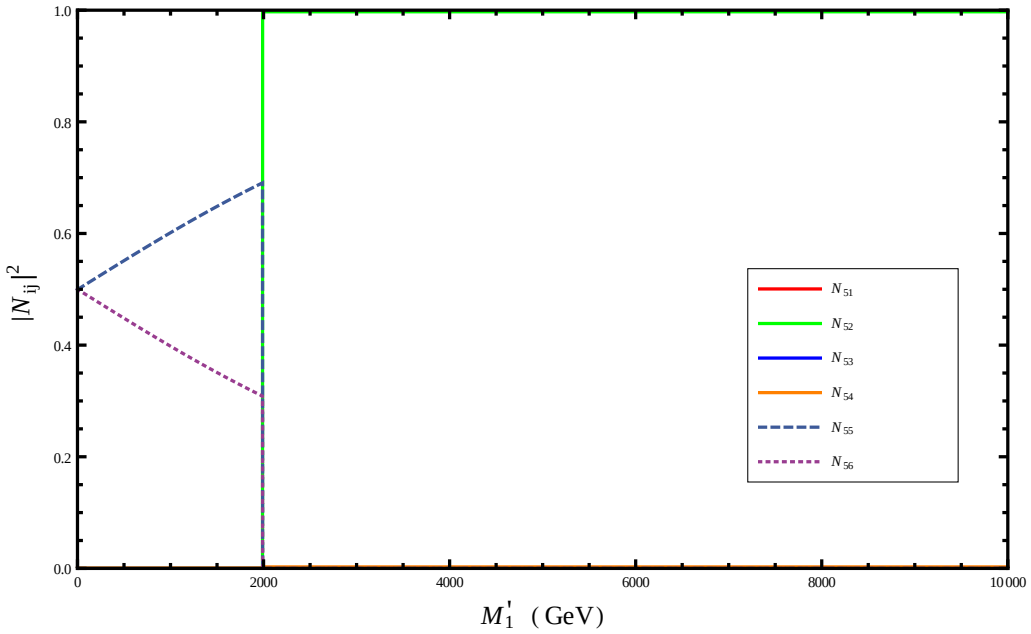

(a) Composition of $\tilde{\chi}_5^0$

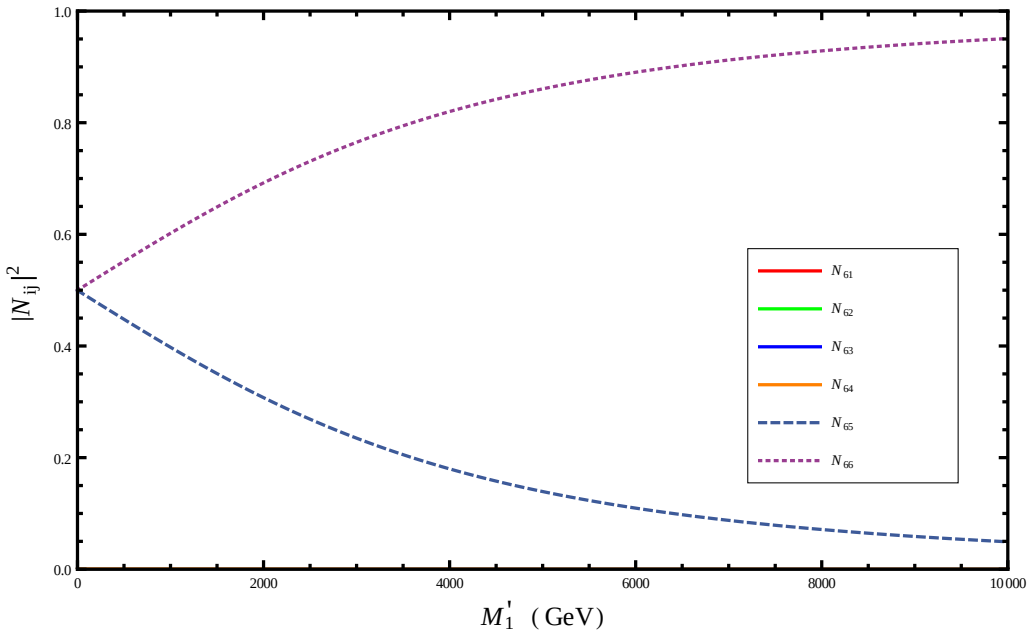

(b) Composition of $\tilde{\chi}_6^0$

Figure 2.8: Gauge eigenstate components $|N_{ij}|^2$ of the 5-th (Fig. 2.8a) and 6-th (Fig. 2.8b) lightest neutralino as a function of M_1'. The mass eigenstates correspond to those of the plot in Fig. 2.6.

For zero Bino primed mass the off-diagonal element of the two dimensional matrix of the extra gaugino sector in eq.(2.155), creates maximal mixing and the two degenerate mass eigenstates which have 50% singlino and 50% Bino primed admixture are quite heavy since the Z' mass is taken to be $M_{Z'} \approx |\tilde{Q}_s| v_s \simeq 2.4$ TeV. Even for very large $M_1' \sim 10$ TeV the singlino gauge eigenstate remains very heavy $m_3 \equiv m_{\tilde{S}} \sim 500$ GeV and becomes the third lightest neutralino with a singlino component $|N_{35}|^2 \sim 95\%$. The remaining component is bino primed $|N_{36}|^2 \sim 5\%$ (see Fig. 2.7b). For a large part of the M_1' range the mostly singlino state with $70\% < |N_{45}|^2 < 90\%$ corresponds to the 4-th lightest neutralino state $\tilde{\chi}_4^0$. For $M_1' < 2$ TeV the $\tilde{\chi}_4^0$ is in a purely Wino state.

2.7 The Chargino Sector

The chargino sector remains unaffected in the UMSSM since the additional gauge singlet S has no charge and does not couple to the either charged gauge eigenstates ($\tilde{W}^+$, $\tilde{H}_u^+$, $\tilde{W}^-$, $\tilde{H}_d^-$). Therefore the current discussion holds for the MSSM as well. The chargino mass terms have three sources, the gaugino-fermion-scalar interaction Lagrangian term eq.(2.19), the explicit soft supersymmetry breaking mass term for the gauginos $M_2 \tilde{W}^+ \tilde{W}^-$ and the F-term contribution to the fermion-fermion-scalar interaction Lagrangian $\lambda S \tilde{H}_u^+ \tilde{H}_d^-$. From the three sources only the first one is the least straightforward. So let us isolate this term in order to obtain the Lagrangian density containing the mass terms for the gauge eigenstates of the charged gauginos and finally construct the mass matrix. From eq.(2.19) for the interactions of the gauginos $\tilde{W}^a$ with the charged and neutral Higgsinos we have

$$\mathcal{L}_{H\tilde{H}\tilde{W}} = -\sum_{a,i} \sqrt{2} g_2 \left(\phi_i^* \ \frac{1}{2}\sigma^a \ \psi_i \right) \ , \tag{2.161}$$

where $a = 1, 2, 3$ and σ^a are the three Pauli matrices and $i = 1, 2$ for the two Higgs doublets $\phi_2 = H_u = (H_u^+ \quad H_u^0)$ and $\phi_1 = H_d = (H_d^0 \quad H_d^-)$ with ψ_1, ψ_2 being the corresponding fermionic superpartners. So the above equation reads in more detail

$$\mathcal{L}_{H\tilde{H}\tilde{W}} = -\sum_{a}^{3} \sqrt{2} g_2 \left(H_u^\dagger \ \frac{1}{2}\sigma^a \ \tilde{H}_u \right) - \sum_{a}^{3} \sqrt{2} g_2 \left(H_d^\dagger \ \frac{1}{2}\sigma^a \ \tilde{H}_d \right) \ , \tag{2.162}$$

now expanding and keeping only terms involving the gauginos $\tilde{W}^{1,2}$ which form the real and imaginary components of the charges gaugino eigenstates $\tilde{W}^\pm = (\tilde{W}^1 \mp i\tilde{W}^2)$ we have

$$\begin{aligned} \mathcal{L}_{H\tilde{H}\tilde{W}^\pm} &= -\sqrt{2}\Big[\Big(\tilde{W}^1 - i\tilde{W}^2 \Big) \tilde{H_d^-} (H_d^0)^* + \Big(\tilde{W}^1 + i\tilde{W}^2 \Big) \tilde{H_u^+} (H_u^0)^* + c.c. \Big] \\ &= -g_2 (H_d^0)^* \tilde{W}^+ \tilde{H}_d^- - g_2 (H_u^0)^* \tilde{W}^- \tilde{H}_u^+ + c.c. \end{aligned} \tag{2.163}$$

after breaking the electroweak symmetry and giving vev's to the Higgs and singlet fields the Lagrangian density containing the mass terms for the charged gaugino and Higgsino eigenstates will be

$$\mathcal{L}_{\psi^\pm\psi^\pm} = \Big(- g_2\frac{v_d}{\sqrt{2}}\tilde{W}^+\tilde{H}_d^- - g_2\frac{v_u}{\sqrt{2}}\tilde{W}^-\tilde{H}_u^+ + h.c.\Big) - \Big(M_2\tilde{W}^+\tilde{W}^- + \frac{\lambda v_s}{\sqrt{2}}\tilde{H}_u^+\tilde{H}_d^- + h.c\Big) \ . \tag{2.164}$$

We can write this in a matrix for as follows

$$\begin{aligned}\mathcal{L}_{mass}^{\psi^\pm} &= -\begin{pmatrix}\tilde{W}^- & \tilde{H}_d^-\end{pmatrix}\begin{pmatrix} M_2 & g_2\frac{v_u}{\sqrt{2}} \\ g_2\frac{v_d}{\sqrt{2}} & \mu_{eff}\end{pmatrix}\begin{pmatrix}\tilde{W}^+ \\ \tilde{H}_u^+\end{pmatrix} + h.c. \\ &= -(\psi^-)^T\mathbf{M_c}\psi^+ + h.c. \ , \end{aligned} \tag{2.165}$$

where we have defined the two column vectors ψ^- (ψ^+) consisting of the negative (positive) charged Higgsino and Wino unphysical eigenstates

$$\psi^- = \begin{pmatrix}\tilde{W}^- \\ \tilde{H}_d^-\end{pmatrix} \ , \qquad \psi^+ = \begin{pmatrix}\tilde{W}^+ \\ \tilde{H}_u^+\end{pmatrix} \ . \tag{2.166}$$

Note that the chargino mass matrix is not symmetric. In order to diagonalize the complex asymmetric matrix and obtain the physical states for the chargino particles we need to find two unitary matrices $\mathbf{V}^+, \mathbf{U}^-$ which diagonalize the hermitian matrices $\mathbf{M_c}^\dagger\mathbf{M_c}$ and $\mathbf{M_c}\mathbf{M_c}^\dagger$, respectively :

$$\mathbf{V}^+\mathbf{M_c}^\dagger\mathbf{M_c}(\mathbf{V}^+)^{-1} = \mathbf{diag}(m^2_{\tilde{\chi}_1^\pm}, m^2_{\tilde{\chi}_2^\pm}) = (\mathbf{U}^{-*})\mathbf{M_c}\mathbf{M_c}^\dagger(\mathbf{U}^{-*})^{-1} \ , \tag{2.167}$$

and $m^2_{\tilde{\chi}_1^\pm}, m^2_{\tilde{\chi}_2^\pm}$ are the positive square roots of the eigenvalues of the hermitian matrix $\mathbf{M_c}^\dagger\mathbf{M_c}$. Then the chargino matrix is diagonalized by the transformation

$$U^{-*}\mathbf{M_c}(V^+)^{-1} = \mathbf{diag}(m^2_{\tilde{\chi}_1^\pm}, m^2_{\tilde{\chi}_2^\pm}) = \mathbf{M_c^{diag}} \ , \tag{2.168}$$

so that

$$\mathcal{L}_{mass}^{\psi^\pm} = -(\chi^-)^T\mathbf{M_c^{diag}}\chi^+ + h.c. \ , \tag{2.169}$$

where the mass eigenstates $\chi_i^\pm$ with $i = 1, 2$ are taken by rotating the unphysical fields

$$\chi^+ \equiv \begin{pmatrix}\chi_1^+ \\ \chi_2^+\end{pmatrix} = V^+\begin{pmatrix}\tilde{W}^+ \\ \tilde{H}_u^+\end{pmatrix} \ , \qquad \chi^- \equiv \begin{pmatrix}\chi_1^- \\ \chi_2^-\end{pmatrix} = U^-\begin{pmatrix}\tilde{W}^- \\ \tilde{H}_d^-\end{pmatrix} \ , \tag{2.170}$$

the singular values of the mass matrix are given by

$$m^2_{\chi^\pm_{1,2}} = \frac{1}{2}\Big(|M_2|^2 + |\mu_{eff}|^2 + 2m_W^2 \pm \sqrt{(|M_2|^2 + |\mu_{eff}|^2 + 2m_W^2)^2 - 4\Big|\mu_{eff}M_2 - m_W^2 \sin(2\beta)\Big|^2}\Big) \ . \quad (2.171)$$

The exclusion limits on the mass of the lightest chargino from LEP searches Ref.[76] at 95%CL $m_{\chi_1^\pm} > 94$ GeV poses a lower bound to the absolute value of the gaugino mass and the effective Higgsino mass $|M_2|, |\mu_{eff}| \gtrsim 100$ GeV. In Fig. 2.9 we show the contours for the lightest chargino mass when we vary both the wino mass and the Higgsino mass. Both parameters are considered to be real. One can see that when the input parameters are approximately less than 100 GeV the chargino mass goes below the lower limit set by LEP.

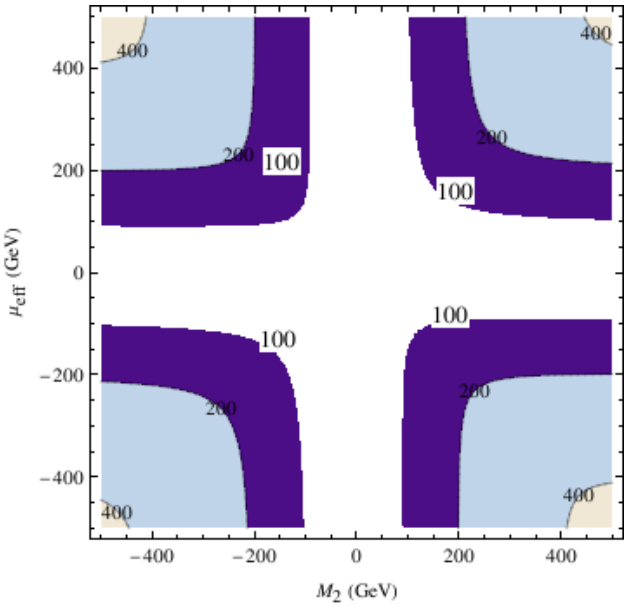

Figure 2.9: Contour plot of the chargino mass $m_{\chi_1^\pm}$ in the plane of the parameter μ_{eff} and the gaugino mass M_2. Both values can be negative as well. In order to pin down the lower limit on these two parameters we focus our scan on relatively small values for both parameters. For $|M_2|, \mu_{eff} < 100$ GeV the chargino mass is lighter than $m_{\chi_1^\pm} \lesssim 100$ GeV and this region is excluded.

Chapter 3

pUMSSM: a gauge extension of MSSM with generic charges

3.1 Introduction and Prior Work

There is an extensive literature on $U(1)'$ extensions of the MSSM with one or more gauge singlets necessary to break the extra gauge symmetry. Usually these models stem from grand unified constructions or string motivated theories in which the extra $U(1)'$ gauge group is the result of the breaking of a larger group such as the $SO(10)$ or E_6. Other constructions are based on the requirement of having an anomaly free theory and assuming family universal $U(1)'$ charges in order to diminish the possibility of having FCNCs. A minimal extension of the MSSM is considering one extra $U(1)'$ gauge symmetry with only one SM gauge singlet S and with no additional exotic matter, usually referred as UMSSM [26, 28]. In principle in these studies [26, 27, 28, 86, 34] the $U(1)'$ charges are taken to have specific values depending on the assumption of the underlying larger group from which the $U(1)'$ broken symmetry comes from. The exotic sector which is present in the complete high-scale theory, it is assumed to decouple and there are no terms entering the superpotential of the low-scale effective theory. Therefore although in this framework one is inclined to restrict the charges relying on a GUT or string motivated theory, once the high-scale degrees of freedom have been integrated out the charges of the extra gauge symmetry can in general be treated as free parameters. For this reason we introduce an effective bottom-up approach in which we parametrise the model by those couplings that are most pertinent to the indirect constraints such as the charges of the Higgs and the stop sector. The remaining charges with a few exceptions, play a minor role in the phenomenology studied here and our work applies both to situations where the charges are

assumed as family universal or non-universal. The experimental discovery of a new Z' boson would have great implications in the phenomenology of collider physics. In principle it is difficult to construct UV complete models which take care of gauge unification, anomaly cancellation, suppression of FCNCs and various other theoretical and phenomenological requirements. The rapidly increasing LHC data suggests the use of "effective" low-energy models which can probe different areas of the parameter space and motivate or reject new discovery modes which can be different than well established ones that are based on sound theoretical models. This basic idea provides the main motivation behind this work presented here and focuses on exploring the effect of different charge assignments on the the phenomenology and naturalness of Z' models. We hope that this work will shed light in the advantages and disadvantages of the gauge extensions of the MSSM and explore different scenarios in a generic framework. This concept of a $U(1)'$ extension of the MSSM with generic parametrization of the charges was first introduced by Cvetic et al [48]. In this paper the authors are considering different supersymmetry breaking scenarios, one which is driven by large trilinear soft supersymmetry breaking terms and a second one where the breaking is due to the running of the singlet soft mass parameter m_s^2 to negative values at low energies. The Higgs, chargino and neutralino sector are presented and several conclusions are made for the charges in order to construct a phenomenological viable scenario with small $Z - Z'$ mixing and avoid tachyonic squared mass parameters for the squarks $m_{\tilde{q}}^2$. The study focuses on Z' bosons of the order of 1 TeV and touches on the fine tuning needed for heavier Z' bosons. A renormalization group analysis is performed relating the weak scale dynamics to the boundary conditions at the string scale. It is concluded that in order to have the desired low energy parameter space which leads to weak scale symmetry breaking according to the proposed scenarios, non universal boundary conditions are preferable. Furthermore the gaugino masses have to be relatively lighter than the rest of the soft SUSY breaking mass parameters at the string scale. At the end the authors present solutions to the anomaly constraint equations in the case of this minimal scenario (UMSSM) with only one gauge singlet and no additional exotics, in order to preserve the approximate gauge unification which is achieved in the MSSM. It is worth mentioning here in more detail that in this non-anomalous $U(1)'$ construction the charges of the two Higgs doublets Q_{H_u}, Q_{H_d} are arbitrary and the first and second families of squarks and sleptons have zero $U(1)'$ charges. They argue that solutions with non-zero charges for all three families can also be attained. Moreover string derived models allow for different values of the $U(1)'$ charges between quarks and leptons making these examples viable. This study was the successor

of a previously published work by Cvetic et al. [49] in which only one Higgs doublet and an additional SM singlet is assumed. In another study conducted by E. Keith and E. Ma in the late 90's [101] an arbitrary $U(1)'$ extension of the MSSM with generic charges which are constrained by the gauge invariance of the superpotential term $\lambda S H_u H_d$ is also considered. The authors construct an effective two Higgs doublet scalar potential with coefficients that depend on the Yukawa coupling λ, the gauge coupling g_1' and the $U(1)'$ charges of the Higgs doublets and singlet field. By including also corrections at 1-loop from the top quark and its scalar superpartner they derive an upper bound for the lightest CP-even Higgs boson of the theory. In the rest of the paper they specialize their study in the case where the extra gauge symmetry is the result of the breakdown of E_6

$$\begin{aligned} E_6 &\rightarrow SO(10) \times U(1)_\psi \rightarrow (SU(5) \times U(1)_\chi) \times U(1)_\psi \\ &\rightarrow SU(3)_c \times SU(2)_L \times U(1)_Y \times U(1)' \ . \end{aligned}$$

Here the extra $U(1)'$ gauge symmetry is a linear combination of the anomaly free subgroups $U(1)_\chi, U(1)_\psi$ parametrized by the mixing angle θ_{E_6}:

$$U(1)' = U(1)_\chi \cos\theta_{E_6} + U(1)_\psi \cos\theta_{E_6} \ , \tag{3.1}$$

where $0 \leq \theta_{E_6} < \pi$ is the only model-dependent parameter. The choice of the mixing angle defines the specific E_6 model. A detailed review can be found in Ref.[112]. In their paper Keith & Ma present their results for this class of models originating from E_6 in a general way by parametrizing for arbitrary values of the angle θ_{E_6}. They go on to discuss the effect of $Z - Z'$ mixing on the electroweak oblique parameters S, T, U and stress the importance of the $U(1)'$ D-terms contributions to the soft supersymmetry breaking masses of the squarks and sleptons by doing an renormalization group analysis assuming universal soft mass parameters at the GUT scale. Other early studies [58, 115, 145, 146] have also been focused on E_6 motivated extra $U(1)$ symmetries. In a more phenomenological study the authors London et al. [120] are exploring implications of Z' bosons on the branching ratios of Z' for various channels, the forward-backward asymmetries and the Drell-Yan production mechanism. They also consider effects on neutral currents and impose constraints on its mass. A very thorough review article on the low-energy phenomenology of E_6 motivated models is given Hewett and Rizzo [94]. The list is by no means exhaustive but it serves as a good reference for this class of models. More recent papers which specialize on a particular E_6 based framework usually referred to as E$_6$SSM can be found here [6, 7, 8, 103, 131]. In these last two papers the focus is on the calculation of the fine tuning in E$_6$SSM. Other interesting studies where the authors examine the possible production modes of exotic

particles which emerge in E_6 constructions is Ref. [21, 22]. In another paper Gherghetta et al. [77] investigate the decay modes of an extra Z' in this type of models parametrizing the charges by the mixing angle θ_{E_6}.

3.2 The Phenomenological UMSSM

We consider a supersymmetric SM extension with gauge group $G = G_{\rm SM} \times U(1)'$. This means assigning $U(1)'$ charges Q_f to the 15 SM matter and the two Higgs supermultiplets. Moreover, we also require a $G_{\rm SM}$ singlet S entering a superpotential term $\lambda S H_u \cdot H_d$ in order to dynamically generate a μ-term, $\mu = \lambda \langle S \rangle$. This gives one constraint $Q_{H_u} + Q_{H_d} + Q_s = 0$ fixing Q_s in terms of the other charges. The singlet vev $v_s = \langle S \rangle \sqrt{2}$ will at the same time break the $U(1)'$ and give mass to the $U(1)'$ gauge boson Z'.

Note here that one could have more than one singlets S_i which would receive vevs of the order of the electroweak scale avoiding to have large supersymmetry breaking scale as in the case of only one gauge singlet [64]. The choice of basis can always be made in such a way so that only one singlet generates the effective μ-term and the others couple only weakly to the SM particles through their $U(1)'$ charges forming a "dark sector". In this scenario the S supermultiplet and the Z' supermultiplet constitute the "portal" to the dark sector. In this way the lower bound on Z' bosons, from exotic searches, is relaxed. In this project we will not consider this option but we keep an open mind for future projects.

In a general $U(1)'$ model, there may also be SM nonsinglet "exotic" matter; to be consistent with SM gauge coupling unification such states should come in complete multiplets of $SU(5)$. Such exotic matter multiplets may have superpotential couplings to the SM fields depending on their $U(1)'$ charges (such as in the case of the several Higgs doublets in E_6-inspired scenarios); unless stated otherwise we will assume that these couplings are either forbidden or negligible in formulating the constraints below.

Since the $U(1)'$ charges appear always in combination with the gauge coupling g_1' we may rescale all charges by setting $g_1 \to 1$ or equivalently $\tilde{Q}_i = g_1' Q_i$ as stated in previous chapters. For simplicity we drop the tilde on top of the charges. In a unified model one would normally require the correctly normalized running g_1' to unify with the SM gauge couplings at the GUT scale. However, the running of the extra gauge coupling present in extended scenarios is sensitive to the exotic/hidden sector field content and thus highly model dependent. Lastly we would like to comment on two complementary papers Ref. [64], [86] which promote a bottom-up approach for gauge extensions with more than one singlets which contribute to the Z' mass. The first one [64] provides the theoretical construction of

the model and a detailed study for unwanted global minima and global symmetries which can lead to two unobserved massless Goldstone bosons. The $U(1)'$ charges are chosen so that this issues are being resolved. Anomaly cancellation and the possibility of having FCNCs are not discussed and the model is not embedded into any larger GUT or string inspired group. This is outside the scope of this study. The second paper [86] studies the phenomenological implications of the models presented in the first paper. By imposing a general constraint on $Z - Z'$ mixing of the order $\mathcal{O}(10^{-3})$ from electroweak precision data and early LEP2 bounds on the Higgs masses the authors study production cross sections for the lightest CP-even Higgs boson as well as the spectrum of the Higgs sector and their couplings with respect to the MSSM. Scans calculating the branching ratios of the lightest Higgs to invisible modes and other SM decay channels are also performed. They conclude that a scenario with small $\tan\beta \sim 1$ is favoured and find Higgs masses up to 170 GeV. They also find that the Higgs boson decays hadronically or invisible for a large region of the parameter space.

This bottom-up approach encourages further studies in that direction and gives insight to different viewpoints of a complex problem such as the construction of a UV-complete extension of the MSSM.

3.3 Constraints on the charges

Restrictions on the visible-sector $U(1)'$ charges follow from requiring the Yukawa terms to be gauge invariant and from anomaly cancellation.

Yukawa constraints. Neglecting flavour mixing, we have one constraint for each non-zero Yukawa coupling. However, due to flavour mixing extra constraints occur. Consider the (or, a) gauge basis, i.e. a basis where each SM gauge multiplet also has a well-defined $U(1)'$ charge. Note that a priori this does not need to coincide with a flavour basis. For instance the right-handed top quark does not have to have a definite $U(1)'$ charge–it could be a superposition. In this basis, for any element $y_{u_{ij}}$ that is nonzero we have a constraint

$$Q_{Q_j} + Q_{\bar{u}_i} + Q_{H_u} = 0 \ , \tag{3.2}$$

and similarly for $y_{d_{ij}}$ and $y_{e_{ij}}$. As a consequence, if a row or a column of a Yukawa matrix contains two nonzero elements, then the left-handed (right-handed) charges of two different multiplets agree. If we require the full Yukawa terms to be $U(1)'$ invariant, then the 3 generations of quark doublets must all have the same charge, $Q_{Q_i} = Q_Q$, for $i = 1, 2, 3$ which implies family universal charges.

One way to evade the conclusion might be that some quark masses are radiatively generated, involving SUSY-breaking terms (thus escaping the SUSY nonrenormalisation theorems). It may be possible to generate the smaller fermion masses at one-loop if non-holomorphic soft terms are present [52]. Perhaps this is also possible for some of the smaller off-diagonal elements. Another possibility are higher-dimensional operators involving singlet fields with a low suppression scale Λ. Such operators would be subject to different charge constraints. This scenario requires new matter at a scale Λ with superpotential couplings to the MSSM fields, possibly also involving exotics. Neither mechanism can generate the large top Yukawa coupling, giving us one constraint

$$Q_{Q_3} + Q_{T^c} + Q_{H_u} = 0 \ . \tag{3.3}$$

If $\tan\beta$ is large, we have two further constraints

$$Q_{Q_3} + Q_{B^c} + Q_{H_d} = 0 \ , \tag{3.4}$$

$$Q_{L_3} + Q_{\tau^c} + Q_{H_d} = 0 \ . \tag{3.5}$$

In fact, (3.5) applies to the non-holomorphic mechanism even at small $\tan\beta$ [52]. However, although we are bound to make assumptions for the charges of the third generation leptons in order to calculate the spectrum with `SPheno`, this assumptions will not affect the purposes of the current analysis. Our results do not depend on these assumptions. Note that the left- and right-handed fermion charges are related via the Higgs charges. In terms of vector and axial-vector Z' couplings, the vectorial couplings are free while the axial-vector couplings are fixed once the Higgs charges are given. Notice that for the third generation of squarks and sleptons we use different notation than the one introduced in Table 2.1, aiming to stress the importance of these parameters in our study and distinguish them from all other charges which are not the focus of the analysis and for that reason are set to fixed values. The above constraints from the gauge invariance of the Yukawa couplings eq.(3.3),(3.4),(3.5) reduce the number of dofs for the $U(1)'$ charges from 9 to 6. The other free parameters in our analysis are: the effective the Higgsino mass parameter μ_{eff} (or λ), the vev of the singlet v_s, the stop trilinear soft supersymmetry breaking parameter A_t, the soft supersymmetry breaking masses of the third generation squarks $m^2_{Q^3}, m^2_{T^c}, m^2_{B^c}$ and the gaugino mass of the additional $\tilde{B}'$. All other parameters will be fixed and their values will be given in the plots or in the text. In the subsequent paragraphs we comment on the perturbativity of the redefined charges[1] and on anomaly cancellation.

[1] Remember the charges depend now on the extra gauge coupling g'_1.

Perturbativity. The $U(1)'$ coupling runs according to (see also eq.(5.18))

$$\mu \frac{\mathrm{d}}{\mathrm{d}\mu} g_1' = \frac{1}{16\pi^2} g_1'^3 \sum_i n_i \tilde{Q}_i^2 \ , \tag{3.6}$$

where n_i is the SM gauge multiplicity of the multiple ϕ_i, e.g. 3 for B^c, 6 for Q_3, and 2 for H_u. Defining $a' = g_1'^2/(16\pi^2)$, the solution is

$$\frac{1}{a'(\mu)} = \frac{1}{a'(\mu_0)} - 2 \ln \frac{\mu}{\mu_0} \sum_i n_i \tilde{Q}_i^2 \ . \tag{3.7}$$

Avoiding a Landau pole below a scale Λ implies the constraint

$$\sum_i n_i Q_i(\mu_0)^2 < \frac{16\pi^2}{2 \ln(\Lambda/\mu_0)} \ , \tag{3.8}$$

where $Q_i(\mu) = g_1' \tilde{Q}_i$. For $\Lambda = 2 \times 10^{16}$ GeV and $\mu_0 = 1$ TeV the bound (right-hand side) is about 2.58.

We can also obtain stricter bounds by requiring "perturbativity" of some couplings below the scale Λ. This is a bit arbitrary in what combination of couplings one chooses to constrain. Perhaps the most obvious object to look at is the β-function itself. Requiring $1/g_1' dg_1'/dt < \epsilon$ implies

$$\sum n_i Q_i(\mu_0)^2 < \frac{16\pi^2 \epsilon}{1 + \Delta 16\pi^2 \epsilon} \ , \tag{3.9}$$

where $\Delta = \frac{1}{8\pi^2} \ln \frac{\mu}{\mu_0} = 0.39 = 1/2.58$ for $\Lambda = 2 \times 10^{16}$ GeV and $\mu_0 = 1$ TeV. For $\epsilon = 0.1$ (which, assuming generic sizes for all terms in the perturbation series, implies that the two-loop contribution is suppressed by one order of magnitude relative to the one-loop one, etc.) at the GUT scale, one has

$$\sum n_i Q_i(\mu_0)^2 < 2.22 \ . \tag{3.10}$$

This is very close already to the Landau pole bound (corresponding to $\epsilon \to \infty$) and contrasts with a bound of 0.72 if one requires $\epsilon = 1/(16\pi^2)$.

Anomaly cancellation. Anomaly cancellation constrains the $U(1)'$ charge assignments. These comprise triangle diagrams involving 3 gauge currents (generators); they must all vanish when summed over internal lines. From $U(1)$ $[Y]$, $U(1)'$ $[Q]$, and the graviton [energy-momentum tensor] one can form potentially anomalous correlators giving the fol-

lowing conditions [48, 52, 112]:

$$YYY \qquad \sum_i Y_i^3 = 0, \tag{3.11}$$

$$YGG \qquad \sum_i Y_i = 0, \tag{3.12}$$

$$QQQ \qquad \sum_i Q_i^3 = 0, \tag{3.13}$$

$$QGG \qquad \sum_i Q_i = 0, \tag{3.14}$$

$$\boldsymbol{YYQ} \qquad \boldsymbol{\sum_i Y_i^2 Q_i = 0,} \tag{3.15}$$

$$\boldsymbol{YQQ} \qquad \boldsymbol{\sum_i Y_i Q_i^2 = 0.} \tag{3.16}$$

If no exotics are present, the first two are automatically satisfied (as in the SM); otherwise they impose a constraint on the exotic sector. The next two equations depend on the full matter content in the dark sector, hence need not be satisfied by the portal singlet S alone. However, the dark fields participating in these equations must be included in the perturbativity constraint. They must also be chiral, hence must receive any of their mass from $U(1)'$ breaking (any pair of oppositely charged dark fields cancels out of all anomaly conditions, and could at the same time have a gauge-invariant mass term). Therefore only the last two equations are dark-sector-independent constraints on the $U(1)'$ charges. They involve only the SM fields including the two Higgs supermultiplets, and any hypercharged exotics, but not the portal singlet S. In the presence of exotics, the first two and last two equations hold only with the exotics included in the sum; so in such a scenario the mixed anomalies do not present us with model-independent constraints on the $U(1)'$ assignments at all. In addition, there are mixed nonabelian-abelian constraints:

$$SU(3)SU(3)Y \qquad \sum_{i\in 3,3^*} Y_i = 0, \tag{3.17}$$

$$SU(2)SU(2)Y \qquad \sum_{i\in 2} Y_i = 0, \tag{3.18}$$

$$\boldsymbol{SU(3)SU(3)Q} \qquad \boldsymbol{\sum_{i\in 3,3^*} Q_i = 0,} \tag{3.19}$$

$$\boldsymbol{SU(2)SU(2)Q} \qquad \boldsymbol{\sum_{i\in 2} Q_i = 0.} \tag{3.20}$$

Again, the first two automatically hold if no exotics are added. The other two constrain the charges of the colored and of the doublet fields, respectively.

Usually all gauge extensions of the MSSM involve the existence of exotic matter in order to cancel the anomalies. Even for a single $U(1)'$ it is difficult to solve the anomaly

conditions by assuming only SM fermions which also have family universal charges under the new gauge symmetry. In a minimal scenario which comprises only one additional $U(1)'$ symmetry [52] and one singlet field S which receives a vev, Demir et al. show that it is possible to solve the anomaly conditions without adding exotic matter fields if one assumes generation non-universal charges. Since the non-universality of the charges can pose problems by creating large FCNCs, all families of quarks are being assigned the same charges. This condition can be evaded in the leptonic sector by assigning charges in a way that the gauge eigenstates are identical to the mass eigenstates. However, this would result in some Yukawa terms to be forbidden from the superpotential and thus the down quarks, the electron and the muon are required to get their mass from non-holomorphic terms. It is worth highlighting that Cvetic et al. [49] also presented solutions for a non-anomalous $U(1)'$ construction without any additional exotics. They have also considered Yukawa terms only for the up-type quarks and assumed that the down-type quarks and leptons receive their masses via other mechanisms. In their solution they have not considered the anomaly conditions coming from graviton-graviton-U(1)$'$.

Another possibility, if one wants to include exotics, would be to add fermions which are non-chiral with respect to the SM group and thus their contributions to the purely SM anomaly conditions cancel out. The charges of these particles would then have to cancel the contributions from the non-exotic matter in the mixed anomalies. However, the presence of extra matter fields would modify the RG equations through new contributions and this would potentially spoil the approximate unification of the gauge couplings at the GUT scale. Although this issue is not as important as gauge invariance and the suppression of FCNCs, it is considered one of the motivations of the MSSM. A way around this problem is to add exotics which transform under the representations of $SU(5)$ ($\mathbf{5}+\bar{\mathbf{5}}$ or $\mathbf{10}+\overline{\mathbf{10}}$). This options is also consistent with non-universality of the $U(1)'$ charges.[2]

In Ref. [62] the anomaly cancellation in the presence of one extra $U(1)'$ is discussed. By adding extra matter fields the author provides solutions which lead to a non-anomalous $U(1)'$ and at the same time preserve gauge couplings unification. One very important outcome of this study seems to be the fact that the solution requires the existence of two SM singlets which acquire a vev after symmetry breaking. Moreover, it is surprising that the solution which corresponds to the best fit of the data, favours $U(1)'$ charges for the SM fermions which are identical to the ones predicted by E_6 inspired models.

As mentioned previously a complete model has to be checked also with regards to the

[2] An underlying string theory allows for different couplings [112].

possibility of creating dangerous FCNCs. Non-universal $U(1)'$ couplings could contribute to rare B-decays at tree-level and explain excesses found in the $Z \to \bar{b}b$ forward backward asymmetry. According to Ref. [24] different couplings for the third families of quarks and leptons in a Z' model seem to be less constraint than the first two families. There is a large literature of Z' studies with non-standard couplings where the new gauge boson is assumed to be weakly coupled to the SM fermions or just the leptons. This idea provides an interesting way of hiding a relatively light Z' from collider searches.

In this study we do not attempt to embed our model into a larger GUT or string inspired group. We aim to motivate the construction of a UV-complete model in the event of interesting areas of the parameter space which would lead to interesting phenomenology without excessive fine tuning.

3.4 W mass constraint and mixing angle

***Z*-*Z′* mixing.** The mixing angles can be expressed in terms of the other parameters in various ways:

$$\tan\theta_W = \frac{g_1}{g_2}, \tag{3.21}$$

$$\cos^2\theta_W = \frac{M_W^2}{M_Z^2}, \tag{3.22}$$

$$\tan 2\theta_{ZZ'} = -2\,\Delta_Z^2/(M_{Z'}^2 - M_Z^2), \tag{3.23}$$

$$\tan^2\theta_{ZZ'} = \frac{M_Z^2 - M_{Z_1}^2}{M_{Z_2}^2 - M_Z^2}, \tag{3.24}$$

$$\sin^2\theta_{ZZ'} = \frac{M_Z^2 - M_{Z_1}^2}{M_{Z_2}^2 - M_{Z_1}^2}, \tag{3.25}$$

$$\cos^2\theta_{ZZ'} = \frac{M_{Z_2}^2 - M_Z^2}{M_{Z_2}^2 - M_{Z_1}^2}. \tag{3.26}$$

***Z* couplings to fermions** The Z_1 couplings in the pUMSSM are determined by rewriting the neutral current Lagrangian in terms of the mass eigenstates according to (2.57),

$$\begin{aligned} -\mathcal{L}_{NC} &= eJ_{\rm em}^\mu A_\mu + g_Z J_1^\mu Z_{1\mu}^0 + J_2^\mu Z_{2\mu}^0 \\ &= eJ_{\rm em}^\mu A_\mu + g_Z J_Z^\mu Z_\mu + J_{Z'}^\mu Z_\mu'. \end{aligned} \tag{3.27}$$

Here the two neutral currents are given by

$$J_Z^\mu = \sum_f \bar{f}\gamma^\mu[(T_{3L}^f - \sin^2\theta_W q_f)P_L - \sin^2\theta_W q_f)]f, \tag{3.28}$$

$$J_{Z'}^\mu = \sum_f \bar{f}\gamma^\mu[Q_f P_L - Q_{f^c} P_R]f. \tag{3.29}$$

Writing the Z current as [140]

$$J_1^\mu = \sum_f \bar{f}\gamma^\mu [g_{Lf} P_L + g_{Rf} P_R] f, \tag{3.30}$$

the left and right-handed couplings of the lighter massive boson Z_1 to fermions follow as

$$g_{Lf} = \cos\theta_{ZZ'}\, g_{Lf}^{\rm SM} + \frac{\sin\theta_{ZZ'}}{g_Z} Q_f \tag{3.31}$$

$$g_{Rf} = \cos\theta_{ZZ'}\, g_{Rf}^{\rm SM} - \frac{\sin\theta_{ZZ'}}{g_Z} Q_{f^c}, \tag{3.32}$$

where the SM couplings are

$$g_{fL}^{\rm SM} = T_{3f} - \sin^2\theta_W\, q_f \tag{3.33}$$

$$g_{fR}^{\rm SM} = -\sin^2\theta_W\, q_f. \tag{3.34}$$

One can in principle use the SM predictions from the determination of the quark and lepton effective coupling $\sin^2\theta_{eff}$ [140] to put constraints on the product of the charges and the mixing angle $\theta_{ZZ'}$. We find that this is not straightforward due to the fact that the two most precise measurements, the left-right asymmetry A_{LR} and the bottom forward-backward asymmetry A_{FB}^b [140] differ from each other more than 3σ. Therefore we construct an alternative way to constrain the mixing angle in a model-independent way in the following paragraph.

***W* mass constraint.** The W mass measurement has significantly improved over the years along with the improved measurement of the top quark mass [71], resulting in a reduction of the theoretical uncertainty in the prediction of the W mass. The W mass is very sensitive to the quantum effects from other particles predicted in a theory and can be used as a powerful tool to constrain possible BSM scenarios [92].

In a renormalisable theory, the number of independent parameters in the Lagrangian does not change. But the relations of the physical quantities to Lagrangian parameters, as well as those between different physical quantities, become modified relative to the tree-level. For instance, $M_W^2 = \frac{g^2}{2}v^2 + \delta M_W^2(\text{couplings, masses, }\dots)$. We can make use of renormalisation freedoms to remove some of the corrections (for example, we could use the physical W mass as a parameter), but we can only do this for as many quantities as there are independent parameters in the Lagrangian, and in a renormalisable theory there are only a finite number. Once this freedom has been exploited, any further observable is an unambigous function of the parameters. parameters as at tree-level, and we could define running M_Z, M_W,etc., in terms of them. The virtue of this is that one gains sensitivity to parameters that do not enter at tree-level, in particular masses and couplings of particles that exist but have not been discovered.

Consider first the SM case, where there are only three independent parameters at tree-level. Two possibilities of fixing them are to measure the set (G_F, M_Z, α) (with G_F measured according to a certain convention in μ decay, and often referred to as G_μ to emphasize this) or the set (M_W, M_Z, α). There are many other ways of choosing three input quantities. The first set has the advantage that it consists of the three most precisely measured quantities and this is why it is widely employed:

$$\alpha^{-1}(0) = 137.035999074(44), \quad \text{Ref. [129]} \tag{3.35}$$

$$G_\mu = 1.166364(5) \times 10^{-5}\,\text{GeV}^{-2}, \quad \text{Ref. [129]} \tag{3.36}$$

$$M_Z = 91.1876(21)\,\text{GeV}, \quad \text{Ref. [71]} \tag{3.37}$$

where the fine structure constant is defined in the Thomson limit $q^2 \to 0$. One can then define the quantities g_2, g_1, g_z, θ_W, M_W, v according to the tree-level relations (note that M_W is not the physical W mass), giving very precise reference values. Any other observable can then be expressed in terms of its reference values (which will have tiny errors), augmented by loop corrections (which depend on the other parameters, but are small). For example, virtual top and bottom quarks give a correction to the physical W mass M_W relative to M_W. This correction is often parameterized in terms of the so-called Δr parameter [141],

$$M_W^2\left(1 - \frac{M_W^2}{M_Z^2}\right) = \frac{\pi\alpha}{\sqrt{2}G_\mu}(1 + \Delta r), \tag{3.38}$$

which can be solved for M_W to give

$$M_W^2 = \frac{M_Z^2}{2}\left(1 + \sqrt{1 - \frac{4\pi\alpha}{\sqrt{2}\,G_\mu M_Z^2}(1 + \Delta r)}\right).$$

Note that this is not strictly a solution, as Δr itself depends on M_W, and a precise determination of M_W requires iterating the expression. However for BSM contributions, where high precision is not needed, or an understanding of the main parametric dependencies, we can Taylor-expand to obtain

$$M_W^2 = M_{W,0}^2\left(1 - \frac{s_{W,0}^2}{c_{W,0}^2 - s_{W,0}^2}\Delta r + \mathcal{O}(\Delta r)^2\right), \tag{3.39}$$

where the reference values $M_{W,0}^2$ [3] and $s_{W,0}^2$ are to be evaluated at tree-level from the input set (α, G_μ, M_Z). The anatomy of Δr (and other EW observables), in the SM and the MSSM is reviewed nicely in [91]. At the one-loop level,

$$\Delta r = \Delta\alpha + \frac{c_W^2}{s_W^2}\Delta\rho + \Delta r_{\text{rem}}, \tag{3.40}$$

[3] We denote the "bare" parameters entering the Lagrangian at tree-level with the subscript 0. The counterterms relating the physical masses to the bare quantities at leading order are given by $\delta M_W^2 = M_W^2 - M_{W,0}^2$.

wherein $\Delta\alpha$ includes light-fermion contributions to the relation between $\alpha(0)$ and $\alpha(M_Z)$, including the so-called hadronic vacuum polarisation $\Delta\alpha^{\rm had}$, $\Delta\rho$ contains the dominant top/bottom (and, in SUSY, stop/sbottom) loops, and the remainder term includes Higgs and other contributions. In the SM, neglecting the bottom and light-quark masses [91],

$$\Delta\rho_{1-\rm loop} \simeq \frac{3\,G_\mu}{8\sqrt{2}\pi^2} m_t^2 .$$

Plugging this into (3.39) via (3.40), one can see that a variation of the top mass by 1 GeV results in a change of M_W by 6.2 MeV, demonstrating the strong sensitivity to the top quark mass. With the precisely known top mass in the LHC era,

$$m_t = (173.21 \pm 0.51 \pm 0.71)\ \text{GeV}\ , \qquad \text{Ref. [71]}$$

and the Higgs mass known, the SM uncertainty is much reduced. An up-to-date theoretical evaluation using the above m_t together with $M_H = 125.64$ GeV [92] gives

$$M_W^{\rm SM} = 80.361\ \text{GeV}\ .$$

For this result, the same authors state parametric uncertainties due to $\Delta\alpha^{\rm had}$ (which has to be extracted from $e^+e^- \to$ hadrons via dispersion relations) of 2 MeV, due to M_Z of 2.5 MeV, and due to M_H of 0.35 GeV (in addition to the top mass dependence). Uncertainties due to higher-order corrections are estimated to be around 4 MeV [9]. The theoretical prediction is to be constrasted with [71]

$$M_W^{\rm exp} = (80.385 \pm 0.015)\ \text{GeV}\ .$$

Adding the theoretical errors in quadrature, one has an error below 10 MeV. As the intepretation of the very precise experimental result for m_t is not completely clear – it is usually identified with the pole mass, but this is not rigorous, and there may be a residual systematic shift of order 1 GeV –, this error may be somewhat understated (and adding in quadrature is also ad hoc). Assuming a total theory error of 15 MeV, the significance of the 24 MeV discrepancy is a bit more than 1σ. Combining the theory and eperimental error in quadrature, the error on the experiment/theory difference is about 21 MeV, and the 1σ and 2σ ranges become 3 MeV $< \delta M_W <$ 45 MeV and -18 MeV $< \delta M_W <$ 66 MeV. In summary, data on M_W and known SM corrections indicate there is about 50 MeV "room" in M_W. Such a size is actually possible in the MSSM while satisfying all experimental constraints [92], but it could also be easily generated by $Z - Z'$ mixing.

The pUMSSM tree-level contribution is easily obtained from (2.62) as follows. First compute $\delta M_Z = M_{Z_1} - M_Z$, this is strictly negative. Identifying M_{Z_1} with the measured

M_Z, one obtains $M_Z = M_{Z_1} - \delta M_Z$. Finally, substituting this into the tree-level expression, one obtains

$$\delta M_{W,\text{mix}} = -\cos\theta_W \delta M_Z. \tag{3.41}$$

For small δM_Z (which is necessary on phenomenological grounds, as just discussed), one can Taylor-expand (2.62) to obtain

$$\delta M_Z = -\frac{1}{2}\frac{(\Delta_Z^2)^2}{M_Z(M_{Z'}^2 - M_Z^2)} + \mathcal{O}(\Delta_Z^2)^3,$$

and finally

$$\Delta_{M_W} \equiv \frac{(\Delta_Z^2)^2}{M_Z(M_{Z'}^2 - M_Z^2)} < \frac{2}{\cos\theta_W}\delta M_W^{\max} \sim 110\,(190)\,\text{MeV} \tag{3.42}$$

at $1(2)\sigma$. Note that the left-hand side can also be written as $M_Z v^2 (Q_{H_u} s_\beta^2 - Q_{H_d} c_\beta^2)^2/(M_{Z'}^2 - M_Z^2)$. Unless the charge term is tiny, this implies that the Z' is much heavier than the Z. For $Q_{H_u} \sim 0.5$ and no cancellation (e.g. large $\tan\beta$), one obtains

$$\frac{M_Z^2}{M_{Z'}^2} < \frac{54(95)\text{MeV}}{M_Z} < 10^{-3},$$

thus Z' is above about 3 TeV. The $Z - Z'$ mixing angle in this case is basically given by the left-hand side, hence also very small. From eq.(3.42) one can see that in the large $\tan\beta$ limit with a heavy Z' (or equivalently large singlet vev, v_s), the quantity Δ_{M_W}, which receives an upper bound from $\delta M_{W,\text{mix}}$, is approximately

$$\Delta_{M_W} \simeq M_Z \frac{v^2}{v_s^2}\left(\frac{Q_{H_u}}{Q_s}\right)^2. \tag{3.43}$$

The above relation shows that the ratio of the $U(1)'$ charges $r = Q_{H_u}/Q_s$ should be preferably smaller than unity in order to pass the W mass constraint for relatively light $U(1)'$ breaking scales. Similarly, the mixing angle in the same limit will be approximately

$$\tan 2\theta_{ZZ'} \simeq \frac{-4M_Z^2}{g_z v_s^2}\left(\frac{r}{Q_s}\right), \tag{3.44}$$

where we can also see the dependence of the mixing angle on the ratio r. We can also rewrite the constraint in terms of masses and the mixing angle. Using (3.23),

$$\delta M_Z = \frac{1}{4}\frac{\Delta_Z^2}{M_Z}\tan 2\theta_{ZZ'} + \mathcal{O}(\Delta_Z^2)^3 = -\frac{1}{8}\frac{(M_{Z'}^2 - M_Z^2)}{M_Z}\tan^2(2\theta_{ZZ'}) + \mathcal{O}(\Delta_Z^2)^3. \tag{3.45}$$

From this we see that a bound on $\delta M_{W,\text{mix}}$ implies a bound on (approximately) the product $M_{Z'}\theta_{ZZ'}$. One can hence relax the bound on $\theta_{ZZ'}$ by decreasing $M_{Z'}$ (rather than increasing it). This requires taking Δ_Z^2 smaller, by either reducing the $U(1)'$ charges or picking $\tan\beta$ to achieve some degree of cancellation.

3.5 Anatomy of Sfermion sector

The third generation of squarks $\tilde{t}_1, \tilde{b}_1$ typically represent the lightest amongst the coloured particles in a natural supersymmetric theory. In section 2.4 we have seen that the scalar superpartners of the SM quarks and fermions unlike the MSSM receive additional D-term contributions $\Delta_{\phi_{i_{U(1)'}}}$ due to the presence of the extra $U(1)'$ symmetry eq.(2.117),(2.129). The squared mass matrices for the top and bottom squarks can be read off from the general expressions of the squared mass matrices of the up and down-type squarks

$$\mathcal{M}^2_{\tilde{t}} = \begin{pmatrix} m^2_{Q_3} + m^2_t + \Delta_{\tilde{u}_L} + Q_3 d' & m_t(A^*_t - \mu_{eff}\cot\beta) \\ m_t(A_t - \mu^*_{eff}\cot\beta) & m^2_{T^c} + m^2_t + \Delta_{\tilde{u}_R} + Q_{T^c} d' \end{pmatrix}, \tag{3.46}$$

$$\mathcal{M}^2_{\tilde{b}} = \begin{pmatrix} m^2_{Q_3} + m^2_b + \Delta_{\tilde{d}_L} + Q_3 d' & m_b(A^*_d - \mu_{eff}\tan\beta) \\ m_b(A_b - \mu^*_{eff}\tan\beta) & m^2_{B^c} + m^2_b + \Delta_{\tilde{d}_R} + Q_{B^c} d' \end{pmatrix}, \tag{3.47}$$

where Δ_{ϕ_i} are the ordinary $U(1)_Y, SU(2)_L$ gauge terms present in the MSSM and

$$d' = \frac{1}{2}\Big(Q_{H_d} v_d^2 + Q_{H_u} v_u^2 + Q_s v_s^2\Big) . \tag{3.48}$$

One immediately understands the importance of the $U(1)'$ D-term contributions in extended models. For large $U(1)'$ supersymmetry breaking scales the effects on the sparticle spectrum do not decouple. The masses of the squarks will always be driven by the extra contributions. The diagonal terms of the stop squared matrix are boosted by the mass of the heavy top quark and in the event where the right-handed top and bottom squarks are charged equally under the $U(1)'$ gauge symmetry, i.e. $Q_{T^c} = Q_{B_c}$ and the soft supersymmetry breaking masses $m^2_{Q_3}, m^2_{T^c}$ are degenerate, this will lead to a mass hierarchy with the bottom squark being slightly lighter than the top squark $m_{\tilde{t}_1} > m_{\tilde{b}_1}$. For models with a heavy Z', where $d' \sim M_{Z'}/2Q_s$, the diagonal elements of the squared matrices can be dominated by these D-terms. Depending on the sign of the charge products $(Q_3 \cdot Q_s)$, $(Q_{T^c} \cdot Q_s)$ and $(Q_{B^c} \cdot Q_s)$ the left-handed squarks, right-handed stops and right-handed sbottoms respectively can either be boosted or driven to unwanted color breaking directions of the scalar potential. In order to avoid $SU(3)_c$ colour or charged breaking minima of the scalar potential where the soft supersymmetry breaking mass parameters of the squarks and/or leptons become tachyonic we will require the first two products which are relevant

in the stop mass matrix to be positive definite $Q_3 \cdot Q_s > 0$ and $Q_{T^c} \cdot Q_s > 0$. Using the first constraint originating from the gauge invariance of the Yukawa term for the up-type quarks in the superpotential eq.(3.3) we understand that the product of the charge for the Higgs doublet and the SM gauge singlet has to be negative $Q_{H_u} Q_s < 0$. Since the right-handed bottom squark mass $m^2_{B^c}$ does not enter the 1-loop beta functions of $m^2_{H_u}$ and thus does not affect the fine tuning, it can be heavier than a few TeV. Therefore we are not considering mandatory to raise the $\tilde{b}^*_R \tilde{b}_R$ diagonal term of the sbottom matrix with large D-terms. In other words the mass of the right-handed bottom squark is going to be determined by its soft mass parameter $m^2_{B^c} \sim (3 \text{ TeV})^2$ and hence can tolerate smaller positive or even negative $U(1)'$ D-term contributions. On the other hand, in principle one would be benefited by boosting the left and right-handed stop masses via larger D-terms. A natural scenario needs light soft supersymmetry breaking stop masses m_{Q_3}, m_{T^c} but heavy mass eigenstates in order to evade the collider searches. For simplicity we will assume that the two chiral $U(1)'$ charges of the top squarks are identical $Q_{Q_3} = Q_{T^c}$ and we will parametrize with respect to the ratio $r = Q_{H_u}/Q_s$ due to the W mass constraint and the fine tuning considerations as we will see in the following chapters. The charge of the right-handed bottom quark is then fixed by the relationship derived by requiring gauge invariance of the bottom quark Yukawa term in the superpotential eq.(3.4). The charge of the singlet is chosen to be negative $Q_s < 0$ in order to satisfy the previous postulates. In Fig. 3.1 we show the masses for the three light squarks for different UMSSM scenarios as a function of $M_{Z'}$. The different charge assignments which are classified with respect to the ratio $r = Q_{H_u}/Q_s$ and the singlet $U(1)'$ charge are shown under each plot. The singlet vev is varied for all four plots within the range 3 TeV $\leq v_s \leq$ 7 TeV. One can see the effect of the different charge assignment on the D-terms and consequently on the masses of the lightest squarks in the spectrum. The squark charges with the assumption that they are equal will be given by $Q_{Q_3} = Q_{T^c} = rQ_s/(-2)$. For large left-handed and right-handed $U(1)'$ charges (Fig. 3.1a) the diagonal terms of the stop and sbottom squared mass matrix are dominated by the large positive D-term contributions due to the massive Z' boson. The masses of all three light squarks is driven to very high values as $M_{Z'}$ becomes heavier. For smaller values of the charges with increasing Z' the effect of the D-terms is relaxed and the increase is lest steep (Figs. 3.1b, 3.1c), but remains positive due to the sign choice. In the fourth plot in Fig. 3.1d we have flipped the sign of the ratio $r > 0$ so that the products $Q_{Q_3} \cdot Q_s < 0$ and $Q_{T^c} \cdot Q_s < 0$. In this case the D-terms have a negative contribution to the diagonal terms of the matrix and for heavier Z' bosons than $(2-3)$ TeV it can lead to

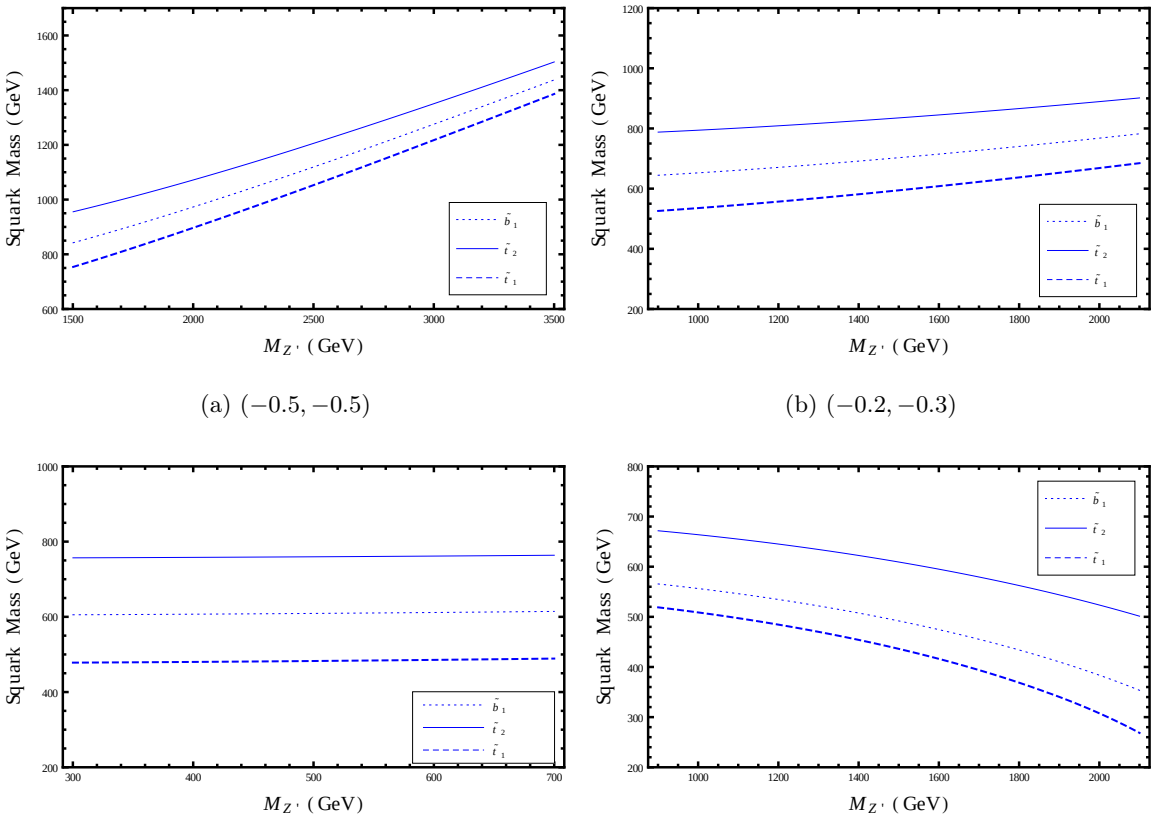

(a) $(-0.5, -0.5)$ (b) $(-0.2, -0.3)$

(c) $(-0.1, -0.1)$ (d) $(0.2, -0.3)$

Figure 3.1: The masses of the 3rd generation $\tilde{t}_1, \tilde{t}_2, \tilde{b}_1$ squarks with respect to the Z' mass for different $U(1)'$ charge assignments ($r = Q_{H_u}/Q_s, Qs$). The masses are calculated at 1-loop using `SARAH + SPheno` interface. The right-handed bottom is taken to be very heavy and is not shown here. Scalar soft masses are $m_{Q_3} = m_{T^c} = 0.7$ TeV and stop trilinear coupling $T_t = y_t A_t = 1$ TeV.

destabilization of the Higgs potential as discussed earlier (tachyonic squark squared mass eigenvalues $m^2_{\tilde{q}} < 0$). Note also that in these plots the right-handed bottom squarks is of the order of 3 TeV with small mixing A_b. The left-handed sbottom ends up in the second mass hierarchical place in the spectrum for this choice of parameters.

In the next plot (Fig. 3.2) we present the masses for the lightest squarks as a function of the soft trilinear coupling A_t for two UMSSM models (black and blue lines) and for the MSSM (red lines). For completeness the lightest CP-even Higgs mass is given for the corresponding models in the right plot. The spectrum consisting of the light squarks is shifted upwards by the $U(1)'$ D-terms for heavier Z' bosons, $M_{Z'} = 3$ TeV (black lines) and $M_{Z'} = 1.8$ TeV (blue lines). For large mixing coming from the soft trilinear coupling $A_t \sim 2$ TeV the lightest stop mass is smaller than in the heavy Z' model by

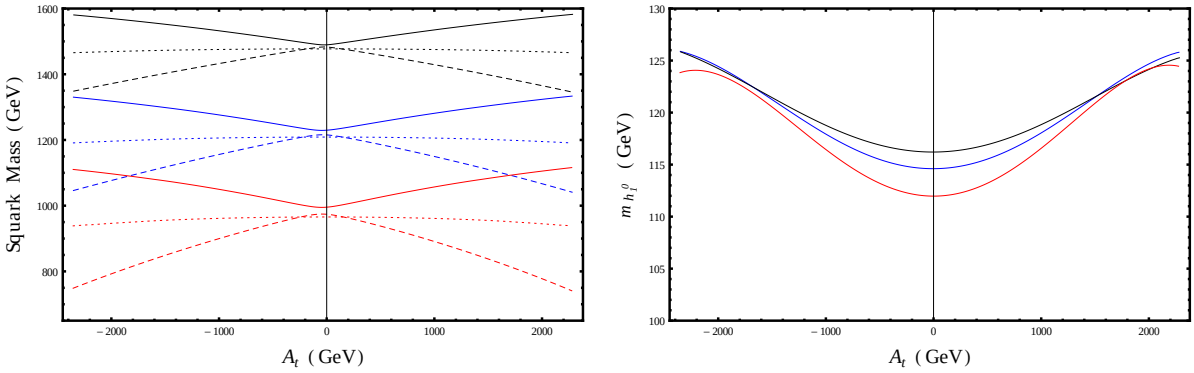

Figure 3.2: Left: Squark masses $\tilde{t}_1$ (Dashed coloured lines), $\tilde{t}_2$ (Solid coloured lines) and $\tilde{b}_1$ (Dotted coloured lines) as a function of the soft trilinear coupling $A_t = T_t/y_t$. Right: Higgs masses $m_{h_1^0}$ calculated at 2-loop accuracy using `SARAH + SPheno`. The black and blue lines correspond to two different UMSSM models, with charge assignments $(r, Q_s) = (-0.5, -0.5)$ and $(-0.6, -0.3)$, respectively. The singlet vev is fixed $v_s = 6$ TeV, $\mu_{eff} = 200$ GeV and $\tan\beta = 20$. The red lines correspond to the MSSM scenario. The relevant soft supersymmetry breaking scalar masses are of the order of 1 TeV.

around $\Delta m_{\tilde{t}_1} \sim 600$ GeV, which can be favourable by future collider searches. In the MSSM for zero mixing A_t the lightest stop is somewhat lighter than 1 TeV at 1-loop accuracy while in the two UMSSM models the squarks are very heavy $m_{\tilde{t}_1} \sim 1.5$ TeV and $m_{\tilde{t}_1} \sim 1.2$ TeV, respectively. This is currently outside the reach of the LHC but probably within its reach at higher center of mass energies of $\sqrt{s} = 14$ TeV or more. As it can be observed from the right plot in Fig. 3.2 the Higgs mass is also boosted by the larger Higgs up quartic coupling. For all three models for large mixing $A_t \sim 2$ TeV the lightest Higgs obtains mass in the LHC Higgs discovery range. For zero mixing $A_t = 0$ the effect is more profound $\Delta m_{h_1^0} \sim 5$ GeV (heavy Z' model), but all models are below the acceptable Higgs mass lower limit $m^{\rm exp}_{h_1^0} \sim 125$ GeV. Note that the Higgsino mass is light in these plots $\mu_{eff} = 200$ GeV. We will see in the next chapter that heavy μ_{eff} (or equivalently[4] large singlet Yukava coupling λ) can boost the tree-level Higgs mass in correlation to the $U(1)'$ charge assignments governing the Higgs sector.

3.6 Anatomy of Higgs Sector

We have seen in section 2.3 that the Higgs Sector in UMSSM consists of 3 CP-even Higgs bosons h_1^0, H_2^0, H_3^0, one CP-odd scalar A^0 and two charged Higgs bosons $H^\pm$. This can have

[4]This is because μ_{eff} is proportional to λ when the singlet vev v_s (or $M_{Z'}$) is fixed.

several implications and potential advantages on the phenomenology over other extensions of the MSSM. For example in the NMSSM like in the UMSSM there are 10 real degrees of freedom coming from the two complex Higgs doublets and the extra SM gauge singlet field. After electroweak symmetry breaking three degrees of freedom are eaten by the gauge bosons $Z, W^{\pm}$ and the remaining dofs result in 3 CP-even Higgs bosons plus two CP-odd A_1^0, A_2^0 and two charged Higgs bosons. The presence of an extra CP-odd Higgs boson can possibly suppress the branching fractions $\gamma\gamma, WW, ZZ, b\bar{b}$, because a SM-like Higgs particle will predominantly decay into the lightest A_1^0 Higgs boson [34, 86]. In the UMSSM this extra degree of freedom is eaten by the Z' boson which appears due to the extra gauge symmetry. The other very interesting observation is that this extra gauge group creates additional $U(1)'$ D-term contributions to the quartic coupling of the Higgs scalar potential which can potentially raise the tree-level lightest Higgs mass [5, 26, 28, 48].

In this section we will explore the implications of this extended sector on the mass of the lightest CP-even Higgs boson h_1^0 which is the candidate to be identified as the Higgs particle discovered at the LHC in 2012. We will investigate how the tree-level mass can be boosted in different UMSSM scenarios with different charge assignments and whether it is affected by other parameters which might have been overlooked in the past. Quantum corrections at 1-loop and 2-loop, using state of the art programs `SARAH + SPheno` will be compared against effective potential techniques in order to test the accuracy of our results and quantify any potential improvement in the calculation of the Higgs mass provided by these programs.

3.6.1 Effect of μ_{eff} on tree-level Higgs mass

In the UMSSM the presence of the additional F-term and $U(1)'$ D-terms in the Higgs potential (2.68),(2.69) can raise the tree-level mass of the lightest Higgs boson h_1^0 above the Z mass ~ 91.2 GeV [122]. An approximate upper limit for $m_{h_1^0}$ can be deduced [48] and for heavy Z' models is given by

$$m_{h_1^0}^2 \lesssim M_Z^2 \cos^2(2\beta) + \frac{1}{2}(\lambda v)^2 \sin^2(2\beta) - \lambda^2 v^2 \left(\frac{\lambda^2}{Q_s^2} + 2\frac{Q_{H_u}}{Q_s} \right) . \tag{3.49}$$

The first term in the above inequality corresponds to the MSSM tree-level upper bound on the Higgs mass, which can be saturated in the large $\tan\beta$ limit. The second term is originating from the λ-term in the superpotential W and is also present in the NMSSM. This term also contributes positively to the upper bound but it depends on the value of $\tan\beta$ competing with the first term. In the large $\tan\beta$ limit where $\beta \sim \pi/2$ this term vanishes and there is no boost on the tree-level Higgs mass greater than the Z mass for

these models. Typically one would favour a large singlet Yukawa coupling λ in order to strengthen the effects of this term as in λ-SUSY scenarios [20, 72, 83]. However λ does not remain perturbative up to a unification scale in this case and typically $\tan\beta$ has to be relatively small. The last term is unique in gauge extensions of the MSSM due to the D-terms contributions from the additional $U(1)$ gauge group. Note that although there is no $\tan\beta$ dependence, the singlet Yukawa coupling and the signs and absolute values of the $U(1)'$ charges can play a significant role in either increasing or decreasing the upper bound on the Higgs mass. It is worth noting that other forms of (3.49) are more popular

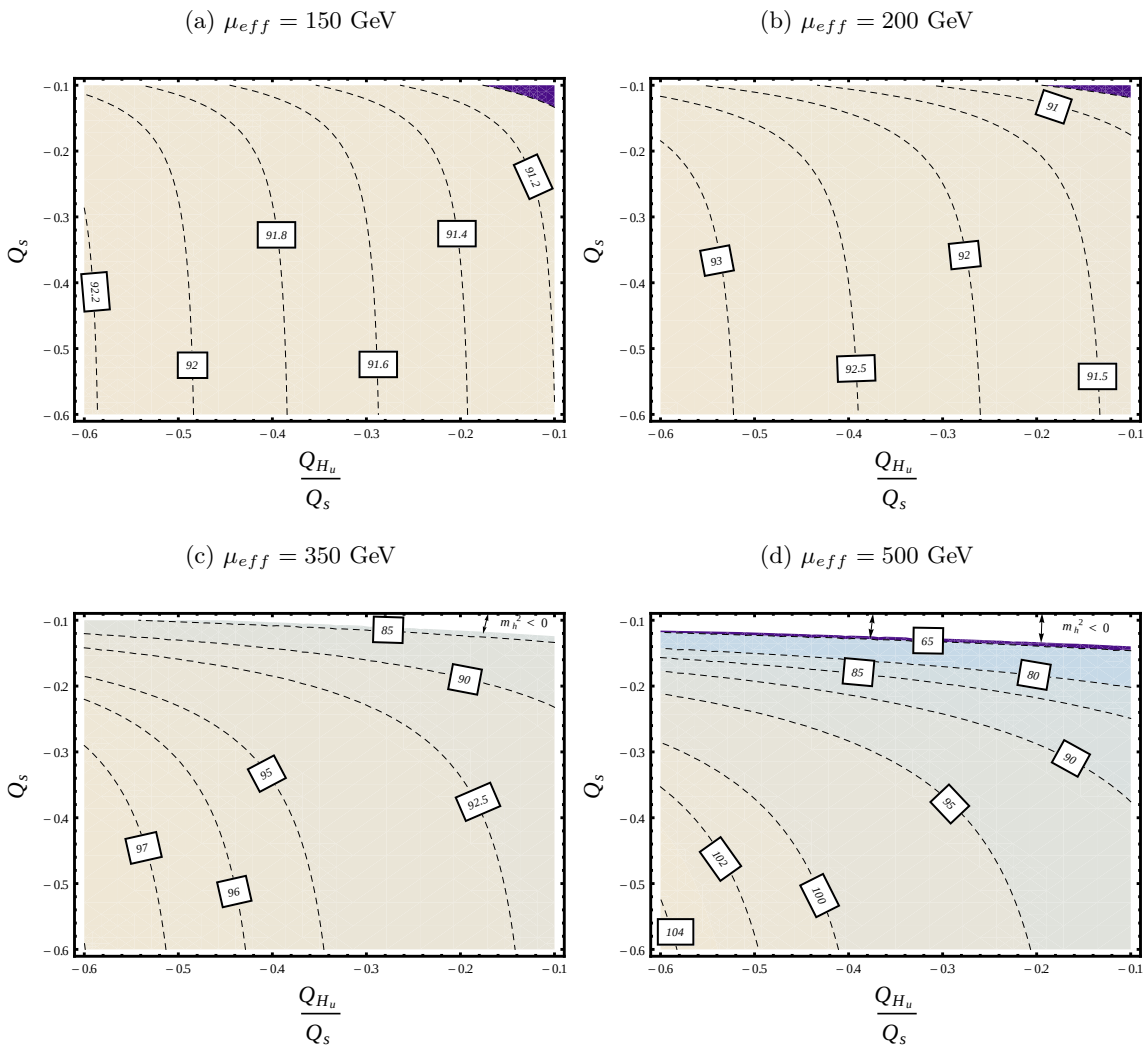

Figure 3.3: Tree-level lightest Higgs mass contours $m^{\text{tree}}_{h^0_1}$ (in units of GeV) on the (r, Q_s) plane for different values of the effective Higgsino mass μ_{eff}. The singlet vev is fixed to $v_s = 3.5$ TeV and $\tan\beta = 20$ in order to saturate the upper bound on $m^{\text{tree}}_{h^0_1}$ in the MSSM (first term in eq.(3.49)) at tree-level.

in the literature but this is the only form that seems to explain analytically our numerical

results on the tree-level mass of h_1^0. Let us rewrite eq.(3.49) taking into account the assumptions for the charges and replacing in the third term the dimensionless coupling λ with dimensionful quantities

$$m_{h_1^0}^2 \lesssim M_Z^2 \cos^2(2\beta) + \frac{1}{2}(\lambda v)^2 \sin^2(2\beta) + 4\mu_{eff}^2 \left(\frac{v}{v_s}\right)^2 \left[\left| \frac{Q_{H_u}}{Q_s} \right| - \left(\frac{\mu_{eff}}{M_{Z'}}\right)^2 \right] , \quad (3.50)$$

the above expression exhibits some of the features one can observe in Fig. 3.3 resulting from our numerical analysis. In this plot we present the tree-level mass contours for the lightest CP-even Higgs boson for different values of μ_{eff}. As one can see from eq.(3.50) for fixed value of the Higgsino mass parameter and the singlet vev the expression inside the bracket determines if the contribution to the Higgs mass is going to be constructive or destructive. This depends on the two ratios $r = Q_{H_u}/Q_s$ and $(\mu_{eff}/M_{Z'})^2$. A light Z' of a comparable size to the Higgsino mass parameter can reduce the Higgs mass if the ratio of the Higgs and singlet charges is small. The ratio $r = Q_{H_u}/Q_s$ not only controls the Z mass shift through the W mass constraint but also controls the upper bound on the tree-level Higgs mass one can achieve in different gauge extensions of the MSSM. When $|r| > (\mu_{eff}/M_{Z'})^2$ then a

(a) $\mu_{eff} = 800$ GeV, $v_s = 3.5$ TeV (b) $\mu_{eff} = 800$ GeV, $v_s = 5.0$ TeV

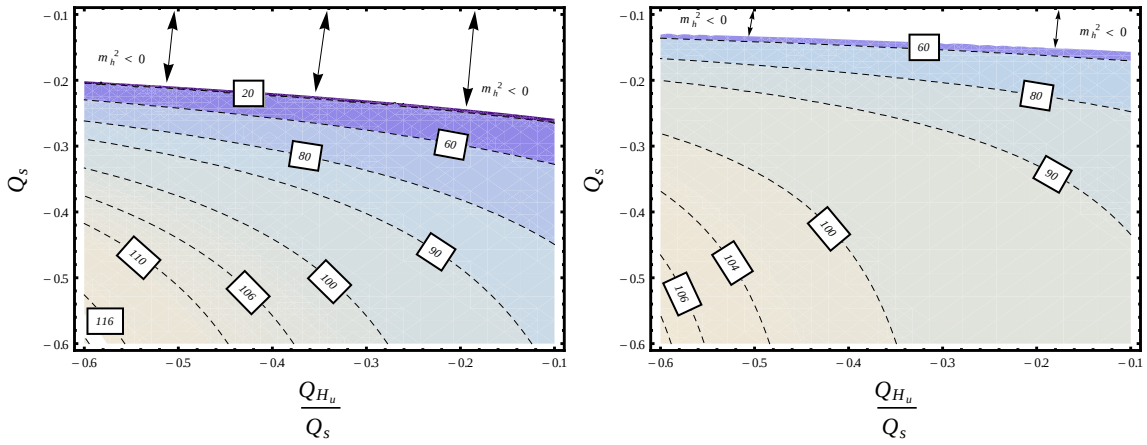

Figure 3.4: Tree-level lightest Higgs mass contours $m_{h_1^0}^{\text{tree}}$ (in GeV) on the (r, Q_s) plane for different values of the effective Higgsino mass μ_{eff}. For these plots we use different values of the singlet vev. For larger values of v_s the upper bound on the Higgs mass decreases for all points in the plane compared to the plot with smaller vev.

heavy Higgsino will contribute positively to the tree-level Higgs mass reducing the need for large radiative corrections. On the other hand when $|r| < (\mu_{eff}/M_{Z'})^2$ the tree-level mass can be lighter than the Z mass (large $\tan\beta$ limit) and one has to require large quantum corrections to the Higgs mass in order to achieve the desirable mass range. This means that

a scenario with a light Z' will not necessarily mean less fine tuning, even if it passes the W mass constraint. Although the light Z' will not contribute to the fine-tuning measure a negative contribution to the Higgs mass at tree-level will enhance the fine tuning coming from the stop sector making it worse than in MSSM models. In the plots of Fig. 3.3 the singlet vev is fixed to $v_s = 3.5$ TeV, hence the lightest Z' is obtained for the smallest singlet charge on the plane $Q_s = -0.1$ which translates to $M_{Z'} \approx 350$ GeV. It is obvious from these plots that as we increase the Higgsino mass, the lightest Higgs for light Z' bosons becomes extremely small and can even enter the color breaking region for which the squared mass eigenvalues of the Higgs become tachyonic. Heavy Z' models are enhanced by raising the Higgsino mass. Furthermore for a fixed value of μ_{eff} a larger ratio $|r|$ enhances the effect of a heavy Higgsino and as we see in the plots the mass contours obtain larger values as we move from right to left increasing the absolute value of the ratio r. This numerical result is exactly what one can read off also from the approximate equation for the upper bound eq.(3.50). For $M_{Z'} \sim 2.1$ TeV the maximum value for the tree-level Higgs obtained for $\mu_{eff} = 800$ GeV is around $m^{\text{tree}}_{h^0_1} \sim (117-118)$ GeV (the contour is not shown in Fig. 3.4a). When the singlet vev increases for fixed μ_{eff} the Higgs mass decreases (Fig. 3.4). The right plot has $v_s = 5.0$ TeV, clearly at the same points on the (r, Q_s) plane the Higgs mass is found to be reduced compared to the left plot with $v_s = 3.5$ TeV. This observation can be explained in terms of eq.(3.50). As one can see, a heavier Z' resulting from a larger $U(1)'$ breaking scale will suppress the second "harmful" term in the bracket which can cause negative contributions if it is order $\mathcal{O}(1)$, but on the other hand the coefficient of the bracket will be suppressed by the ratio $(v/v_s)^2$ reducing the upper bound. So in this case of $M_{Z'} \gg \mu_{eff}$ although one is not concerned about negative contributions to the Higgs mass, the heavier the singlet vev the larger the suppression of the positive contribution to the tree-level Higgs upper bound. There are two ways to increase the Z' mass, either by increasing its coupling Q_s or by increasing the $U(1)'$ breaking scale v_s. According to our analysis the first way (increasing Q_s) can result in negative contributions if the ratio does not satisfy the approximate relation $|r| > (\mu_{eff}/M_{Z'})^2$ but can achieve very heavy Higgs masses otherwise when also μ_{eff} is heavy. However we have to be careful because for large ratios $|r|$, as we have argued in the previous sections, the W mass constraint can be challenging, and thus unavoidably we need a sufficient large singlet vev to overcome this constraint. The second method although it is more safe from the point of view of having negative contributions (note that also the tachyonic mass area is shrinking in the right plot of Fig. 3.4) it will suppress the positive contributions to the upper bound of the tree-

level Higgs mass. Ultimately for extremely large breaking scales $m^{\text{tree}}_{h^0_1} \sim M_Z$ will become MSSM like (in the large $\tan\beta$ limit). The above discussion strengthens and supports the parametrization and classification of the different UMSSM models by the ratio r and the singlet $U(1)'$ charge Q_s.

3.6.2 Radiative corrections to h^0_1

In this section we investigate the 1-loop corrections to the lightest Higgs boson using effective potential techniques and we compare with the full 1-loop and 2-loop radiative corrections calculated using the state of the art programs for BSM phenomenology studies `SARAH & SPheno` Ref.[138, 139, 142, 143]. We will show that 1-loop corrections to the lightest Higgs particle involving the top quark and its scalar superpartners $\tilde{t}_{1,2}$ can lead to exaggerated corrections $\Delta m^2_{h^0_1}$ which can exceed even the full 2-loop calculation by more than $m^{\text{1-Eff}}_{h^0_1} - m^{\text{2-loop}}_{h^0_1} \simeq 10$ GeV. In the post Higgs discovery era it is crucial to calculate the lightest CP-even Higgs mass with high accuracy in order to get conclusive results. Therefore, previous calculations used in older pre-Higgs discovery studies are found to be inefficient for this matter. We improve our study by including the 2-loop calculation of the Higgs sector.

One-loop effective potential $\mathbf{V_{eff}}$. We will consider contributions from the top quark and the two top squarks in the loop. For very large $\tan\beta > 40$ the contribution from the bottom squarks become sizeable [5] due to the fact that the bottom Yukawa coupling becomes large in this limit $y_b \sim \mathcal{O}(1)$. The Coleman-Weinberg correction to the scalar potential including the stops and the top quark is given by [39]

$$V^1 = \frac{3}{32\pi^2}\Big[\sum_{j=1}^{2} m^4_{\tilde{t}_j}\Big(\ln\frac{m^2_{\tilde{t}_j}}{Q^2} - \frac{3}{2}\Big) - 2\bar{m}^4_t\Big(\ln\frac{\bar{m}^2_t}{Q^2} - \frac{3}{2}\Big)\Big]\,, \tag{3.51}$$

where $\bar{m}^2_t = y^2_t|H^0_u|^2$ is the field dependent mass of the top quark and Q is the renormalization scale in the $\overline{\text{DR}}$ scheme. The field dependent stop squared masses $\bar{m}^2_{\tilde{t}_{1,2}}$ are taken to be the eigenvalues of the stop squared matrix before electroweak symmetry breaking takes place see eq.(2.107),(2.108),(2.110) and eq.(2.109). The field dependent mass matrix

$$\overline{\mathcal{M}}^2_{\tilde{t}} = \begin{pmatrix} \overline{\mathcal{M}}^2_{\tilde{t}^*_L\tilde{t}_L} & \overline{\mathcal{M}}^2_{\tilde{t}^*_L\tilde{t}_R} \\ \\ \overline{\mathcal{M}}^2_{\tilde{t}^*_R\tilde{t}_L} & \overline{\mathcal{M}}^2_{\tilde{t}^*_R\tilde{t}_R} \end{pmatrix}\,, \tag{3.52}$$

where we have used the bar notation to denote the fact that the elements are field dependent quantities and are given by eq.(2.107),(2.108),(2.110) and eq.(2.109)

$$\begin{aligned}\overline{\mathcal{M}}^2_{\tilde{t}^*_L\tilde{t}_L} &= \left(|H^0_d|^2 - |H^0_u|^2\right)\left(\frac{g_2^2}{4} + \frac{g_1^2}{12}\right) \\ &+ g_1'^2\Big(Q_{H_d}|H^0_d|^2 + Q_{H_u}|H^0_u|^2 + Q_s|S|^2\Big)Q_{Q_3} + |y_t|^2|H^0_u|^2 + m^2_{Q_3}\ , \end{aligned} \tag{3.53}$$

$$\begin{aligned}\overline{\mathcal{M}}^2_{\tilde{t}^*_R\tilde{t}_R} &= g_1^2\left(\frac{|H^0_d|^2}{3} + \frac{|H^0_u|^2}{3}\right) + g_1'^2\Big(Q_{H_d}|H^0_d|^2 + Q_{H_u}|H^0_u|^2 + Q_s|S|^2\Big)Q_{T^c} \\ &+ |y_t|^2|H^0_u|^2 + m^2_{T^c}\ , \end{aligned} \tag{3.54}$$

and finally the off-diagonal terms of the matrix which are related by complex conjugation

$$\overline{\mathcal{M}}^2_{\tilde{t}^*_L\tilde{t}_R} = -y_t^*\lambda S H^0_d + y_t^* H^{0\,*}_u A^*_t = \left(\overline{\mathcal{M}}^2_{\tilde{t}^*_R\tilde{t}_L}\right)^*\ . \tag{3.55}$$

the field dependent eigenvalues $\bar{m}^2_{\tilde{t}_{1,2}}$ of the matrix will then be given by

$$\bar{m}^2_{\tilde{t}_{1,2}} = \frac{1}{2}\mathrm{Tr}\left[\overline{\mathcal{M}}^2_{\tilde{t}}\right] \pm \frac{1}{2}\sqrt{\left(\mathrm{Tr}\left[\overline{\mathcal{M}}^2_{\tilde{t}}\right]\right)^2 - 4\mathrm{Det}\left[\overline{\mathcal{M}}^2_{\tilde{t}}\right]} \tag{3.56}$$

the one-loop corrections to the tree-level squared mass matrix $\mathcal{M}^2_{\text{CP-even}}$ of the Higgs bosons are then given by taking the second derivative of the Coleman-Weinberg potential V^1 and subtracting the appropriate terms from the diagonal elements which take care of the shift of the potential and allow one to use the same tree-level minimization conditions, i.e.

$$(\mathcal{M}^1_{\text{CP-even}})_{ij} = \frac{\partial^2 V^1}{\partial\phi_i\partial\phi_j}\Big|_{\text{min}} - \delta_{ij}\frac{1}{v_i}\frac{\partial V^1}{\partial\phi_i}\Big|_{\text{min}}\ , \tag{3.57}$$

where $\phi = H_u^0, H_d^0, S$. After performing the derivation using eq.(3.51) one will get [5, 26] the elements of the mass matrix which provides the one-loop corrections to be

$$(\mathcal{M}^1_{\text{CP-even}})_{11} = k\left[\left(\frac{(\widetilde{m}_1^2)^2}{(m^2_{\tilde{t}_1}-m^2_{\tilde{t}_2})^2}\mathcal{G}\right)v_d^2 + \left(\frac{\lambda y_t^2 A_t}{2\sqrt{2}}\mathcal{F}\right)\frac{v_u v_s}{v_d}\right] , \tag{3.58}$$

$$(\mathcal{M}^1_{\text{CP-even}})_{12} = k\left[\left(\frac{\widetilde{m}_1^2\widetilde{m}_2^2}{(m^2_{\tilde{t}_1}-m^2_{\tilde{t}_2})^2}\mathcal{G} + \frac{y_t^2\widetilde{m}_1^2}{m^2_{\tilde{t}_1}+m^2_{\tilde{t}_2}}(2-\mathcal{G})\right)v_d v_u - \left(\frac{\lambda y_t^2 A_t}{2\sqrt{2}}\mathcal{F}\right)v_s\right] , \tag{3.59}$$

$$(\mathcal{M}^1_{\text{CP-even}})_{13} = k\left[\left(\frac{\widetilde{m}_1^2\widetilde{m}_s^2}{(m^2_{\tilde{t}_1}-m^2_{\tilde{t}_2})^2}\mathcal{G} + \frac{\lambda^2 y_t^2}{2}\mathcal{F}\right)v_d v_s - \left(\frac{\lambda y_t^2 A_t}{2\sqrt{2}}\mathcal{F}\right)v_u\right] , \tag{3.60}$$

$$\begin{aligned}(\mathcal{M}^1_{\text{CP-even}})_{22} &= k\left(\frac{(\widetilde{m}_2^2)^2}{(m^2_{\tilde{t}_1}-m^2_{\tilde{t}_2})^2}\mathcal{G} + \frac{2y_t^2\widetilde{m}_2^2}{m^2_{\tilde{t}_1}+m^2_{\tilde{t}_2}}(2-\mathcal{G}) + y_t^4\ln\frac{m^2_{\tilde{t}_1}m^2_{\tilde{t}_2}}{m_t^4}\right)v_u^2 \\ &+ k\left(\frac{\lambda y_t^2 A_t}{2\sqrt{2}}\mathcal{F}\right)\frac{v_d v_s}{v_u} ,\end{aligned} \tag{3.61}$$

$$(\mathcal{M}^1_{\text{CP-even}})_{23} = k\left[\left(\frac{\widetilde{m}_2^2\widetilde{m}_s^2}{(m^2_{\tilde{t}_1}-m^2_{\tilde{t}_2})^2}\mathcal{G} + \frac{y_t^2\widetilde{m}_s^2}{m^2_{\tilde{t}_1}+m^2_{\tilde{t}_2}}(2-\mathcal{G})\right)v_u v_s - \left(\frac{\lambda y_t^2 A_t}{2\sqrt{2}}\mathcal{F}\right)v_d\right] , \tag{3.62}$$

$$(\mathcal{M}^1_{\text{CP-even}})_{33} = k\left[\left(\frac{(\widetilde{m}_s^2)^2}{(m^2_{\tilde{t}_1}-m^2_{\tilde{t}_2})^2}\mathcal{G}\right)v_s^2 + \left(\frac{\lambda y_t^2 A_t}{2\sqrt{2}}\mathcal{F}\right)\frac{v_d v_u}{v_s}\right] . \tag{3.63}$$

Here the coefficient $k = \frac{3}{(4\pi)^2}$ and the functions $\mathcal{G}$ and $\mathcal{F}$ are given by

$$\mathcal{G}(m^2_{\tilde{t}_1}, m^2_{\tilde{t}_2}) = 2\left[1 - \frac{m^2_{\tilde{t}_1}+m^2_{\tilde{t}_2}}{m^2_{\tilde{t}_1}-m^2_{\tilde{t}_2}}\log\left(\frac{m_{\tilde{t}_1}}{m_{\tilde{t}_2}}\right)\right] , \tag{3.64}$$

$$\mathcal{F} = \log\left(\frac{m^2_{\tilde{t}_1}m^2_{\tilde{t}_2}}{Q^4}\right) - \mathcal{G}(m^2_{\tilde{t}_1}, m^2_{\tilde{t}_2}) . \tag{3.65}$$

The mass squared parameters $\widetilde{m}_1^2, \widetilde{m}_2^2, \widetilde{m}_s^2$ are defined as

$$\widetilde{m}_1^2 = y_t^2\mu_{eff}\left(\mu_{eff} - A_t\tan\beta\right) , \tag{3.66}$$

$$\widetilde{m}_2^2 = y_t^2 A_t\left(A_t - \mu_{eff}\cot\beta\right) , \tag{3.67}$$

$$\widetilde{m}_s^2 = \frac{v_d^2}{v_s^2}y_t^2\mu_{eff}\left(\mu_{eff} - A_t\tan\beta\right) . \tag{3.68}$$

The corresponding effective potential calculation for the MSSM can be found in Ref.[30]. One can see that in the limit where the UMSSM becomes MSSM-like the loop corrections are matching. For completeness we present in Fig. 3.5 two plots which depict the lightest

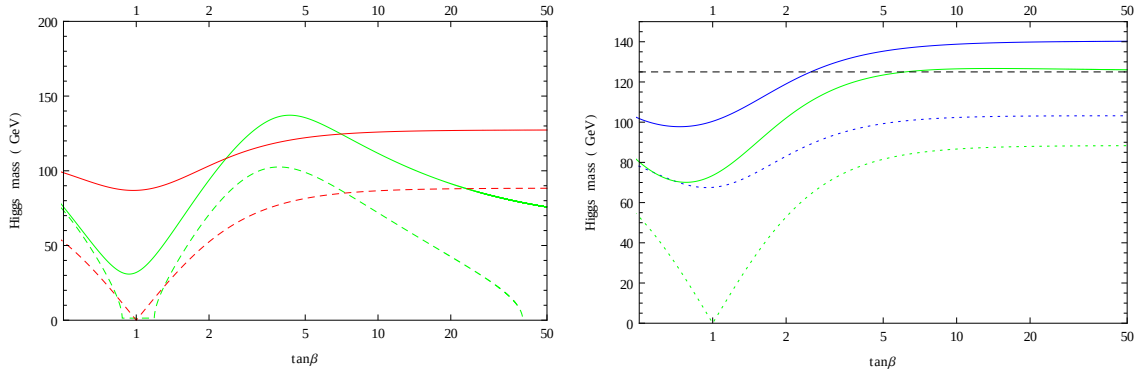

(a) Higgs mass in the MSSM (solid red line) and UMSSM (solid green line). The dashed lines correspond to the tree-level masses in both scenarios. For this plot $m_{Q_3} = m_{T^c} = 1$ TeV, $v_s = 0.5$ TeV, $\lambda = 0.5$. Furthermore a moderate mixing is considered $A_t = 1$ TeV.

(b) For this plot we choose $m_{Q_3} = m_{T^c} = 0.4$ TeV, $v_s = 2.5$ TeV, $\lambda = 0.3$ and same soft trilinear coupling A_t with (a). Blue (Green) solid line: UMSSM (MSSM) 1-loop and dashed line UMSSM (MSSM) at tree-level.

Figure 3.5: Higgs masses in the UMSSM and the MSSM using the 1-loop effective potential method including the stops in the loop. For the $U(1)'$ charges we have used the E$_6$SSM charge assignments Ref.[103].

Higgs mass in UMSSM and in MSSM as a function of $\tan\beta$ using the 1-loop effective potential method. Note that these plots are given only for pedagogical purposes here and intend to show as argued earlier that this method does not provide us with enough accuracy in the post-Higgs discovery era. We choose the charges to be $Q'_{H_u} = -2/\sqrt{40}$, $Q'_{H_d} = -3/\sqrt{40}$ and $Q'_s = 5/\sqrt{40}$ and $g'_1 \simeq 0.46$ which is usually assumed to result from unification of the gauge couplings. Note that in our parametrization introduced in the previous sections this corresponds to the ratio $r = -0.4 < 0$ with $Q_s \equiv g'_1 Q'_s = 0.36$. It is worth also mentioning that the sfermion charges are also positive coinciding with our requirements for positive $U(1)'$ D-term contributions to the sfermion masses. The vev for the left plot is very small $v_s = 500$ GeV and the model fails to pass the W mass constraint and is away from the central value by around 20σ deviation, which of course is not acceptable ($\theta_{ZZ'} = 0.113$). For the second plot the W mass constraint is within 2σ and the mixing angle is approximately $\theta_{ZZ'} \simeq 3.6 \times 10^{-3}$. The 1-loop Higgs mass for the UMSSM is overshooting the line of $m_{h_1^0} = 125$ GeV at around $\tan\beta = 2.5$ and obtains a maximum value of around $m_{h_1^0} = 140$ GeV for large $\tan\beta = 50$ when the MSSM upper bound is saturated. The soft masses for the third generation squarks are taken to be very small. It is also surprising that even the MSSM reaches the black dashed horizontal line at around $\tan\beta = 5$. In the MSSM as we will see later on in the next chapters, it is

well-known that in order to reach the Higgs mass of $m_{h_1^0} = 125$ GeV, large stops of the order $\mathcal{O}(1)$ TeV are needed along with maximal mixing $A_t \sim 2$ TeV. In the next plot we will elaborate on this observation and we will actually compare the loop corrections using the two available methods.

Calculating two-loop Higgs radiative corrections with `SARAH`. In the MSSM the radiative corrections to the Higgs bosons are known to high accuracy. Leading two-loop corrections using effective potential techniques or diagrammatic calculation of order $\mathcal{O}(\alpha_s\alpha_t)$, $\mathcal{O}(\alpha_t^2)$, $\mathcal{O}(\alpha_b\alpha_s)$ and $\mathcal{O}(\alpha_t\alpha_b + \alpha_b^2)$ with zero external momentum have been available for a while and have been implemented in publicly available codes such as `SoftSUSY` [4, 74], and `SPheno` [138, 139]. Three-loop calculations with the effective potential method have been performed Ref.[125] and lately two-loop QCD corrections of $\mathcal{O}(\alpha_s\alpha_t)$, $\mathcal{O}(\alpha_t^2)$ Ref.[50], including the effect of non-vanishing external momenta in the self-energies have become available, in order to reduce the theoretical uncertainties to match the impressive experimental uncertainty. The picture is less impressive when one decides to study a model beyond the MSSM. In the previous section we have taken a glimpse into this issue and convinced ourselves that we need higher accuracy in order to be able to obtain some conclusive results which are going to point in the right direction and not distort our judgement either in favour or against a particular model.

The program `SARAH` gave us the ability to overcome this barrier and go beyond 1-loop corrections using effective potential methods with only the third-generation squarks in the loop. The program provides the 2-loop calculation of the Higgs masses with two different methods: (a) an effective potential method (b) a fully diagrammatic calculation. This way one can verify their results since there is no literature to compare it with at the moment. The calculation includes all 2-loop corrections which do not involve the electroweak corrections. By appropriately modifying the `SARAH` files one can create an output for `SPheno` which is a powerful spectrum generator written in `Fortran` code. The latter calculates all other masses in the spectrum at one-loop order using the routines provided by `SARAH`. Additionally it calculates the branching ratios, decay widths, flavour observables and more Ref.[138, 139, 143, 144]. In the following we present results from our numerical analysis on the lightest Higgs mass in the generic pUMSSM scenario.

In Figure 3.6 we have plotted the Higgs mass up to two-loop order using `SARAH` (black dashed line) along with the tree-level mass and at one-loop order using the effective potential V^1 eq.(3.51). The charges are chosen in our parametrization to be $(r, Q_s) = (-0.6, -0.5)$ and all other input parameters are taken at the electroweak scale.

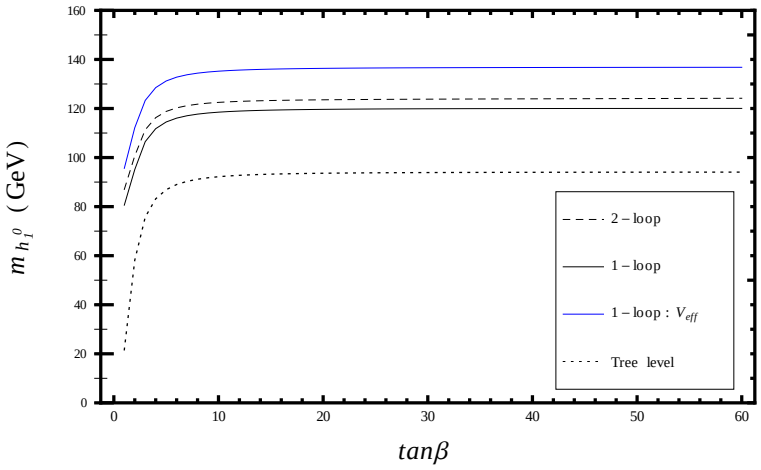

Figure 3.6: Higgs mass at one-loop (black solid line) and two-loop (dashed black line) using `SARAH + SPheno`. The corrections using one-loop effective potential with only stops in the loop are also shown in blue. Finally the tree-level mass is shown for comparison. One can see that the blue line exceeds the two-loop calculation by around 10 GeV, see Table 3.1.

Quantum Corrections Order	$\tan\beta = 20$	$\tan\beta = 60$
$m_{h_1^0}$ 2-loop with `SARAH`	123.5 GeV	124.2 GeV
$m_{h_1^0}$ 1-loop with `SARAH`	119.6 GeV	120.0 GeV
$m_{h_1^0}$ 1-loop V_{eff}^1	136.4 GeV	136.8 GeV
$m_{h_1^0}$ tree-level	93.6 GeV	94.1 GeV

Table 3.1: Table showing the values of the lightest Higgs mass corresponding to Fig. 3.6 for $\tan\beta = 20$ and $\tan\beta = 60$.

The left-handed and right-handed soft supersymmetry breaking masses of the stops are assumed degenerate in mass with $m_{Q_3} = 800$ GeV and the singlet vev is $v_s = 5$ TeV. The soft trilinear coupling $A_t = 1.5$ TeV and the Higgsino mass is $\mu_{eff} = 300$ GeV. The singlet soft trilinear coupling is taken to be fixed $A_s = 250$ GeV throughout this project in order to maximize the effects on the Higgs mass. In Table 3.1 we give the values of the Higgs mass for the pUMSSM models shown in Fig. 3.6 at $\tan\beta = 20, 60$ so that one can compare the accuracy of the different loop orders and methods. The one-loop corrections using V_{eff}^1 in eq.(3.51) provides a large contribution to the tree-level Higgs mass which exceeds even the two-loop accuracy obtained with `SARAH`. This is due to the fact that many scalar contributions apart from the two stops are not taken into account which can reduce the

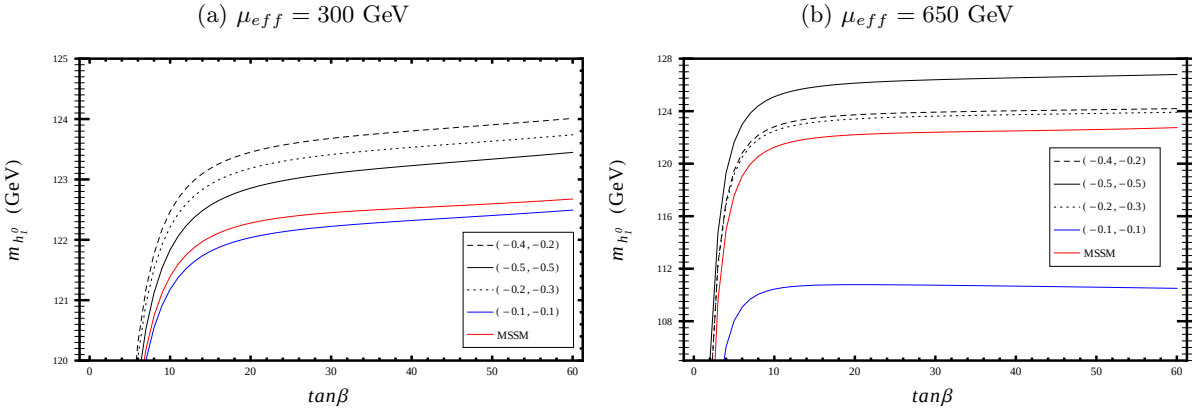

Figure 3.7: Lightest CP-even Higgs mass in different pUMSSM models. The effective Higgsino mass parameter is increased in the right plot and everything else remains the same. The soft masses at the electroweak scale are $m_{Q_3} = m_{T^c} = 800$ GeV, $A_t = 1.5$ TeV and the singlet vev $v_s = 6$ TeV. Color lines are kept the same across the plots for specific models.

positive contributions to the radiative corrections on the Higgs mass. The tree-level Higgs mass appears slightly larger than Z mass due to the large $U(1)'$ couplings and the effective Higgsino mass value. In Fig. 3.7 we show the Higgs mass at two-loop for different pUMSSM scenarios. The charge assignments are given in the legend. For the left plot the Higgsino mass is taken to be $\mu_{eff} = 300$ GeV and for the right one is increased to $\mu_{eff} = 650$ GeV in order to boost the tree-level Higgs mass. The maximum values obtained for every model are shown in Table 3.2. The blue line with charges $(-0.1, -0.1)$ appears to have slightly suppressed Higgs mass compared to the MSSM for light Higgsino but the maximum Higgs mass is over 122 GeV. When the Higgsino mass increases we see that due to the small ratio $r = -0.1$, the tree-level Higgs mass receives negative contributions and reduces the Higgs mass below 110 GeV. On the other hand the models with larger $|r|$ are enhanced in this case. It is interesting that the black line with charges $(-0.5, -0.5)$, in the left plot corresponds to the third heaviest Higgs mass with maximum value $m_{h_1^0}^{\text{Max}} \simeq 123.4$ GeV and in the right plot the model achieves the heaviest Higgs mass $m_{h_1^0}^{\text{Max}} \simeq 126.8$ GeV.

Conclusion

In this section we have introduced the phenomenological version of UMSSM (pUMSSM) with generic charges and discussed the constraints from gauge invariance of the Yukawa terms in the superpotential and the perturbativity bounds on the $U(1)'$ effective charges which have absorbed the $U(1)'$ gauge coupling. We have stressed the importance of anomaly cancellation and the possible problems arising from FCNCs but we do not treat them

$U(1)'$ Charges (r, Q_s)	$m_{h_1^0}^{\text{Max}}$ for $\mu_{eff} = 300$ GeV	$m_{h_1^0}^{\text{Max}}$ for $\mu_{eff} = 650$ GeV
$(-0.5, -0.5)$	123.4 GeV	126.8 GeV
$(-0.2, -0.3)$	123.8 GeV	123.9 GeV
$(-0.4, -0.2)$	124.0 GeV	124.2 GeV
$(-0.1, -0.1)$	122.5 GeV	110.8 GeV
MSSM	122.7 GeV	122.7 GeV

Table 3.2: Maximum values of the Higgs mass of the lightest boson h_1^0 corresponding to the two plots in Fig. 3.7.

in this project. Since the mixing angle constraint are highly model dependent Ref.[63, 65] we tackle the problem of the Z mass shift in a way suitable for gauge extensions with generic charges by imposing constraints from the W mass experimental measurement. We identify the importance of the ratio $r = Q_{H_u}/Q_s$ in satisfying the W mass constraint and we parametrize our study accordingly. In the heavy Z' limit where $M_{Z'} \gg M_Z$, the quantity Δ_{M_W}, which is constrained from the W mass precision measurement, is proportional to the square of the ratio r for fixed singlet vev v_s while the mixing is proportional to r itself. Ratios larger than one would require large v_s and consequently heavy Z' to pass the constraint. Hence we require $r < 0, |r| < 1$, the first inequality comes from the requirement of having positive $U(1)'$ D-term contributions to the 3rd generation squark masses. Furthermore, we show that the Higgs upper bound is also sensitive to r. We show numerically that in the bottom left corner of the (r, Q_s) plane (large $|r|$,$|Q_s|$ region) the tree-level Higgs mass can be substantially enhanced at tree-level for heavy effective Higgsino masses which can potentially be beneficial for reducing the fine-tuning measure. On the other hand a large $U(1)'$ breaking scale v_s which results in heavy Z' bosons for large $|Q_s| \sim 0.6$, can suppress the Higgs mass as seen in the plots. Moreover, we show that the squark sector can be very different from the MSSM, with mass hierarchies which can be entirely directed by large $U(1)'$ D-terms. We improve the accuracy of our study by calculating the Higgs mass at two-loop order using the publicly available programs `SARAH`, `SPheno` and compare with effective potential techniques with only the stops in the loop. Plots of the lightest Higgs mass for different charge assignments are given as a function of $\tan\beta$ and the MSSM has been included for comparison.

Chapter 4

Fine-Tuning in pMSSM. Collider constraints using Fastlim

4.1 Low scale fine tuning in the MSSM

In the MSSM the EW scale (at large $\tan\beta$) is given by the expression

$$\frac{M_Z^2}{2} = -m_{H_u}^2 - \mu^2 \ , \tag{4.1}$$

at tree-level. For naturalness to be preserved, we would want both terms to be of the order of the EW scale otherwise large cancellations would have to occur. It is possible that these terms are much larger than the EW scale and some underlying fundamental theory dictates the cancellations to take place. In this case the fine-tuning has to be checked at the radiative level to make sure that this cancellation is not ruined by large loop corrections to the soft parameters of the theory. This situation is present in models like the pUMSSM where the D-term contributions to the soft parameters can be dominant at tree-level and thus destabilize the EW scale. For this reason one could attribute the occurring cancellation to a fundamental theory as mentioned above and consider worrisome the fine-tuning stemming from the radiative corrections to the left-hand side of the EW stability equation. In the MSSM one can define the fine tuning in the Higgs potential according to the Kitano-Nomura definition [106] where

$$\Delta_h = \frac{\delta m_{H_u}^2}{(m_h^2/2)} \ . \tag{4.2}$$

Here $\delta m_{H_u}^2$ denotes the radiative corrections to the soft supersymmetry breaking mass $m_{H_u}^2$. A similar definition measures the fine-tuning in the EW scale using eq.(4.1) and

thus normalizing with respect to the Z mass and not the Higgs mass, i.e.

$$\Delta_Z = \frac{\delta m_{H_u}^2}{(M_Z^2/2)} \ . \tag{4.3}$$

Note that the second term does not receive large corrections due to the fact that μ^2 is a supersymmetry preserving parameter and thus its beta function is proportional to the parameter itself [124]. For this reason the tree-level contributions from the Higgsino mass parameter μ^2 to the fine-tuning are always larger than the radiative corrections $\delta(\mu^2)$, since the beta function of μ^2 is small. In general in the absence of fine-tuning one would require that the radiative corrections of each term in the right-hand side of eq.(4.1) to be of the order of the EW scale and define the measure as

$$\Delta = \max_i \frac{|B_i|}{(M_Z^2/2)} \ , \tag{4.4}$$

with $B_i = \delta m_{H_u}^2$, $\delta\mu^2$, $m_{H_u}^2|_{tree}$, $\mu^2|_{tree}$. At the loop level the contributions to the fine-tuning from $\delta m_{H_u}^2, \delta\mu^2$ are suppressed by the ratio of the logarithm to the loop factor $\ln(\Lambda/1 \text{ TeV})/16\pi^2$. Therefore, the tree-level contribution of μ^2 is much larger than the radiative corrections of these two terms, see above. For this reason naturalness criteria imposes stringent bounds on the Higgsinos which as we will see later have to be lighter than $\mu \leq 200$ GeV [12, 14, 136]. Combining this with the LEP bound on charginos which translates to a lower bound on the Higgsino mass parameter μ we have 100 GeV $\leq \mu \leq$ 200 GeV, which is a rather restricted range, leaving not much room for natural models. The Barbieri-Giudice measure proposed in [19, 61] applies to UV- complete models and is not suitable for measuring the fine-tuning from low-energy EW input alone. Other measures useful for these types of models have been proposed in [8] and have been applied to superstring inspired models like the E_6SSM in [7]. In [10, 11, 12, 15] the authors have proposed a new model independent measure of EW fine-tuning Δ_{EW} suitable for low-energy effective theories valid up to a messenger scale Λ close to $M_{\rm SUSY}$. This measure is similar but not the same as the Kitano-Nomura measure [105, 106] and contains no information about any possible high-scale origin. In the study [14] the authors compare different fine-tuning measures with the new measure of the electroweak fine-tuning Δ_{EW} presenting advantages and caveats for these measures. As noted in [14] a low-energy EW fine-tuning measure does not necessarily mean that the model is not fine tuned and represents the minimal fine tuning that is present in the weak scale spectrum of the supersymmetric theory. A large fine tuning at the weak scale would imply that the theory will be fine tuned. The existence of areas of low EW fine-tuning would motivate the likelihood of an underlying high-scale theory which also exhibits low values of fine tuning. In the following chapters

we will explore if a low-scale Z' model can have low values of fine tuning and motivate the construction of high-scale complete models based on the naturalness criterion. An extensive list of references is available for the MSSM [11, 12, 13, 15] and the NMSSM [72, 83, 100], but only a few attempts have been made to calculate the fine tuning in Z' models [7, 101]. In the MSSM as we discussed earlier at tree-level the largest contribution to the fine tuning comes from μ^2 which leads to the following Higgsino upper limit [136],

$$\mu \lesssim 190 \text{ GeV} \left(\frac{m_{h^0}}{120 \text{ GeV}}\right) \left(\frac{\Delta_\mu^{tree}}{5}\right)^{1/2} . \tag{4.5}$$

For $\Delta_\mu = 5$ and $m_h \sim 125$ GeV the upper bound on the Higgsinos will be $\mu \lesssim 200$ GeV as stated before. Due to different definitions of the fine tuning measure if one uses eq.(4.3) will get a stringent bound for the same amount of fine tuning, due to the fact that $M_Z = 91.2$ GeV is lighter than the observed Higgs mass $m_{h^0} \simeq 125$ GeV

$$\mu \lesssim 144 \text{ GeV} \left(\frac{\Delta_\mu^{tree}}{5}\right)^{1/2} \xrightarrow{\Delta_\mu=5} \mu \lesssim 144 \text{ GeV} . \tag{4.6}$$

In order to "match" the two different definitions so that we are getting approximately the same limits we would have to accept larger value for the absence of fine tuning in the latter case $\Delta_\mu = 10$. The smallness of the quartic coupling in the MSSM

$$\lambda = \frac{1}{8}(g_1^2 + g_2^2)\cos^2 2\beta , \tag{4.7}$$

requires large radiative corrections so that the tree-level Higgs mass is lifted up to the observed value of $m_{h^0} \approx 125$ GeV. As we have seen earlier, in the MSSM one has [56, 126] (see eq.(1.21))

$$m_{h_0}^2 = M_Z^2 \cos 2\beta^2 + \frac{3g_2^2}{8\pi^2}\frac{m_t^4}{m_W^2}\left[\ln\frac{m_{\tilde{t}_1} m_{\tilde{t}_2}}{m_t^2} + \frac{X_t^2}{m_{\tilde{t}_1} m_{\tilde{t}_2}}\left(1 - \frac{X_t^2}{12 m_{\tilde{t}_1} m_{\tilde{t}_2}}\right)\right] , \tag{4.8}$$

where $X_t = A_t - \mu \cot\beta$ and one can make the approximation $M_{\text{SUSY}}^2 \equiv m_{\tilde{t}_1} m_{\tilde{t}_2} \approx m_{Q_3} m_{T^c}$. This is a one-loop approximate result including only the stop loop effect. From this equation one can easily see that in order for the radiative corrections to be large enough to compensate for the smallness of the tree-level value of the Higgs mass, the stop masses and thus the soft supersymmetry breaking masses m_{Q_3}, m_{T^c} have to be heavy. Furthermore a large mixing X_t is usually necessary, especially if one needs the third generation squarks to be light and maintain a natural spectrum. The question is why stops have to be light from a natural perspective and then how light do they have to be? From eq.(4.2) we see that at the loop level the fine-tuning responsible in the MSSM is coming from the corrections

to the soft mass of the Higgs up doublet $m^2_{H_u}$. The beta function of $m^2_{H_u}$ in the MSSM at 1-loop level is given by [124]

$$\begin{aligned}\beta^{(MSSM,1)}_{m^2_{H_u}} &= 6|y_t|^2(m^2_{H_u}+m^2_{Q_3}+m^2_{T^c}+|A_t|^2)-6g_2^2|M_2|^2 \\ &- \frac{6}{5}g_1^2|M_1^2|+\frac{3}{5}g_1^2 S\ .\end{aligned} \tag{4.9}$$

By integrating this equation from a higher scale Λ down to the $M_{\rm SUSY}\sim 1$ TeV where the stop masses exist and neglecting the gauge terms, which are small if the gaugino masses are not extremely heavy, [1] we will have

$$\delta m^2_{H_u} = -\frac{-3y_t^2}{8\pi^2}(m^2_{Q_3}+m^2_{T^c}+|A_t|^2)\ln\frac{\Lambda}{M_{\rm SUSY}}\ . \tag{4.10}$$

Here Λ is the scale where the soft masses are generated (not the scale at which SUSY is broken) and it can be as high as the GUT scale or a much lower scale $\mathcal{O}(10-100)$ TeV. This is the scale at which a hidden soft supersymmetry breaking sector starts to communicate through interactions with the visible sector, and is usually called the messenger scale M_{mess} [32]. It is clear from the above equation that due to the large top Yukawa coupling the effect of the stop soft masses and thus the top squarks to the fine tuning is substantial. Large stop masses needed to elevate the Higgs mass to the observed value and maximal mixing X_t will drive the fine tuning measure to large values. Furthermore if the logarithm associated with the scale Λ at which the underlying theory transmits the SUSY breaking sector to the visible sector, is large the fine-tuning can be significantly enhanced. For $\Lambda = M_{GUT}\sim(10^{15}-10^{16})$ GeV this logarithm is of the order of 30, but if a lower messenger scale is assumed like in gauge mediation scenarios the logarithm is reduced to $2.4-4.6$. In the case of GUT motivated theories, SUSY is broken radiatively by running the RGEs from the GUT scale down to the EW scale and due to these large logarithms the fine tuning will be always enhanced [20, 68]. This is the origin of the large coefficients in the solutions of the RGEs. Considering low mediation scale alleviates this problem and relaxes the fine tuning [105, 106, 136]. From this observation using eq.(4.10),(4.2) we can extract some useful information about the stop masses in a natural supersymmetric spectrum

$$\sqrt{m^2_{\tilde{t}_1}+m^2_{\tilde{t}_2}}\lesssim 625\ \text{GeV}\frac{\sin\beta}{(1+\overline{X}_t^2)^{1/2}}\left(\frac{3}{\ln\frac{\Lambda}{M_{\rm SUSY}}}\right)^{1/2}\frac{m_{h^0}}{125\ \text{GeV}}\left(\frac{\Delta_h}{5}\right)^{1/2}\ , \tag{4.11}$$

[1] We will see that in order to interpret collider search results using `Fastlim` the gaugino masses have to be heavy

where $\overline{X}_t = |A_t|/\sqrt{m^2_{\tilde{t}_1} + m^2_{\tilde{t}_2}}$. For $\Delta = 5$, $\tan\beta = 10$, a Higgs mass of 125 GeV and a low-scale mediation $\Lambda = 10$ TeV we get an upper limit to the stops and sbottoms

$$m_{\tilde{t}_1,\tilde{b}_1} \lesssim 700 \text{ GeV} , \tag{4.12}$$

for high-scale models where $\Lambda = M_{\text{GUT}}$ it is easy to see that the limits are becoming even more stringent

$$m_{\tilde{t}_1,\tilde{b}_1} \lesssim 200 \text{ GeV} . \tag{4.13}$$

Defining the fine-tuning measure with respect to the Z mass as in eq.(4.3) the corresponding equations would read[2]

$$\sqrt{m^2_{\tilde{t}_1} + m^2_{\tilde{t}_2}} \lesssim 450 \text{ GeV} \frac{\sin\beta}{(1+\overline{X}^2_t)^{1/2}} \left(\frac{3}{\ln\frac{\Lambda}{M_{\text{SUSY}}}}\right)^{1/2} \frac{M_Z}{91.2 \text{ GeV}} \left(\frac{\Delta_Z}{5}\right)^{1/2} , \tag{4.14}$$

and the upper bounds on the third-generation squarks translate into the tighter ones below

$$m_{\tilde{t}_1,\tilde{b}_1} \lesssim 500 \text{ GeV} . \tag{4.15}$$

If we assume that $m_{\tilde{t}_1}, m_{\tilde{t}_2} \approx m_{Q_3} = m_{T^c}$ then this upper limit corresponds to $m_{Q_3} \approx 360$ GeV for $X_t = 0$. Comparing the two eq.(4.11),(4.14) to get the same limits we see that $\Delta_h/\Delta_Z \approx (1.4)^2 \approx 2$. Relaxing the requirement of fine-tuning absence to $\Delta_Z = 10$ we retrieve the previous limit of $m_{\tilde{t}_1} \lesssim 700$ GeV for the stop masses when we consider a light messenger scale. The gluino mass parameter can also be constrained in the same manner since it contributes the Higgsino mass parameter at 2-loop level through its contribution to the stop soft masses at 1-loop [136]. We can then write down the following relationship for the gluino mass

$$|M_3| \lesssim 904 \text{ GeV} \cdot \sin\beta \cdot \frac{m_{h^0}}{125 \text{ GeV}} \left(\frac{\Delta_h}{5}\right)^{1/2} \left(\frac{3}{\ln\frac{\Lambda}{M_{\text{SUSY}}}}\right)^{1/2} . \tag{4.16}$$

Using the same rationale one can derive similar inequalities for the other gaugino masses M_1, M_2 with the wino being much more constrained due to the large coefficient with which it enters the 1-loop RGEs in eq.(4.9). It is clear from the above discussion that in the MSSM the heavier the higher scale Λ the larger the fine tuning one can expect. In an effort to compare the fine tuning expected in the minimal scenario to the fine tuning one can have in $U(1)'$ gauge extensions we will use as higher scale $\Lambda \sim 10^{15}$ GeV. Although a small logarithm can provide a quick "fix" in the case of MSSM reducing the nominal amount of fine tuning, the same solution is not working in the case of pUMSSM. The

[2] we explicitly write the Z mass to remind the reader of the different definition of Δ_Z

extra D-terms entering the minimization conditions drive the Higgs soft mass parameters to large values at tree-level, in turn contributing to the fine tuning. In other words, as we can see from the definition of the fine tuning in eq.(4.4), the tree-level soft masses will be dominant over the loop contributions and thus determine the fine tuning of the model. This means that we can no longer extract meaningful information for high-scale scenarios and most importantly we are unable to make use of a possible large Higgs quartic in the case of pUMSSM in order to improve fine tuning. This is going to become clearer in the following sections.

4.2 Phenomenology and naturalness of MSSM

In this study we re-interpret data from LHC collider searches for supersymmetric particles using the program `Fastlim` [137]. The spectrum is calculated with `SARAH` and `SPheno` at one-loop level for all scalars and at two-loops for the Higgs sector. `Fastlim` reconstructs the visible cross section for a given event topology by taking into account the contributions of the relevant simplified event topologies and thus without the need of running Monte Carlo simulations. We have created an interface that links `Fastlim` to the spectrum generator SPheno from which `Fastlim` reads all the information about the masses of the particles and the branching ratios of the decays which enter the calculation of the contributing event topologies. It is important to note that `Fastlim`'s power to reconstruct the visible cross section for a specific signal region (defined by experimental collaborations) is limited by the existence of the pre-calculated efficiency tables ϵ_i for every implemented topology i. The efficiency of an event topology is multiplied by its cross section and the integrated luminosity in order to generate the number of events for every contribution to the total number of events. When the efficiency of a contributing topology is absent then the number of events cannot be calculated and thus the total number of events is going to be underestimated. Therefore if a topology has not been implemented for this scenario then the program can only provide limits with small coverage which translates to an underestimation of the visible cross section. For this reason the results must be interpreted with caution bearing in mind that for complicated scenarios the limits can only be conservative. The program is rather successful for models with a natural spectrum i.e. for theories where the lightest SUSY particles are the third generation squarks, the Higgsinos, and the gluinos. In order to achieve large coverage well above $(90-95)\%$ the wino and bino masses have to be a few TeV and the gluino mass has to be around 2 TeV.

Throughout this paper the first and second family squark soft masses are assumed to be

Name	Short description	E_{CM}	$\mathcal{L}_{\text{int}}$	# SRs	Ref.
AC2013024	0 lepton + (2 b-)jets + MET [Heavy stop]	8	20.5	3	[2]
AC2013035	3 leptons + MET [EW production]	8	20.7	6	[1]
AC2013037	1 lepton + 4(1 b-)jets + MET [Medium/heavy stop]	8	20.7	5	[3]
AC2013047	0 leptons + 2-6 jets + MET [squarks & gluinos]	8	20.3	10	[46]
AC2013048	2 leptons (+ jets) + MET [Medium stop]	8	20.3	4	[43]
AC2013049	2 leptons + MET [EW production]	8	20.3	9	[41]
AC2013053	0 leptons + 2 b-jets + MET [Sbottom/stop]	8	20.1	6	[42]
AC2013054	0 leptons + $\geq$ 7-10 jets + MET [squarks & gluinos]	8	20.3	19	[44]
AC2013061	0-1 leptons + $\geq$ 3 b-jets + MET [3rd gen. squarks]	8	20.1	9	[47]
AC2013062	1-2 leptons + 3-6 jets + MET [squarks & gluinos]	8	20.3	13	[45]
AC2013093	1 lepton + bb(H) + Etmiss [EW production]	8	20.3	2	[40]

Table 4.1: The analyses available in `Fastlim` version 1.0 [137]. The units for the centre of mass energy, E_{CM}, and the integrated luminosity, $\mathcal{L}_{\text{int}}$, are TeV and fb^{-1}, respectively. The number of signal regions in each analysis and the references are also shown. Note that we use a concise name for every ATLAS conference note.

of the order of 3 TeV. Although in recent studies authors [15] have found that non-universal gaugino masses with a hierarchy $M_1, M_2 > M_3$ lead to points of the parameter space with reduced EW fine tuning, this can only be due to the fact that heavy gaugino masses create cancellations within the beta function of $m^2_{H_u}$ which contradicts the assumptions of previous studies where the gaugino terms are considered very light and thus are omitted from the calculation of the fine tuning. The cancellations due to the heavy wino and bino masses Ref.[15] seem to create the right amount of cancellation against the heavy third generation soft masses of the top squarks in the MSSM, which are needed in order to achieve a Higgs mass around 125 GeV. Since in the pUMSSM, as we will see later on, the soft masses of the left-handed and right-handed stops can be substantially lighter than in the minimal scenario this would mean that heavy gauginos would dominate the fine tuning. In other words in order to get low fine tuning in these extended scenarios the cancellation needed from the gaugino sector would be much smaller, making the need of light gauginos preferable from a naturalness perspective of the theory. Furthermore if gaugino masses

are light this would mean that the lightest neutralino $\tilde{\chi}_1^0$ would now have a sizeable bino $\tilde{B}$ and wino $\tilde{W}$ component reducing its Higgsino $\tilde{H}_u, \tilde{H}_d$ component. This reduces the branching ratios $BR(\tilde{t}_1 \to t\tilde{\chi}_1^0)$ of the lightest top squark decaying into the top and the lightest neutralino, making it easier to mask itself against collider searches.

The experimental analysis available in `Fastlim` are shown in Table 4.1 from Ref.[137]. In the case of light top squarks (bottom squarks) the relevant ATLAS searches which are expected to impose the most stringent constraints are the following: 1) AC2013024 2) AC2013053 3) AC2013037 4) AC2013048. In these experimental studies the main production mechanism of the top superpartner is considered to be the direct pair production mechanism $pp \to \tilde{t}_1 \tilde{t_1}^*$. The two scalar particles are decaying subsequently either into their top fermionic partner and the lightest neutralino ($\tilde{t}_1 \to t\ \tilde{\chi}_1^0$) or into a bottom quark and the lightest chargino ($\tilde{t}_1 \to b\ \tilde{\chi}_1^\pm$). In the latter case the chargino decays into a virtual W boson and the lightest neutralino resulting in the 3-body decay ($\tilde{t}_1 \to b\ W\tilde{\chi}_1^0$). Strong assumptions have been made from the experimental collaborations on the mixings and couplings (e.g. $BR(\tilde{t}_1 \to t\ \tilde{\chi}_1^0) = 1, BR(\tilde{t}_1 \to b\ \tilde{\chi}_1^\pm) = 1$) of the decaying particles in order to set strict bounds on the masses of the superpartners. The truth is that in

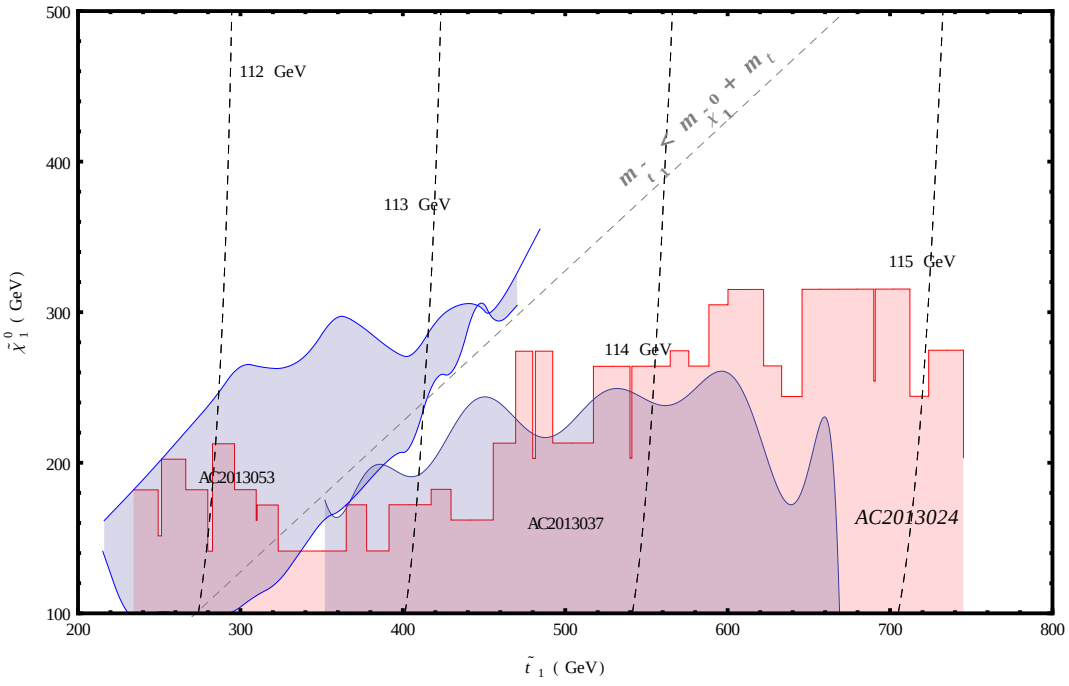

Figure 4.1: Exclusion regions on the $(\tilde{\chi}_1^0, \tilde{t}_1)$ mass plane for the three ATLAS searches: AC2013024 (red shaded area) AC2013053 (light blue shaded area on the left) AC2013037 (light blue shaded area on the right). Contributions from the other searches have not been included in this plot. The coverage for this plot we get with `Fastlim` is nearly 100%

any realistic scenario this bounds tend to be weakened since these assumptions cannot be fully matched most of the time. To get strong constraints from these collider searches and extract meaningful results we need to "simulate" the experimental assumptions. Therefore for the purpose of imposing constraints from collider searches using `Fastlim` we are bound to assume that the wino and bino masses have to be relatively heavy compared to the Higgsino mass parameter μ which has to be light in the MSSM for naturalness reasons. This way the lightest neutralino $\tilde{\chi}_1^0$, in this scenario appears mostly in a Higgsino state $\tilde{H}_u, \tilde{H}_d$ leading to an enhanced branching ratio for the decay channel $BR(\tilde{t}_1 \to t\ \tilde{\chi}_1^0)$ due to the large top Yukawa coupling $y_t \tilde{t}_R^* t_L \tilde{H}_u^0$ or $y_t t_R^* \tilde{t}_L \tilde{H}_u^0$. If the stop mixing is large by setting $m_{Q_3} \sim m_{T^c}$ then the branching ratios are expected to be small, but if there is a large hierarchy between the soft masses which will result in small mixing then the branching ratios are expected to become largish leading to stronger constraints. When this channel is closed due to kinematic reasons the decay of the top scalar superpartner into a bottom quark and a chargino becomes dominant $BR(\tilde{t}_1 \to b\ \tilde{\chi}_1^\pm) = 100\%$ in this scenario.

In Fig. 4.1 we have plotted the three dominant exclusion regions of the lightest top squark mass $\tilde{t}_1$ with respect to the mass of the lightest neutralino $\tilde{\chi}_1^0$. We have created a grid of 6161 points assuming that the soft masses of the stops have a mass hierarchy with 340 GeV $\leq m_{Q_3} \leq$ 1200 GeV and $m_{T^c} = 2.8$ TeV, the Higgsino mass parameter μ runs between 100 GeV $\leq \mu \leq$ 800 GeV where the lower bound comes from the LEP bound on the lightest chargino. The soft trilinear couplings of the top and bottom squarks are taken to be $T_t = y_t A_t = 100$ GeV, $T_b = 1$ TeV in order to avoid tachyonic masses for very small values of m_{Q_3}. The 3-shaded areas correspond to the ATLAS searches AC2013024, AC2013037, AC2013053 as shown in the plot. For masses of the lightest neutralino $\tilde{\chi}_1^0$ less than around 300 GeV the mass of the lightest stop is excluded up to 750 GeV at 95% CL. Note that for stop masses around 750 GeV the lightest Higgs mass is not much heavier than 115 GeV. The Higgs mass contours (black dashed lines) are almost parallel to the neutralino axis, showing no significant dependence on the mass of the lightest Higgsino-like neutralino.

The ATLAS search AC2013053 is predominantly looking at the topology $pp \to \tilde{t}_1 \tilde{t}_1^*$ where the stops decay into a bottom quark and the lightest chargino $\tilde{t}_1 \to b\tilde{\chi}_1^\pm$. The chargino decays subsequently into a virtual W boson and the lightest neutralino $\tilde{\chi}_1^\pm \to W\tilde{\chi}_1^0$ with the signal regions defined by two b-jets and missing transverse energy $\not{E}_T$ (MET). The lightest chargino and the lightest neutralino are considered to have small mass splitting. As we see in Fig. 4.1 this topology excludes mostly the points in the region where the decay

of the lightest stop into the top and the lightest neutralino $\tilde{t}_1 \to t\tilde{\chi}_1^0$, is kinematically forbidden. Since the two topologies $\tilde{t}_1 \to t\tilde{\chi}_1^0$ and $\tilde{t}_1 \to b\tilde{\chi}_1^\pm$ are characterized by identical final state products which consist of either 2 b-jets + 2-leptons + $\not{E}_T$ or 2 b-jets + 4-jets + $\not{E}_T$ the program reconstructs the number of events using the kinematically allowed topology and thus excludes points residing in either side of the line $m_{\tilde{t}_1} < m_{\tilde{\chi}_1^0} + m_t$. This is especially relevant for the exclusion region that we obtain from the ATLAS search AC2013024 which assumes that the top squark is decaying exclusively to a top and the lightest neutralino. This decay is not allowed above the line $m_{\tilde{t}_1} < m_{\tilde{\chi}_1^0} + m_t$ but the program uses the kinematically allowed topology which has the same final state products to reconstruct the visible cross section and set limits. These points as we see on the plot are overshadowed by the AC2013053 analysis which is specifically designed to work well in this region since the rate of the decay $\tilde{t}_1 \to b\tilde{\chi}_1^\pm$ is 100%. As the channel $\tilde{t}_1 \to t\tilde{\chi}_1^0$ opens up and the branching ratio $BR(\tilde{t}_1 \to b\tilde{\chi}_1^\pm)$ becomes smaller the analysis AC2013053 becomes less effective. Note that the branching ratio for the topology $\tilde{t}_1 \to t\tilde{\chi}_1^0$ is approximately 50%, while the lightest stop is mostly left-handed since we have chosen a large mass splitting for the soft masses m_{Q_3} and m_{T^c}.

In Fig. 4.2a we show the contours of the lightest CP-even Higgs boson h_1^0 in the MSSM (solid black lines) along with the lightest stop mass contours $\tilde{t}_1$ (red dashed lines) and the collider constraints using `Fastlim` (colour shaded areas). The figure on the right Fig. 4.2b depicts the fine tuning contours for the same scenario. The LHC constraints have now been removed to make the plot more readable. The Higgino mass parameter is $\mu = 105$ GeV, providing a spectrum with nearly degenerate lightest neutralinos $\tilde{\chi}_1^0, \tilde{\chi}_2^0$ and lightest chargino $\tilde{\chi}_1^\pm$. We see that the most stringent constraints come from the searches AC2013024 (blue shaded area), AC2013053 (light yellow shaded area) which exclude stop masses up to 750GeV for zero trilinear coupling $A_t = 0$ i.e. small mixing in the stop sector. The soft masses of the left-handed and right-handed top squarks are considered to be degenerate $m_{Q_3} = m_{T^c}$. The right-handed sbottom soft mass is taken to be quite heavy around $m_{B^c} \approx 3$ TeV like the other heavy particles in the spectrum. The green shaded area corresponds to the ATLAS search AC2013037 while the red and black shaded area correspond to the searches AC2013048 and AC2013093, respectively. Note that the latter experimental ATLAS study AC2013093 gives some exclusion points since it has the same signature 1-lepton+2-b jets+ $\not{E}_T$ with the green shaded region. The gray area corresponds to the region where the spectrum results in tachyonic masses. From this plot we see that the Higgs mass of around 125 GeV resides well above the current experimental limits,

Fig. 4.2b on the right shows the fine tuning contours for this MSSM scenario using low-energy information. As we can see the points of lowest fine tuning for a Higgs mass between 124 GeV $\leq m_{h_1^0} \leq$ 127 GeV is approximately $\Delta_Z \sim 1.13 \times 10^3$. This is consistent with what other authors find when studying high-scale models and calculate the fine tuning doing broad scans Ref.[14, 15].

(a) LHC constraints (b) Fine tuning contours

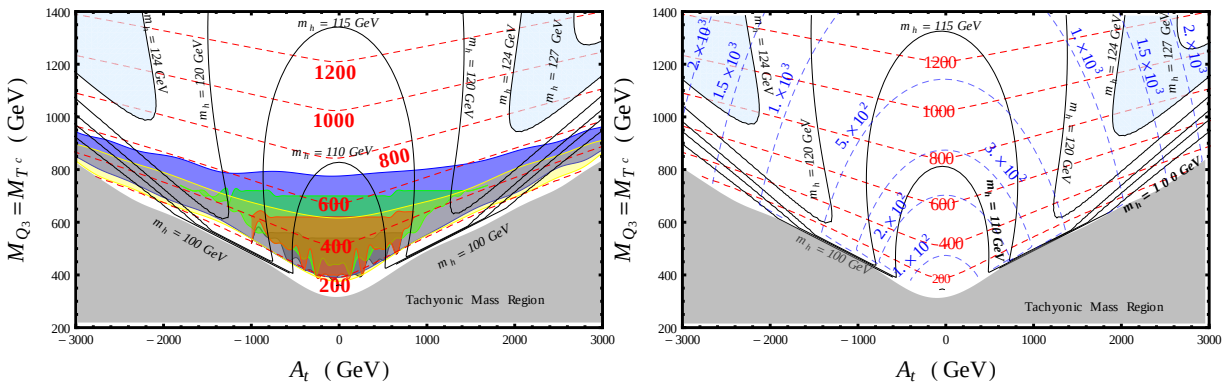

Figure 4.2: Here we plot the lightest CP-even Higgs mass contours h_1^0 (solid black lines), the lightest stop mass contours $\tilde{t}_1$ (red dashed lines, in units of GeV) in the MSSM with: Fig. 4.2a the LHC constraints from various ATLAS searches using `Fastlim` and Fig. 4.2b the fine tuning contours. We fix $\tan\beta = 20$ in order to saturate the upper limit of the tree-level Higgs mass in MSSM. Higgsino mass parameter is $\mu = 105$ GeV. The shaded areas correspond to the exclusion regions from the following ATLAS studies: AC2013024 (blue) AC2013053 (yellow) AC2013037 (green) AC2013048 (red) and AC2013093 (black).

The plot shows that in order to achieve the observed Higgs mass $m_{h_1^0} \simeq 125$ GeV the soft masses have to be of the order of 1 TeV with large mixing, $A_t \simeq 2$ TeV, and corresponds to the schematic representation of our previous analytic discussion on the origin of the fine tuning in the MSSM. As we have anticipated for large mixing in the stop sector $A_t \simeq 2$ TeV the limits set by collider constraints are weakened. The blue region forbids stops up to 750 GeV for zero trilinear coupling but as we increase A_t the stop masses are excluded up to 600 GeV, so the bound is relaxed by around 150 GeV. For large $T_t = 2040$ GeV (and $m_{Q_3} = 0.8$ TeV) soft trilinear coupling the off-diagonal element of the stop matrix, due to the large Yukawa coupling is large, creating maximal mixing between the top squarks. The lightest stop $\tilde{t}_1$ composition is found to be $|R_{11}^{(\tilde{t})}|^2 \sim 0.511$ ($\tilde{t}_L$ component) and $|R_{12}^{(\tilde{t})}|^2 \sim 0.489$ ($\tilde{t}_R$ component). Since the couplings of the top squark depend on the left-handed and right-handed admixture, maximal mixing leads to

reduced branching ratios $BR(\tilde{t}_1 \to t\tilde{\chi}_1^0) \approx 0.35$, $BR(\tilde{t}_1 \to t\tilde{\chi}_2^0) \approx 0.196$ and increased $BR(\tilde{t}_1 \to b\tilde{\chi}_1^\pm) \approx 0.453$ and thus weaker bounds from the relevant topologies used in those studies. For zero trilinear coupling $A_t = 0$ the branching ratios have the values $BR(\tilde{t}_1 \to t\tilde{\chi}_1^0) \approx 0.45$, $BR(\tilde{t}_1 \to t\tilde{\chi}_2^0) \approx 0.435$ and $BR(\tilde{t}_1 \to b\tilde{\chi}_1^\pm) \approx 0.12$ while the left and right-handed component of the lightest top squark is found to be $|R_{11}^{(\tilde{t})}|^2 \sim 0.972$ and $|R_{12}^{(\tilde{t})}|^2 \sim 0.028$, respectively.

(a) LHC constraints (b) Fine tuning contours

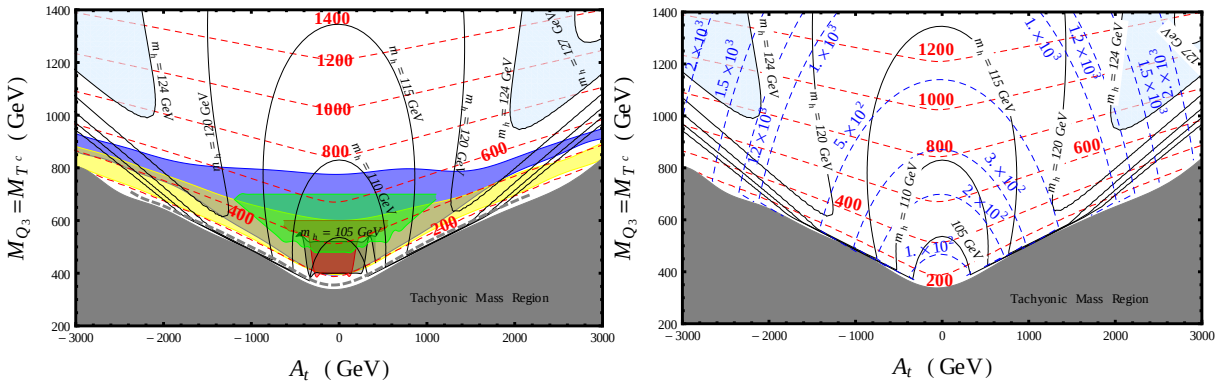

Figure 4.3: The plot shows the lightest CP-even Higgs mass contours h_1^0 (solid black lines), the lightest stop mass contours $\tilde{t}_1$ (red dashed lines, in units of GeV) in the MSSM with: Fig. 4.3a the LHC constraints from various ATLAS searches using `Fastlim` and Fig. 4.3b the fine tuning contours. We fix $\tan\beta = 20$ in order to saturate the upper limit of the tree-level Higgs mass in MSSM. Higgsino mass parameter is $\mu = 150$ GeV. The shaded areas correspond to the exclusion regions from the following ATLAS studies: AC2013024 (blue) AC2013053 (yellow) AC2013037 (green) AC2013048 (red) and AC2013093 (black). Below the gray dashed line $\tilde{t}_1$ becomes lighter than $\tilde{\chi}_1^0$.

In Fig. 4.3 we present the same plot as in Fig. 4.2 but now we have increased the Higgsino mass to $\mu = 150$ GeV. The gray dashed line depicts the line below which the stops become lighter than the lightest neutralino and the spectrum has a charged LSP. The fine tuning contours of course are not changed and they are just shown here for completeness. Notice that the limits set by the blue region are relaxing a bit more for large A_t compared to the previous Figure 4.2 for $\mu = 105$ GeV, but are not yet weakened significantly. In order to see how these experimental constraints depend on the mass of the lightest neutralino which is basically given by the Higgsino mass parameter μ in this scenario, where the other gaugino masses are heavy, we have created Figures 4.4a and 4.4b. The left plot in Fig. 4.4 shows the Higgs mass and the lightest stop mass in the MSSM scenario where the lightest

neutralino is $m_{\tilde{\chi}_1^0} \approx 203$ GeV and we have assumed again degenerate soft masses of the left-handed and right-handed top squarks. Note that the blue region which corresponds to

(a) $\mu = 200$ GeV (b) $\mu = 300$ GeV

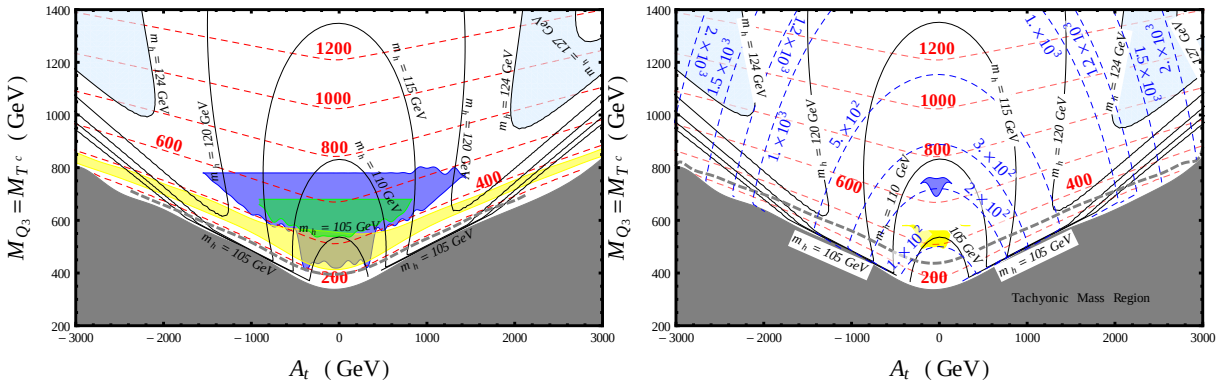

Figure 4.4: Left Figure 4.4a depicts the Higgs mass contours and the lightest stop mass contours (red dashed lines, in units of GeV) along with the experimental limits created with Fastlim, Higgsino mass is fixed at $\mu = 200$ GeV. Right Figure 4.4b contains also the fine tuning contours which are the same for both plots and are only given in the right plot for better visibility. Blue shaded area corresponds to experimental results based on the ATLAS study AC2013024. Similarly, yellow area corresponds to AC2013053 study and green area to AC2013037. Note that since large mixing reduces the $BR(\tilde{t}_1 \to t\tilde{\chi}_1^0)$ points for small A_t is more likely to be excluded.

the limits set against the experimental ATLAS study AC2013024, is truncated compared to Figs. 4.2, 4.3 since for this topology the decay rate of the lightest stop transmuting into the top partner and the $\tilde{\chi}_1^0$ is now smaller $BR(\tilde{t}_1 \to t\tilde{\chi}_1^0) \approx 0.30$ for the same benchmark point at large A_t. On the other hand since the channel $\tilde{t}_1 \to b\tilde{\chi}_1^{\pm}$ becomes more favourable and $BR(\tilde{t}_1 \to b\tilde{\chi}_1^{\pm}) \simeq 0.681$ the ATLAS study AC2013053 still provides exclusion points for large stop mixing. Below the gray dashed line the stops become lighter than the LSP in case we have heavy wino and bino masses. Lighter gaugino masses as argued earlier would change the composition of the lightest neutralino and make things more complicated. The LSP ($\tilde{\chi}_1^0$) could also be much lighter avoiding charged LSP but this observation is not so important since the observed Higgs mass is rather heavy. For Higgsino mass $\mu = 300$ GeV it is clear that the limits become very weak. In this case the reconstructed visible cross section is very small and only a few points are excluded for $A_t = 0$.

Now it would be interesting to see how the Higgs, the stop mass and the LHC constraints are modified in the case of non-degenerate soft masses $m_{Q_3} \neq m_{T^c}$. In Figs. 4.5, 4.6 we

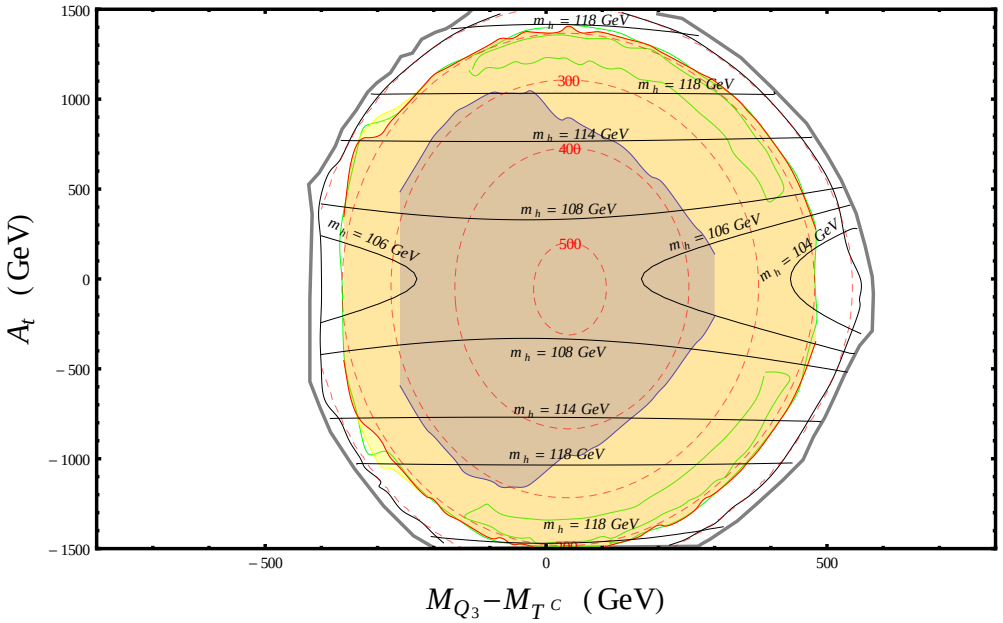

Figure 4.5: In this plot we fix the fine tuning coming from the stop masses by setting $\sqrt{m_{Q_3}^2 + m_{T^c}^2} = C = 600\sqrt{2}$ GeV and varying the difference $X = m_{Q_3} - m_{T^c}$ between the soft mass parameters. The Higgs mass contours are shown by the black lines and stop masses by the red dashed contours. The green, red ,blue shaded areas represent the limits from the searches AC2013024, AC2013053, AC2013037, respectively. The lightest neutralino $\tilde{\chi}_1^0$ is Higgsino like and $\mu = 105$ GeV fixed.

fix the fine tuning coming from the soft masses by setting their sum of the squares to a constant value i.e. we define in eq.(4.10) $m_{Q_3}^2 + m_{T^c}^2 = C^2$. The soft trilinear coupling is a free parameter along with the difference between the left-handed soft mass of the third generation squarks and the right-handed stop mass $X = m_{Q_3} - m_{T^c}$. From these two equations we can express the soft masses as a function of the fixed value C and the difference of the soft masses X, $m_{Q_3} = (X + \sqrt{2C^2 - X^2})/2$, $m_{T^c} = (-X + \sqrt{2C^2 - X^2})/2$. Note that this is the only acceptable solution which results in positive soft mass parameters. In these plots the fine tuning will now depend only on the trilinear soft coupling A_t (y-axis) and therefore it will increase as we move away from the center of the graph while staying constant as we move parallel to the change of the X values (x-axis). In Fig. 4.5 we choose a moderate value $C = 600\sqrt{2}$ GeV and we create a grid of 8181 points where we vary -800 GeV $\leq X \leq 800$ GeV and -1.5 TeV $\leq T_t \leq 1.5$ TeV with a step size 20 GeV and 30 GeV, respectively. The white region outside the solid gray contour gives tachyonic masses and it is excluded. The red dashed lines correspond as in previous

graphs to the mass of the lightest top squark while the solid black lines depict the Higgs mass contours. We present LHC constraints coming from the following ATLAS searches: AC2013024 (green region), AC2013053 (red region) AC2013037 (blue region). As one would expect the Higgs mass even for maximal mixing in the stop sector is not capable of reaching the observed LHC Higgs mass window. The lightest stop ($\tilde{t}_1$) contours form homocentric circles roughly around the point $(X, A_t) = (43, -57)$ GeV and their eigenvalue reduces as we move away from the center of the graph. Large mixing A_t creates large splitting between the eigenvalues of the two top squarks while a large mass difference between the two soft parameters m_{Q_3}, m_{T^c} leads to a hierarchy of the diagonal matrix elements in the stop sector, splitting the two stops even for zero mixing in the off-diagonal element. The strongest constraint is coming again from the ATLAS study AC2013024 which excludes all the points for stop masses lighter than (500-513) GeV. Note that `Fastlim` cannot exclude the points for very light stop masses $m_{\tilde{t}_1} < 180$ GeV. These points are in principle excluded by older LEP analyses Ref. [17, 140]. The mass of the lightest bottom squark $\tilde{b}_1$ will vary as we move parallel to the x-axis but it is not affected by the trilinear coupling of the top squark A_t and thus has to remain constant across the y-axis. At the point $(X, A_t) = (-300, 0)$ GeV (ref. point **A**), since X is negative and consequently $m_{Q_3} < m_{T^c}$, the lightest top squark $m_{\tilde{t}_1} = 275$ GeV is mostly left-handed $\tilde{t}_1 \sim \tilde{t}_L$ and appears slightly heavier than the bottom squark $m_{\tilde{b}_1} = 244$ GeV. This is because the left-handed stop mass $m_{\tilde{t}_L}$ is boosted by the top quark mass resulting in a spectrum with the sbottom being the lightest squark. As we move to the right side of the plot m_{Q_3} increases gradually until it becomes equal to the right-handed soft mass m_{T^c} at $X = 0$ and then it becomes larger for all $X > 0$. Since the right-handed sbottom mass parameter $m_{B^c} \simeq 3$ TeV is relatively very heavy, the lightest sbottom will always be mostly left-handed $\tilde{b}_1 \sim \tilde{b}_L$ and will increase in mass as we move to the right. For $(X, A_t) = (0, 0)$ GeV (**B**) the masses of the lightest third generation squarks are found to be $m_{\tilde{t}_1} = 513$ GeV and $m_{\tilde{b}_1} = 498$ GeV and at the point $(X, A_t) = (440, 0)$ GeV (**C**) we have $m_{\tilde{t}_1} = 241$ GeV, $m_{\tilde{b}_1} = 716$ GeV. The stop $\tilde{t}_1$ is mostly left-handed at point (**B**) and it becomes mostly right-handed $\tilde{t}_1 \sim \tilde{t}_R$ at point (**C**). It is interesting to see the implications of these observations on the phenomenology. At the reference point (**A**) the production cross section $\sigma(pp \to \tilde{b}_1\tilde{b}_1^*) \approx 6369$ fb (**@**8 TeV) dominates over the stop pair production cross section $\sigma(pp \to \tilde{t}_1\tilde{t}_1^*) \approx 3259$ fb and therefore a large contribution to the number of events comes from the topology where the sbottom decays into a bottom quark and a neutralino with a rate $BR(\tilde{b}_1 \to b\tilde{\chi}_1^0) \simeq 0.51$. The other contribution comes from the decay of the stop into a bottom quark and a lightest

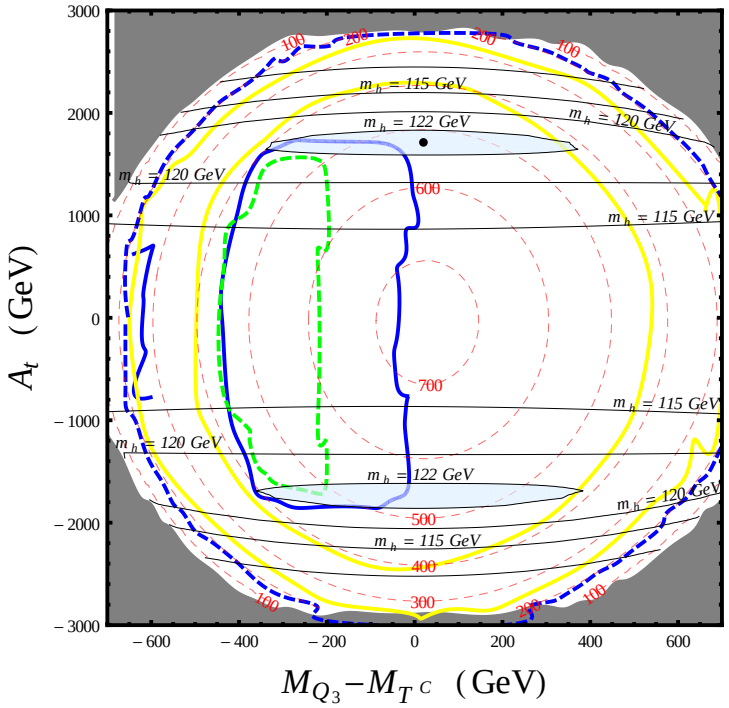

Figure 4.6: In this plot we fix the fine tuning coming from the stop masses by setting $\sqrt{m_{Q_3}^2 + m_{T^c}^2} = C = 800\sqrt{2}$ GeV and varying the difference $X = m_{Q_3} - m_{T^c}$ between the soft mass parameters. The Higgs mass contours are shown by the black lines and stop masses by the red dashed contours. The area inside the yellow (AC2013053), blue (AC2013024) and green (AC2013037) contours is excluded by the respective ATLAS searches shown in the parentheses. The lightest neutralino $\tilde{\chi}_1^0$ is Higgsino like and $\mu = 200$ GeV fixed. The gray region corrsponds to tachyonic masses and outside the blue dashed line the stops become ligher than the neutralino.

chargino with rate $BR(\tilde{t}_1 \to b\tilde{\chi}_1^{\pm}) = 1$ followed by $BR(\tilde{\chi}_1^{\pm} \to \tilde{\chi}_1^0 f\bar{f}') = 1$, since the direct decay to a top is kinematically forbidden. Moving to the right see e.g. point (**B**), the stop and sbottom mass increases and the decay to a top quark now becomes possible. The decay rates of $BR(\tilde{t}_1 \to t\tilde{\chi}_1^0) \simeq 0.447$ and $BR(\tilde{b}_1 \to t\tilde{\chi}_1^{\pm}) \simeq 0.875$ become large and the dominant topologies are $\tilde{t}_1\tilde{t}_1^* \to (t\tilde{\chi}_1^0)(t\tilde{\chi}_1^0)^*$ and $\tilde{b}_1\tilde{b}_1^* \to tf\bar{f}'\tilde{\chi}_1^0(tf\bar{f}'\tilde{\chi}_1^0)^*$ with signatures searched by ATLAS studies mentioned on the plot. At the far right point see (**C**) the mass of the stop is very light compared to the sbottom as seen earlier and thus the production cross section $\sigma(pp \to \tilde{t}_1\tilde{t}_1^*) \approx 6776$ fb represents the 99.8% of the total cross section. The top squarks decay exclusively to a bottom quark and a light chargino as in point (**A**). In Fig. 4.6 we have increased the fine tuning coming from the stop soft masses by setting $C = 800\sqrt{2}$ GeV. The maximum Higgs mass now is around $m_{h_1^0} = 122.3$ GeV

and is shown by the black thick dot in the plot. The maximum values of the lightest top and bottom squarks are, respectively $m_{\tilde{t}_1} = 763$ GeV and $m_{\tilde{b}_1} = 1043$ GeV. The general observations derived from Fig. 4.5 apply here. The strongest constraints are coming from the ATLAS searches AC2013024 (blue contour), AC2013053 (yellow disk) and AC2013037 (green contour). The points inside the areas defined by theses contours are excluded. As we can see from the figure the points for which the right-handed stop mass is lighter than the left-handed soft mass of the third generation squarks $m_{T^c} < m_{Q_3}$, are not excluded by any of these analyses implemented in the program (see Table 4.1). The analysis AC2013053 excludes all points inside the yellow band for light stops $\tilde{t}_1$. Inside these yellow band the mass splitting between the squarks $(\tilde{t}_1, \tilde{b}_1)$ and the lightest neutralino $\tilde{\chi}_1^0$ is small and thus the events fall into the signal region B (SRB) of the analysis AC2013053 (for more details see [42]) which is most sensitive in this case. As we have seen previously in Fig. 4.5 moving from the left side of the plot to the right side, the mass of the bottom squark increases gradually as X increases from negative to positive values. Therefore the production cross section $\sigma(pp \to \tilde{b}_1\tilde{b}_1)$ decreases. Fig. 4.7 shows the cross section for the pair production of stops $\tilde{t}_1\tilde{t}_1^*$ (and sbottoms $\tilde{b}_1\tilde{b}_1^*$) using the program NLL-fast as a function of the average mass of the particles.

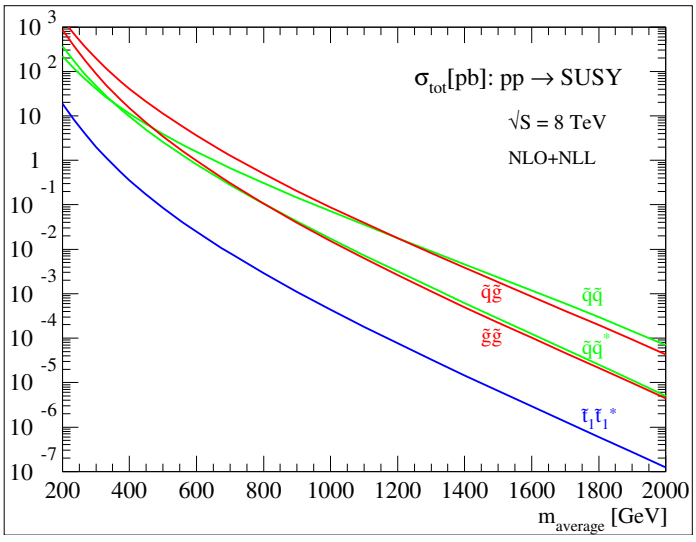

Figure 4.7: Production cross section (NLL+NLO) for various SUSY particles at the center of mass energy of $\sqrt{s} = 8$ TeV using `NLL-fast`. Plot from `NLL-fast` collaboration website Ref. [29, 109, 110]. The errors from the theoretical uncertainties and the parton distribution functions are not shown here. The squark and gluino masses are considered degenerate.

To highlight this we note that at the point with $(X, A_t) = (-600, 0)$ GeV the production cross section of a pair of bottom squarks is found to be $\sigma(pp \to \tilde{b}_1\tilde{b}_1) \approx 3921$ fb while at the point $(X, A_t) = (600, 0)$ GeV on the right side of the plot is $\sigma(pp \to \tilde{b}_1\tilde{b}_1) \approx 0.389$ fb. Combining this with the fact that the stop pair production is maximum at the edges and becomes smaller as we approach the center of the plot, we understand that the total

production cross section for $X > 0$ for the same mass of the lightest top squark $m_{\tilde{t}_1}$, decreases. The point at $(X, A_t) = (400, 0)$ GeV ($\mathbf{B}'$) with $m_{\tilde{t}_1} = 535$ GeV, $m_{\tilde{b}_1} = 938$ GeV has a total production cross section of $\sigma_{tot} = 56$ fb while the point $(X, A_t) = (-400, 0)$ GeV ($\mathbf{A}'$) with $m_{\tilde{t}_1} = 514$ GeV and $m_{\tilde{b}_1} = 497$ GeV has a total production cross section $\sigma_{tot} = 161$ fb. The latter point ($\mathbf{A}'$) is excluded by the experimental search AC2013014 since it is sensitive to the topologies involving the decays $\tilde{b}_1 \to t\tilde{\chi}_1^0$ and $\tilde{t}_1 \to t\tilde{\chi}_1^0$, which give the main contributions to the reconstruction of the visible cross section. The branching ratios are found to be $Br(\tilde{b}_1 \to t\tilde{\chi}_1^0) = 0.862$ and $Br(\tilde{t}_1 \to t\tilde{\chi}_1^0) = 0.434$. On the other hand point ($\mathbf{B}'$) has significantly smaller cross section and thus the two dominant topologies with 1) both stops decaying into $\tilde{t}_1 \to t\tilde{\chi}_1^0$ and 2) one stop decaying into $\tilde{t}_1 \to \tilde{\chi}_1^0$ and the other one into $\tilde{t}_1 \to b\tilde{\chi}_1^+$ give a visible cross section smaller than the observed one by the experimental collaborations and thus not excluded. The fine tuning for the maximum value of the Higgs mass as we can see from Fig. 4.2b is around $\Delta_Z \sim 800$ and we see that in the case where $X > 0$ the SUSY collider searches is possible that they have missed the detection of these particles. It remains to be studied in the future, how these limits are going to be affected at the center of mass energy of $\sqrt{s} = (13, 14)$ TeV or higher. In order to do that one needs a dedicated study using Monte Carlo simulations in order to approximate the efficiencies for each signal region defined by future experimental searches. In Fig. 4.8b we have plotted

(a) Gluino pair production cross section

(b) Stop (sbottom) pair production cross section

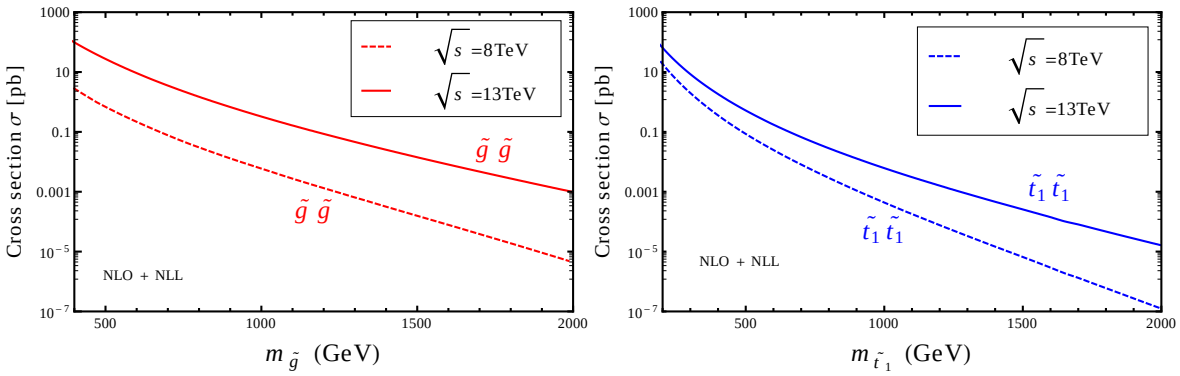

Figure 4.8: Gluino (a) and stop (b) pair production cross section as a function of the mass of the gluino and stop (sbottom) for two different center of mass energies $\sqrt{s} = (8, 13)$ TeV, using tables from LHC SUSY cross section working group. For these simplified topologies the squarks (in left plot) and the squarks (first and second generation) and gluinos (in right plot) are considered to be decoupled from the rest of the spectrum.

the production cross sections for a pair of top squarks $\sigma(pp \to \tilde{t}_1\tilde{t}_1)$ (and sbottoms) as a

function of the mass of the stops $\tilde{t}_1$ (sbottoms) for two different center of mass energies $\sqrt{s} = 8$ TeV and $\sqrt{s} = 13$ TeV. In Fig. 4.8a we show the cross sections for a pair of gluinos. All the other particles are considered to be decoupled which is exactly what we assume in a natural scenario studied with `Fastlim`. For these plots we have used the available cross section tables for simplified topologies from the LHC SUSY cross section working group [108]. The tables have been calculated using the program NLL-fast [29, 109, 110]. In Fig. 4.9 we plot again the lightest stop mass contours $m_{\tilde{t}_1}$ (red dashed contours) and the Higgs mass contours $m_{h_1^0}$ (solid black contours) on the (X, A_t) plane. We fix the fine tuning coming from the stop sector by setting the sum of the squares of the soft masses equal to $C = 1000\sqrt{2}$ GeV. The Higgsino mass parameter is fixed to $\mu = 105$ GeV. The maximum value of the Higgs mass is $m_{h_1^0}^{max} = 124.6$ GeV at the point $(X, A_t) = (40, 2187)$ GeV. The light blue areas around $A_t = \pm 2$ TeV show the region where the Higgs mass is heavier than 124 GeV and lighter than the maximum value $m_{h_1^0}^{max}$. Since the fine tuning in these plots depends only on the soft trilinear coupling of the stop A_t (for fixed C), we have overlaid these figures with the fine tuning curve (dotted blue line) as a function of A_t. The values of the fine tuning for different A_t values and $C = 1000\sqrt{2}$ GeV are given on the top of the plot. As seen in the figure the fine tuning for the blue area where the Higgs mass is around 124 GeV is $1 \times 10^3 \lesssim \Delta_Z \lesssim 1.5 \times 10^3$. For $A_t = 0$ the fine tuning coming only from the soft masses of the third generation squarks is $\Delta_{Z_{(A_t=0)}} \approx 386.5$. A large mixing is needed even for large differences of the soft masses $X = m_{Q_3} - m_{T^c}$ in order to achieve the observed lightest CP-even Higgs mass. The blue solid contour which corresponds to the re-interpretation of the data for the ATLAS experimental search AC2013024 using simplified topologies, excludes in principle, for $X \lesssim -300$ GeV all points for which the lightest stop mass is lighter than $(700 - 730)$ GeV, and for -200 GeV$\lesssim X \lesssim 700$ GeV it excludes points for which the lightest stop is lighter than around $(500-550)$ GeV. As we have argued earlier, we notice that when the difference between the stop masses X increases the experimental constraints become weaker. The maximum value of the lightest bottom squark mass is found to be $m_{\tilde{b}_1} = 1276$ GeV for $X = 700$ GeV while the maximum value of the lightest top squark is $m_{\tilde{t}_1} = 962$ GeV. The yellow contour excludes points where the stop $\tilde{t}_1$ is lighter than around 500 GeV for $X \gtrsim 400$ GeV and lighter than around $(300 - 350)$ GeV when $X \lesssim -550$ GeV, it is based on the ATLAS experimental analysis AC2013053. The dashed green and solid red exclusion curves correspond to the experimental searches AC2013037 and AC2013048, respectively and all the points between the boundaries of these curves and the plot axes are not allowed by these searches. Notice that the green

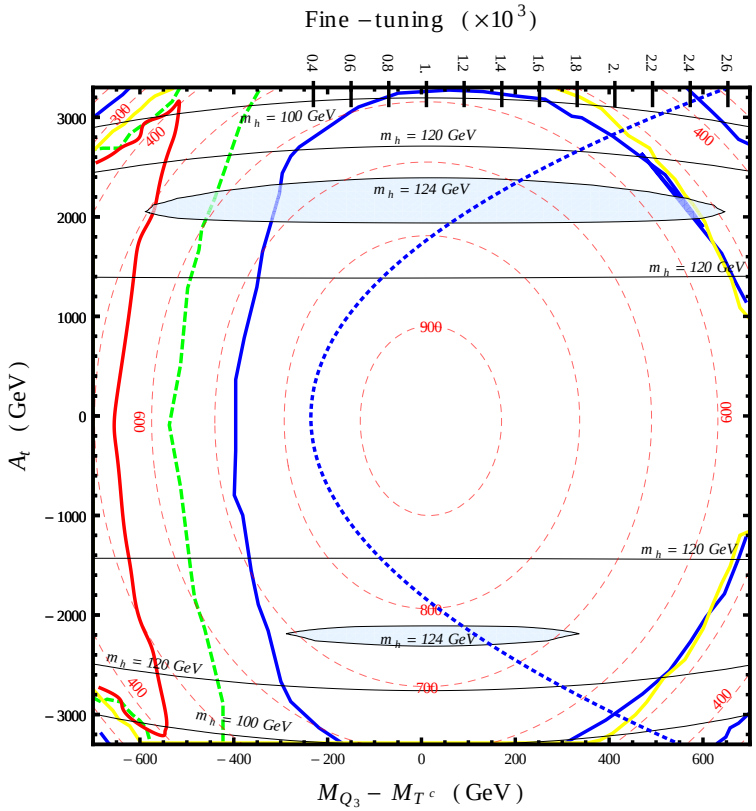

Figure 4.9: In this plot the fine tuning coming from the stop masses is fixed $C = \sqrt{m_{Q_3}^2 + m_{T^c}^2} = 1000\sqrt{2}$ GeV and the Higgsino mass is $\mu = 105$ GeV.The difference $X = m_{Q_3} - m_{T^c}$ between the soft mass parameters is varied. The area outside the closed solid blue (AC2013024) contour is excluded, the area inside the solid red (AC2013048) and dashed green (AC2013037) contours are also excluded by the corresponding experimental analyses given inside the parentheses. The analysis AC2013053 shown by the yellow contours excludes points where the stop masses are lighter than around 550 GeV for $X > 0$ and lighter than 350 GeV for $X < 0$. The dotted blue curve depicts the fine tuning as a function of the soft trilinear coupling A_t, the values are shown on the top of the figure. The Higgs mass and the lightest stop correspond to the solid black and dashed red contours respectively.

curve excludes points for which $m_{\tilde{t}_1} \lesssim (600 - 620)$ GeV and $X \lesssim -500$ GeV. The red curve (AC2013048) provides weak constraints for soft mass differences less than around $X \lesssim -550$ GeV and excludes stop masses lighter than 550 GeV even for very large mixing A_t. At the point **A**(-400,0) GeV in Fig. 4.9, which is excluded only by the blue curve (AC2013024), the main production mechanisms involve the pair production of stops and sbottoms with almost equal probability $\sigma(pp \to \tilde{t}_1\tilde{t}_1) = 6.0$ fb and $\sigma(pp \to \tilde{b}_1\tilde{b}_1) = 6.8$ fb.

The implemented topologies cover the 99.7% of all possible event topologies. The lightest bottom squark is slightly lighter $m_{\tilde{b}_1} = 717$ GeV than the lightest stop $m_{\tilde{t}_1} = 728$ GeV contributing a bit more to the total production cross section σ_{tot}. The dominant event topologies that contribute to the reconstruction of the number of events involve the decays of the sbottom and top squark to a top and the lightest neutralino $\tilde{b}_1 \to t\tilde{\chi}_1^0$ and $\tilde{t}_1 \to t\tilde{\chi}_1^0$. Since in this set up the lightest neutralino $\tilde{\chi}_1^0$ as well as the lightest chargino $\tilde{\chi}_1^\pm$ is mostly Higgsino the branching ratio $BR(\tilde{b}_1 \to t\tilde{\chi}_1^-) \simeq 0.893$ will be large. As we can see from the superpotential term $-u_R^\dagger y_u d_L H_u^+$, the coupling strength of a left-handed bottom squark $\tilde{b}_L$ to a right-handed top quark and a mostly Higgsino chargino will be proportional to the top Yukawa coupling y_t and thus it will be of order one. On the other hand the decay of the lightest sbottom into a bottom quark and the lightest neutralino $\tilde{b}_1 \to b\tilde{\chi}_1^0$ has a small rate $BR(\tilde{b}_1 \to b\tilde{\chi}_1^0) \simeq 0.054$ due to the fact that this coupling is proportional to the bottom Yukawa coupling which is smaller. Therefore such a topology involving this decay will have a small contribution to the number of events. The mixed topology $pp \to \tilde{b}_1\tilde{b}_1 \to (b\tilde{\chi}_1^0)(t\tilde{\chi}_1^0)$ (in `Fastlim` nomenclature `B1bN1_B1tN1`, see Ref. [137]) has a cross section times branching ratio

$$\begin{aligned}
\sigma_1 = \quad & \sigma(\tilde{b}_1\tilde{b}_1) \times BR(\tilde{b}_1 \to t\tilde{\chi}_1^-) \times BR(\tilde{\chi}_1^- \to \tilde{\chi}_1^0 W^-) \times BR(\tilde{b}_1 \to b\tilde{\chi}_1^0) \times 2 \\
= \quad & 6.810 \times 8.93 \cdot 10^{-1} \times 1 \times 5.39 \times 10^{-2} \times 2 \\
= \quad & 0.656 \text{ fb} \,. \qquad (4.17)
\end{aligned}$$

It is worth noting that this is not the only event topology which contributes to the topology with the same final state particles denoted as `B1bN1_B1tN1`. Since the lightest particles in the spectrum have very small mass splitting $m_{\tilde{\chi}_1^\pm} = 108$ GeV, $m_{\tilde{\chi}_1^0} = 106$ GeV, $m_{\tilde{\chi}_2^0} = 109$ GeV, a second possible topology arises which has to be added to the previous one seen above

$$\begin{aligned}
\sigma_2 \quad & = \sigma(\tilde{b}_1\tilde{b}_1) \times BR(\tilde{b}_1 \to t\tilde{\chi}_1^-) \times BR(\tilde{\chi}_1^- \to \tilde{\chi}_1^0 W^-) \times BR(\tilde{b}_1 \to b\tilde{\chi}_2^0) \times \\
& \quad BR(\tilde{\chi}_2^0 \to \tilde{\chi}_1^0) \times 2 \\
= \quad & 6.810 \times 8.93 \cdot 10^{-1} \times 5.25 \times 10^{-2} \times 2 \\
= \quad & 0.639 \text{ fb} \,. \qquad (4.18)
\end{aligned}$$

Adding up the contributions from these two topologies we find that the total contribution for this final state topology $(\tilde{b}_1\tilde{b}_1 \to (b\tilde{\chi}_1^0)(t\tilde{\chi}_1^0))$ is approximately $\sigma_1 + \sigma_2 = 1.29$ fb and therefore does not produce a significant number of reconstructed events. The main contribution to the total number of events thus comes from the topologies $\tilde{b}_1\tilde{b}_1 \to (t\tilde{\chi}_1^0)(t\tilde{\chi}_1^0)$ and

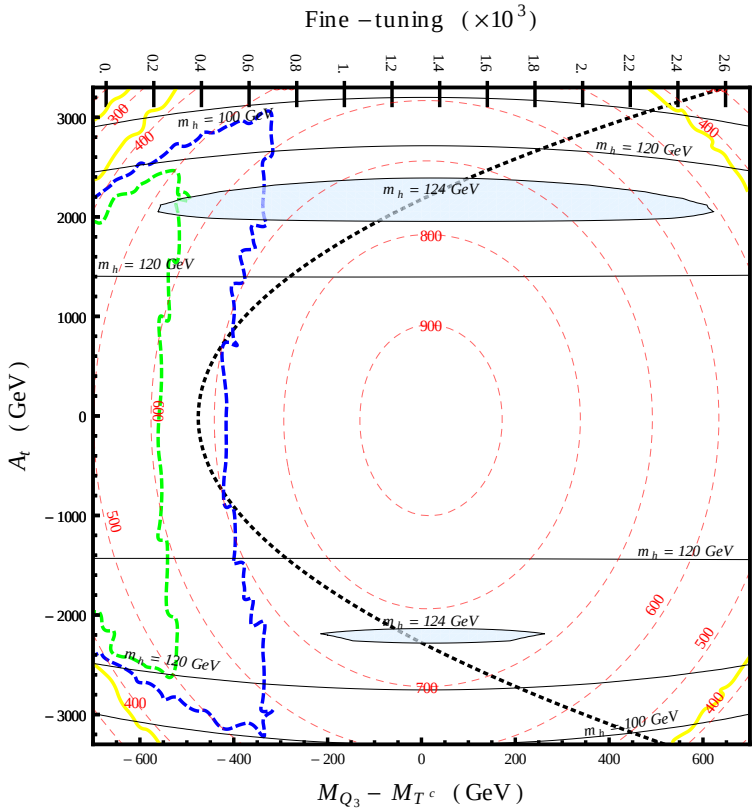

Figure 4.10: In this plot the fine tuning coming from the stop masses is fixed $C = \sqrt{m_{Q_3}^2 + m_{T^c}^2} = 1000\sqrt{2}$ GeV and the Higgsino mass is $\mu = 200$ GeV. The difference $X = m_{Q_3} - m_{T^c}$ between the soft mass parameters is varied. The area inside the closed solid blue (AC2013024) contour and the solid red (AC2013048) contour is excluded by the corresponding experimental analyses given inside the parentheses. The analysis shown by the yellow contours (AC2013053) excludes points where the stop masses are lighter than around 400 GeV for $X > 0$ and lighter than 350 GeV for $X < 0$. The dotted black curve depicts the fine tuning as a function of the soft trilinear coupling A_t, the values are shown on the top of the figure. The Higgs mass and the lightest stop correspond to the solid black and dashed red contours, respectively.

$\tilde{t}_1\tilde{t}_1 \to (t\tilde{\chi}_1^0)(t\tilde{\chi}_1^0)$ with cross sections times branching ratios 5.43 fb and 4.82 fb, respectively. The total number of events is slightly larger than the experimental upper limit at 95% CL, $N_{vis} = 3.6$ excluding this point from the allowed parameter space. At the point **B**(0,0) GeV of Fig. 4.9 the three lightest 3rd generation squarks have masses very close to each other $m_{\tilde{t}_1} = 973$ GeV, $m_{\tilde{b}_1} = 965$ GeV and $m_{\tilde{t}_2} = 995$ GeV. Therefore the production cross section for the pair production of each squark is almost equal giving a total production cross section $\sigma_{tot} = 1.6$ fb. The contributing topologies are mainly those in

which the two sbottoms $\tilde{b}_1$ (or stops $\tilde{t}_1$) decay into a top quark and the lightest neutralino $\tilde{b}_1\tilde{b}_1 \to (t\tilde{\chi}_1^0)(t\tilde{\chi}_1^0)$ and the mixed topology $\tilde{t}_2\tilde{t}_2 \to (b\tilde{\chi}_1^0)(t\tilde{\chi}_1^0)$ where one of the heaviest top squarks decays into a bottom quark and a neutralino and the second one into a top and the lightest neutralino. As we see the statistics is very small giving a small number of events compared to the experimental limits, thus the point is allowed by current analyses implemented in the program. Let us now investigate another point which is excluded by the yellow and blue exclusion curve, point **C** (600, 2052) GeV. At this point since the soft mass difference X is large and the stop trilinear coupling, which induces a large mixing in the stop sector, is also large results in a light stop $m_{\tilde{t}_1} = 522$ GeV which is responsible for the 99.8% of the total production cross section ($\sigma_{tot} = 64.3$ fb) at the center of mass energy of 8 TeV. The lightest sbottom and $\tilde{t}_2$ are both slightly heavier than 1.2 TeV with the left-handed bottom squark being the lightest of the two. In Fig. 4.10 we fix $C = 1000\sqrt{2}$ GeV as in Fig. 4.9 and we increase the Higgsino mass to $\mu = 200$ GeV, thus relaxing the experimental bounds. One can observe that for $X < -400$ GeV the stop masses are excluded up to $m_{\tilde{t}_1} \simeq 700$ GeV. At the center of the plot for $X = 0,\ A_t = 0$ the stops are heavier than $m_{\tilde{t}_1} > 900$ GeV. The Higgs mass can be reached for large mixing and for relatively large splitting X between the soft masses, similar to previous Fig. 4.9.

Chapter 5

Fine-Tuning in the pUMSSM

The original motivation of the U(1)$'$ extensions of the MSSM, apart from the fact that it provides a neat solution to the μ problem present in the minimal scenario, is that it raises the Higgs mass at tree-level, alleviating the need for large soft masses. As we have seen in the previous chapter, the smallness of the Higgs quartic coupling makes the need for heavy soft mass parameters $m_{Q_3}, m_{T^c} \sim 1$ TeV and very large mixing $A_t \sim 2$ TeV imperative in order to achieve a Higgs mass within the LHC observed range. This creates two problems for supersymmetric models. The first one is that supersymmetry in this form is still confronted with a fine tuning problem, which although is much less reduced compared to the SM, it spoils the theoretical motivation which lead SUSY to become one of the most favourable candidates of physics beyond the SM. The second problem seems to be phenomenological. The top squarks $\tilde{t}_1$ with masses around (700-750) GeV seem to be not heavy enough to evade future experimental constraints in some scenarios, raising the scepticism against SUSY. In this chapter we will explore the pros and cons of the singlet gauge extensions of the MSSM and study the possibility of having a less fine tuned theory which can evade current and possible future experimental results.

5.1 Stability of the EW scale under the presence of radiative corrections

As we have seen earlier the fine tuning measure checks the stability of the EW scale eq.(4.1) at tree-level and in the presence of large radiative corrections. In the case of pUMSSM the equation that exhibits the stability of the Z mass eq.(4.1) is being modified due to the presence of the extra gauge singlet S, which alters the minimization conditions. One can re-write the minimization conditions of the Higgs potential as follows

$$m_{H_u}^2 - M_Z^2/2\cos 2\beta - \frac{\lambda A_\lambda v_s \cot\beta}{\sqrt{2}} + \frac{\lambda^2}{2}(v_s^2 + v^2\cos^2\beta) + Q_{H_u} d' = 0 \ , \tag{5.1}$$

$$m_{H_d}^2 + M_Z^2/2\cos 2\beta - \frac{\lambda A_\lambda v_s \tan\beta}{\sqrt{2}} + \frac{\lambda^2}{2}(v_s^2 + v^2\sin^2\beta) + Q_{H_d} d' = 0 \ , \tag{5.2}$$

$$m_s^2 - \frac{v^2}{v_s}\frac{\sin\beta\cos\beta}{\sqrt{2}}\lambda A_\lambda + \lambda^2\frac{v^2}{2} + Q_s d' = 0 \ , \tag{5.3}$$

where d' are the D-terms coming from the extra $U(1)$ gauge group, see eq.(3.48). In complete analogy with the MSSM we consider $M_Z^2, \tan\beta$ as output and all the other parameters as input. By adding the first two equations together we can solve with respect to $\sin 2\beta$ and we obtain

$$\sin 2\beta = \frac{\sqrt{2}\lambda A_\lambda v_s}{m_{H_u}^2 + m_{H_d}^2 + 2\mu_{eff}^2 + \lambda^2\frac{v^2}{2} + d'(Q_{H_u} + Q_{H_d})} \ . \tag{5.4}$$

Now by subtracting the first two equations in (5.1), plugging in (5.4) and using the trigonometric identities we arrive at the expression

$$\boxed{\frac{M_Z^2}{2} = \frac{m_{H_d}^2 - m_{H_u}^2\tan^2\beta}{\tan^2\beta - 1} - \mu_{eff}^2 + d'\left(\frac{Q_{H_d} - Q_{H_u}\tan^2\beta}{\tan^2\beta - 1}\right)} \ , \tag{5.5}$$

which describes the stability of the EW scale at tree-level. The above equation resembles the corresponding equation in the minimal supersymmetric extension and differs by the presence of the extra term which is proportional to the d', i.e. the $U(1)'$ D-term contributions. Note that in the above relation no assumption has been made for $\tan\beta$ which is typically taken to be large. In this case where $\tan\beta \gg 1$ is assumed to be very large the above equation simplifies to

$$\frac{M_Z^2}{2} = -m_{H_u}^2 - \mu_{eff}^2 - d' Q_{H_u} \ , \tag{5.6}$$

with $d' \simeq \frac{1}{2}(Q_{H_u} v^2 + Q_s v_s^2)$. From the above equation we see that the source of fine tuning in the MSSM is still present here with the addition of an extra term which can make the fine tuning worse or can potentially create cancellations if $Q_{H_u}\cdot Q_s < 0$ and thus flip the relative sign of this extra contribution. To be able to analyse this possibility we have to study the effect of the quantum corrections to the right-hand side of the above equation. Let us first express eq.(5.5) in such a way that is easy to include the quantum contributions to the right-hand side through the RGEs of the soft masses and couplings. For values of $\tan\beta > 10$ we can safely assume that $\cos\beta \simeq 0$ and thus we retrieve eq.(5.6). From the third minimization condition in eq.(5.1) we will then have for the scalar soft mass

$$m_s^2 = -\frac{\lambda^2 v^2}{2} - Q_s d' \ . \tag{5.7}$$

Plugging in the expression for d' when $\tan\beta$ is large we will have an expression for the vev of the singlet v_s as a function of the scalar soft mass and the weak scale vev v

$$v_s^2 = -2\frac{m_s^2}{Q_s^2} - v^2\left(\frac{\lambda^2}{Q_s^2} + \frac{Q_{H_u}}{Q_s}\right) \ . \tag{5.8}$$

Inserting eq.(5.8) into eq.(5.6) and rewriting the vev v with respect to M_Z, we can then move this contribution to the left-hand side to obtain

$$\boxed{\frac{1}{2}M_Z^2\left[1 - 4\frac{\lambda^2}{g_z^2}\left(2\frac{Q_{H_u}}{Q_s} + \frac{\lambda^2}{Q_s^2}\right)\right] = -m_{H_u}^2 + m_s^2\left(\frac{Q_{H_u}}{Q_s} + \frac{\lambda^2}{Q_s^2}\right)} \ . \tag{5.9}$$

Here we denote the coefficient of M_Z^2 on the left-hand side as ξ. Note that the sign inside the bracket is minus and since in principle $Q_{H_u}\cdot Q_s < 0$ in order to avoid tachyonic stop masses we see that if

$$\frac{|Q_{H_u}|}{|Q_s|} > \frac{1}{2}\frac{|\lambda|^2}{|Q_s|^2} \ , \tag{5.10}$$

then the coefficient ξ reduces the fine tuning by a factor $1/\xi$. The 1-loop corrections to the right-hand side of eq.(5.9) are given by

$$\delta(-m_{H_u}^2 + \alpha m_s^2) = \frac{1}{16\pi^2}\ln\frac{\Lambda}{\mu_0}\left(-\beta^{(1)}_{m_{H_u}^2} + \alpha\beta^{(1)}_{m_s^2} + m_s^2\beta^{(1)}_{\alpha}\right) \ , \tag{5.11}$$

where $\alpha = \frac{Q_{H_u}}{Q_s} + \frac{\lambda^2}{Q_s^2}$ is the coefficient of the singlet soft mass m_s^2 on the right-hand side of eq.(5.9). We calculate the RGEs at 1-loop using the program `SARAH` [142, 143, 144] and we generalize the results for non-universal $U(1)'$ charges. The beta functions for the soft masses $m_{H_u}^2, m_s^2$ are given by:

$$\begin{aligned}\beta^{(1)}_{m_{H_u}^2} &= 6|y_t|^2\left(m_{H_u}^2 + m_{Q_3}^2 + m_{T^c}^2 + |A_t|^2\right) + 2|\lambda|^2\left(m_{H_u}^2 + m_{H_d}^2 + m_s^2 + |A_s|^2\right) \\ &- \frac{6}{5}g_1^2|M_1|^2 - 6g_2^2|M_2|^2 + \frac{3}{5}g_1^2 S + 2Q_{H_u}S_1 - 8Q_{H_u}^2|M_1'|^2 \ ,\end{aligned} \tag{5.12}$$

where we should remind the reader that we have absorbed the extra $U(1)$ gauge coupling into the charges. To regain explicit dependence on g_1' one should set $Q_i \equiv g_1' Q_i$. Furthermore,

$$\beta^{(1)}_{m_s^2} = 4|\lambda|^2\left(m_{H_d}^2 + m_{H_u}^2 + m_s^2 + |A_\lambda|^2\right) + 2Q_s S_1 - 8Q_s^2|M_1'|^2 \ . \tag{5.13}$$

The coefficient S is a function of the soft mass parameters only

$$\begin{aligned}S &= -2Tr(m_{\bar{u}}^2) - Tr(m_L^2) - m_{H_d}^2 + m_{H_u}^2 + Tr(m_{\bar{d}}^2) + Tr(m_{\bar{e}}^2) + Tr(m_Q^2) \\ &= -2\sum_i^3 m_{\bar{u}_i}^2 - \sum_i^3 m_{L_i}^2 + \sum_i^3 m_{\bar{d}_i}^2 + \sum_i^3 m_{\bar{e}_i}^2 + \sum_i^3 m_{Q_i}^2 + m_{H_u}^2 + m_{H_d}^2 \ ,\end{aligned} \tag{5.14}$$

while the coefficient S_1 depends on the soft masses and the $U(1)'$ charges

$$\begin{aligned} S_1 &= 2m_{H_d}^2 Q_{H_d} + 2m_{H_u}^2 Q_{H_u} + 2Q_L Tr(m_L^2) + 3Q_{\bar{d}} Tr(m_{\bar{d}}^2) + 3Q_{\bar{u}} Tr(m_{\bar{d}}^2) \\ &+ 6Q_Q Tr(m_Q^2) + m_s^2 Q_s + Q_{\bar{e}} Tr(m_{\bar{e}}^2) \\ &= 2m_{H_d}^2 Q_{H_d} + 2m_{H_u}^2 Q_{H_u} + 2\sum_i^3 (Q_{L_i} m_{L_i}^2) + 3\sum_i^3 (Q_{\bar{d}_i} m_{\bar{d}_i}^2) \\ &+ 3\sum_i^3 (Q_{\bar{u}_i} m_{\bar{u}_i}^2) + 6\sum_i^3 (Q_{Q_i} m_{Q_i}^2) + m_s^2 Q_s + \sum_i^3 (Q_{\bar{e}_i} m_{\bar{e}_i}^2) \ . \end{aligned} \tag{5.15}$$

Here we have used the assumption that the 3×3 soft mass matrices m_{soft}^2 are all diagonal in the family space and we have generalized the relations for non-universal charges. Although the first term $\frac{Q_{H_u}}{Q_s}$ of the coefficient α is independent of the renormalization scale, the second term will run with the scale λ. It is easy to see that the beta function of the coefficient α at 1-loop will be

$$\beta_\alpha^{(1)} \equiv \beta_{\frac{\lambda^2}{Q_s^2}} = 2\frac{\lambda^2}{Q_s^2}\left(\frac{1}{\lambda}\beta_\lambda^{(1)} - \frac{1}{g_1'}\beta_{g_1'}^{(1)}\right) \ , \tag{5.16}$$

where beta functions of singlet trilinear coupling λ and the extra U(1) gauge coupling g_1' are given by

$$\begin{aligned} \beta_\lambda^{(1)} &= \lambda\Big[3\left(Tr(Y_d Y_d^\dagger) + Tr(Y_u Y_u^\dagger)\right) + Tr(Y_e Y_e^\dagger) + 4|\lambda|^2 - 2Q_{H_u}^2 \\ &- 2Q_{H_d}^2 - 2Q_s^2 - \frac{3}{5}g_1^2 - 3g_2^2\Big] \\ &= \lambda\Big[3\left(y_t^2 + y_b^2\right) + y_\tau + 4|\lambda|^2 - 2Q_{H_u}^2 - 2Q_{H_d}^2 - 2Q_s^2 - \frac{3}{5}g_1^2 - 3g_2^2\Big] \ . \end{aligned} \tag{5.17}$$

Here we have used the fact that the Yukawa matrices are diagonal and only the y_t, y_b, y_τ are non-zero. In addition

$$\begin{aligned} \beta_{g_1'}^{(1)} &= g_1' \sum_i^3 \left(6Q_{Q_i}^2 + 2Q_{L_i}^2 + 3Q_{\bar{u}_i}^2 + Q_{\bar{e}_i}^2 + 3Q_{\bar{d}_i}^2\right) + g_1'\Big(2Q_{H_u}^2 + 2Q_{H_d}^2 \\ &+ Q_s^2\Big) \ . \end{aligned} \tag{5.18}$$

Having calculated the 1-loop corrections to the terms in eq.(5.9), causing the fine tuning we can now define the fine tuning measure following the lines of eq.(4.4). We get

$$\Delta_Z = \max_i \frac{|B_i/\xi|}{(M_Z^2/2)} \ , \tag{5.19}$$

where $B_i = \{m_{H_u}^2,\ \delta m_{H_u}^2, \alpha m_s^2, \delta(\alpha m_s^2)\}$. Note that in our definition there is no μ_{eff}^2 or $\delta\mu_{eff}^2$ term as in the MSSM. Although we have written explicitly the μ_{eff} term in the EW scale stability equation (5.5) in order to resemble the MSSM case, we have to stress the fact that μ_{eff} emerges from the singlet soft mass m_s^2 and does not enter the equation directly.

After all this is why we have introduced the gauge singlet in the first place in scenarios like the $U(1)'$ extensions and the NMSSM in order to solve the μ problem in the MSSM. The singlet soft mass m_s^2 breaks the extra $U(1)'$ gauge symmetry at some higher scale and gives a vev to the gauge singlet S. If one disentangles the two parameters in view of resembling the MSSM relationship that exhibits the EW stability, in a way reintroduces the μ problem by cutting the link between μ_{eff} and m_s^2 and inherits one of the disadvantages of the MSSM. As we have discussed in the previous chapter in the MSSM the Higgsino parameter μ already at tree-level, is responsible for the main contribution to the fine tuning. For this reason the mass of the Higgsinos receive a stringent constraint to be of the order of 200 GeV or less in order for the theory to remain natural (see eq.(4.5),(4.6)). In the pUMSSM scenario things seem to be different. The solution to the μ problem and the connection to the soft SUSY breaking parameter m_s^2 removes the μ_{eff} term from directly entering the formula of EW stability and thus evading the constraint for light Higgsinos. As we have discussed in section 3.6.1 this observation is very crucial for $U(1)'$ extensions, because the tree-level Higgs mass can be boosted for heavy Higgsino masses. Additionally heavy Higgsinos in the extended models can possibly create cancellations within the m_s^2 terms and reduce slightly the fine tuning caused by these terms. Let us summarize here our main observations on fine tuning analytic expressions before we go on with the numerical analysis:

- Although the fine tuning coming from the effective Higgsino mass parameter μ_{eff} is suppressed in pUMSSM there is a critical value for which the fine tuning can blow up. In our definition of the fine tuning measure eq.(4.4) there is a multiplying factor $1/\xi$, which can increase the fine tuning if ξ is too small. It is obvious that if $\xi \to 0$ the fine tuning goes to infinity. The coefficient ξ is the multiplying factor of the Z mass in eq.(5.9)

$$\xi = 1 - 4\frac{\lambda^2}{g_z^2}\left(2\frac{Q_{H_u}}{Q_s} + \frac{\lambda^2}{Q_s^2}\right) \ . \tag{5.20}$$

  To find the critical value for λ_c and consequently for μ_{eff}^c we only have a simple quartic equation with respect to λ

$$-C_1\lambda_c^4 + C_2\lambda_c^2 + 1 = 0 \ , \tag{5.21}$$

  where the coefficients C_1, C_2 are functions of the ratio $Q_s, r = Q_{H_u}/Q_s$, respectively. The coefficients are given as

$$C_1(Q_s) = \frac{4}{g_z^2}\frac{1}{Q_s^2} \ , \qquad C_2(r) = \frac{8}{g_z^2}|r| \ . \tag{5.22}$$

For a real positive solution $\lambda_c > 0$ of the quartic equation it follows that

$$\lambda_c = \left(\frac{C_2 + \sqrt{C_2^2 + 4C_1}}{2C_1} \right)^{1/2} , \tag{5.23}$$

and thus the critical value for μ_{eff} is given by

$$\mu_{eff}^c = v_s \left(\frac{C_2 + \sqrt{C_2^2 + 4C_1}}{4C_1} \right)^{1/2} . \tag{5.24}$$

Since we are using as input the value of the singlet vev v_s and the effective Higgsino

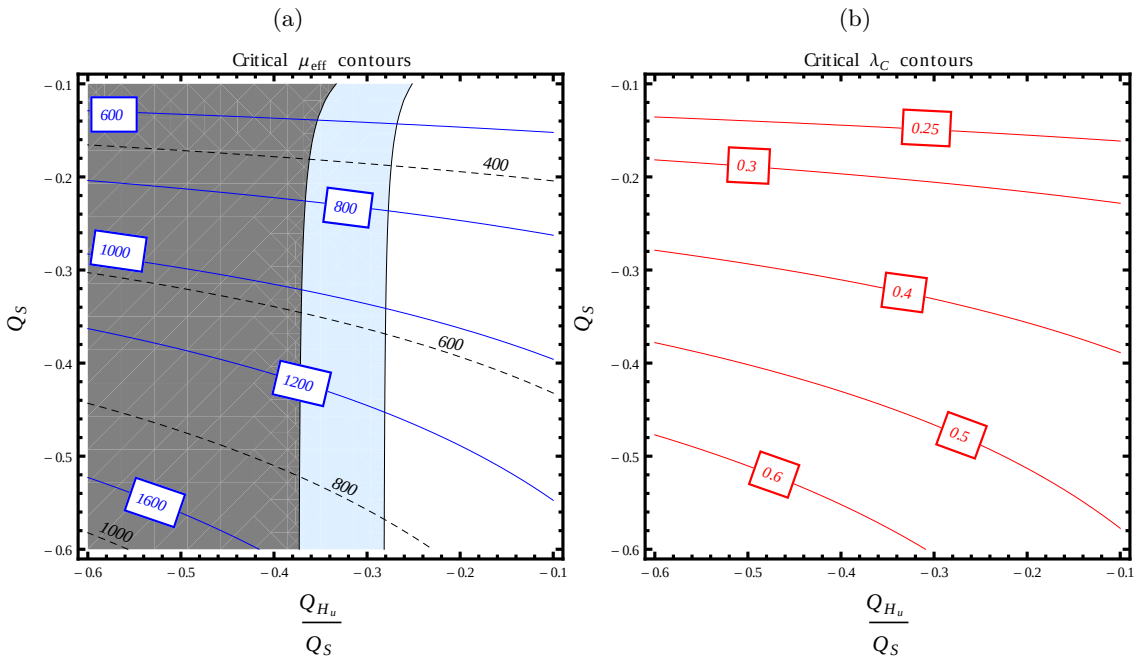

Figure 5.1: Fig. 5.1b: shows the critical values of the singlet trilinear coupling λ_c for which the parameter $\xi = 0$ and thus causing the fine tuning to blow up, see eq.(4.4). Fig. 5.1a: Critical μ_{eff} contours for two different values of the singlet vev (i) $v_s = 2$ TeV (black dashed lines) (ii) $v_s = 3.5$ TeV (blue solid lines). The light blue area corresponds to W mass values within 2σ deviation from the central measured value and the gray area corresponds to more than 2σ error. The W mass contours have been created for the lower value of $v_s = 2$ TeV and large $\tan\beta = 20$. For the second value of $v_s = 3.5$ TeV all the points on this plane are within 2σ.

mass parameter μ_{eff}, it is more convenient to translate the λ_c contours into the μ_{eff}^c contours. In Fig. 5.1 we have plotted the contours of the critical μ_{eff} (Fig. 5.1a) and λ_c values (Fig. 5.1b) in the (r, Q_s) plane. In order to keep each term at the TeV scale we will consider values for μ_{eff} well below 1 TeV. As we see from the figure the heavier the Z' mass the larger the critical value of μ_{eff}. This means that one

has to be careful in case of light Z' masses where the critical value can be small but in principle heavier than (200-300) GeV. In this case we will use light Higgsinos $\mu_{eff} \sim (105 - 150)$ GeV because, as we have seen in section 3.6.1, heavy Higgsinos tend to decrease the tree-level mass of the lightest CP-even Higgs boson.

- In order to suppress fine tuning the multiplying factor ξ in eq.(5.9) has to be either $\xi > 1$ or $\xi < -1$. For $|\xi| = 1$ we are not gaining any advantage from ξ on reducing the fine tuning. In the first case where $\xi \leq -1$ one has two solve a similar quartic equation to eq.(5.21). For a singlet Yukawa coupling λ greater than the solution of this equation which is defined by the Higgs $U(1)'$ couplings

$$\lambda_{\xi\leq -1} \geq \left(\frac{C_2 + \sqrt{C_2^2 + 8C_1}}{2C_1} \right)^{1/2} \longrightarrow \xi \leq -1 \ , \tag{5.25}$$

the fine tuning will be suppressed. Note that $\lambda_{\xi\leq -1}$ is somewhat larger than the critical value $\lambda_{\xi\leq -1} > \lambda_c$. For $\xi \geq 1$ then it is easy to see that the singlet Yukawa coupling has to be smaller than

$$\lambda_{\xi\geq 1} \leq |Q_s|(2|r|)^{1/2} \longrightarrow \xi \geq 1 \ . \tag{5.26}$$

The first case is common in a study where one would fix λ and allow μ_{eff} to vary as the singlet vev grows to larger values. The latter case is what in principle happens in our current approach where the Higgsino mass μ_{eff} is kept constant and below the TeV scale while v_s is allowed to be a free parameter of the theory. The first case is also very interesting since it would involve heavy Higgsino states which according to our previous discussion would potentially further reduce the fine tuning by creating cancellations within the beta function of the singlet soft mass. Moreover light singlino states would create a large mixing in the neutralino sector and thus affecting the couplings of the neutralino physical states to the other matter fields making it difficult to be detected by current and near future analyses. There is also a special case in which the coefficient $\alpha = 0$ becomes identically zero and this happens when $\lambda_{\alpha=0} = \lambda_{\xi=1}/\sqrt{2}$.

- For large $M_{Z'}$ scenarios one can write the D-terms in (3.48) as

$$d' \simeq -\frac{1}{2} Q_s v_s^2 = -\frac{1}{2} M_{Z'}^2/Q_s \ ,$$

so that $m_s^2 \simeq -\frac{1}{2} M_{Z'}^2$ and thus equation (5.9) can be viewed as follows

$$\frac{1}{2} M_Z^2 \left[1 - 4\frac{\lambda^2}{g_z^2} \left(2\frac{Q_{H_u}}{Q_s} + \frac{\lambda^2}{Q_s^2} \right) \right] = -m_{H_u}^2 - \frac{1}{2} M_{Z'}^2 \left(\frac{Q_{H_u}}{Q_s} + \frac{\lambda^2}{Q_s^2} \right) \ . \tag{5.27}$$

In this form we understand that, in the limit of heavy Z' boson the models with extra $U(1)$ gauge symmetries will encounter large fine tuning already at tree-level. The second term for a given order one ratio Q_{H_u}/Q_s seems to dominate the fine tuning. One should not forget at this point that not only m_s^2 is driven to large values by the D-terms d' but also the Higgs soft masses $m_{H_u}^2, m_{H_d}^2$. The Higgs up soft mass parameter which is the one to blame for the fine tuning in the MSSM, is also driven to large values by the existence of a heavy Z'. From the minimization conditions one can see that for heavy $M_{Z'}$ we can write the approximation for $m_{H_u}^2$

$$m_{H_u}^2 \simeq -Q_{H_u} d' = -\frac{1}{2} M_{Z'}^2 \frac{Q_{H_u}}{Q_s} \ . \tag{5.28}$$

It seems that in the heavy Z' scenario both terms in eq.(5.9) are enhanced already at tree-level and there is a common factor, the ratio of the two $U(1)'$ charges $r = Q_{H_u}/Q_s$ which can potentially reduce the effect of these terms on the fine tuning. Note that if one would choose $Q_{H_u} = 0$ then these terms vanish and the fine tuning is no longer driven by heavy Z' masses. On the other hand a zero Higgs up $U(1)'$ charge does not seem favourable either and it serves only to construct our argument, that the ratio r plays an important role not only for achieving a small $Z - Z'$ mixing but also in potentially reducing the fine tuning. In the extreme case where $Q_{H_u} = 0$ then we lose the advantage of a larger Higgs quartic coupling and consequently a boosted tree-level Higgs mass. This would potentially lead to MSSM like fine tuning with the twist that the theory predicts extra matter which has many phenomenological implications. A small ratio $|r|$ would be favourable if the LHC bounds on Z' searches push its mass even higher.

- Moving on to study the fine tuning entering at the loop level, we have to look at the leading logarithmic solutions to the RGEs eq.(5.12),(5.13) and (5.11). Although this is a crude a approximation and one should resummate the logarithms by solving numerically the RGEs from the high-scale Λ down to the EW scale, it is sufficient for the purposes of this project. A low fine tuning would motivate further investigation for specific areas of the parameter space whereas if there are no such areas this would mean that it is impossible to improve it by using a more sophisticated resummation. The results have to be interpreted with caution, but this should be the case with any fine tuning study. In our approximation one should spot a difference between the beta function of $m_{H_u}^2$ in UMSSM eq.(5.12) and the solutions used to calculate the fine tuning in the MSSM eq.(4.10). The soft mass $m_{H_u}^2$ has to be included in this leading

logarithm (LL) approximation since the soft mass in UMSSM is no longer small but as we have seen for heavy Z' bosons will be driven to very large values by the D-terms. In the MSSM this term usually is being omitted due to its smallness compared to the heavy stop masses m_{Q_3}, m_{T^c} and the large off-diagonal mixing caused by the trilinear soft coupling A_t. In the pUMSSM the Higgs up soft mass if we consider the limit where the singlet vev is large eq.(5.28), has an overall positive sign since the ratio $r = Q_{H_u}/Q_s < 0$ is taken to be negative due to the desired enhancement of the D-terms on the stop masses. This has tremendous consequences for the fine tuning measure since it adds up to the other sources increasing the fine tuning. For moderate values of Z' the effect of this term will not be so drastic but as we increase the mass of the Z' this term would dominate the fine tuning. Another worrisome term in eq.(5.12) is $2Q_{H_u}S_1$. This term gives the 1-loop corrections originating from the $U(1)'$ gauge coupling of the Higgs up doublet to the matter fields. Thus the coefficient S_1 as seen in eq.(5.15) is a function of the $U(1)'$ couplings and the soft masses of all squark and slepton fields. This term which is present due to the extra $U(1)$ gauge symmetry is absent in the MSSM. Heavy sfermion masses well above 1 TeV, of the first two families with largish $U(1)'$ couplings will enhance this term and contribute to the fine tuning. This is another new feature of the theory which can be tackled by considering non-universal charges which are small for the first two families of squarks and sleptons. This is also important for preserving perturbativity up to the high-scale Λ up to which the theory is valid. The term competing $\delta m^2_{H_u}$ in our definition of the fine tuning measure in eq.(4.4) is

$$\delta(\alpha m_s^2) = \frac{1}{16\pi^2}\ln\frac{\Lambda}{\mu_0}\left(\alpha\beta^{(1)}_{m_s^2} + m_s^2\beta^{(1)}_{\alpha}\right) \ , \tag{5.29}$$

the second term if we combine eq.(5.16) and the fact that $m_s^2 = -1/2(Q_s v_s)^2$ in the large v_s limit and $\mu_{eff} = \lambda v_s/\sqrt{2}$ becomes

$$\begin{aligned} m_s^2\beta^{(1)}_{\alpha} &= m_s^2 \cdot 2\frac{|\lambda|^2}{Q_s^2}\mathcal{B} = -\frac{1}{2}\Big(Q_s v_s\Big)^2\, 2\frac{|\lambda|^2}{Q_s^2}\mathcal{B} \\ &= -2\mu^2_{eff}\mathcal{B} \ . \end{aligned} \tag{5.30}$$

Here the coefficient $\mathcal{B}$ is a sum of the squares of the $U(1)'$ charges and Yukawa couplings

$$\begin{aligned} \mathcal{B} &= 3(y_b^2 + y_t^2) + y_\tau^2 + 4\lambda^2 - 4(Q^2_{H_u} + Q^2_{H_d}) - 2Q_s^2 + \\ &+ \sum_i \left(6Q^2_{Q_i} + Q^2_{\bar{e}_i} + 3Q^2_{\bar{d}_i} + 2Q^2_{L_i} + 3Q^2_{\bar{u}_i}\right) . \end{aligned} \tag{5.31}$$

From eq.(5.30) we can understand that this term cannot push the fine tuning measure to high values when $\mu_{eff} \sim \mathcal{O}(1\text{ TeV})$. As stated earlier for our study we keep the effective Higgsino mass below the TeV scale and avoid in the present study any large accidental cancellations. The worrisome term in eq.(5.29) for that reason appears to be the first term $\alpha\beta_{m_s^2}$. It is obvious that if the coefficient $|\alpha| \leqslant 1$ will suppress or enhance the effect of this term on the fine tuning. Another special case would be that, for which this coefficient vanishes $\alpha = 0$ and thus the second term on the right-hand side of eq.(5.9) as well as $\alpha\beta_{m_s^2}$ vanishes identically. In principle looking at eq.(5.10) and from the fact that we vary the singlet vev v_s while fixing the effective Higgsino mass parameter μ_{eff}, we understand that small values of λ are preferred. In the limit where $|r| \gg (\lambda/Q_s)^2$ then $\alpha \approx -|r|$ and one can see that the term $2Q_{H_u}S_1 \in \alpha\beta_{m_s^2}$ appears and can affect the fine tuning. To see how the charges and the soft masses of the first two families of squarks and sleptons contribute to the fine tuning we have made the following two plots, Fig. 5.2a and Fig. 5.2b. Since the number of free parameters is large for simplicity in our project we are considering all $U(1)'$ charges $Q_{\tilde{f}}$ and soft masses m_{soft} of the first two families of sfermions equal. In Fig. 5.2a we have plotted the fine tuning contours on the $(m_{soft}, Q_{\tilde{f}})$ plane. In the

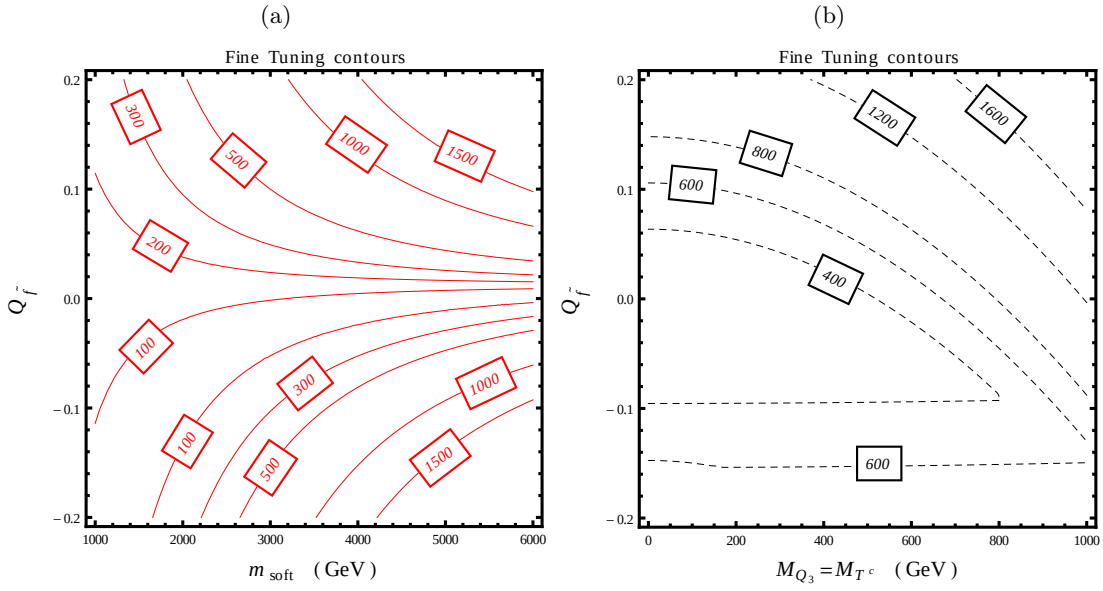

Figure 5.2: Fine tuning contours on (a) the $(m_{soft}, Q_{\tilde{f}})$ plane and (b) on the $(m_{Q_3}, Q_{\tilde{f}})$ plane. (a) For this plot we fix the third generation squark masses $m_{Q_3} = m_{T^c} = 0.5$ TeV, $m_{B^c} = 3$ TeV and $A_t = 0.5$ TeV and we vary the charges $Q_{\tilde{f}}$ and soft mass for first, second family of sfermions m_{soft}. (b) The soft masses are fixed $m_{soft} = 3$ TeV and we vary $m_{Q_3} = m_{T^c} = A_t/2$. $r = Q_{H_u}/Q_s = -0.5$ and $Q_s = -0.5$ for both plots.

case where $(r, Q_s) = (-0.5, -0.5)$ we expect the Higgs mass to be boosted at tree-level and we are considering lighter soft masses $m_{Q_3} = m_{T^c} = 0.5$ TeV and small trilinear coupling $A_t = 0.5$ TeV for this plot but only for the sake of our argument without claiming that at the moment we are calculating the Higgs mass to be around the LHC experimental value. We aim here to get an idea of how these extra gauge terms in the beta functions of the singlet and Higgs soft masses affect the fine tuning in our study of pUMSSM. The singlet vev is taken $v_s = 3.5$ TeV and $\mu_{eff} = 800$ GeV is largish. It can be seen from Fig. 5.2 that soft masses heavier than a few TeV and charges with absolute values larger than $|Q_{\tilde{f}}| > 10^{-1}$ will increase the fine tuning. On the right Figure 5.2b the soft masses of the stops are considered equal and are varied along with the stop trilinear coupling $A_t = 2m_{Q_3}$. The singlet vev is taken to be $v_s = 4$ TeV and the effective Higgsino mass $\mu_{eff} = 500$ GeV. For negative values of the charges $Q_{\tilde{f}}$ the contours are flat with respect to the m_{Q_3} axis which means that the variation of the soft masses and the trilinear coupling does not alter the fine tuning measure. This happens because the term $\delta(\alpha m_s^2)$ is causing the fine tuning and overpowers $\delta m_{H_u}^2$. It seems that for positive charges the picture changes and $\delta m_{H_u}^2$ is enhanced and is responsible for the fine tuning. This situation looks like a see-saw where both edges cannot be at the minimum at the same time. Since one can reduce the fine tuning coming from $\delta m_{H_u}^2$ by enhancing the Higgs quartic coupling, in principle it would be desirable that the fine tuning originates from this term. Moreover if one can reduce the fine tuning coming from the stop sector then the overall value will be suppressed compared to other extended $U(1)'$ models or even the MSSM scenario. We ought to mention that in some cases the terms $2Q_{H_u}S_1$, $2Q_sS_1$ can also create large cancellations and reduce the overall fine tuning but this would be just an artefact of the chosen parameters which cannot be based on sound theoretical arguments. For this reason we will choose for our calculations the soft masses of the first and second family of sfermions to be $m_{soft} = 3$ TeV and the charges to be very small, therefore we set $Q_{\tilde{f}} = 1/20$ or 0. Small $U(1)'$ charges are also justified if one would want to evade constraints from exotic searches on the heavy gauge boson Z'.

- The gaugino masses M_1, M_2, M_1' enter the beta functions of the soft masses eq.(5.12), (5.13) with opposite signs to the terms ruling the fine tuning i.e. those terms proportional to the top Yukawa coupling. Therefore the bino, wino, and bino primed masses can potentially reduce the fine tuning by creating large cancellations within the beta functions of $m_{H_u}^2$ and m_s^2. As we have seen in our discussion for the MSSM,

in recent studies [15] points with low fine tuning are found to have heavy bino and wino masses of a few TeV. It almost seems like an unavoidable conspiracy between the cancelling terms which brings the fine tuning down by two orders of magnitude. In Fig. 5.3 we draw the fine tuning as a function of the bino mass M_1. The wino

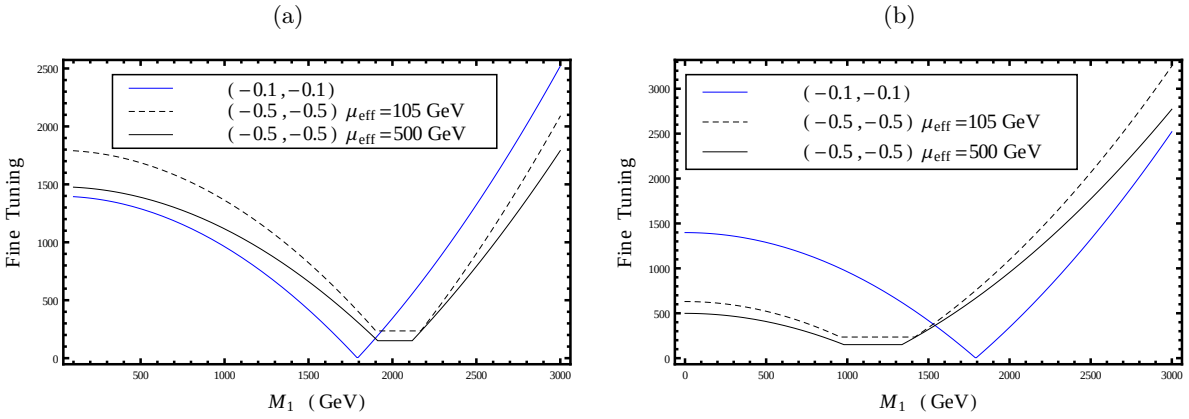

Figure 5.3: Fine tuning Δ_Z as a function of the gaugino mass $M_1 = M_2/2$. The $\tilde{B}'$ mass is zero for this plot $M_1' = 0$. The blue lines in both plots are the same and have small Higgs quartic coupling $Q_{H_u} = 0.01$. The stop soft mass parameters are $m_{Q_3} = m_{T^c} = 1$ TeV with large $A_t = 2$ TeV in the left plot. The black lines correspond to large $U(1)'$ charge $Q_{H_u} = 1/4$. The soft supersymmetric breaking parameters for the right plot are fixed to smaller values $m_{Q_3} = m_{T^c} = 0.5$ TeV and $A_t = 0.5$ TeV. The black solid line corresponds to larger Higgsino mass μ_{eff} which reduces the fine tuning by a factor of $\xi \sim 1.2$. Note that in order to be consistent, the bino mass is chosen so that $M_2 > 200$ GeV well above the LEP chargino constraint. $Q_{\text{other}} = 1/18$.

mass is taken to be twice as heavy as the bino mass $M_2 = 2M_1$ whereas the mass of the $\tilde{B}'$ is considered to be zero here $M_1' = 0$. This means that the two extra neutralinos $\tilde{S}, \tilde{B}'$ are nearly degenerate with the heavy Z' boson and have maximal mixing. In the left plot Fig. 5.3a the soft masses and the stop trilinear coupling A_t which define the fine tuning originating from stop sector for all three lines are taken to be MSSM like with respect to the lightest Higgs mass $m_{Q_3} = m_{T^c} = 1$ TeV and $A_t = 2$ TeV. For the right plot Fig. 5.3b the fixed parameters for the blue line remain unchanged for comparison whereas for the black lines are changed to smaller values $m_{Q_3} = m_{T^c} = 0.5$ TeV and $A_t = 0.5$ TeV. The black solid lines have quartic coupling $Q_{H_u} = 1/4$ and $\mu_{eff} = 0.5$ TeV which boosts the tree-level Higgs and allows for smaller soft stop masses. The black dashed lines have light effective Higgsino mass $\mu_{eff} = 105$ GeV which does not have the same effect on the tree-level mass of the

Higgs boson as we have seen earlier in sec. 3.6.1. There are several remarks that we have to make concerning this plot. First note that in both plots the solid black line has smaller fine tuning than the dashed line. This is because the larger effective $\mu_{eff} = 500$ GeV parameter corresponds to a larger coefficient $\xi \simeq 1.2$ which reduces the fine tuning as we have anticipated whereas for $\mu_{eff} = 105$ GeV it is smaller $\xi \simeq 1$. The blue line which has a tiny quartic $Q_{H_u} = 0.01$ and $\mu_{eff} = 105$ GeV has also $\xi \sim 1$ and as we can see by increasing the mass of the gaugino mass $M_1 = M_2/2$ the fine tuning is reduced dramatically. For $M_1 \approx 1.8$ TeV the fine tuning is reduced to $\Delta_Z \approx 10$. The black lines in the left plot Fig. 5.3a obtain a minimum fine tuning $\Delta_Z \approx 155.2$ for bino mass approximately $M_1 \approx 1.9$ TeV. The Z' mass for the black lines is $M_{Z'} \approx |Q_s| v_s = 2$ TeV which enhances the fine tuning already at tree-level. At $M_1 = 1.9$ TeV the solid and dashed black lines become flat for a while and then when the gaugino masses dominate the fine tuning they start to increase again, driving Δ_Z to high values. At these points where the two curves become flat the fine tuning comes from the tree-level values $m^2_{H_u}$ (solid black) and m^2_s (dashed black). In the right plot Fig. 5.3b the stop sector creates much smaller tuning $\Delta_Z \approx 500$ and thus smaller gaugino masses are needed to reduce it. For $M_1 \approx 1$ TeV the measure is $\Delta_Z \approx 150$, again at this point the tree-level soft masses are ruling the fine tuning due to the heavy Z' mass and therefore we cannot reduce it further by increasing the gaugino masses. The blue line has lighter Z' boson, $M_{Z'} = 400$ GeV and consequently lighter soft mass parameters $m^2_{H_u}, m^2_s$ at tree-level which allow for larger reduction of the fine tuning by having heavier gaugino masses. So far in our discussion we had the bino primed mass switched off M'_1 in order to understand how the other gaugino masses can reduce the fine tuning. We have seen that the largest effect comes from the wino mass M_2 due to the large coefficient with which it enters the 1-loop RGEs eq.(5.12). Let us now examine what happens if we switch M'_1 on. The $\tilde{B}'$ mass enters the RGEs with large coefficients proportional to the squares of the $U(1)'$ charges Q_{H_u} and Q_s eq.(5.12),(5.13). For large quartic coupling Q_{H_u} this term $-8Q^2_{H_u}|M'_1|^2$ will soon dominate for even light $\tilde{B}'$ mass and will increase the fine tuning as M'_1 becomes heavier. In the beta function of the singlet soft mass eq.(5.13) the term dependent on M'_1 mass will also overpower the other terms for moderate values of the bino primed mass given a large Higgs quartic.[1] This means that for heavy Z' with large Higgs quartic coupling the $\tilde{B}'$ cannot become too heavy before it drives the fine tuning to

[1] Since the ratio $|r| < 1$ if the quartic coupling is large then this implies a large singlet charge.

very high values, therefore a very light singlino LSP in this case with low fine tuning is not possible. A light singlino of a few hundred GeV with small Δ_Z would favour a light Z' with small $U(1)'$ charges. In Fig. 5.4 we have plotted Δ_Z with increasing M_1'

(a) $(r, Q_s) = (-0.1, -0.1)$ (b) $(r, Q_s) = (-0.5, -0.5)$

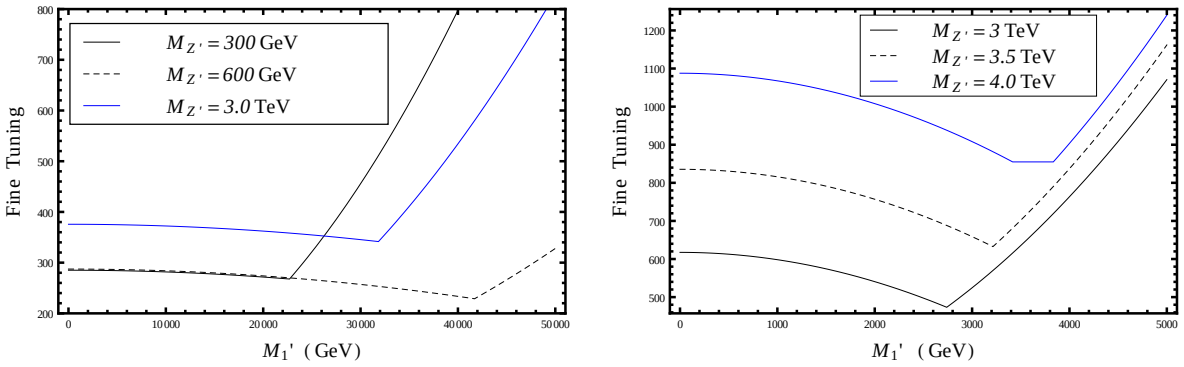

Figure 5.4: Fine tuning Δ_Z in pUMSSM as a function of the $\tilde{B}'$ mass parameter M_1' (a) for small $U(1)'$ Higgs quartic coupling $Q_{H_u} = 10^{-2}$ and (b) for large charge $Q_{H_u} = 1/4$. On the left plot we are considering the case of two relatively light Z' bosons (black lines) and a heavy Z' with mass around $M_{Z'} \approx |Q_s| v_s = 3$ TeV. In the right plot the large $U(1)'$ couplings indicate heavy Z' masses in order to pass the W mass constraint and thus we consider $M_{Z'} \approx 3$ TeV, 3.5 TeV, 4 TeV. The other two gaugino masses M_1, M_2 are taken to be well above TeV scale in order to reduce Δ_Z below 10^3 at $M_1' = 0$. The plot aims to exhibit how Δ_Z is affected by the increase of M_1' with respect to different models of Z' (different $U(1)'$ charges).

in order to get an idea of the effect of the extra $\tilde{B}'$ mass on the fine tuning measure for different charge assignments. The bino and wino masses are set above the TeV scale and create cancellations as we have discussed previously, bringing Δ_Z down dramatically as in the MSSM. The soft masses for the left plot Fig. 5.4a are set to large values $m_{Q_3} = m_{T^c} = 1$ TeV and $A_t = 2$ TeV due to the smallness of the $U(1)'$ Higgs quartic coupling, again in light of the Higgs mass. The Higgsino mass is light $\mu_{eff} = 105$ GeV for all three curves. For the right plot Fig. 5.4b the Higgsino mass is taken to be heavy $\mu_{eff} = 500$ GeV and degenerate with the stop soft masses and $A_t = 0.5$ TeV. For light Z' the extra gauge charges are small and as one can observe from Fig. 5.4a, the $\tilde{B}'$ mass can become very heavy before it starts dominating the fine tuning. For $M_{Z'} = 300$ GeV and zero bino primed mass, $\Delta_Z \sim 3 \times 10^2$ and is gradually decreasing because of the small cancellations within $\delta m_{H_u}^2$ from the term

which depends on M_1'. At the same time the fine tuning coming from $\delta(\alpha m_s^2)$ is increasing and at around $M_1' = 23$ TeV overpowers the other term and Δ_Z is rising again. It is worth noting that at the lowest point of $\Delta_Z \approx 270$ the lightest neutralino mass at tree-level is $m_{\tilde{\chi}_1^0} = 4$ GeV with a singlino component $|N_{15}|^2 = 99.3\%$. For heavy Z' the blue line on the left plot starts off with a larger $\Delta_Z \sim 4 \times 10^2$ and slightly decreases with M_1' until $M_1' \approx 32$ TeV, due to the small $U(1)'$ charges. At the lowest point the fine tuning is roughly $\Delta_Z \approx 341$. The third lightest neutralino appears to be in a mostly singlino state with component $|N_{15}|^2 = 99.1\%$ and has a mass $m_{\tilde{\chi}_3^0} = 279$ GeV. The two lightest neutralinos are Higgsino like with masses given by the effective μ_{eff} parameter $m_{\tilde{\chi}_1^0} = 103$ GeV and $m_{\tilde{\chi}_1^0} = 106$ GeV. In the right Fig. 5.4b the fine tuning measure is substantially larger due to the heavier Z' bosons. Due to the large $U(1)'$ couplings the fine tuning related to the singlet soft mass becomes large for relatively small values of the bino primed mass compared to the case explored in Fig. 5.4a and raises the fine tuning. A combination of a heavy Z' and consequently heavy off-diagonal terms in the 2×2 neutralino matrix eq.(2.155) with a comparable size of M_1' will result in two heavy mass eigenstates comparable to the mass of the Z'. For the lowest fine tuning point of the solid black line with $M_{Z'} = 3$ TeV, we find that the fifth lightest physical neutralino state has a mass $m_{\tilde{\chi}_5^0} = 1940$ GeV and is a mixture of singlino $|N_{55}|^2 = 70.5\%$ and bino primed $|N_{56}|^2 = 29.5\%$ gauge eigenstates. For the heaviest Z' (solid blue line) the fine tuning at the lowest point is about $\Delta_Z = 850$ with the fifth lightest neutralino being mostly singlino ($|N_{55}|^2 = 71.4\%$) and the heaviest $\tilde{B}'$ like neutralino having mass around $m_{\tilde{\chi}_6^0} = 6.3$ TeV and decoupling from the rest of the states.

- We conclude from the previous study that heavy gaugino masses would in principle create cancellations as in the MSSM reducing the fine tuning drastically. It appears that in the case of the pUMSSM the heavier the Z' boson and the larger the $U(1)'$ charges it is difficult to reduce the fine tuning below a certain amount due to the heavy tree-level soft masses $m_{H_u}^2, m_s^2$ which will dominate Δ_Z. In order to have an MSSM like reduction effect ($\Delta_Z \sim \mathcal{O}(10-20)$) having heavy gaugino masses the Z' boson has to be relatively light (sub-TeV) with small $U(1)'$ charges. We stress here the fact that these observation have a qualitative character and should motivate further study for the accurate calculation of the fine tuning measure by resumming the logarithms and linking the weak scale dynamics to the high-scale model input.

- Although the fine tuning coming from the tree-level quantities appears to be an

impervious barrier (in case we have convinced ourselves that the solution of heavy gauginos is not just a spurious cancellation but is indicated by the high-scale theory) we have to mention some important distinguishing differences in the phenomenology of the two models pUMSSM and MSSM, emanating from the previous observations on the analytic expressions of the fine tuning measure Δ_Z. As we have previously discussed in Chapter 4 a natural MSSM requires a spectrum with light Higgsino μ, light stops $\tilde{t}_1$, light sbottoms $\tilde{b}_1$ and a light gluino $\tilde{g}$ not much heavier than 1 TeV. On the other hand for the reasons we have explicated in this section as well as in Chapter 4, a natural MSSM spectrum also requires that the bino $\tilde{B}$ and wino $\tilde{W}^0$ masses are fairly heavy of the order of a few TeV. From a phenomenological point of view this translates into large couplings of the Higgsino like LSP with the lightest third generation squarks and thus providing a discovery method which involves the pair production and decays of the lightest stops and sbottoms. Using similar assumptions for the natural spectrum, these decay channels are being used by experimental collaborations to set limits on the visible cross sections [1, 2, 42]. The pUMSSM seems to diverge from this concept. In the $U(1)'$ extended scenarios with an enhanced tree-level Higgs boson and lighter soft masses the wino and bino masses have to be much lighter than in the MSSM, as we have seen because otherwise they will dominate the fine tuning and drive it to very large values. Therefore the Higgsinos will mix more strongly with the $\tilde{B}$ and $\tilde{W}^0$ to form the lightest mass eigenstates which will result in suppressed branching ratios and the possibility of evading current experimental analyses. In combination with the fact that the lightest stops are enhanced by the extra D-term contributions, this results in a reduction of the production cross sections for these sparticles.

- In this survey we will not consider cancellations stemming from the gaugino masses when calculating the fine tuning measure Δ_Z, and therefore we will fix the gaugino masses below TeV. On the other hand in order to impose the stringent constraints from available experimental analyses and achieve large coverage with `Fastlim` we have no other option but follow the same lines of our previous analysis for the MSSM and decouple the gaugino masses $M_1,\ M_2,\ M_3$ to be of the order of a few TeV, except the bino primed mass which is taken to be small $M_1' = 10$ GeV.

5.2 Phenomenology and naturalness of pUMSSM. Numerical Analysis

In this section we will present the results of our numerical analysis. We examine the fine tuning of the phenomenological UMSSM with generic charges and we impose constraints from the perturbativity of the extra gauge coupling, the LHC data for the Higgs mass and from supersymmetry searches of the lightest superpartners. We compare our results with the study on the MSSM and point out potentially interesting scenarios.

(a) Universal Charges (b) Non Universal Charges

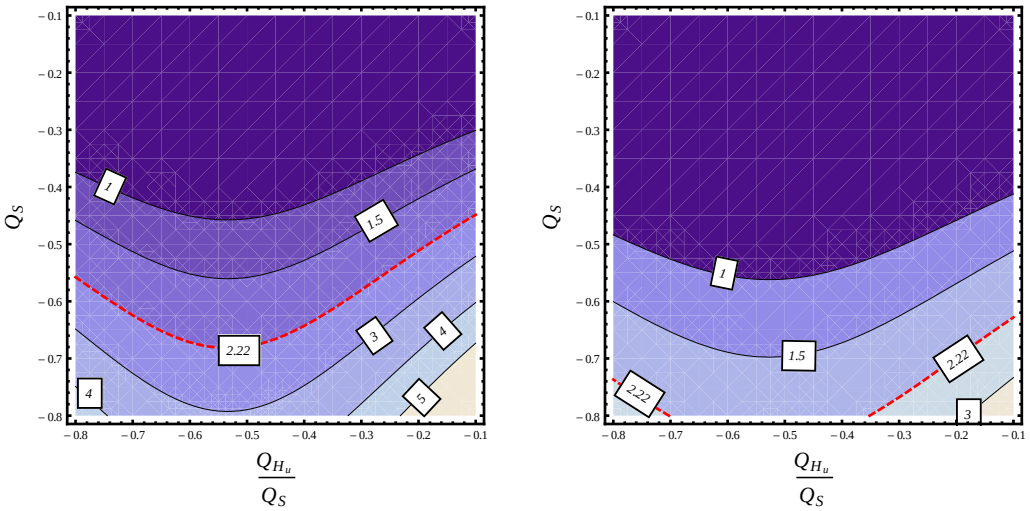

Figure 5.5: Plot of $\sum_i n_i Q_i$ in eq.(3.10) on the (r, Q_s) plane for universal and non-universal charges. (a) we consider $Q_Q = Q_{\bar{u}}$ and $Q_L = Q_{\bar{e}}$. (b) $Q_{Q_3} = Q_{T^c}$ and $Q_{L_3} = Q_{E^c}$. All other charges except third generation sfermions are considered to have fixed value $Q_{\text{other}} = 1/20$. The red line depicts the stricter upper limit $\sum_i n_i Q_i < 2.22$.

Perturbativity of charges. Having introduced our parametrization of the Higgs sector $U(1)'$ charges by the pair (r, Q_s), we proceed to investigate how the perturbativity bound given in eq.(3.10) imposes a constraint on our charge assignments. In Fig. 5.5 we plot the sum $\sum_i n_i Q_i$ which enters the beta function of the extra gauge coupling and is constrained from the requirement that g_1' has to be perturbative up to the GUT scale eq.(3.10). The left plot assumes family universal charges with the assumption that $Q_Q = Q_{\bar{u}}$ and $Q_L = Q_{\bar{e}}$ while the right plot is made with the same assumption for the third families of squarks and sleptons and all other charges are considered to have a fixed $U(1)'$ charge $Q_{\text{other}} = 1/20$. For $Q_{\text{other}} = 0$ the bounds are not significantly altered in Fig. 5.5 and therefore the plot is not shown here. We show in the plot only the strict bound $\sum_i n_i Q_i < 2.22$ (red line). We see that even in the universal scenario if we choose ranges $-0.6 \leq r \leq -0.1$ and

$-0.6 \leq Q_s \leq -0.1$ we are safe up to $r \lesssim -0.35$. In the case of non-universal charges one can tolerate even larger couplings. Notice that the point $(-0.6, -0.6)$ renders a sum of $\sum_i n_i Q_i = 1.77$ in the universal case and $\sum_i n_i Q_i = 1.16$ for the non-universal one. This is a propitious result since, as we have shown in Chapter 3 the bottom left corner of the (r, Q_s) plane is also favoured due to the boost on the tree-level Higgs mass. Therefore, we will use the conservative ranges above for our study which satisfy the stricter bound.

Contour plots $\mathbf{m_{Q_3}}$vs$\mathbf{A_t}$. In these section we present plots on the plane (A_t, m_{Q_3}). We consider for all plots that the right and left-handed soft masses of the top squarks are degenerate i.e. $m_{Q_3} = m_{T^c}$. Like in the MSSM, the case of having a hierarchy between the two soft parameters would be very interesting, especially when $m_{T^c} < m_{Q_3}$ but it will not be dealt with in these plots. We will classify the results in terms of the Z' mass and we will split them in two categories: (1) light Z' scenarios and (2) heavy Z' scenarios. The first one will contain sub-TeV Z' bosons and the second one will deal with Z' masses above 1 TeV.

In the ($\mathbf{m_{Q_3}}$vs$\mathbf{A_t}$) plots the mass of the Z' boson and the effective Higgsino mass μ_{eff} are fixed, $\tan\beta = 20$. The charges are also fixed by the pair (r, Q_s), the first and second generation of sfermions are all assumed to have very small $U(1)'$ charges and therefore we set $Q_{\text{other}} = 0$ for the calculation of the fine tuning. This way we diminish the effect of the terms $2Q_{H_u}S_1$ and $2Q_sS_1$ and we focus on the fine tuning coming from the stop masses and the Z' boson. The only parameters which are varied, are the soft supersymmetry breaking masses $m_{Q_3} = m_{T^c}$ and the soft trilinear coupling A_t. Hence the fine tuning due to the Z' boson is fixed and Δ_Z is controlled by the fine tuning stemming from the third generation squark sector. The importance of these plots therefore focuses on the Higgs mass. A boosted Higgs mass, which falls into the vicinity of the Higgs measured mass for light soft masses would potentially be beneficial. We present the plots as follows: Every figure contains two plots, both plots contain the Higgs mass contours (black lines), the lightest stop mass contours (red dashed lines) and the tachyonic mass region where either colour breaking is taking place or the minimum of the potential is unstable (saddle point). The allowed Higgs mass region is taken to be 124 GeV $\leq m_{h_1^0} \leq$ 127 GeV and is depicted by a light blue shaded area. The left plot contains additionally the re-interpreted collider constraints from exotic searches, using the program `Fastlim`. The coloured areas correspond to the different ATLAS experimental studies and are shown in the caption. The right plot contains additionally only the fine tuning contours and is placed next to each other for better visibility. The deviation from the W mass constraint and the mixing

angle will also be stated for each plot. Finally we will comment on the interpretation of these results.

(1) Light Z'

(a) Exclusion Regions from Collider Searches (b) Fine Tuning Contours

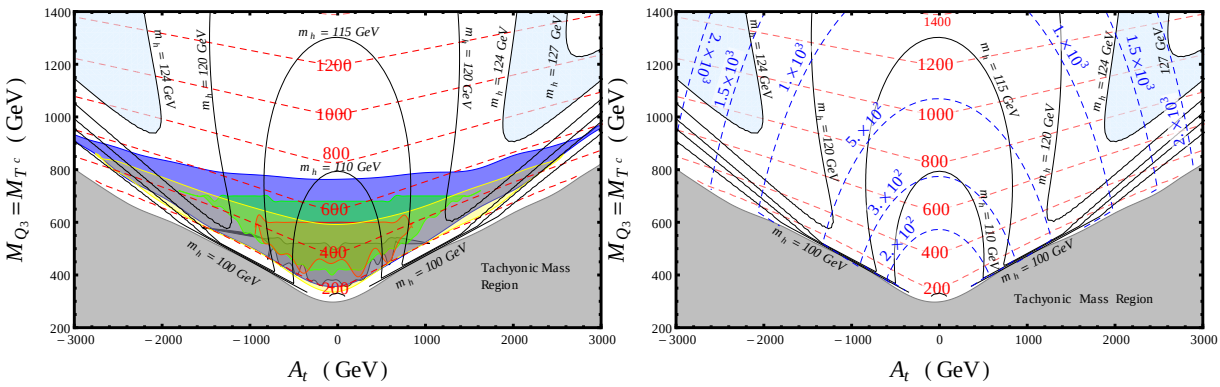

Figure 5.6: The charges are $(r, Q_s) = (-0.6, -0.1)$ and the mass of the Z' is $M_{Z'} = 450$ GeV. **Left plot**: five ATLAS searches impose strong constraints: 1) AC2013024 (dark blue) 2) AC2013053 (yellow) 3) AC2013037 (green) 4) AC2013048 (red) 5) AC2013093 (black). **Right plot**: The lightest Higgs is slightly boosted and for the lowest point in the blue region with $m_{h_1^0} = 124$ GeV the stop soft masses are $m_{Q_3} \approx 910.3$ GeV for $A_t = 1.97$ TeV. In the MSSM the values for the lowest point are $m_{Q_3} \approx 943.2$ GeV for $A_t = 2.03$ TeV. Although the Higgs mass is obtained for slightly lighter soft masses and smaller mixing, especially for $A_t > 0$, the fine tuning remains at the MSSM level $\Delta_Z \sim (1.1 - 1.2) \times 10^3$. The Higgs mass boost is not dramatic since the Higgsino mass is very small $\mu_{eff} = 105$ GeV. As we have seen earlier when we are sitting on the top left corner of the (r, Q_s) plane we have to be careful with the stability of the scalar potential. If μ_{eff} is too large the masses $m^2_{h_1^0}$ run negative. The Higgs mass at tree-level is found to be $m^{\text{tree}}_{h_1^0} = 91.3$ GeV.

Supplementary Comments on Fig. 5.6:

Stop masses are excluded up to $m_{\tilde{t}_1} \simeq 700$ GeV for zero mixing but the Higgs mass, $m_{h_1^0} \simeq 110$ GeV is nowhere near the observed Higgs mass. The coefficients α, ξ which can reduce the fine tuning have values $\xi = 1.009$ and $\alpha = -0.49$. Therefore only the second coefficient can have a positive effect on suppressing the fine tuning. The W mass constraint is within 1σ and the mixing angle is $\theta_{ZZ'} = -6.89 \times 10^{-3}$.

(a) Exclusion Regions from Collider Searches (b) Fine Tuning Contours

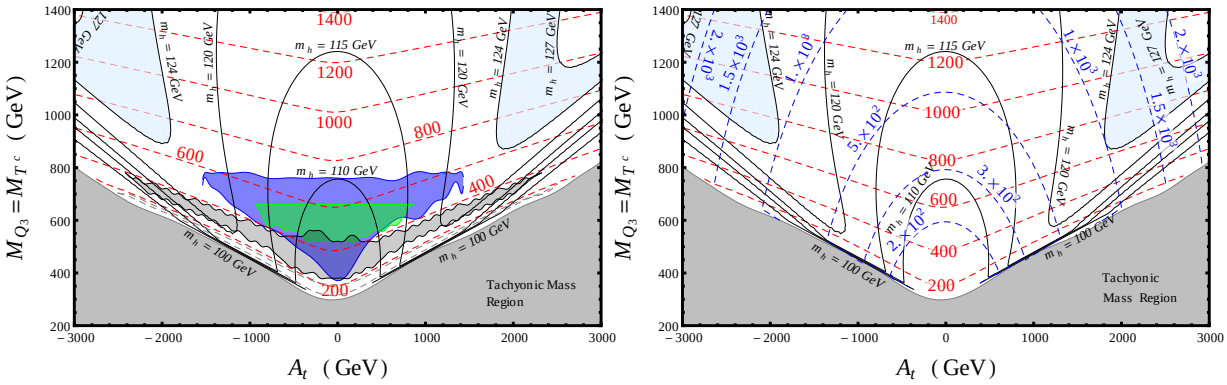

Figure 5.7: The charges are $(r, Q_s) = (-0.6, -0.1)$ and the mass of the Z' is $M_{Z'} = 450$ GeV as in Fig. 5.6. In this plot $\mu_{eff} = 200$ GeV has increased. **Left plot**: 3 ATLAS searches impose the strongest constraints: 1) AC2013024 (dark blue) 2) AC2013037 (green) 3) AC2013053 (black). The lowest point for which $m_{h_1^0} = 124$ GeV is for $A_t \simeq 1.88$ TeV where $m_{Q_3} = 869.2$ GeV. Notice that the Higgs mass contour almost touches the stop mass contour (red line) with mass $m_{\tilde{t}_1} = 600$ GeV. This point is currently not excluded by experimental searches. The larger Higgsino LSP mass combined with the large mixing reduces the branching ratio of $\tilde{t}_1$ decaying to Higgsino reducing the number of observable events. The gray dashed line depicts the area where the stops become lighter than the LSP. **Right plot**: The fine tuning appears slightly reduced and the lower points with the Higgs mass $m_{h_1^0} = 124$ GeV have $\Delta_Z = 10^3$. The W mass constraint is within 1σ and $\theta_{ZZ'} = -6.89 \times 10^{-3}$ as in Fig. 5.6. The coefficients ξ, α are also modified since μ_{eff} has increased $\xi = 1.023$ and $\alpha = -0.21$. The Higgs mass at tree-level is found to be $m_{h_1^0}^{\text{tree}} = 92$ GeV.

(a) Exclusion Regions from Collider Searches (b) Fine Tuning Contours

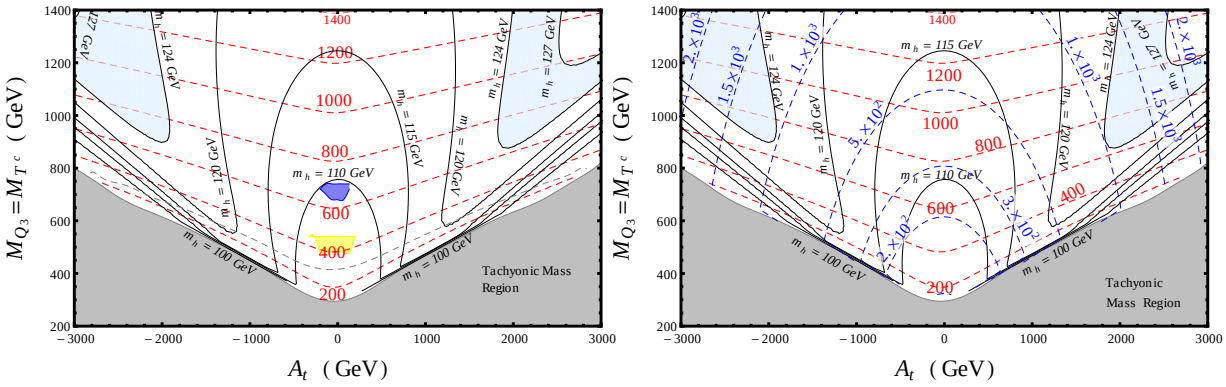

Figure 5.8: For completeness we show this plot which has the same parameter values with Fig. 5.6 and Fig. 5.7 but now $\mu_{eff} = 300$ GeV. The collider constraints (left plot) are minimal due to the heavy Higgsino LSP. Only two very small regions are excluded 1) AC2013024 (blue) 2) AC2013053 (yellow). Again these regions achieve very light Higgs mass and are not interesting. The lightest stop is no longer enhanced by the heavy Higgsinos. For heavier Higgsinos we anticipate that the Higgs mass is going to be reduced. The fine tuning for the lowest point with $m_{h_1^0} = 124$ GeV is $\Delta_Z = 10^3$. The coefficients have values $\xi = 1.02$ and $\alpha = 0.29$. The area below the gray dashed line gives the charged LSP region which is excluded. Finally $m_{h_1^0}^{\text{tree}} = 92$ GeV.

(a) Exclusion Regions from Collider Searches (b) Fine Tuning Contours

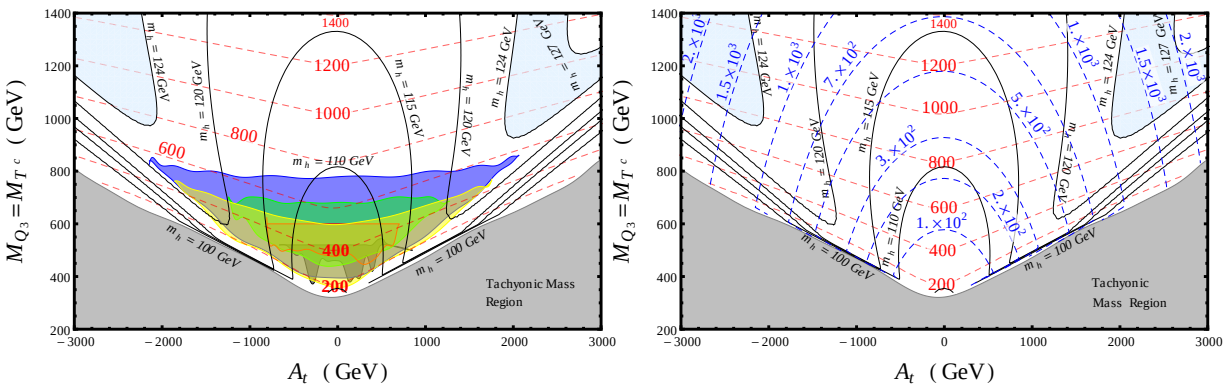

Figure 5.9: In this plot we explore the bottom-right corner of the $(r, Q_s) = (-0.1, -0.6)$ plane. Due to the fact that $|r|$ is small we can obtain a light Z' with mass $M_{Z'} = 360$ GeV within less than 2σ deviation from the W mass constraint. The mixing angle is $\theta_{ZZ'} \simeq -10^{-2}$. The Higgsino mass is $\mu_{eff} = 120$ GeV to avoid negative large contributions to the Higgs mass since $|r| < (\mu_{eff}/M_{Z'})^2 = 0.11$ already at this point, $m_{h_1^0}^{\text{tree}} = 92$ GeV. **Left plot**: The exclusion regions from ATLAS searches are 1) AC2013024 (blue) 2) AC2013053 (yellow) 3) AC2013048 (red) 4) AC2013093 (black) 5) AC2013024 (green). The Higgs mass is MSSM like, the lowest points in the light blue area have ($A_t \simeq -2.1$ TeV, $m_{Q_3} = 972$ GeV) and ($A_t \simeq 2.03$ TeV, $m_{Q_3} = 923$ GeV). As anticipated Δ_Z is also MSSM like. The coefficients have values $\xi = 0.987$ and $\alpha = 0.122$.

(a) Exclusion Regions from Collider Searches (b) Fine Tuning Contours

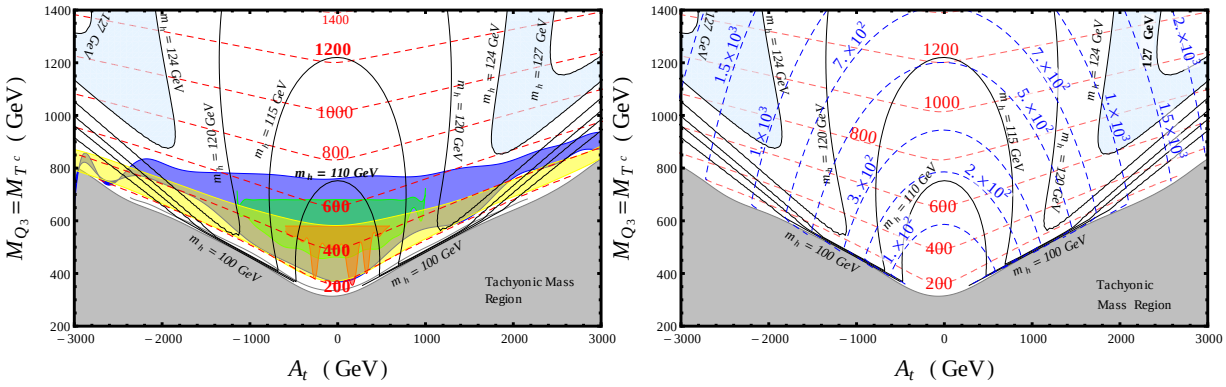

Figure 5.10: $(r, Q_s) = (-0.1, -0.6)$ with $M_{Z'} = 600$ GeV and Higgsino mass $\mu_{eff} = 120$ GeV. **Left plot:** Exclusion regions: 1) AC2013024 (blue) 2) AC2013053 (yellow) 3) AC2013037 (green) 4) AC2013048 (red). This is an interesting case where the Higgs mass is enhanced for a light Z'. At the lowest point inside the light blue region where $A_t = 1.84$ TeV and $m_{Q_3} = 851.3$ GeV the stop mass is very light $m_{\tilde{t}_1} = 600$ GeV evading the collider constraints. The deviation from the W mass is less than 1σ and $\theta_{ZZ'} = -3.7\times10^{-3}$. **Right plot:** The fine tuning is clearly reduced compared to the MSSM, $\Delta_Z \sim 850$ but not dramatically. Note that $m^{\text{tree}}_{h^0_1} = 92.2$ GeV. The coefficients $\xi = 1.025$ and $\alpha = -0.02$.

(a) Exclusion Regions from Collider Searches (b) Fine Tuning Contours

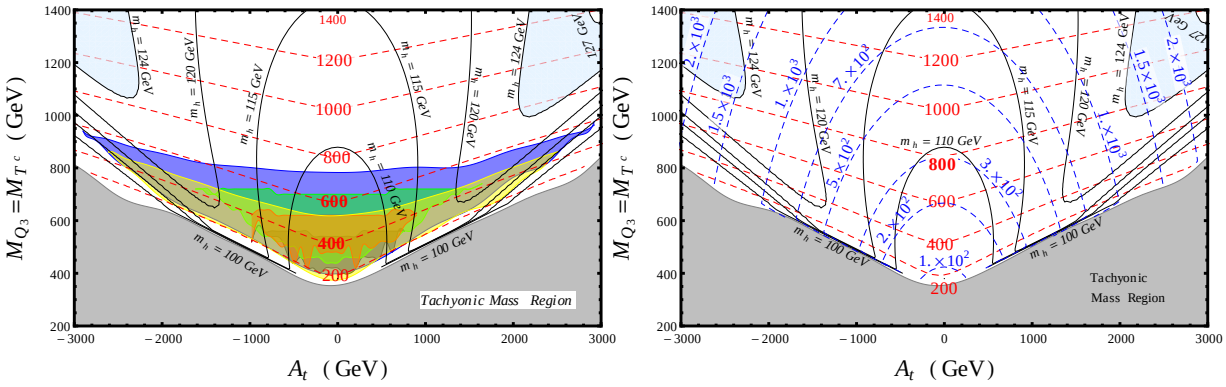

Figure 5.11: This plot investigates the top-right corner of the plane with $(r, Q_s) = (-0.1, -0.1)$ and light Z' mass near the electroweak scale $M_{Z'} = 200$ GeV. The Higgsino mass is chosen $\mu_{eff} = 105$ GeV to avoid tachyonic masses. **Left plot:** Exclusion regions 1)AC2013024 (dark blue) 2) AC2013053 (yellow) 3) AC2013037 (green) 4) AC2013048 (red) 5) AC2013093 (black). In this case the light Z' causes larger fine tuning due to the suppressed $m^{\text{tree}}_{h^0_1} = 89.8$ GeV. For $A_t \simeq 2.16$ TeV and $m_{Q_3} = 994.9$ GeV we have the lowest point in the allowed Higgs mass region (light blue). On top of that the coefficients $\xi = 0.973 < 1$ and $\alpha = 0.62$ also affect $\Delta_Z \sim 1.3 \times 10^3$ to increase. The W mass is within 1σ and the mixing angle takes the value $\theta_{ZZ'} = -6.9 \times 10^{-3}$.

Summary and comments. In these plots we have examined the possibility of a light Z' boson and its effect on the fine tuning. Although a light Z' has a small contribution to Δ_Z, it can lead as we saw in the previous plots to a larger fine tuning than in MSSM, because of the inability to reach the Higgs mass for light m_{Q_3}, m_{T^c}. As we have seen in Section 3.6.1 the top-left and top-right corners of the (r, Q_s) plane are extremely sensitive to the Higgsino mass and they can result in a suppressed tree-level Higgs mass $m_{h_1^0}^{\text{tree}}$. Therefore in some cases the amount of fine tuning coming from the stop soft masses can be greater than in the MSSM. In order to get a light Z' near the weak scale we need small couplings and relatively large $U(1)'$ breaking scales in order to pass the W mass constraint. If one assumes couplings $(r, Q_s) = (-0.1, -0.1)$, a light Z' with a mass $M_{Z'} \geq 120$ GeV is possible within 1σ deviation from the W mass constraint. We have seen that for $M_{Z'} = 200$ GeV (Fig. 5.11) the fine tuning becomes worse than in the MSSM for these reasons. The small couplings and light Z' boson mass result in small $U(1)'$ D-term contributions to the masses of the scalars and thus the lightest stops and sbottoms have MSSM-like masses. The experimental searches exclude masses for the lightest stops $\tilde{t}_1$ up to $m_{\tilde{t}_1} \lesssim 750$ GeV for zero mixing, very similar to the MSSM.

Larger ratio $|r|$ requires heavier $M_{Z'}$ masses to pass the W mass constraint. In this corner of the plane with $(r, Q_s) = (-0.6, -0.1)$, one can achieve an enhancement to the tree-level Higgs mass for slightly heavy Higgsino masses and have $\Delta_Z \sim 10^3$. For the corner with $(r, Q_s) = (-0.1, -0.6)$, small $|r|$ makes it easier to pass the W mass constraint and we can achieve $M_{Z'} \sim 450$ GeV and be within 1σ deviation from the W mass constraint. For slightly heavier $M_{Z'} = 600$ GeV one can have a slightly improved $\Delta_Z \sim 850$.

There is also the possibility of having a Z' boson with mass less than the mass of the Z boson. Such a light boson $M_{Z'} \leq (50 - 60)$ GeV would require couplings $(r, Q_s) = (-0.1, -0.1)$ to pass the W mass constraint and it seems impossible to achieve the observed Higgs mass. The Higgs potential is very unstable for this choice of the parameters and we have checked that $m_h^2 < 0$ goes negative, therefore we do not look at this case here.

From the analysis above we understand that a light Z' does not necessarily mean better fine tuning amongst the gauge extensions of the MSSM. Although it seems that the fine tuning for light Z' bosons is of the order of the MSSM, there are regions on the (r, Q_s) plane which can make the fine tuning to be worse than in the MSSM. A light Z' scenario with $(r, Q_s) = (-0.1, -0.1)$, as we have seen in the previous section, has small tree-level fine tuning and therefore one can benefit from an MSSM like reduction of Δ_Z due to heavy gauginos M_1, M_2 and/or M_1'. One would then end up with a spectrum which has light

Higgsinos and heavy binos and winos and possibly very light singlinos which would modify the phenomenology of pUMSSM compared to MSSM significantly.

(2) Heavy Z'

In this section we are looking at the most interesting corner of the $(r, Q_s) = (-0.6, -0.6)$ plane, because of the significant enhancement one can get not only by having larger $U(1)'$ charges but also from having a heavy effective Higgsino mass μ_{eff}. There is an interesting observation here, a heavy Higgsino in models with small couplings, like we discussed in the previous case of a relatively light Z', can cause a suppression of the tree-level Higgs and increase Δ_Z. Moreover, in this type of models the spectrum will also be accommodated by light top squarks and sbottoms due the fact that there will be no significant boost to the diagonal elements of the squark matrix from the $U(1)'$ D-terms. If no supersymmetric particles are observed in the next run of the LHC, these scenarios will be highly constrained as we can see from the previous plots. In heavy Z' scenarios the situation is different, the Higgs mass is achieved easier without the need of very heavy soft masses but the stops and sbottoms are driven to acquire heavy masses from the $U(1)'$ D-terms. Consequently heavy stops and sbottoms can easier hide themselves from experimental searches as we will show in the plots. We also perform calculations in the other corners of the (r, Q_s) plane to spot the differences with the other cases.

(a) $M_{Z'} = 2.1$ TeV and $\mu_{eff} = 200$ GeV (b) $M_{Z'} = 2.1$ TeV and $\mu_{eff} = 505$ GeV

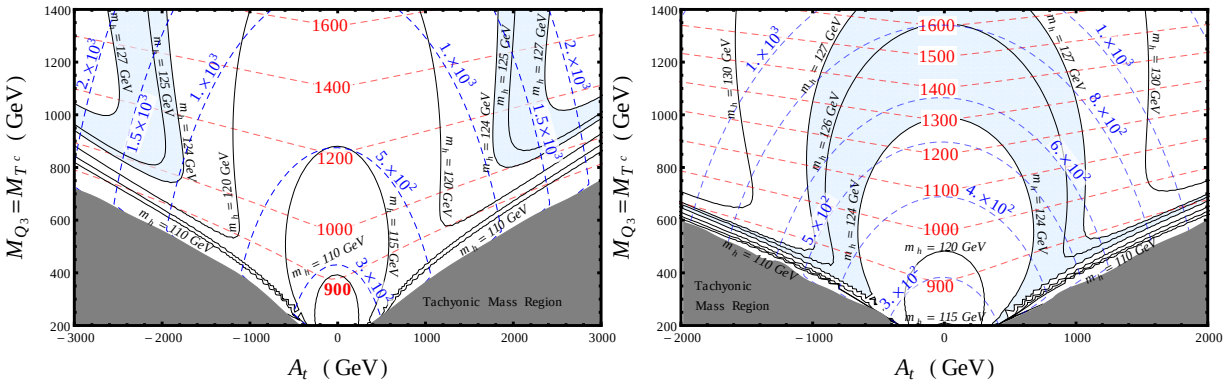

Figure 5.12: Both plots have charges $(r, Q_s) = (-0.6, -0.6)$. All points in both plots pass the constrains from all the experimental searches included in `Fastlim`, and therefore there are no excluded regions. The stop masses are now very heavy, evading the constraints. **Left plot:** The Higgs mass is enhanced at tree-level $m^{\text{tree}}_{h^0_1} = 93.3$ GeV and the lowest point in the shaded light blue area with $m_{h^0_1} \simeq 124$ GeV is achieved for $A_t = -1.86$ TeV and soft masses $m_{Q_3} = 741.2$ GeV. The lowest fine tuning at $A_t = -1.76$ TeV and $m_{Q_3} = 775.2$ GeV has the value $\Delta_Z \simeq 985$. The coefficients have values $\xi = 1.06$ and $\alpha = -0.58$. Although the Higgs mass is lifted up and it is easier to achieve the observed Higgs mass for low soft masses, the Δ_Z contours have moved closer to the origin due to the heavy Z' contribution to the fine tuning. Hence the improvement is not significant compared to the other cases and to MSSM. **Right plot:** Higgsino mass is increased to $\mu_{eff} = 505$ GeV. The tree-level Higgs mass is $m^{\text{tree}}_{h^0_1} = 104.6$ GeV and one can get the observed Higgs mass for very light soft masses and small mixing A_t. The lowest fine tuning is around $\Delta_Z \simeq 300$. The coefficients $\xi = 1.32$ and $\alpha = -0.48$. The mixing angle for both plots is $\theta_{ZZ'} = -1.8 \times 10^{-3}$ and the W mass is within 2σ error. Note that the tree-level fine tuning coming from $m^2_{H_u}$ is around $\Delta_Z \simeq 193$. This means that even if the gaugino masses are quite heavy the fine tuning cannot be reduced to a lower value.

(a) $M_{Z'} = 2.1$ TeV and $\mu_{eff} = 800$ GeV (b) $M_{Z'} = 2.7$ TeV and $\mu_{eff} = 800$ GeV

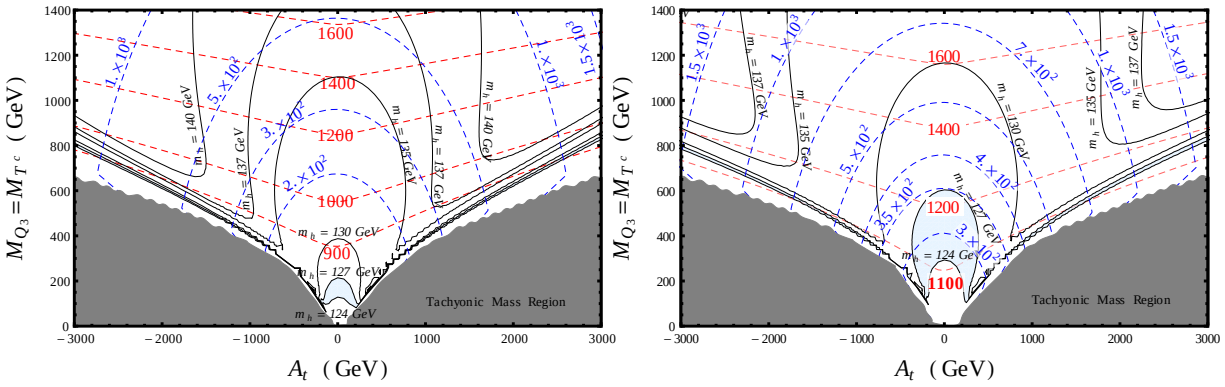

Figure 5.13: Both plots $(r, Q_s) = (-0.6, -0.6)$ **Left plot:** The tree-level Higgs mass is $m^{\text{tree}}_{h^0_1} = 118.3$ GeV very close to the observed Higgs mass. The lowest fine tuning for Higgs masses within the allowed region is $\Delta_Z \simeq 105$. Also note that $\Delta_Z(m^2_{H_u}) \simeq 97.4$. Notice that $\xi = 1.69$ and therefore suppresses Δ_Z by the same factor, that is why the contours have moved away from the origin compared to previous plots. Also $\alpha = -0.31$ which also benefits Δ_Z. $\theta_{ZZ'} = -1.8 \times 10^{-3}$ and the W mass is within 2σ error. **Right plot:** The tree-level Higgs mass is $m^{\text{tree}}_{h^0_1} = 110.2$ GeV. $\xi = 1.47$ and $\alpha = -0.42$. The lowest fine tuning is $\Delta_Z \simeq 267$. The mixing angle is $\theta_{ZZ'} = -1.1 \times 10^{-3}$ and the W mass is within 1σ error. Note that both plots all points pass the collider constraints.

(a) $M_{Z'} = 3.3$ TeV and $\mu_{eff} = 800$ GeV (b) $M_{Z'} = 3.9$ TeV and $\mu_{eff} = 500$ GeV

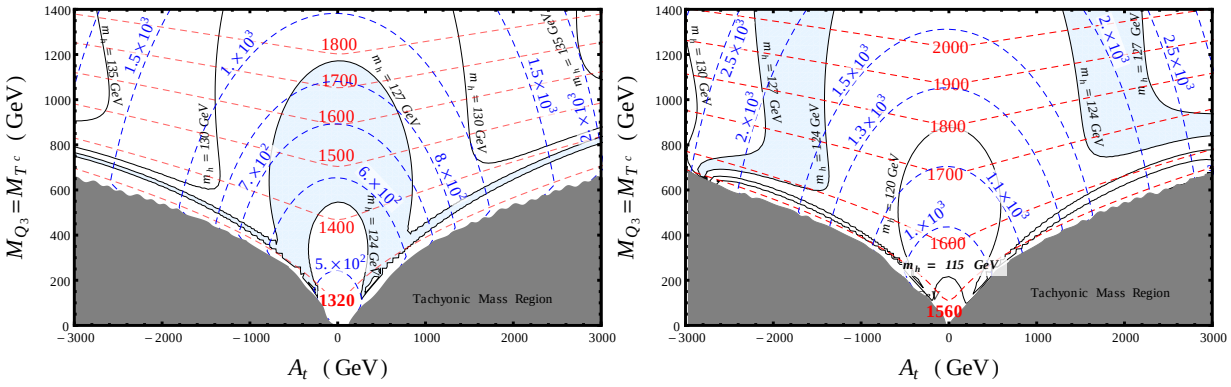

Figure 5.14: $(r, Q_s) = (-0.6, -0.6)$ **Left Plot:** The tree-level Higgs mass is now reduced $m^{\text{tree}}_{h^0_1} = 105$ GeV because of the heavier $M_{Z'}$. In order to get larger enhancement we would have to require heavier Higgsinos near the TeV scale or above. The coefficients obtain values $\xi = 1.33$, $\alpha = -0.48$ which reduce Δ_Z. The minimum value of fine tuning within the blue region is around $\Delta_Z \simeq 500$. Notice that the $\xi = 1.33$ is smaller compared to Figs. 5.13b, 5.13a and also Z' is heavier, therefore Δ_Z contours have moved closer to the origin. For lighter soft masses and smaller mixing A_t the fine tuning is now larger. The W mass is within 1σ error and $\theta_{ZZ'} = -7.3 \times 10^{-4}$. **Right plot:** $m^{\text{tree}}_{h^0_1} = 95.4$ GeV and $\xi = 1.1$ and $\alpha = -0.56$. Δ_Z has increased tremendously and even for very light stop soft masses and $m_{h^0_1} \simeq 125$ GeV, $\Delta_Z \sim 1.5 \times 10^3$. The mixing angle is $\theta_{ZZ'} \sim -5.3 \times 10^{-4}$.

(a) Exclusion Regions from Collider Searches (b) Fine Tuning Contours

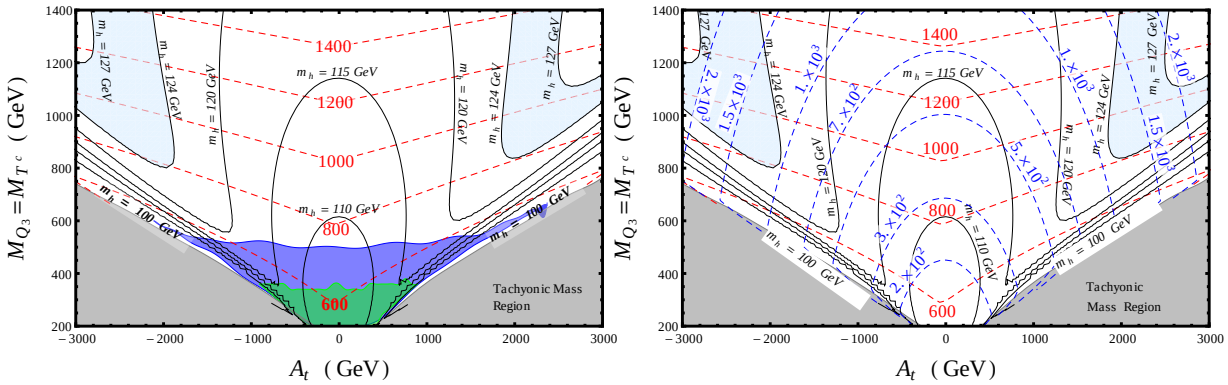

Figure 5.15: **Left plot:** $(r, Q_s) = (-0.1, -0.6)$, $M_{Z'} = 3.6$ TeV and Higgsino mass $\mu_{eff} = 150$ GeV. The W mass is within 1σ and $\theta_{ZZ'} = -1.01 \times 10^{-4}$. Note that in this case the stop charges are also small and the $U(1)'$ D-term contributions to the stop masses is not as large as in the $(-0.6, -0.6)$ case where we had very heavy stops. We have constraints from two experimental searches 1) AC2013024 (blue) 2) AC2013037 (green). The tree-level Higgs mass is $m_{h_1^0}^{\text{tree}} = 91$ GeV. For $A_t = -1.98$ TeV and $m_{Q_3} = 800$ GeV, $m_{h_1^0} = 124$ GeV and $m_{\tilde{t}_1} \simeq 800$ GeV. **Right plot:** The coefficients entering Δ_Z are $\xi = 1.00$ and $\alpha = -0.061$. Due to the small ratio r the effect of the heavy Z' on Δ_Z is not excessive. Furthermore, small α suppresses $\Delta_Z(\delta(\alpha m_s^2))$. The fine tuning is MSSM-like with lowest point at $\Delta_Z \sim 10^3$. MSSM-like Δ_Z with very heavy Z' and relatively light stops.

(a) Exclusion Regions from Collider Searches (b) Fine Tuning Contours

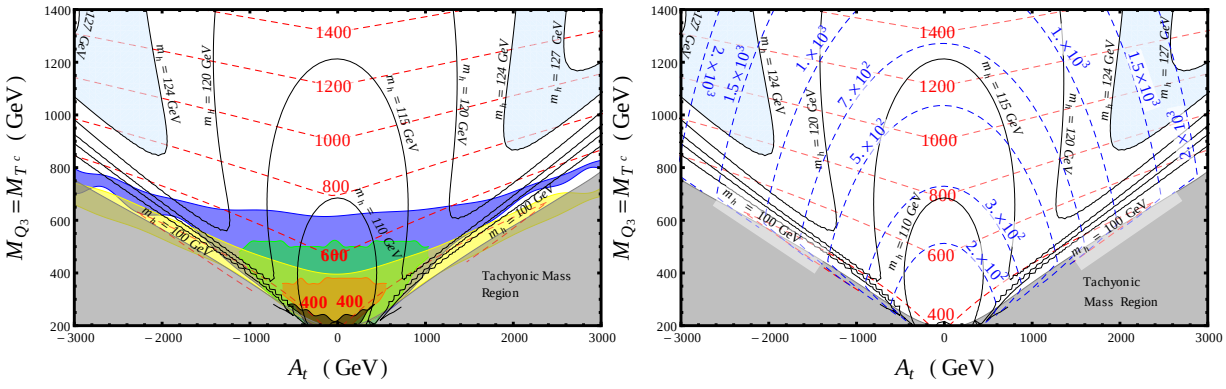

Figure 5.16: **Left plot:** $(r, Q_s) = (-0.1, -0.1)$, $M_{Z'} = 3.0$ TeV and Higgsino mass $\mu_{eff} = 150$ GeV. The W mass is within 1σ and $\theta_{ZZ'} = -2.4 \times 10^{-5}$. The stop masses are slightly heavier again than the MSSM by around 100 GeV. Their larger $\sigma(pp \to \tilde{t}_1\tilde{t}_1)$ results in exclusion regions 1) AC2013024 (blue) 2) AC2013037 (green) 3)AC2013053 (yellow) 4) AC2013093 (black) and 5) AC2013048 (red). Tree-level Higgs mass $m_{h_1^0}^{\text{tree}} = 100$ GeV. **Right plot:** The lowest fine tuning is around $\Delta_Z \sim (1.1 - 1.2) \times 10^3$. The coefficients $\xi = 1$ and $\alpha = -0.095$. So here again, we have a heavy Z' with relatively light stops and MSSM-like fine tuning.

Summary and comments. We have identified an interesting region on the (r, Q_s) plane which can reduce the amount of fine tuning in gauge extensions of the MSSM, due to the large enhancement of the Higgs mass. We find that for the bottom-left corner with $(r, Q_s) = (-0.6, -0.6)$ where the effect from heavy Higgsinos is maximal, that we can achieve fine tuning within the region $100 \lesssim \Delta_Z \lesssim 500$ for Z' bosons with masses 2.1 TeV $\lesssim M_{Z'} \lesssim$ 3.3 TeV and $\mu_{eff} = 800$ GeV. Note that the lower limit is set by the W mass constraint and at this point a lighter Z' mass would lead to a more than 2σ deviation from the central value. This corner with heavy Z', cannot achieve a fine tuning of the order of $\Delta_Z \sim \mathcal{O}(10 - 20)$ because of the large tree-level fine tuning coming from the soft masses $m^2_{H_u}, m^2_s$. Heavy gauginos can reduce the fine tuning up to a certain point until the tree-level soft masses dominate Δ_Z. The other corners of the plane will still suffer from the tree-level fine tuning which will determine the lowest possible Δ_Z one can achieve in a given model and additionally will not benefit from an enhanced Higgs mass. Therefore in these cases heavy gauginos will be needed to reduce Δ_Z.

The corner $(r, Q_s) = (-0.6, -0.6)$ offers an interesting case with heavy Higgsinos and heavy third generation squarks which can evade the experimental searches. The binos and winos can be relatively light compared to the MSSM and modify the light spectrum compared to a natural MSSM scenario. This can have implications to current experimental search strategies since the couplings and branching ratios are also modified. The $\tilde{B}'$ is preferably light in order to avoid large contributions to Δ_Z, resulting in heavy singlinos and heavy bino primed neutralinos which have approximately the same mass with $M_{Z'}$.

Contour plots on (r, Q_s) plane. In these plots we present the Higgs contours (black solid lines) and the lightest stop mass contours (red lines) along with exclusion regions made with `Fastlim` (left plot) and the fine tuning contours (right plot: blue dashed lines). The masses are given in units of GeV. For those plots that we do not get exclusion regions we give only one figure. The soft SUSY breaking masses of the stops and the Higgsino mass is fixed and shown in the plots. The Z' masses vary with Q_s.

(a) Exclusion Regions from Collider Searches (b) Fine Tuning Contours

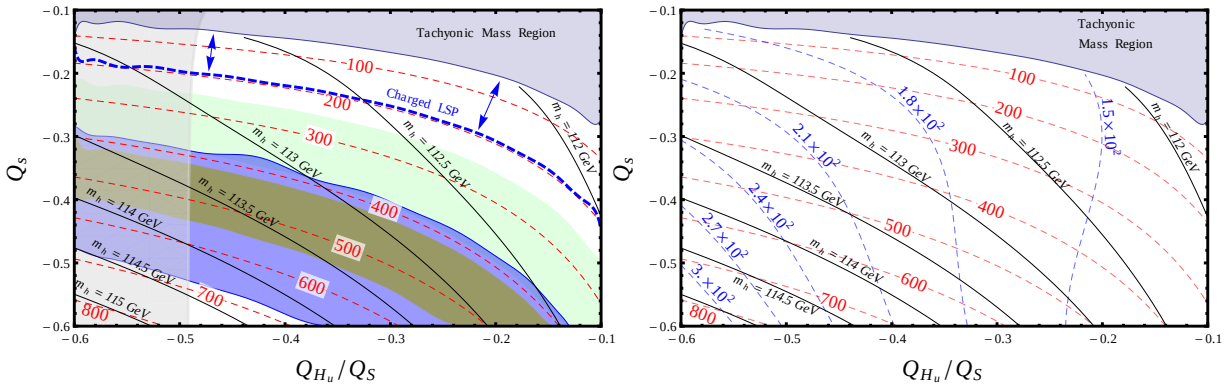

Figure 5.17: The soft stop masses are fixed $m_{Q_3} = m_{T^c} = 400$ GeV. Stop trilinear coupling $T_t = y_t A_t = 500$ GeV and Higgsino mass $\mu_{eff} = 200$ GeV. The mass of the Z' is varied with Q_s within the range 350 GeV $\leq M_{Z'} \leq$ 2.1 TeV. **Left:** Exclusion regions: 1) AC2013024 (blue) 2) AC2013037 (yellow) 3) AC2013053 (light green). The Higgsino mass is very light to produce any positive effect on the tree-level Higgs mass, hence $m_{h_1^0}^{\max} \sim 115$ GeV. Stop masses are excluded up to $m_{\tilde{t}_1} < 700$ GeV. Note that for very light stops $m_{\tilde{t}_1} < 180$ GeV `Fastlim` does not produce output because in the efficiency tables the lightest stops are $m_{\tilde{t}_1} = 180$ GeV. Thus the interpolation to reconstruct the visible cross section cannot proceed, giving no output. The blue dashed region shows the charged LSP region. **Right:** Δ_Z is increasing as Z' becomes heavier and is reduced as we move to the right for smaller values of the ratio $|r| = |Q_{H_u}/Q_s|$. One can see the dependence on the Higgs mass on r. Moving to the right not only reduces the fine tuning but also suppresses the Higgs mass. The light gray region on the left shows the W mass constraint within 2σ. All the points on the right of the gray area are within 1σ error. Moving to smaller values of $|r|$ makes it easier to pass the W mass constraint but again removes the benefits from an enhanced Higgs mass.

(a) Exclusion Regions from Collider Searches (b) Fine Tuning Contours

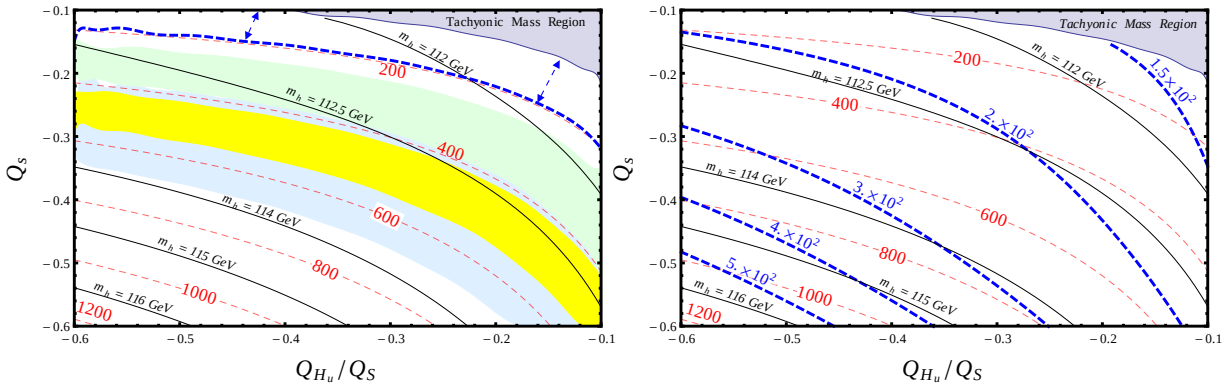

Figure 5.18: For this plots $m_{Q_3} = m_{T^c} = 400$ GeV, $T_t = 500$ GeV, $\mu_{eff} = 200$ GeV and 500 GeV $\leq M_{Z'} \leq$ 3.0 TeV. **Left:** Exclusion regions: 1) AC2013024 (blue) 2) AC2013037 (yellow) 3)AC2013053 (light green). All points within 1σ error of the W mass.

(a) 3.5 TeV $\leq M_{Z'} \leq$ 6.0 TeV

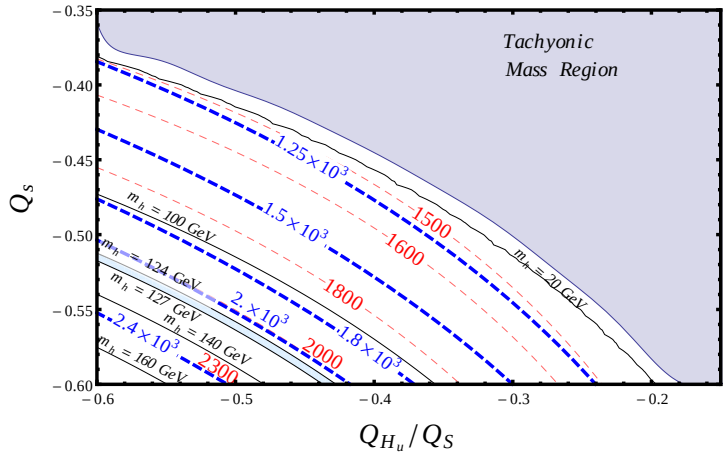

Figure 5.19: For this plot $m_{Q_3} = m_{T^c} = 400$ GeV, $T_t = 1$ TeV, $\mu_{eff} = 200$ GeV and 3.5 TeV $\leq M_{Z'} \leq$ 6.0 TeV. Due to the large trilinear coupling T_t a large region gives tachyonic masses (light blue). The Higgs mass is achieved for $M_{Z'} \simeq 5.1$ TeV for $r = -0.6$. Increasing $M_{Z'}$ increases the Higgs mass and smaller ratio $|r|$ is needed to achieve $m_{h_1^0} \sim 125$ GeV. The fine tuning contours (blue dashed lines) are moving almost parallel to the Higgs mass contours. Note that the Higgsino mass is light. Heavier Higgsino would move the allowed Higgs mass region towards the top-right corner of the plot. The stops are heavier than $m_{\tilde{t}_1} > 2$ TeV due to the large $U(1)'$ D-terms and all points pass the experimental constraints. The W mass constraint is well within 1σ error.

(a) Exclusion Regions from Collider Searches

(b) Fine Tuning Contours

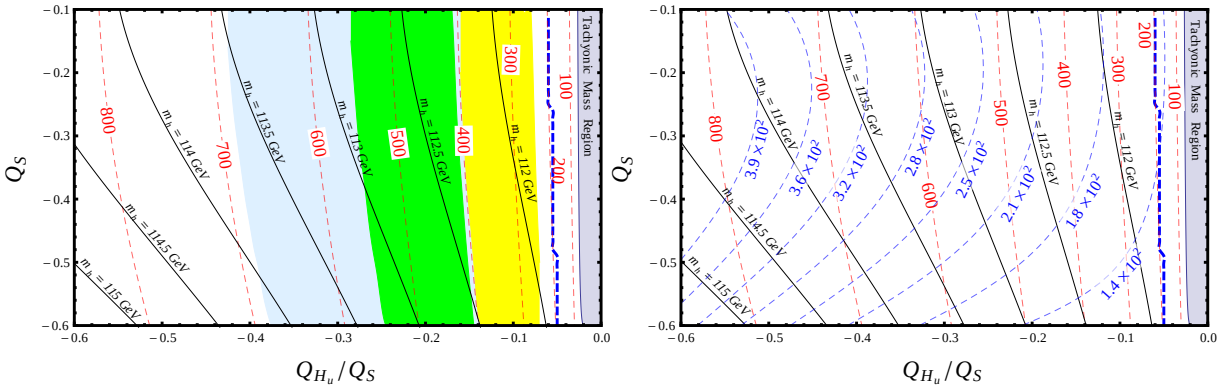

Figure 5.20: In this plot $M_{Z'} = 2.1$ TeV is fixed. Higgsino mass has the value $\mu_{eff} = 200$ GeV and $m_{Q_3} = m_{T^c} = 0.4$ TeV and $T_t = 0.5$ TeV. **Left:** Eclusion regions: 1) AC2013024 (light blue) 2) AC2013037 (yellow) 3) AC2013053 (green). All points are within 2σ error of the W mass. The maximum Higgs mass is below the observed value. **Right:** For $M_{Z'}$ = fixed increasing $|Q_s|$ decreases Δ_Z. Increasing the ratio $|r|$ increases Δ_Z as we would have expected.

Contour plot on $(X = m_{Q_3} - m_{T^c}, A_t)$ plane. Here we present a plot similar to those presented for the MSSM in Figs. 4.5, 4.6, 4.9. The sum of the squares of the left-handed and right-handed stop soft masses $m^2_{Q_3} + m^2_{T^c} = C^2$ is fixed and we vary the difference $X = m_{Q_3} - m_{T^c}$ between them and the soft trilinear coupling A_t. The Z' boson mass it is also fixed and the fine tuning depends only on A_t. The fine tuning contours Δ_Z are simply straight lines parallel to the horizontal axis $X = m_{Q_3} - m_{T^c}$.

(a) $C = 600\sqrt{2}$ GeV and $M_{Z'} = 2.1$ TeV (b) Δ_Z contours

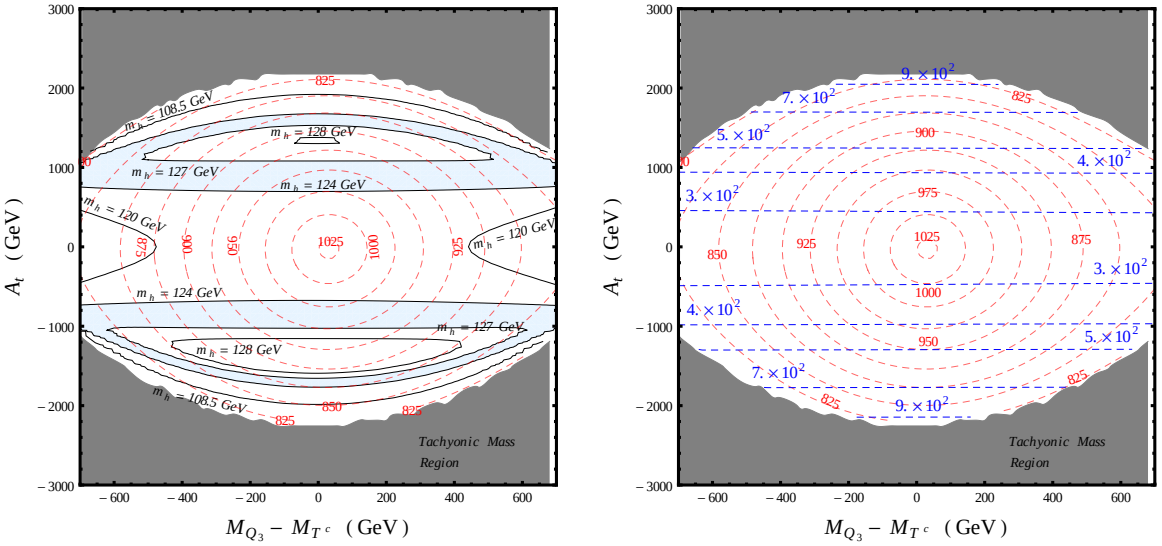

Figure 5.21: $(r, Q_s) = (-0.6, -0.6)$ and the Higgsino mass is $\mu_{eff} = 500$ GeV in order to boost the tree-level Higgs mass. **Left**: The black contours correspond to the Higgs mass contours and the shaded area is the allowed region within 124 GeV $\leq m_{h^0_1} \leq$ 127 GeV. The stop masses are shown in red dashed contours. **Right:** The stop contours (red) are shown with Δ_Z contours (blue). One can achieve $m_{h^0_1} \sim 125$ GeV for $A_t < 1$ TeV even for $m_{Q_3} \neq m_{T^c}$. All the points pass the experimental searches available in `Fastlim`. The stop masses are heavier than $m_{\tilde{t}_1} > 825$ GeV and at the center of the plot $m_{\tilde{t}_1} \simeq 1$ TeV. The fine tuning is around $\Delta_Z \sim 350$ for the smaller A_t in the blue region (right plot). Compare this plot with Fig. 4.9. pUMSSM with heavy stops driven by the $U(1)'$ terms can evade current and possibly future searches. In Table 5.1 we give the total production cross sections for several points with zero trilinear coupling A_t. Moving from left to right in the plot, one can see how the lightest sbottoms become heavier as we increase the left-handed soft mass of the third generation of squarks m_{Q_3}. Note also how the total cross section changes as we move to the right of the plot. For $X = m_{Q_3} - m_{T^c} = -X_1 < 0$ and $A_t = 0$ the cross section is smaller than $X = m_{Q_3} - m_{T^c} = X_1$ and $A_t = 0$ since the bottom squarks are becoming heavier.

$A_t = 0$, X (GeV) =	-600	-400	-200	0	200	400	600
$m_{\tilde{t}_1}$ (GeV)	846	898	961	1024	983	924	874
$m_{\tilde{t}_2}$ (GeV)	1189	1151	1101	1044	1084	1136	1175
$m_{\tilde{b}_1}$ (GeV)	836	889	952	1016	1076	1128	1168
σ_{tot} (fb)	4.0	2.4	1.5	1.02	0.94	1.15	1.6

Table 5.1: The masses of $\tilde{t}_1$, $\tilde{b}_1$, $\tilde{t}_2$ and the cross sections for the points $(X, A_t = 0)$ in Fig. 5.21. The masses are calculated with `SARAH + SPheno` and the total cross sections with `Fastlim`.

Summary. In Figures 5.17, 5.18 one can see that for the same Z' boson mass, i.e. for lines parallel to the $r = Q_{H_u}/Q_s$ axis, in order to evade the constraints from collider searches $|r|$ has to be relatively large, depending on the $M_{Z'}$ mass. In these plots even for $M_{Z'} = 3$ TeV the Higgs mass does not go beyond $m_{h_1^0} \simeq 117$ GeV. In Fig. 5.19, we see that we need $M_{Z'} \simeq 5.1$ TeV to get $m_{h_1^0} \sim 125$ GeV and this causes a large $\Delta_Z \sim 2.1 \times 10^3$. The stops appear to be very heavy $m_{\tilde{t}_1} > 2$ TeV, outside the reach of current experimental analyses. The fine tuning contours move almost parallel to the Higgs contours showing a correlation. Heavier Higgsinos would move the Higgs band $m_{h_1^0} \sim 125$ GeV, towards the top-right corner making it easier to achieve the Higgs mass for lighter $M_{Z'}$ and smaller charges, reducing the fine tuning. Fig. 5.20 shows that for $M_{Z'} =$ fixed, larger $|Q_s|$ charges and smaller ratio $|r|$ can reduce Δ_Z. On the other hand larger ratio $|r|$ is preferred in order to enhance the $U(1)'$ D-terms in the sfermion squared mass matrix and evade collider constraints. In the last Figure 5.21 which someone should compare with the Figures 4.5, 4.6, 4.9 for the MSSM, we can see that all points pass the collider constraints available in `Fastlim`. Third generation squarks are all heavier than $m_{\tilde{q}} > 830$ GeV and have very small production cross sections. The observed Higgs mass can be achieved for large hierarchies between the left-handed and right-handed stop soft masses. As in MSSM, the case where $m_{Q_3} > m_{T^c}$ results in heavy bottom squarks $m_{\tilde{b}_1}$ and is more likely to pass future experimental constraints. Even when the same parameter points will be ruled out in MSSM, they will still be allowed in a pUMSSM scenario with large $(|r|, |Q_s|)$ and heavy Higgsinos.

Chapter 6

Conclusions

In a bottom-up approach we have considered a gauge extension of the MSSM with generic non-universal $U(1)'$ charges which are constrained by gauge invariance and perturbativity. We have investigated the fine tuning in the MSSM and in different pUMSSM scenarios, imposing constraints from Higgs data, the W mass measurement and collider searches on supersymmetric particles. We summarize here our main observations as a result of this project:

The W mass constraint provides a model-independent method to impose constraints on the mixing angle $\theta_{ZZ'}$. In non-universal scenarios with leptophobic Z' bosons this constraint can provide a stricter bound on the mixing angle than the other precision electroweak observables. We find that the W mass constraint is sensitive to the ratio $r = \frac{Q_{H_u}}{Q_s}$ of the $U(1)'$ charges entering the Higgs sector. Small values of $|r|$ relax the need for large $U(1)'$ breaking scales and thus allows for light Z' bosons near the EW scale without tuning $\tan\beta$ to receive a critical value indicated by the requirement of having zero mixing angle $\tan\beta_c = \sqrt{Q_{H_d}/Q_{H_u}}$. This would restrict the study to a specific point of the parameter space.

We study the Higgs sector and we identify a strong dependence of the lightest CP-even Higgs boson on the Higgsino mass μ_{eff} for different points on the (r, Q_s) plane. We parametrize our study based on the previous observations with respect to the ratio r and Q_s which also plays an important role in the fine tuning. We understand that heavy gauginos in MSSM scenarios and also in pUMSSM models with light Z' bosons can reduce the fine tuning Δ_Z to low values $\Delta_Z \sim \mathcal{O}(10-20)$ but not in heavy Z' models due to the large tree-level fine tuning coming from the soft masses $m^2_{H_u}, m^2_s$. In this case binos and winos can be lighter compared to MSSM modifying the phenomenology. Furthermore, in models with a light Z' and small couplings $(|r|, |Q_s|)$, one can have a light singlino which

can even be the LSP of the theory. This has implications on the phenomenology of these models and can differ significantly from that of the MSSM, thus motivating further study. In heavy Z' pUMSSM scenarios one cannot have a light singlino without excessive fine tuning coming from the $\tilde{B}'$ gaugino mass.

A light Z' scenario does not necessarily lead to smaller Δ_Z amongst gauge extensions of the MSSM. We show that for some points on the (r, Q_s) plane one can have worse fine tuning than heavy Z' scenarios and the MSSM if one assumes light gauginos which do not reduce Δ_Z. This is a consequence of the suppressed tree-level Higgs mass. We also indicate points on the plane $(r, Q_s) = (-0.1, -0.6)$ with light Z' for which the fine tuning can be improved $\Delta_Z \sim 850$. We stress the fact that a light Z', due to small tree-level Δ_Z coming from the soft masses $m^2_{H_u}, m^2_s$, can benefit from heavy gauginos as in the MSSM to reduce $\Delta_Z \sim \mathcal{O}(10-20)$. More importantly, we find an interesting region close to the bottom-left

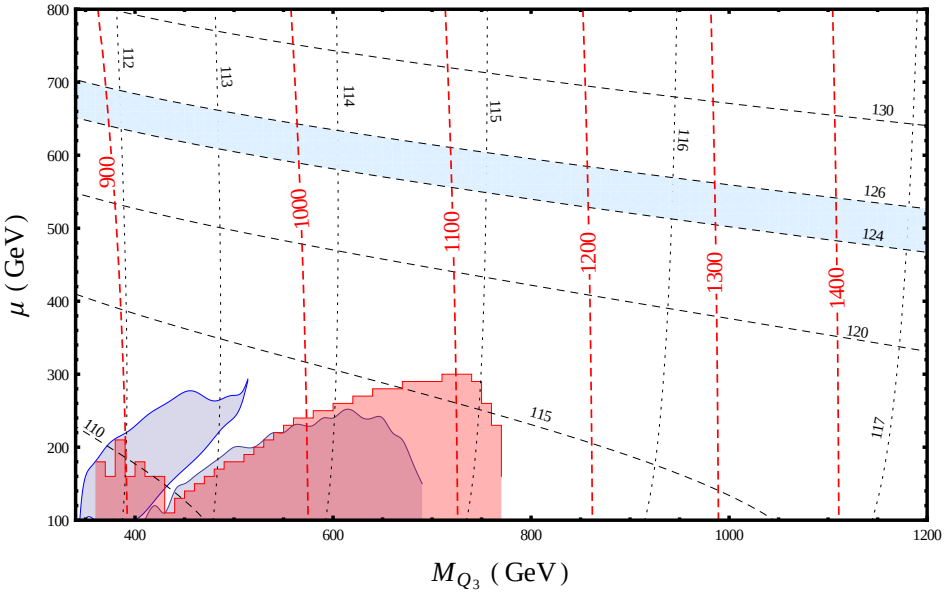

Figure 6.1: Higgsino mass μ plotted against the SUSY breaking soft mass $m_{Q_3} = m_{T^c}$ in the MSSM and pUMSSM for $(r, Q_s) = (-0.6, -0.6)$ and $M_{Z'} = 2.1$ TeV. The exclusion areas from 1) AC2013024 (red) 2) AC2013053 (blue top) 3) AC2013037 (blue bottom) apply only to the MSSM. All points are allowed in the pUMSSM scenario. The "vertical" black dotted lines correspond to the MSSM Higgs mass (in units of GeV) while the almost "horizontal" black dashed show $m_{h^0_1}$ (in GeV) in the pUMSSM scenario. The red dashed lines depict $m_{\tilde{t}_1}$ (in units of GeV) in pUMSSM. The soft trilinear coupling is $T_t = y_t A_t = 100$ GeV. The blue band shows the allowed Higgs mass in the pUMSSM (compare with Fig. 4.1).

corner of the plane $(r, Q_s) = (-0.6, -0.6)$ for which we can have a relatively low fine tuning within the region $100 \lesssim \Delta_Z \lesssim 500$ for Z' bosons with masses 2.1 TeV $\lesssim M_{Z'} \lesssim$ 3.3 TeV

and heavy Higgsinos $\mu_{eff} = 800$ GeV. We understand that this scenario cannot achieve a low Δ_Z below the tree-level fine tuning indicated by the soft masses $m^2_{H_u}, m^2_s$ even if we benefit from relatively heavy gauginos as in MSSM. It provides an improvement amongst $U(1)'$ extensions of the MSSM. Moreover, this scenario differs from the MSSM substantially and can evade current and future experimental searches. The heavy Z' masses and the large $U(1)'$ stop couplings create large $U(1)'$ D-term contributions to the diagonal terms of the squared squark mass matrices resulting in very heavy physical states for the third generation squarks. At the points we investigate, we find that $m_{\tilde{t}_1,\tilde{b}_1} > 800$ GeV for very light soft masses. All points are passing current constraints with `Fastlim`. The heavier the Z' bosons the heavier the lighter squarks and the higher the energy needed at the LHC in order to probe this region of the parameter space. Furthermore, large splitting between the soft masses $X = m_{Q_3} - m_{T^c} > 0$ are very interesting because it can account for Higgs mass around 125 GeV and relax constraints from future experimental searches due to the heavy sbottoms and the small productions cross sections. We have shown that this is also an interesting scenario for MSSM.

Additionally we conclude that in this scenario the Higgsinos are not restricted from naturalness to be light but on the contrary we see that heavy Higgsinos can reduce the fine tuning in gauge extensions of the MSSM. If one also considers the fact that bino and wino can be light compared to MSSM, which needs heavy gauginos (but not very heavy gluino), then we see that in this case we have a spectrum with heavy third generation squarks $m_{\tilde{q}} \sim 1$ TeV, heavy Higgsinos $\mu_{eff} \sim (0.8 - 1)$ TeV and possibly light bino and wino. In Fig. 6.1 we summarize the main differences between the MSSM and the interesting model of pUMSSM which resides in the bottom-left corner of the (r, Q_s) plane presented here. Note that this plot has been constructed using the same scan we used for Fig. 4.1.

Bibliography

[1] ATLAS Collaboration, "Search for direct production of charginos and neutralinos in events with three leptons and missing transverse momentum in 21 fb^{-1} of pp collisions at $\sqrt{s} = 8\,\text{TeV}$ with the ATLAS detector," ATLAS-CONF-2013-035. 1, 88, 120

[2] ATLAS Collaboration, "Search for direct production of the top squark in the all-hadronic ttbar + etmiss final state in 21 fb^{-1} of pp collisions at $\sqrt{(s)} = 8$ TeV with the ATLAS detector," ATLAS-CONF-2013-024. 1, 88, 120

[3] ATLAS Collaboration, "Search for direct top squark pair production in final states with one isolated lepton, jets, and missing transverse momentum in $\sqrt{s} = 8$ TeV pp collisions using 21 fb^{-1} of ATLAS data," ATLAS-CONF-2013-037. 88

[4] B. C. Allanach, "SOFTSUSY: a program for calculating supersymmetric spectra," Comput. Phys. Commun. **143** (2002) 305 [hep-ph/0104145]. 78

[5] H. Amini, "Radiative corrections to Higgs masses in Z-prime models," New J. Phys. **5** (2003) 49 [hep-ph/0210086]. 70, 74, 76

[6] P. Athron, M. Mühlleitner, R. Nevzorov and A. G. Williams, "Non-Standard Higgs Decays in U(1) Extensions of the MSSM," JHEP **1501** (2015) 153 [arXiv:1410.6288 [hep-ph]]. 54

[7] P. Athron, M. Binjonaid and S. F. King, "Fine Tuning in the Constrained Exceptional Supersymmetric Standard Model," Phys. Rev. D **87** (2013) no.11, 115023 [arXiv:1302.5291 [hep-ph]]. 54, 83, 84

[8] P. Athron and D. J. Miller, "A New Measure of Fine Tuning," Phys. Rev. D **76** (2007) 075010 [arXiv:0705.2241 [hep-ph]]. 54, 83

[9] M. Awramik, M. Czakon, A. Freitas and G. Weiglein, "Precise prediction for the W boson mass in the standard model," Phys. Rev. D **69** (2004) 053006 [hep-ph/0311148]. 64

[10] H. Baer, "Radiative natural supersymmetry with mixed axion/higgsino cold dark matter," AIP Conf. Proc. **1534** (2012) 39 [arXiv:1210.7852 [hep-ph]]. 83

[11] H. Baer, V. Barger, P. Huang, D. Mickelson, A. Mustafayev and X. Tata, "Post-LHC7 fine-tuning in the minimal supergravity/CMSSM model with a 125 GeV Higgs boson," Phys. Rev. D **87** (2013) no.3, 035017 [arXiv:1210.3019 [hep-ph]]. 83, 84

[12] H. Baer, V. Barger, P. Huang, D. Mickelson, A. Mustafayev and X. Tata, "Radiative natural supersymmetry: Reconciling electroweak fine-tuning and the Higgs boson mass," Phys. Rev. D **87** (2013) no.11, 115028 [arXiv:1212.2655 [hep-ph]]. 83, 84

[13] H. Baer, V. Barger, P. Huang, A. Mustafayev and X. Tata, "Radiative natural SUSY with a 125 GeV Higgs boson," Phys. Rev. Lett. **109** (2012) 161802 [arXiv:1207.3343 [hep-ph]]. 84

[14] H. Baer, V. Barger and D. Mickelson, "How conventional measures overestimate electroweak fine-tuning in supersymmetric theory," Phys. Rev. D **88** (2013) no.9, 095013 [arXiv:1309.2984 [hep-ph]]. 83, 92

[15] H. Baer, V. Barger and M. Padeffke-Kirkland, "Electroweak versus high scale finetuning in the 19-parameter SUGRA model," Phys. Rev. D **88** (2013) 055026 [arXiv:1304.6732 [hep-ph]]. 83, 84, 88, 92, 116

[16] H. Baer, D. Dicus, M. Drees and X. Tata, "Higgs Boson Signals in Superstring Inspired Models at Hadron Supercolliders," Phys. Rev. D **36** (1987) 1363. [PhysRevD.36.1363]

[17] R. Barate *et al.* [ALEPH Collaboration], "Searches for sleptons and squarks in e+ e- collisions at 189-GeV," Phys. Lett. B **469** (1999) 303. [http://inspirehep.net/ record/509442] 96

[18] R. Barbieri, M. Frigeni, F. Giuliani and H. E. Haber, "Precision Measurements in Electroweak Physics and Supersymmetry," Nucl. Phys. B **341** (1990) 309. [http://inspirehep.net/record/285468]

[19] R. Barbieri and G. F. Giudice, "Upper Bounds on Supersymmetric Particle Masses," Nucl. Phys. B **306** (1988) 63. [https://inspirehep.net/record/248280] 83

[20] R. Barbieri, L. J. Hall, Y. Nomura and V. S. Rychkov, "Supersymmetry without a Light Higgs Boson," Phys. Rev. D **75** (2007) 035007 [hep-ph/0607332]. 71, 85

[21] V. D. Barger, N. Deshpande, R. J. N. Phillips and K. Whisnant, "Extra Fermions in E6 Superstring Theories," Phys. Rev. D **33** (1986) 1912 [PhysRevD.33.1912] 55

[22] V. D. Barger, N. Deshpande, R. J. N. Phillips and K. Whisnant, "Extra Fermions in E6 Superstring Theories," Erratum: Phys. Rev. D **35** (1987) 1741 [PhysRevD.35.1741] 55

[23] V. D. Barger, N. G. Deshpande and K. Whisnant, "Phenomenological Mass Limits on Extra Z of E6 Superstrings," Phys. Rev. Lett. **56** (1986) 30. [PhysRevLett.56.30]

[24] V. Barger, C. W. Chiang, P. Langacker and H. S. Lee, "Z' mediated flavor changing neutral currents in B meson decays," Phys. Lett. B **580** (2004) 186 [hep-ph/0310073]. 61

[25] V. Barger, P. Langacker and H. S. Lee, "Lightest neutralino in extensions of the MSSM," Phys. Lett. B **630** (2005) 85 [hep-ph/0508027]. 40

[26] V. Barger, P. Langacker, H. S. Lee and G. Shaughnessy, "Higgs Sector in Extensions of the MSSM," Phys. Rev. D **73** (2006) 115010 [hep-ph/0603247]. 52, 70, 76

[27] V. Barger, P. Langacker and G. Shaughnessy, "Collider Signatures of Singlet Extended Higgs Sectors," Phys. Rev. D **75** (2007) 055013 [hep-ph/0611239]. 52

[28] V. Barger, P. Langacker and G. Shaughnessy, "Singlet extensions of the MSSM," AIP Conf. Proc. **903** (2007) 32 [hep-ph/0611112]. 52, 70

[29] W. Beenakker, R. Hopker, M. Spira and P. M. Zerwas, "Squark and gluino production at hadron colliders," Nucl. Phys. B **492** (1997) 51 [hep-ph/9610490]. 98, 100

[30] M. Carena, J. R. Espinosa, M. Quiros and C. E. M. Wagner, "Analytical expressions for radiatively corrected Higgs masses and couplings in the MSSM," Phys. Lett. B **355** (1995) 209 [hep-ph/9504316]. 76

[31] M. Carena, M. Quiros and C. E. M. Wagner, "Effective potential methods and the Higgs mass spectrum in the MSSM," Nucl. Phys. B **461** (1996) 407 [hep-ph/9508343].

[32] J. A. Casas, J. R. Espinosa and I. Hidalgo, "The MSSM fine tuning problem: A Way out," JHEP **0401** (2004) 008 [hep-ph/0310137]. 85

[33] J. A. Casas and C. Munoz, "A Natural solution to the mu problem," Phys. Lett. B **306** (1993) 288 [hep-ph/9302227].

[34] C. F. Chang, K. Cheung, Y. C. Lin and T. C. Yuan, "Mimicking the Standard Model Higgs Boson in UMSSM," JHEP **1206** (2012) 128 [arXiv:1202.0054 [hep-ph]]. 52, 70

[35] G. C. Cho and K. Hagiwara, "Supersymmetry versus precision experiments revisited," Nucl. Phys. B **574** (2000) 623 [hep-ph/9912260].

[36] G. C. Cho, K. Hagiwara, Y. Matsumoto and D. Nomura, "The MSSM confronts the precision electroweak data and the muon g-2," JHEP **1111** (2011) 068 [arXiv:1104.1769 [hep-ph]].

[37] G. C. Cho, K. Hagiwara and Y. Umeda, "Z' bosons in supersymmetric E_6 models confront electroweak data," Nucl. Phys. B **531** (1998) 65, Erratum: [Nucl. Phys. B **555** (1999) 651] Erratum: [Nucl. Phys. B **565** (2000) 483] [hep-ph/9805448].

[38] S. Y. Choi, H. E. Haber, J. Kalinowski and P. M. Zerwas, "The Neutralino sector in the U(1)-extended supersymmetric standard model," Nucl. Phys. B **778** (2007) 85 [hep-ph/0612218]. 40

[39] S. R. Coleman and E. J. Weinberg, "Radiative Corrections as the Origin of Spontaneous Symmetry Breaking," Phys. Rev. D **7** (1973) 1888. [PhysRevD.7.1888] 74

[40] The ATLAS collaboration, "Search for chargino and neutralino production in final states with one lepton, two b-jets consistent with a Higgs boson, and missing transverse momentum with the ATLAS detector in 20.3 fb^{-1} of $\sqrt{s} = 8$ TeV pp collisions," ATLAS-CONF-2013-093. 88

[41] The ATLAS collaboration, "Search for direct-slepton and direct-chargino production in final states with two opposite-sign leptons, missing transverse momentum and no jets in 20.3 fb^{-1} of pp collisions at $\sqrt{s} = 8$ TeV with the ATLAS detector," ATLAS-CONF-2013-049. 88

[42] The ATLAS collaboration, "Search for direct third generation squark pair production in final states with missing transverse momentum and two b-jets in $\sqrt{s} = 8$ TeV pp collisions with the ATLAS detector.," ATLAS-CONF-2013-053. 88, 98, 120

[43] The ATLAS collaboration, "Search for direct top squark pair production in final states with two leptons in $\sqrt{s} = 8$ TeV pp collisions using 20 fb^{-1} of ATLAS data.," ATLAS-CONF-2013-048. 88

[44] The ATLAS collaboration, "Search for new phenomena using final states with large jet multiplicities and missing transverse momentum with ATLAS in 20 fb^{-1} of $\sqrt{s} = 8$ TeV proton-proton collisions," ATLAS-CONF-2013-054. 88

[45] The ATLAS collaboration, "Search for squarks and gluinos in events with isolated leptons, jets and missing transverse momentum at $\sqrt{s} = 8$ TeV with the ATLAS detector," ATLAS-CONF-2013-062. 88

[46] The ATLAS collaboration, "Search for squarks and gluinos with the ATLAS detector in final states with jets and missing transverse momentum and 20.3 fb^{-1} of $\sqrt{s} = 8$ TeV proton-proton collision data," ATLAS-CONF-2013-047. 88

[47] The ATLAS collaboration [ATLAS Collaboration], "Search for strong production of supersymmetric particles in final states with missing transverse momentum and at least three b-jets using 20.1 fb^{-1} of pp collisions at $\sqrt{s} = 8$ TeV with the ATLAS Detector.," ATLAS-CONF-2013-061. 88

[48] M. Cvetic, D. A. Demir, J. R. Espinosa, L. L. Everett and P. Langacker, "Electroweak breaking and the mu problem in supergravity models with an additional U(1)," Phys. Rev. D **56** (1997) 2861, Erratum: [Phys. Rev. D **58** (1998) 119905] [hep-ph/9703317]. 53, 59, 70

[49] M. Cvetic and P. Langacker, "New gauge bosons from string models," Mod. Phys. Lett. A **11** (1996) 1247 [hep-ph/9602424]. 54, 60

[50] G. Degrassi, S. Di Vita and P. Slavich, "Two-loop QCD corrections to the MSSM Higgs masses beyond the effective-potential approximation," Eur. Phys. J. C **75** (2015) no.2, 61 [arXiv:1410.3432 [hep-ph]]. 78

[51] F. del Aguila, J. de Blas and M. Perez-Victoria, "Electroweak Limits on General New Vector Bosons," JHEP **1009** (2010) 033 [arXiv:1005.3998 [hep-ph]].

[52] D. A. Demir, G. L. Kane and T. T. Wang, "The Minimal U(1)' extension of the MSSM," Phys. Rev. D **72** (2005) 015012 [hep-ph/0503290]. 57, 59, 60

[53] D. A. Demir and N. K. Pak, "One loop effects in supergravity models with an additional U(1)," Phys. Rev. D **57** (1998) 6609 [hep-ph/9809357].

[54] M. Dine, "Naturalness Under Stress," Ann. Rev. Nucl. Part. Sci. **65** (2015) 43 [arXiv:1501.01035 [hep-ph]].

[55] A. Djouadi, "The Anatomy of electro-weak symmetry breaking. I: The Higgs boson in the standard model," Phys. Rept. **457** (2008) 1 [hep-ph/0503172].

[56] A. Djouadi, "The Anatomy of electro-weak symmetry breaking. II. The Higgs bosons in the minimal supersymmetric model," Phys. Rept. **459** (2008) 1 [hep-ph/0503173]. 8, 84

[57] F. Domingo and T. Lenz, "W mass and Leptonic Z-decays in the NMSSM," JHEP **1107** (2011) 101 [arXiv:1101.4758 [hep-ph]].

[58] M. Drees, "Comment on 'Higgs Boson Mass Bound in $E(6)$ Based Supersymmetric Theories.'," Phys. Rev. D **35** (1987) 2910. [PhysRevD.35.2910] 54

[59] M. Drees, R. Godbole and P. Roy, "Theory and phenomenology of sparticles: An account of four-dimensional N=1 supersymmetry in high energy physics," Hackensack, USA: World Scientific (2004) 555 p 2

[60] L. S. Durkin and P. Langacker, "Neutral Current Constraints on Heavy Z Bosons," Phys. Lett. B **166** (1986) 436. [INSPIRE]

[61] J. R. Ellis, K. Enqvist, D. V. Nanopoulos and F. Zwirner, "Observables in Low-Energy Superstring Models," Mod. Phys. Lett. A **1** (1986) 57. [INSPIRE] 83

[62] J. Erler, "Chiral models of weak scale supersymmetry," Nucl. Phys. B **586** (2000) 73. [hep-ph/0006051] 60

[63] J. Erler and P. Langacker, "Constraints on extended neutral gauge structures," Phys. Lett. B **456** (1999) 68 [hep-ph/9903476]. 81

[64] J. Erler, P. Langacker and T. j. Li, "The Z - Z' mass hierarchy in a supersymmetric model with a secluded U(1) -prime breaking sector," Phys. Rev. D **66** (2002) 015002 [hep-ph/0205001]. 55

[65] J. Erler, P. Langacker, S. Munir and E. Rojas, "Improved Constraints on Z-prime Bosons from Electroweak Precision Data," JHEP **0908** (2009) 017 [arXiv:0906.2435 [hep-ph]]. 81

[66] J. Erler, P. Langacker, S. Munir and E. Rojas, "Z' Bosons at Colliders: a Bayesian Viewpoint," JHEP **1111** (2011) 076 [arXiv:1103.2659 [hep-ph]].

[67] J. Erler and D. M. Pierce, "Bounds on supersymmetry from electroweak precision analysis," Nucl. Phys. B **526** (1998) 53 [hep-ph/9801238].

[68] J. R. Espinosa, "Fine tuning in EW symmetry breaking," AIP Conf. Proc. **805** (2006) 240. [INSPIRE] 85

[69] J. R. Espinosa and M. Quiros, "On Higgs boson masses in non-minimal supersymmetric standard models," Phys. Lett. B **279** (1992) 92. [INSPIRE]

[70] J. R. Espinosa and M. Quiros, "Upper bounds on the lightest Higgs boson mass in general supersymmetric Standard Models," Phys. Lett. B **302** (1993) 51 [hep-ph/9212305].

[71] K. A. Olive *et al.* [Particle Data Group Collaboration], "Review of Particle Physics," Chin. Phys. C **38** (2014) 090001. [INSPIRE] [IOPscience] 62, 63, 64

[72] M. Farina, M. Perelstein and B. Shakya, "Higgs Couplings and Naturalness in λ-SUSY," JHEP **1404** (2014) 108 [arXiv:1310.0459 [hep-ph]]. 71, 84

[73] P. Fayet, "Extra U(1)'s and New Forces," Nucl. Phys. B **347** (1990) 743. [INSPIRE]

[74] J. L. Feng, P. Kant, S. Profumo and D. Sanford, "Three-Loop Corrections to the Higgs Boson Mass and Implications for Supersymmetry at the LHC," Phys. Rev. Lett. **111** (2013) 131802 [arXiv:1306.2318 [hep-ph]]. 78

[75] F. Franke and S. Hesselbach, "Production of singlino dominated neutralinos in extended supersymmetric models," Phys. Lett. B **526** (2002) 370 [hep-ph/0111285]. 40

[76] G. Ganis [ALEPH Collaboration], "Search for charginos and neutralinos in e^+e^- collisions at $\sqrt{s} = 188.6$ GeV and mass limit for the lightest neutralino," CERN-OPEN-99-294, ALEPH-99-011. 51

[77] T. Gherghetta, C. F. Kolda and S. P. Martin, "Flat directions in the scalar potential of the supersymmetric standard model," Nucl. Phys. B **468** (1996) 37 [hep-ph/9510370]. 55

[78] G. F. Giudice and A. Masiero, "A Natural Solution to the μ Problem in Supergravity Theories," Phys. Lett. B **206** (1988) 480. [INSPIRE]

[79] H. E. Haber and G. L. Kane, "The Search for Supersymmetry: Probing Physics Beyond the Standard Model," Phys. Rept. **117** (1985) 75. [INSPIRE]

[80] H. E. Haber and R. Hempfling, "The Renormalization group improved Higgs sector of the minimal supersymmetric model," Phys. Rev. D **48** (1993) 4280 [hep-ph/9307201].

[81] H. E. Haber, R. Hempfling and A. H. Hoang, "Approximating the radiatively corrected Higgs mass in the minimal supersymmetric model," Z. Phys. C **75** (1997) 539 [hep-ph/9609331].

[82] H. E. Haber and M. Sher, "Higgs-Boson Mass Bound in $E(6)$ Based Supersymmetric Theories," Phys. Rev. D **35** (1987) 2206. [INSPIRE]

[83] L. J. Hall, D. Pinner and J. T. Ruderman, "A Natural SUSY Higgs Near 126 GeV," JHEP **1204** (2012) 131 [arXiv:1112.2703 [hep-ph]]. 71, 84

[84] S. W. Ham, E. J. Yoo, S. K. Oh and D. Son, "Higgs bosons of a supersymmetric U(1)-prime model at the ILC," Phys. Rev. D **77** (2008) 114011 [arXiv:0801.4640 [hep-ph]].

[85] S. W. Ham and S. K. Oh, "Exotic quark effects on the Higgs sector of the USSM at the LHC," J. Phys. G **37** (2010) 045003 [arXiv:0906.5526 [hep-ph]].

[86] T. Han, P. Langacker and B. McElrath, "The Higgs sector in a U(1)-prime extension of the MSSM," Phys. Rev. D **70** (2004) 115006 [hep-ph/0405244]. 52, 55, 56, 70

[87] Z. Han, A. Katz, M. Son and B. Tweedie, "Boosting searches for natural supersymmetry with R-parity violation via gluino cascades," Phys. Rev. D **87** (2013) no.7, 075003 [arXiv:1211.4025 [hep-ph]].

[88] E. Hardy and J. March-Russell, "Retrofitted Natural Supersymmetry from a U(1)," JHEP **1305** (2013) 120 [arXiv:1302.5423 [hep-ph]].

[89] S. Heinemeyer, "MSSM Higgs physics at higher orders," Int. J. Mod. Phys. A **21** (2006) 2659 [hep-ph/0407244].

[90] S. Heinemeyer, W. Hollik, D. Stockinger, A. M. Weber and G. Weiglein, "Precise prediction for M(W) in the MSSM," JHEP **0608** (2006) 052 [hep-ph/0604147].

[91] S. Heinemeyer, W. Hollik and G. Weiglein, "Electroweak precision observables in the minimal supersymmetric standard model," Phys. Rept. **425** (2006) 265 [hep-ph/0412214]. 63, 64

[92] S. Heinemeyer, W. Hollik, G. Weiglein and L. Zeune, "Implications of LHC search results on the W boson mass prediction in the MSSM," JHEP **1312** (2013) 084 [arXiv:1311.1663 [hep-ph]]. 62, 64

[93] S. Hesselbach, F. Franke and H. Fraas, "Neutralinos in E(6) inspired supersymmetric U(1)-prime models," Eur. Phys. J. C **23** (2002) 149 [hep-ph/0107080]. 40

[94] J. L. Hewett and T. G. Rizzo, "Low-Energy Phenomenology of Superstring Inspired E(6) Models," Phys. Rept. **183** (1989) 193. [INSPIRE] 54

[95] B. Holdom, "Oblique electroweak corrections and an extra gauge boson," Phys. Lett. B **259** (1991) 329. [INSPIRE]

[96] R. Howl, "E_6 Inspired Supersymmetric Models," [PhD Thesis, INSPIRE-1264622]

[97] T. Hur, H. S. Lee and S. Nasri, "A Supersymmetric U(1)-prime model with multiple dark matters," Phys. Rev. D **77** (2008) 015008 [arXiv:0710.2653 [hep-ph]].

[98] D. Jarecka, J. Kalinowski, S. F. King and J. P. Roberts, "Dark Matter in the U(1) Extended SUSY," eConf C **0705302** (2007) SUS15 [arXiv:0709.1862 [hep-ph]].

[99] J. Kalinowski, S. F. King and J. P. Roberts, "Neutralino Dark Matter in the USSM," JHEP **0901** (2009) 066 [arXiv:0811.2204 [hep-ph]].

[100] Z. Kang, J. Li and T. Li, "On Naturalness of the MSSM and NMSSM," JHEP **1211** (2012) 024 [arXiv:1201.5305 [hep-ph]]. 84

[101] E. Keith and E. Ma, "Generic consequences of a supersymmetric U(1) gauge factor at the TeV scale," Phys. Rev. D **56** (1997) 7155 [hep-ph/9704441]. 54, 84

[102] J. E. Kim and H. P. Nilles, "The μ Problem and the Strong CP Problem," Phys. Lett. B **138** (1984) 150. [INSPIRE]

[103] S. F. King, S. Moretti and R. Nevzorov, "Theory and phenomenology of an exceptional supersymmetric standard model," Phys. Rev. D **73** (2006) 035009 [hep-ph/0510419]. 54, 77

[104] S. F. King, M. Mühlleitner, R. Nevzorov and K. Walz, "Natural NMSSM Higgs Bosons," Nucl. Phys. B **870** (2013) 323 [arXiv:1211.5074 [hep-ph]].

[105] R. Kitano and Y. Nomura, "A Solution to the supersymmetric fine-tuning problem within the MSSM," Phys. Lett. B **631** (2005) 58 [hep-ph/0509039]. 83, 85

[106] R. Kitano and Y. Nomura, "Supersymmetry, naturalness, and signatures at the LHC," Phys. Rev. D **73** (2006) 095004 [hep-ph/0602096]. 82, 83, 85

[107] K. Kowalska and E. M. Sessolo, "Natural MSSM after the LHC 8 TeV run," Phys. Rev. D **88** (2013) no.7, 075001 [arXiv:1307.5790 [hep-ph]].

[108] M. Kramer, A. Kulesza, R. van der Leeuw, M. Mangano, S. Padhi, T. Plehn and X. Portell, "Supersymmetry production cross sections in pp collisions at $\sqrt{s} = 7$ TeV," [arXiv:1206.2892 [hep-ph]]. 100

[109] A. Kulesza and L. Motyka, "Soft gluon resummation for the production of gluino-gluino and squark-antisquark pairs at the LHC," Phys. Rev. D **80** (2009) 095004 [arXiv:0905.4749 [hep-ph]]. 98, 100

[110] A. Kulesza and L. Motyka, "Threshold resummation for squark-antisquark and gluino-pair production at the LHC," Phys. Rev. Lett. **102** (2009) 111802 [arXiv:0807.2405 [hep-ph]]. 98, 100

[111] P. Langacker, "Beyond the MSSM," (2004) [hep-ph/0402203].

[112] P. Langacker, "The Physics of Heavy Z' Gauge Bosons," Rev. Mod. Phys. **81** (2009) 1199 [arXiv:0801.1345 [hep-ph]]. 54, 59, 60

[113] P. Langacker, "The Physics of New U(1)-prime Gauge Bosons," AIP Conf. Proc. **1200** (2010) 55 [arXiv:0909.3260 [hep-ph]].

[114] P. Langacker and M. x. Luo, "Constraints on additional Z bosons," Phys. Rev. D **45** (1992) 278. [INSPIRE]

[115] P. Langacker and J. Wang, "U(1)-prime symmetry breaking in supersymmetric E(6) models," Phys. Rev. D **58** (1998) 115010 [hep-ph/9804428]. 54

[116] H. S. Lee, K. T. Matchev and T. T. Wang, "A U(1)-prime solution to the μ-problem and the proton decay problem in supersymmetry without R-parity," Phys. Rev. D **77** (2008) 015016 [arXiv:0709.0763 [hep-ph]].

[117] H. M. Lee, S. Raby, M. Ratz, G. G. Ross, R. Schieren, K. Schmidt-Hoberg and P. K. S. Vaudrevange, "Discrete R symmetries for the MSSM and its singlet extensions," Nucl. Phys. B **850** (2011) 1 [arXiv:1102.3595 [hep-ph]].

[118] A. Leike, "Model independent Z-prime constraints from measurements at the Z peak," Phys. Lett. B **396** (1997) 245 [hep-ph/9612410].

[119] A. Leike, "The Phenomenology of extra neutral gauge bosons," Phys. Rept. **317** (1999) 143 [hep-ph/9805494].

[120] D. London and J. L. Rosner, "Extra Gauge Bosons in E(6)," Phys. Rev. D **34** (1986) 1530. [INSPIRE] 54

[121] E. Ma, "Exceeding the MSSM Higgs Mass Bound in a Special Class of U(1) Gauge Models," Phys. Lett. B **705** (2011) 320 [arXiv:1108.4029 [hep-ph]].

[122] E. Ma and M. Maniatis, "Effective Two Higgs Doublets in Nonminimal Supersymmetric Models," Eur. Phys. J. C **71** (2011) 1610 [arXiv:1005.3305 [hep-ph]]. 70

[123] M. Maniatis, "The Next-to-Minimal Supersymmetric extension of the Standard Model reviewed," Int. J. Mod. Phys. A **25** (2010) 3505 [arXiv:0906.0777 [hep-ph]]. 9

[124] S. P. Martin, "A Supersymmetry primer," Adv. Ser. Direct. High Energy Phys. **21** (2010) 1 [Adv. Ser. Direct. High Energy Phys. **18** (1998) 1] [hep-ph/9709356]. vi, 2, 6, 7, 9, 83, 85

[125] S. P. Martin, "Three-loop Standard Model effective potential at leading order in strong and top Yukawa couplings," Phys. Rev. D **89** (2014) no.1, 013003 [arXiv:1310.7553 [hep-ph]]. 78

[126] S. P. Martin, K. Tobe and J. D. Wells, "Virtual effects of light gauginos and higgsinos: A Precision electroweak analysis of split supersymmetry," Phys. Rev. D **71** (2005) 073014 [hep-ph/0412424]. 84

[127] R. Martinez, F. Ochoa and J. P. Rubio, "Some phenomenological aspects of a new $U(1)'$ model," Phys. Rev. D **89** (2014) no.5, 056008 [arXiv:1303.2734 [hep-ph]].

[128] D. J. Miller, R. Nevzorov and P. M. Zerwas, "The Higgs sector of the next-to-minimal supersymmetric standard model," Nucl. Phys. B **681** (2004) 3 [hep-ph/0304049].

[129] P. J. Mohr, B. N. Taylor and D. B. Newell, "CODATA Recommended Values of the Fundamental Physical Constants: 2010," Rev. Mod. Phys. **84** (2012) 1527 [arXiv:1203.5425 [physics.atom-ph]]. 63

[130] S. Nakamura and D. Suematsu, "Supersymmetric extra U(1) models with a singlino dominated LSP," Phys. Rev. D **75** (2007) 055004 [hep-ph/0609061].

[131] R. Nevzorov, "E_6 inspired supersymmetric models with exact custodial symmetry," Phys. Rev. D **87** (2013) no.1, 015029 [arXiv:1205.5967 [hep-ph]]. 54

[132] H. P. Nilles, "Supersymmetry, Supergravity and Particle Physics," Phys. Rept. **110** (1984) 1. [INSPIRE]

[133] Y. Nomura, D. Poland and B. Tweedie, "Minimally fine-tuned supersymmetric standard models with intermediate-scale supersymmetry breaking," Nucl. Phys. B **745** (2006) 29 [hep-ph/0509243].

[134] C. Panagiotakopoulos and K. Tamvakis, "Stabilized NMSSM without domain walls," Phys. Lett. B **446** (1999) 224 [hep-ph/9809475]. 9

[135] P. N. Pandita, "One loop radiative corrections to the lightest Higgs scalar mass in nonminimal supersymmetric Standard Model," Phys. Lett. B **318** (1993) 338. [INSPIRE]

[136] M. Papucci, J. T. Ruderman and A. Weiler, "Natural SUSY Endures," JHEP **1209** (2012) 035 [arXiv:1110.6926 [hep-ph]]. 83, 84, 85, 86

[137] M. Papucci, K. Sakurai, A. Weiler and L. Zeune, "Fastlim: a fast LHC limit calculator," Eur. Phys. J. C **74** (2014) no.11, 3163 [arXiv:1402.0492 [hep-ph]]. vi, 87, 88, 89, 102

[138] W. Porod and F. Staub, "SPheno 3.1: Extensions including flavour, CP-phases and models beyond the MSSM," Comput. Phys. Commun. **183** (2012) 2458 [arXiv:1104.1573 [hep-ph]]. 74, 78

[139] W. Porod, "SPheno, a program for calculating supersymmetric spectra, SUSY particle decays and SUSY particle production at e^+e^- colliders," Comput. Phys. Commun. **153** (2003) 275 [hep-ph/0301101]. 74, 78

[140] S. Schael *et al.* [ALEPH and DELPHI and L3 and OPAL and SLD and LEP Electroweak Working Group and SLD Electroweak Group and SLD Heavy Flavour Group Collaborations], "Precision electroweak measurements on the Z resonance," Phys. Rept. **427** (2006) 257 [hep-ex/0509008]. 62, 96

[141] A. Sirlin, "Radiative Corrections in the $SU(2)_L \times U(1)$ Theory: A Simple Renormalization Framework," Phys. Rev. D **22** (1980) 971. [INSPIRE] 63

[142] F. Staub, "Sarah," [arXiv:0806.0538 [hep-ph]]. 74, 107

[143] F. Staub, "SARAH 4 : A tool for (not only SUSY) model builders," Comput. Phys. Commun. **185** (2014) 1773 [arXiv:1309.7223 [hep-ph]]. 74, 78, 107

[144] F. Staub, "Exploring new models in all detail with SARAH," Adv. High Energy Phys. **2015** (2015) 840780 [arXiv:1503.04200 [hep-ph]]. 78, 107

[145] D. Suematsu, "Vacuum structure of the μ problem solvable extra U(1) models," Phys. Rev. D **59** (1999) 055017 [hep-ph/9808409]. 9, 54

[146] D. Suematsu and Y. Yamagishi, "Radiative symmetry breaking in a supersymmetric model with an extra U(1)," Int. J. Mod. Phys. A **10** (1995) 4521 [hep-ph/9411239]. 9, 54

[147] Y. Umeda, G. C. Cho and K. Hagiwara, "Constraints on leptophobic Z' models from electroweak experiments," Phys. Rev. D **58** (1998) 115008 [hep-ph/9805447].

Appendix A

Magnified plots

In this appendix we present some of the plots in a larger scale in order to enhance the visibility of their details.

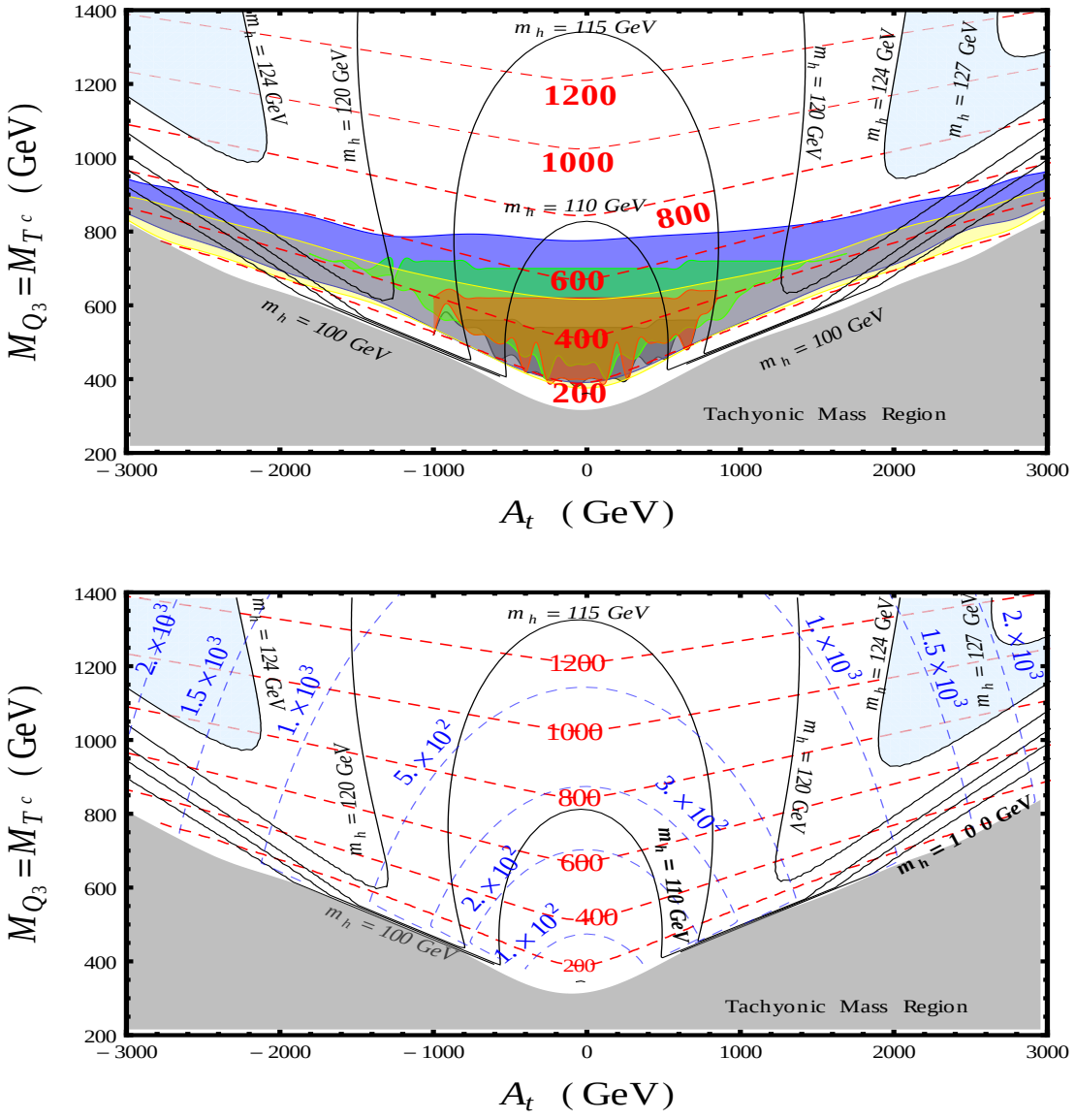

Figure A.1: Plots on page 92. Top: Fig. 4.2a. Bottom: Fig. 4.2b

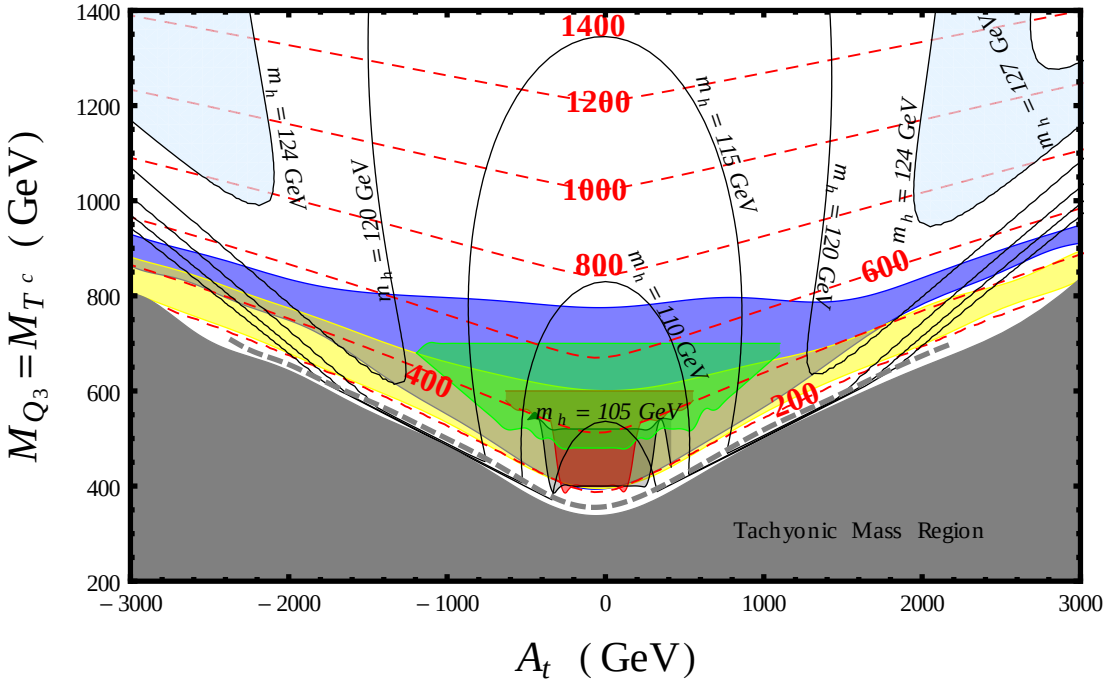

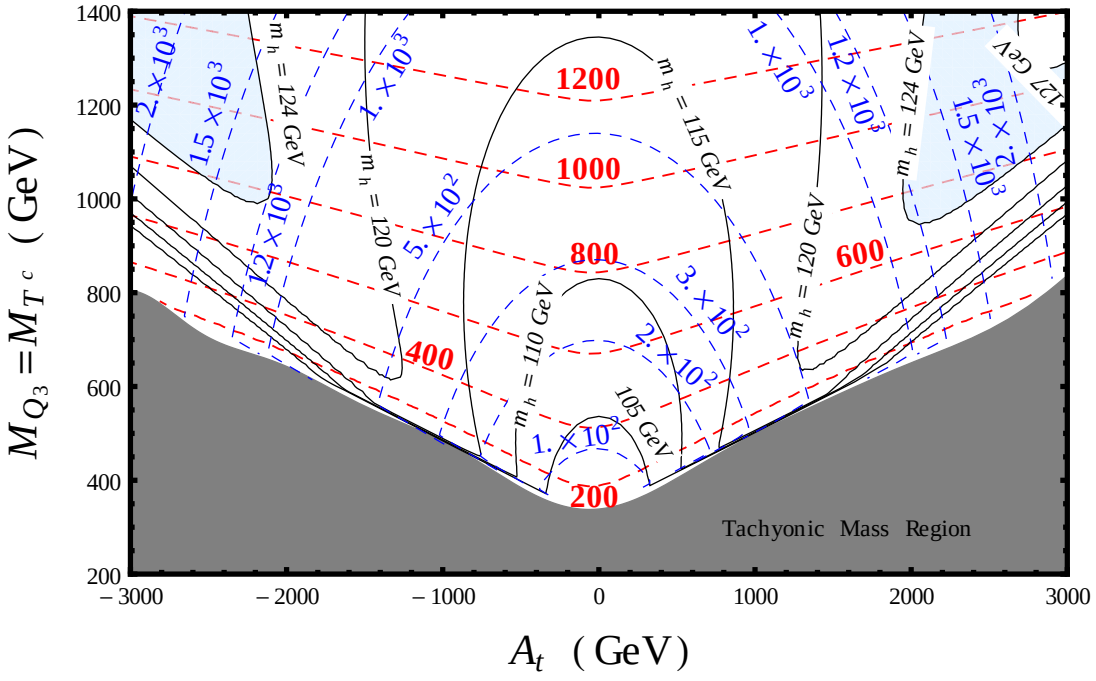

Figure A.2: Plots on page 93. Top: Fig. 4.3a. Bottom: Fig. 4.3b

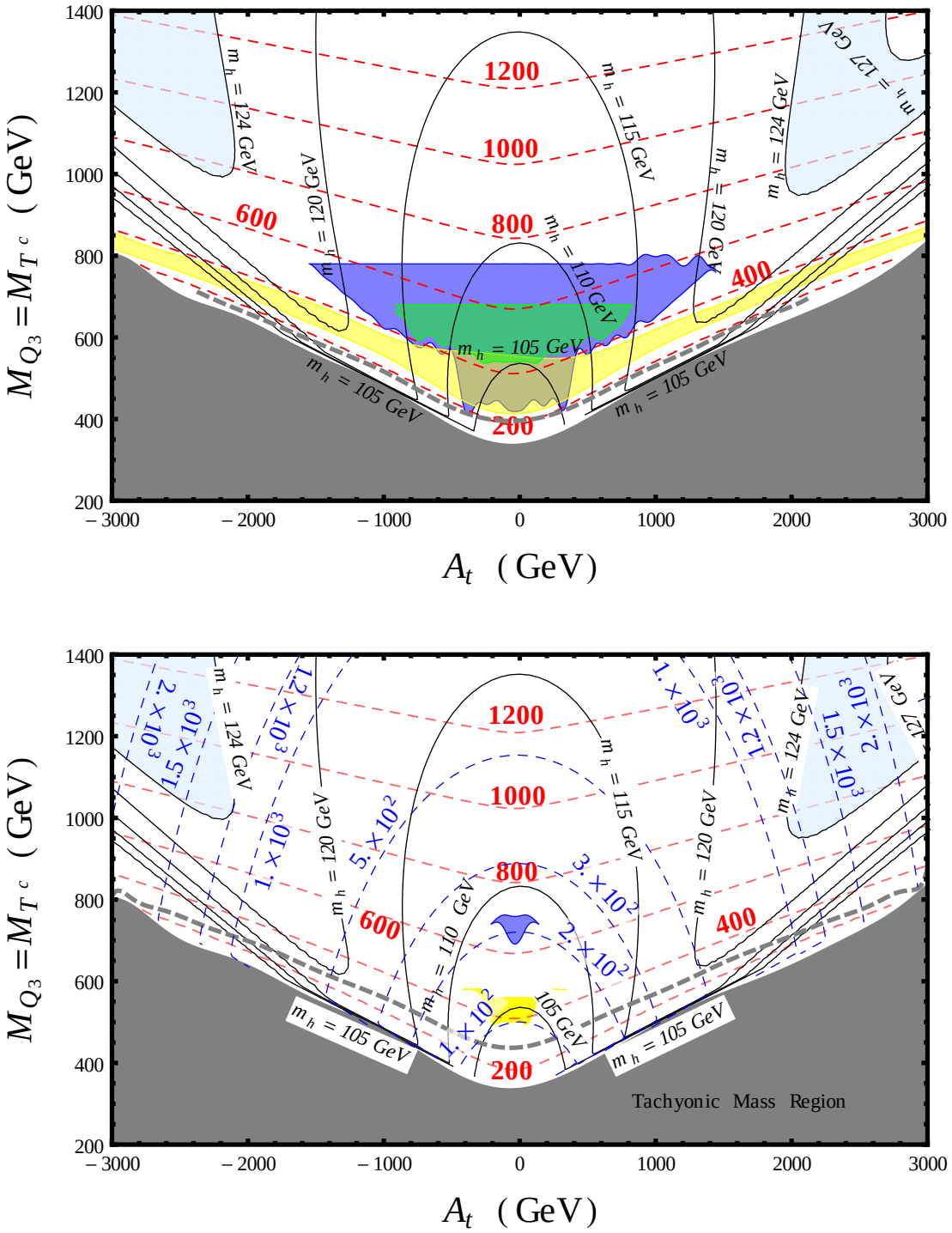

Figure A.3: Plots on page 94. Top: Fig. 4.4a. Bottom: Fig. 4.4b

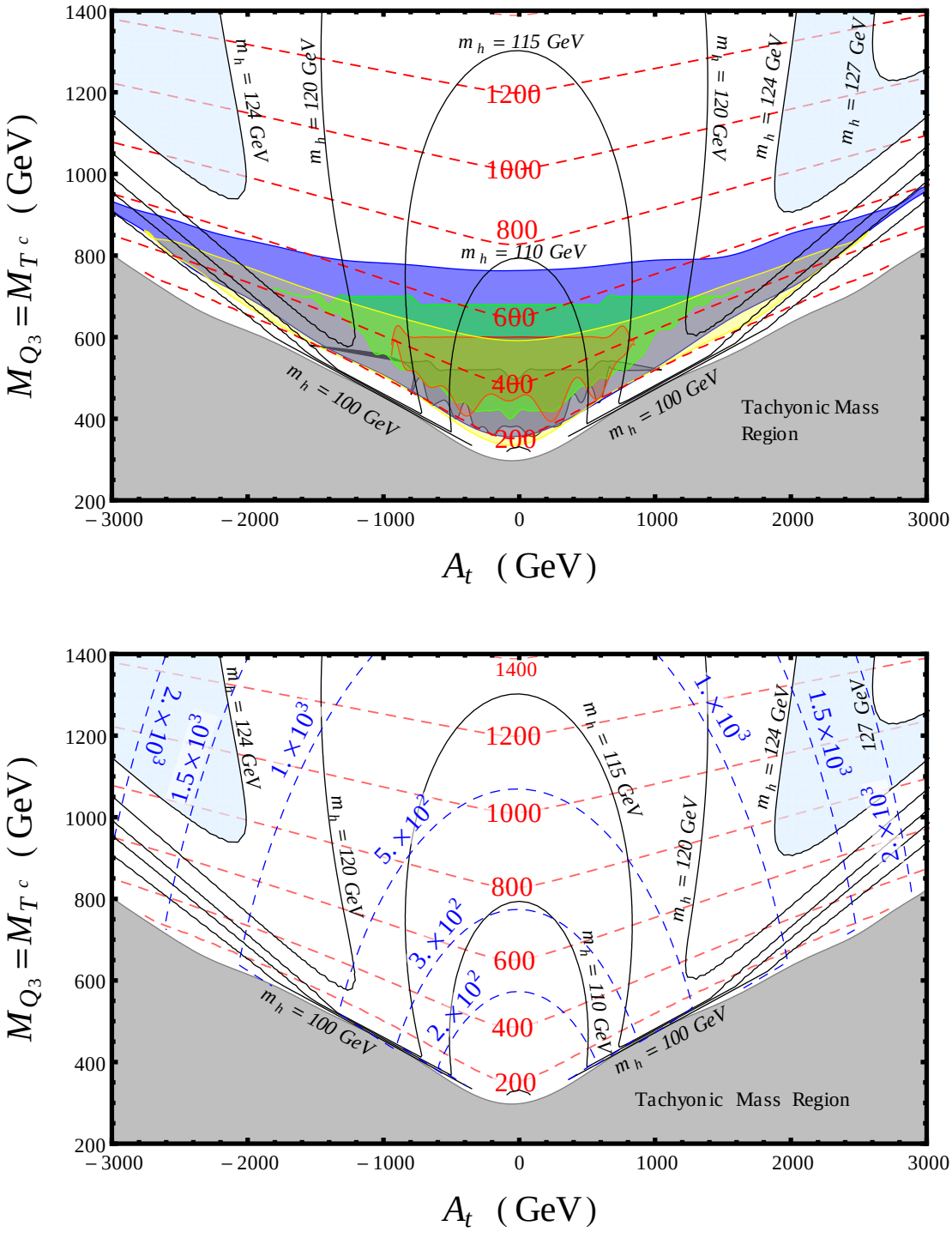

Figure A.4: Plots on page 123. Top: Fig. 5.6a. Bottom: Fig. 5.6b

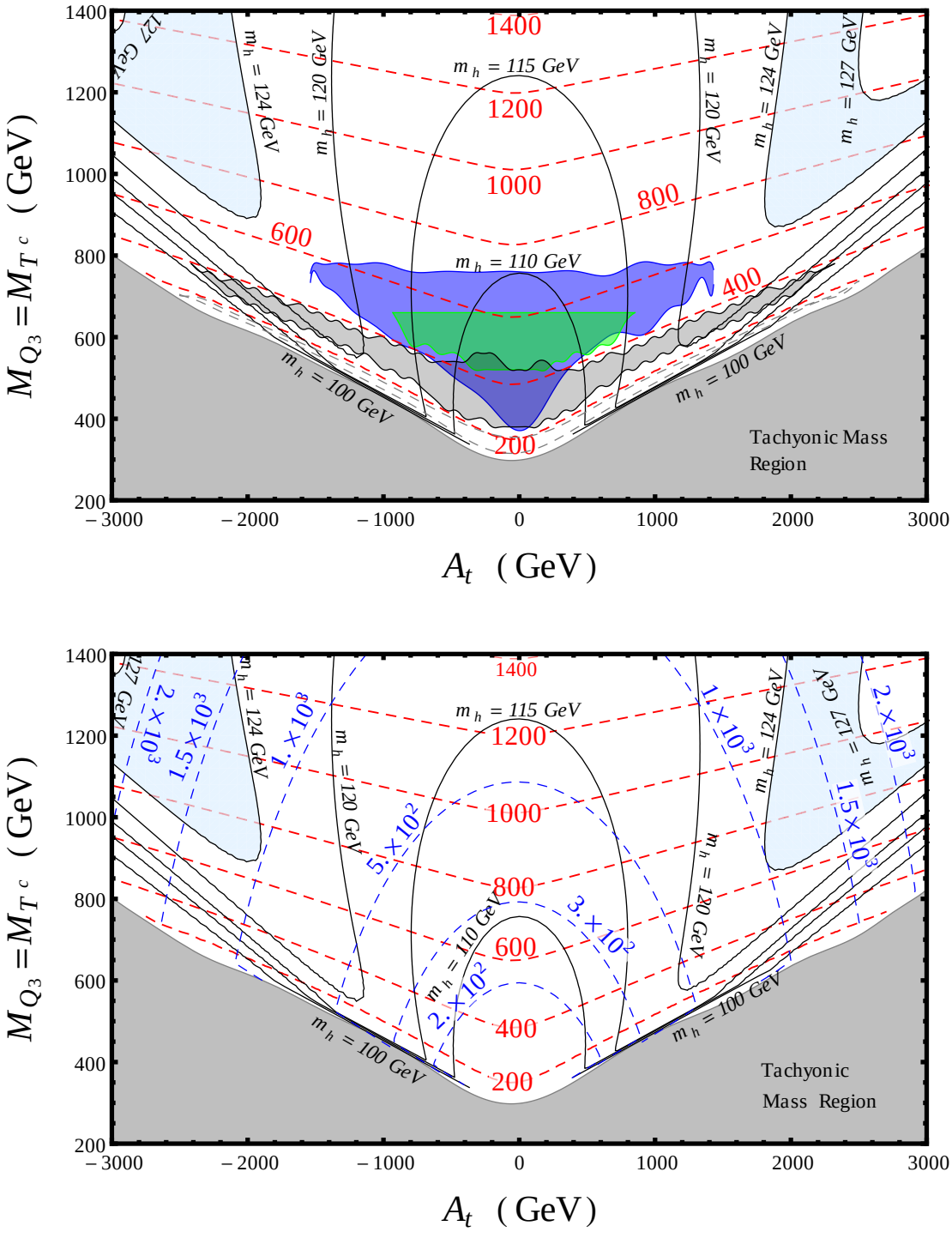

Figure A.5: Plots on page 124. Top: Fig. 5.7a. Bottom: Fig. 5.7b

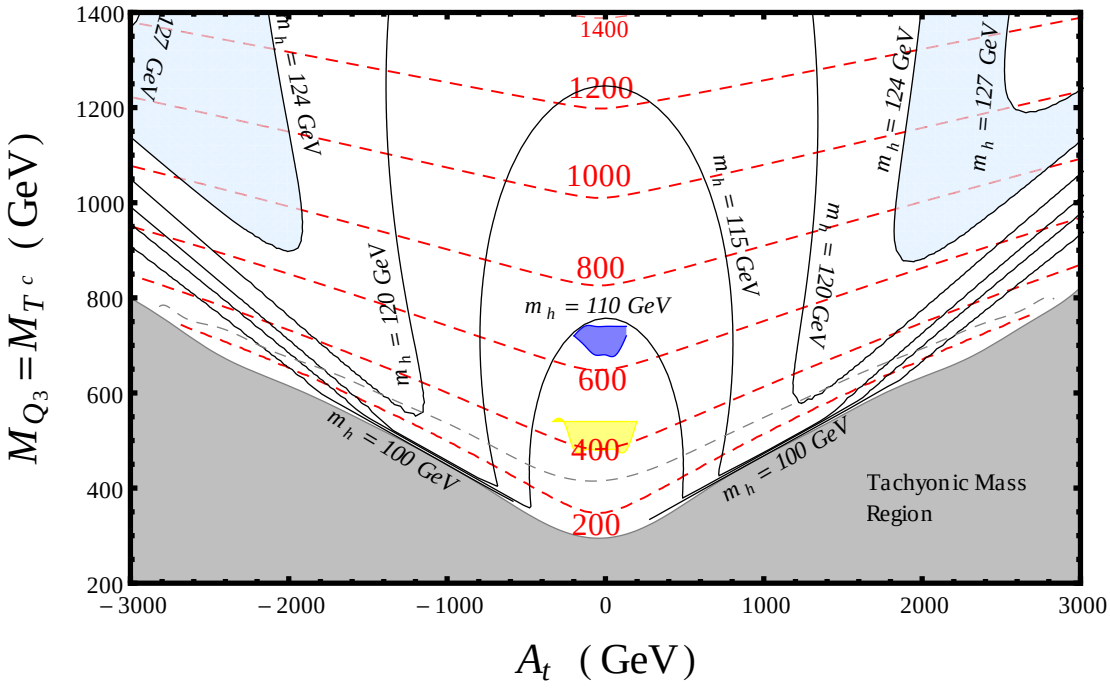

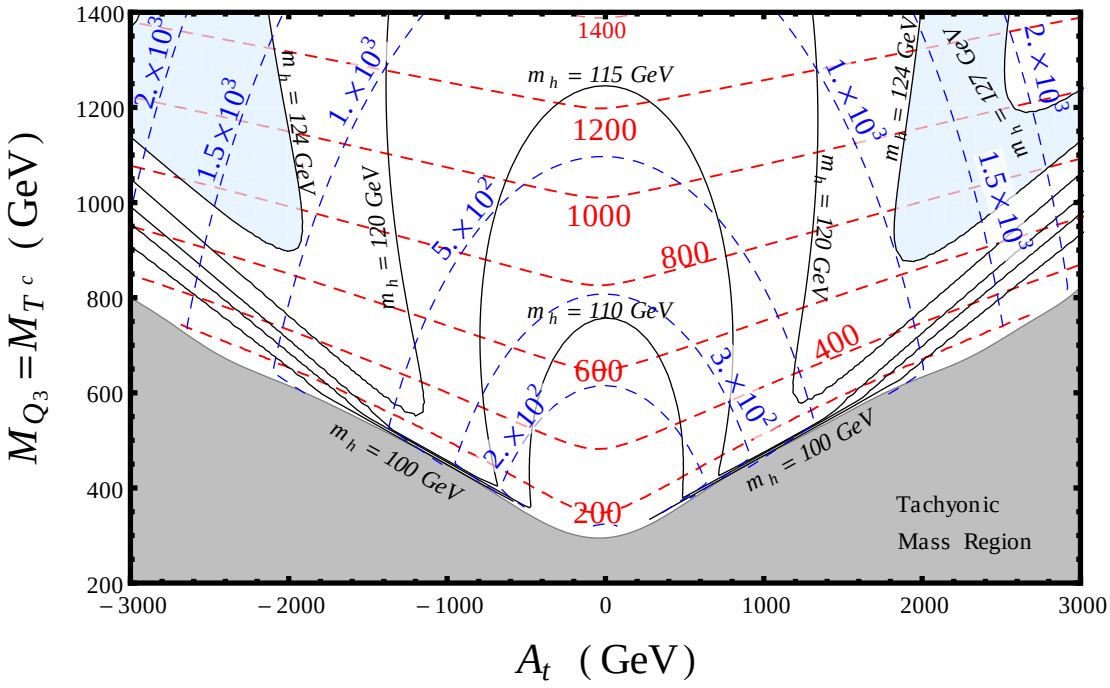

Figure A.6: Plots on page 125. Top: Fig. 5.8a. Bottom: Fig. 5.8b

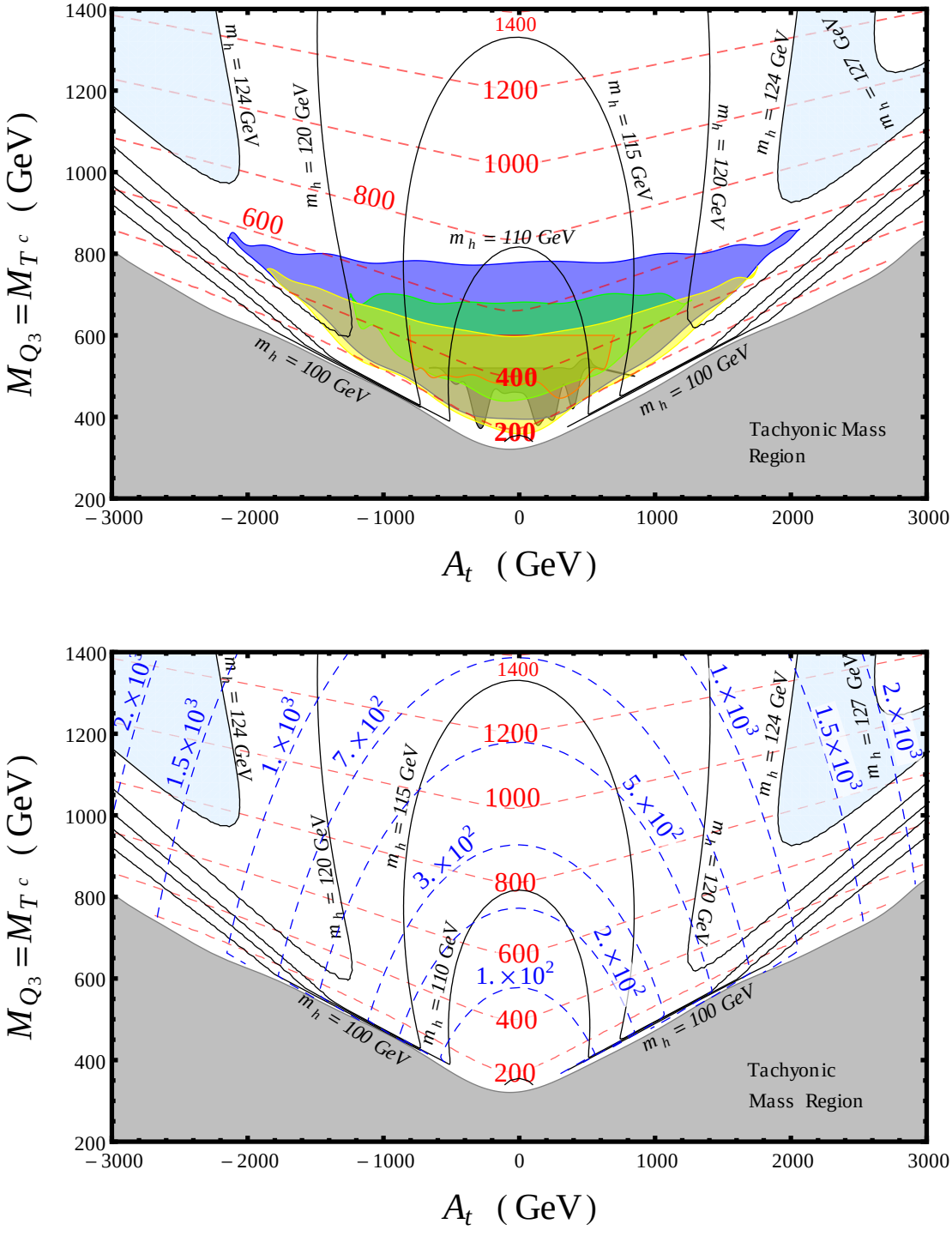

Figure A.7: Plots on page 125. Top: Fig. 5.9a. Bottom: Fig. 5.9b

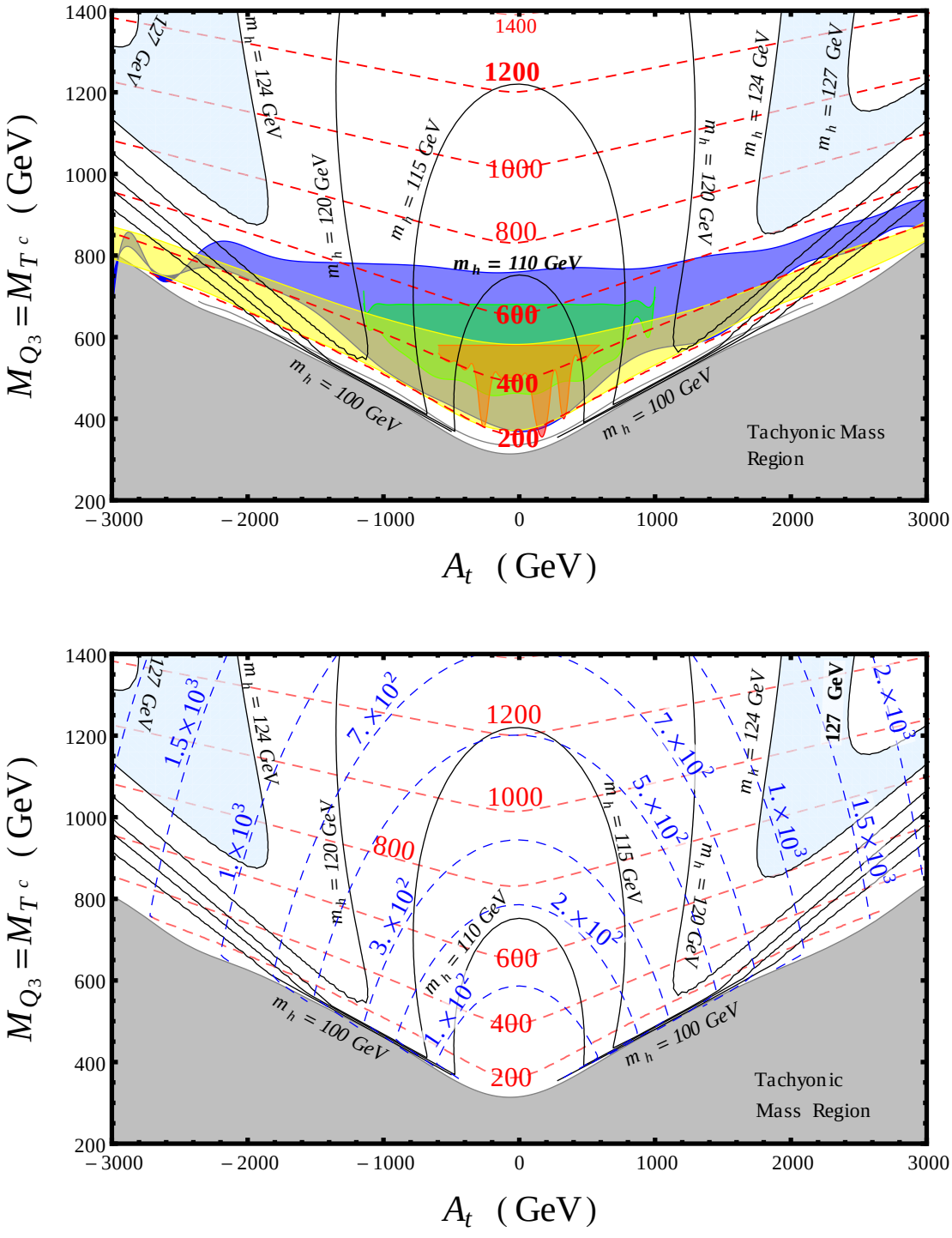

Figure A.8: Plots on page 126. Top: Fig. 5.10a. Bottom: Fig. 5.10b

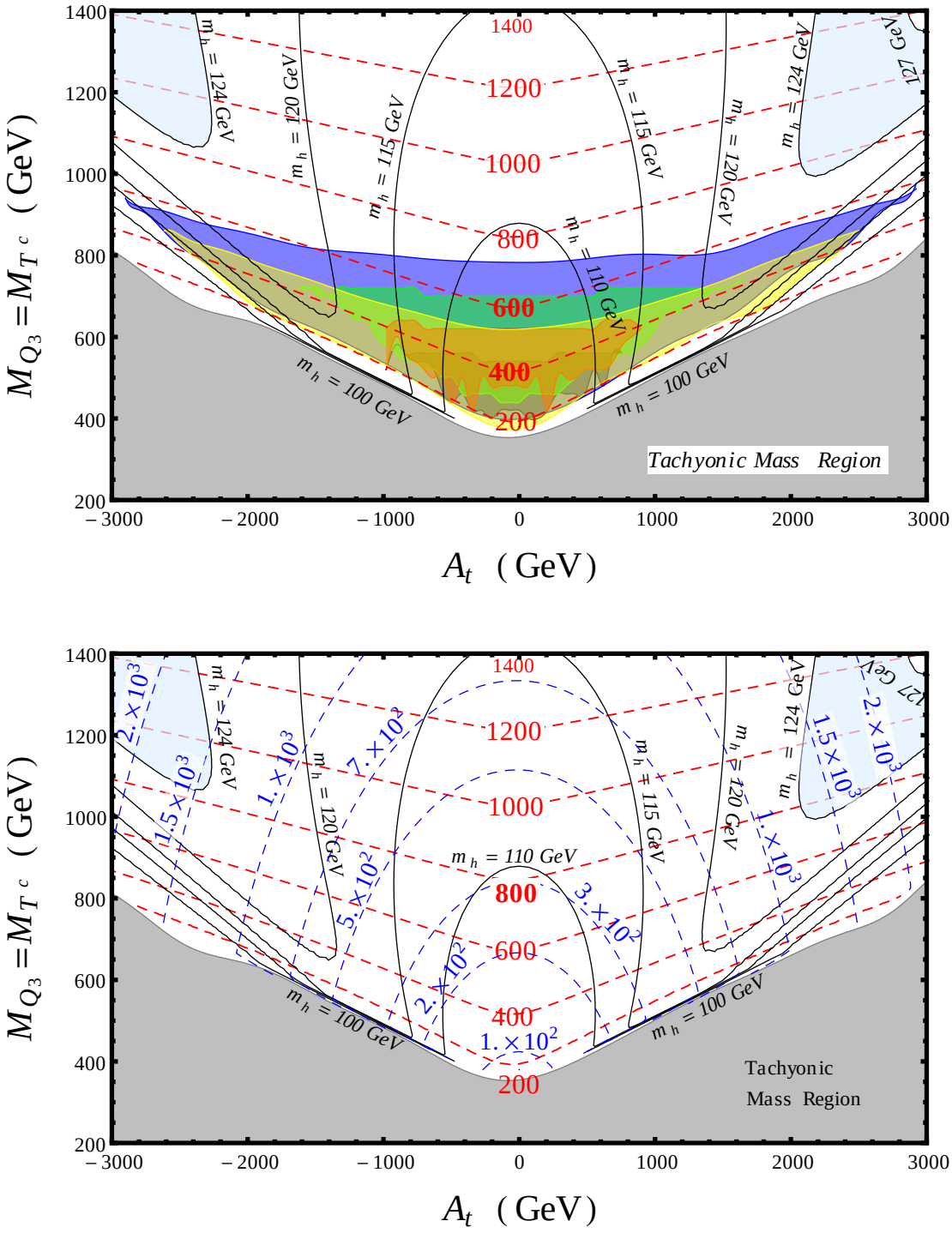

Figure A.9: Plots on page 126. Top: Fig. 5.11a. Bottom: Fig. 5.11b

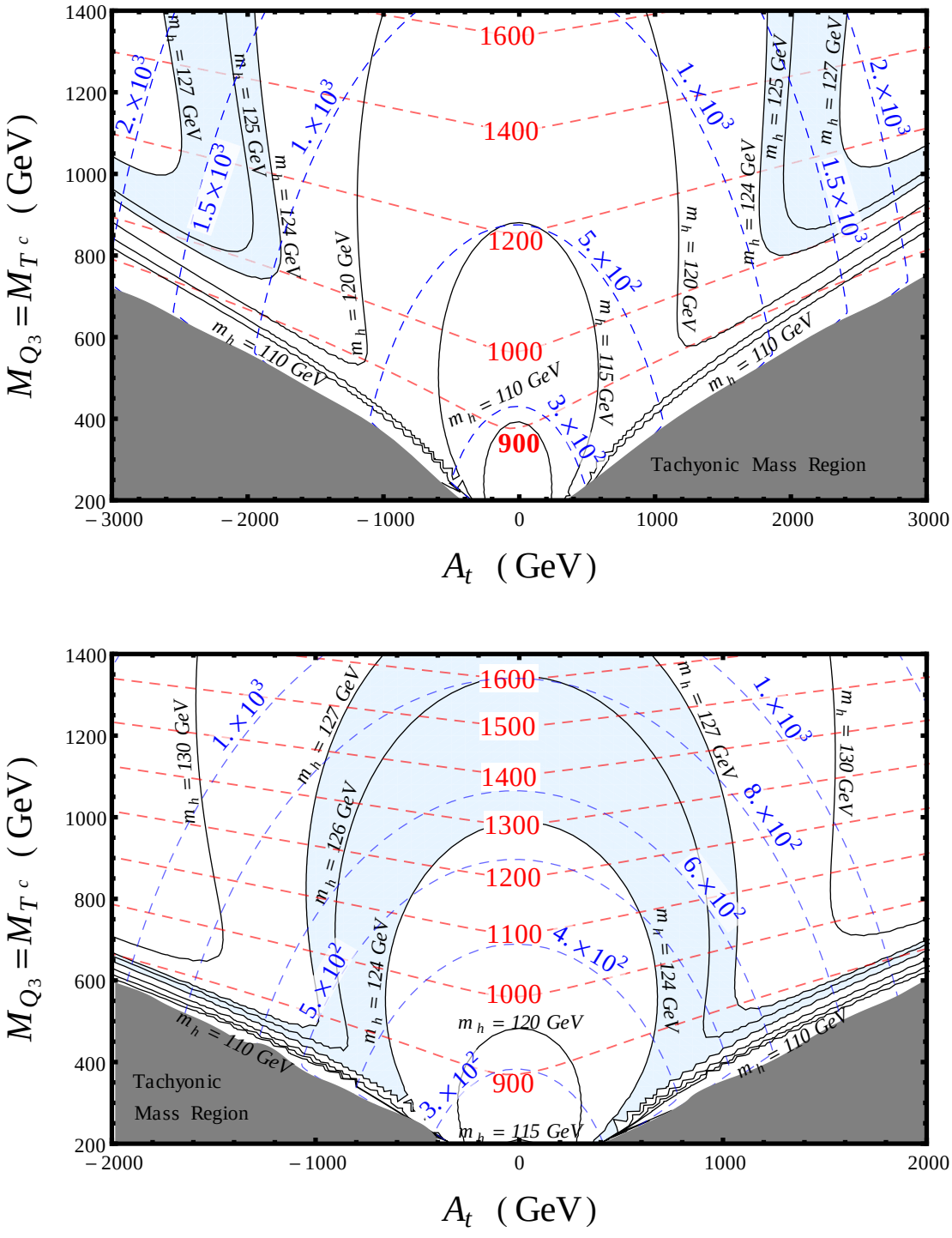

Figure A.10: Plots on page 129. Top: Fig. 5.12a. Bottom: Fig. 5.12b

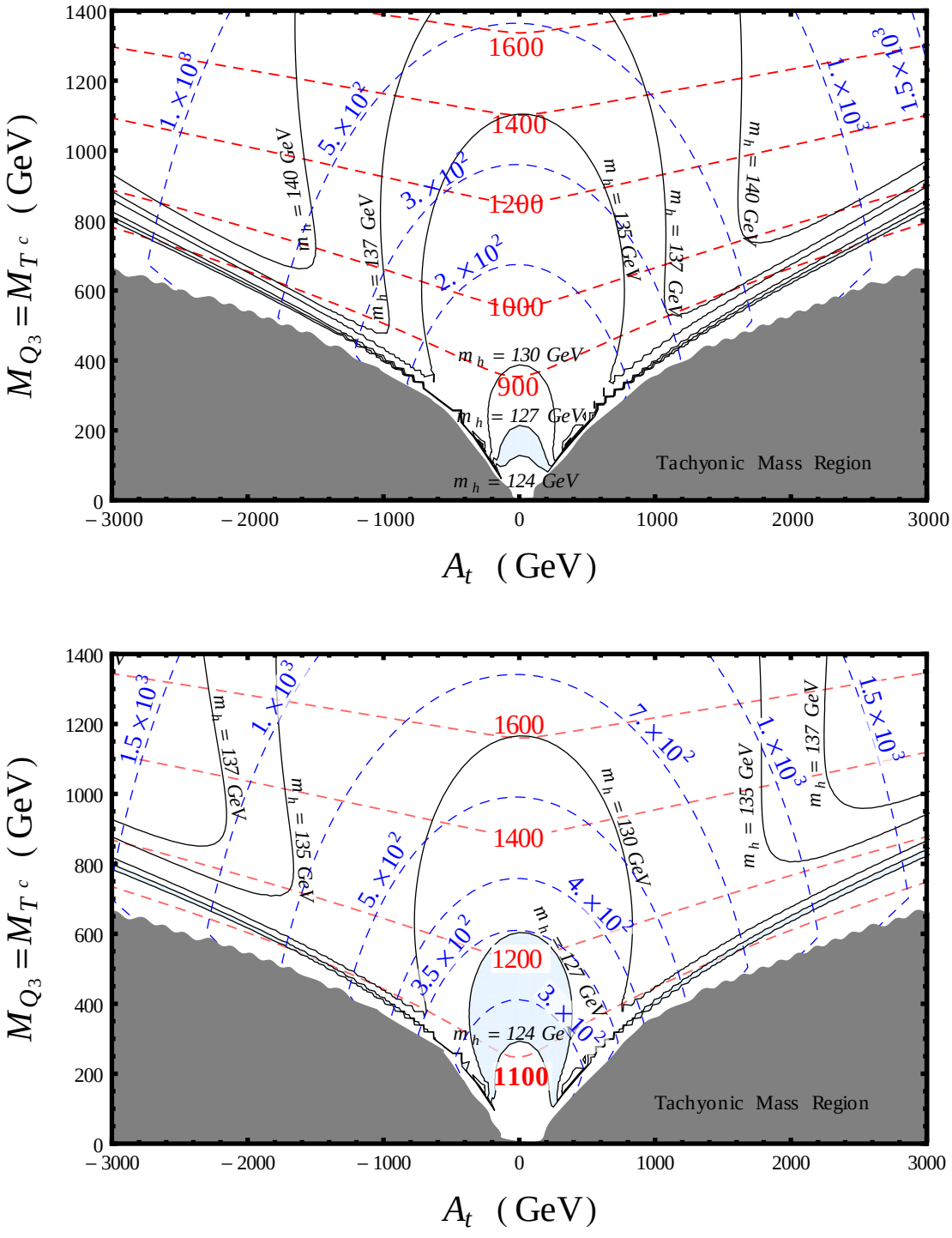

Figure A.11: Plots on page 130. Top: Fig. 5.13a. Bottom: Fig. 5.13b

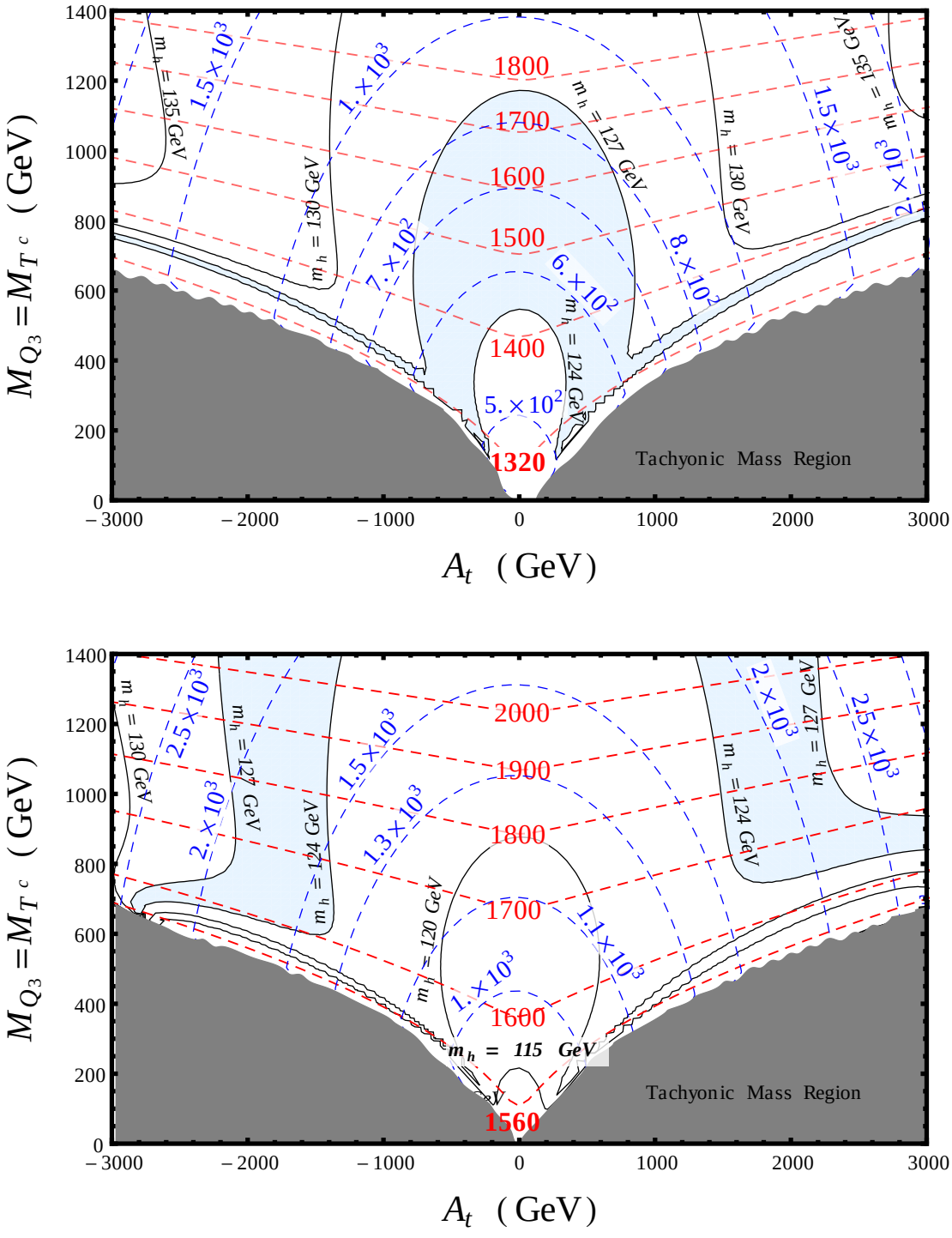

Figure A.12: Plots on page 130. Top: Fig. 5.14a. Bottom: Fig. 5.14b

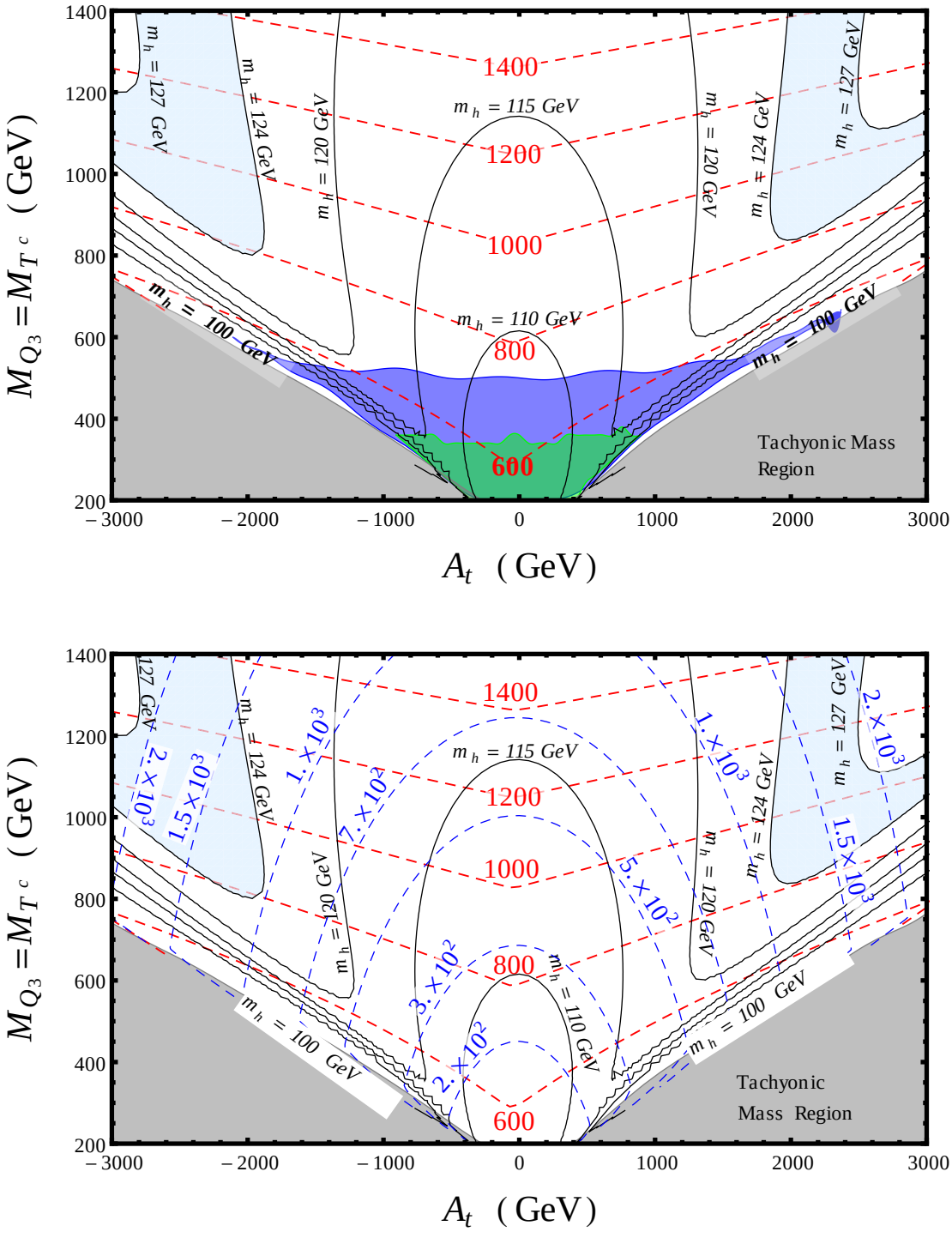

Figure A.13: Plots on page 131. Top: Fig. 5.15a. Bottom: Fig. 5.15b

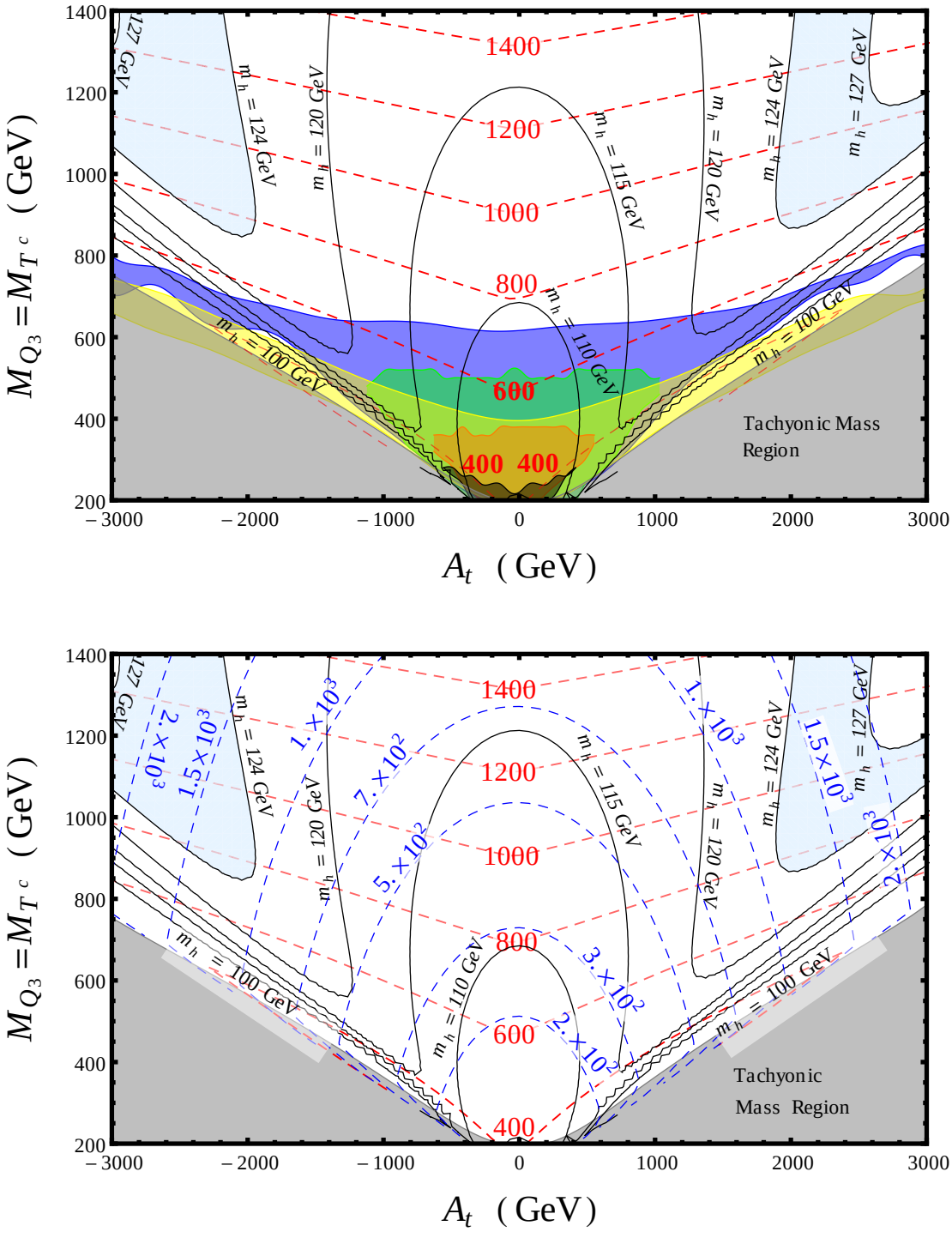

Figure A.14: Plots on page 131. Top: Fig. 5.16a. Bottom: Fig. 5.16b

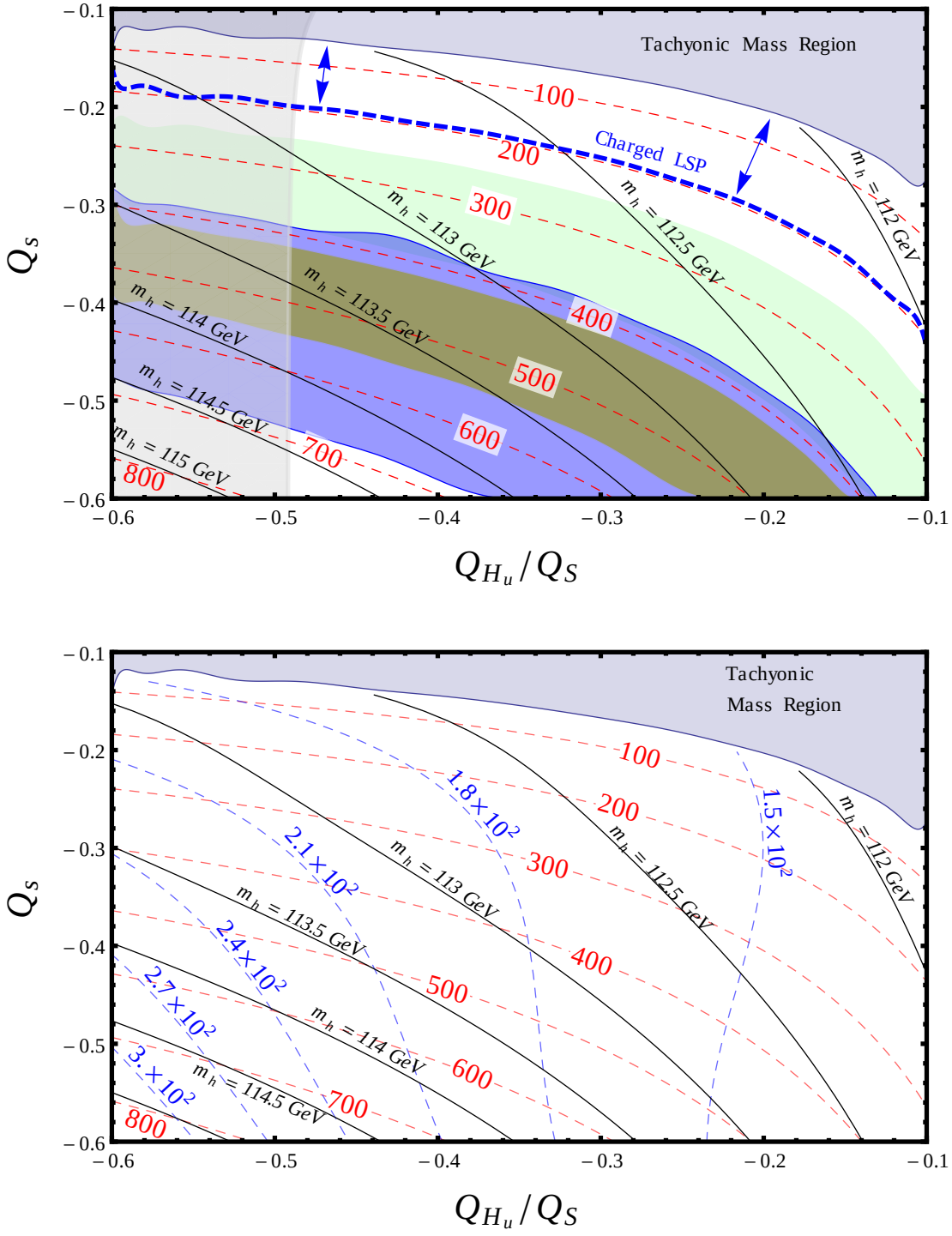

Figure A.15: Plots on page 133. Top: Fig. 5.17a. Bottom: Fig. 5.17b

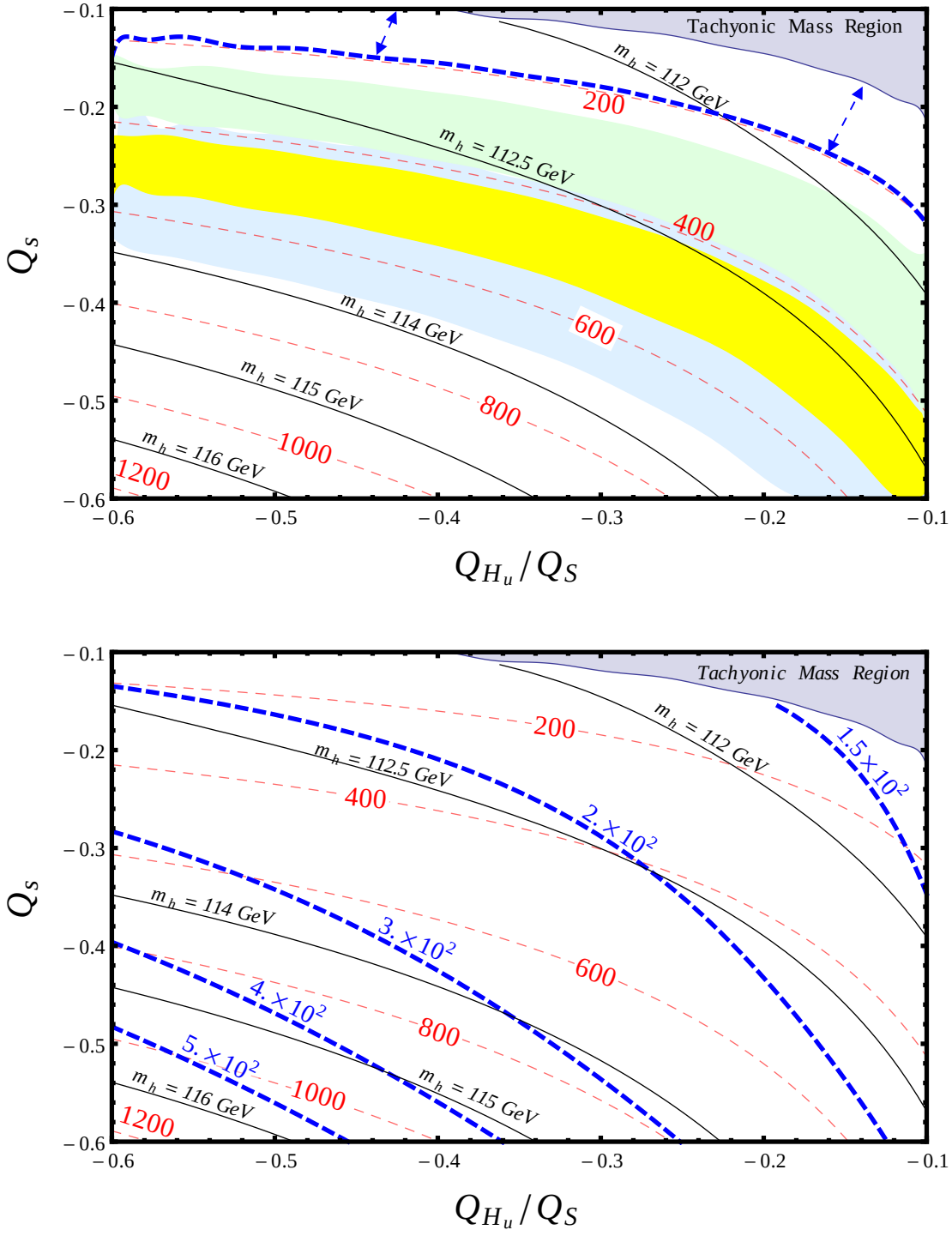

Figure A.16: Plots on page 133. Top: Fig. 5.18a. Bottom: Fig. 5.18b

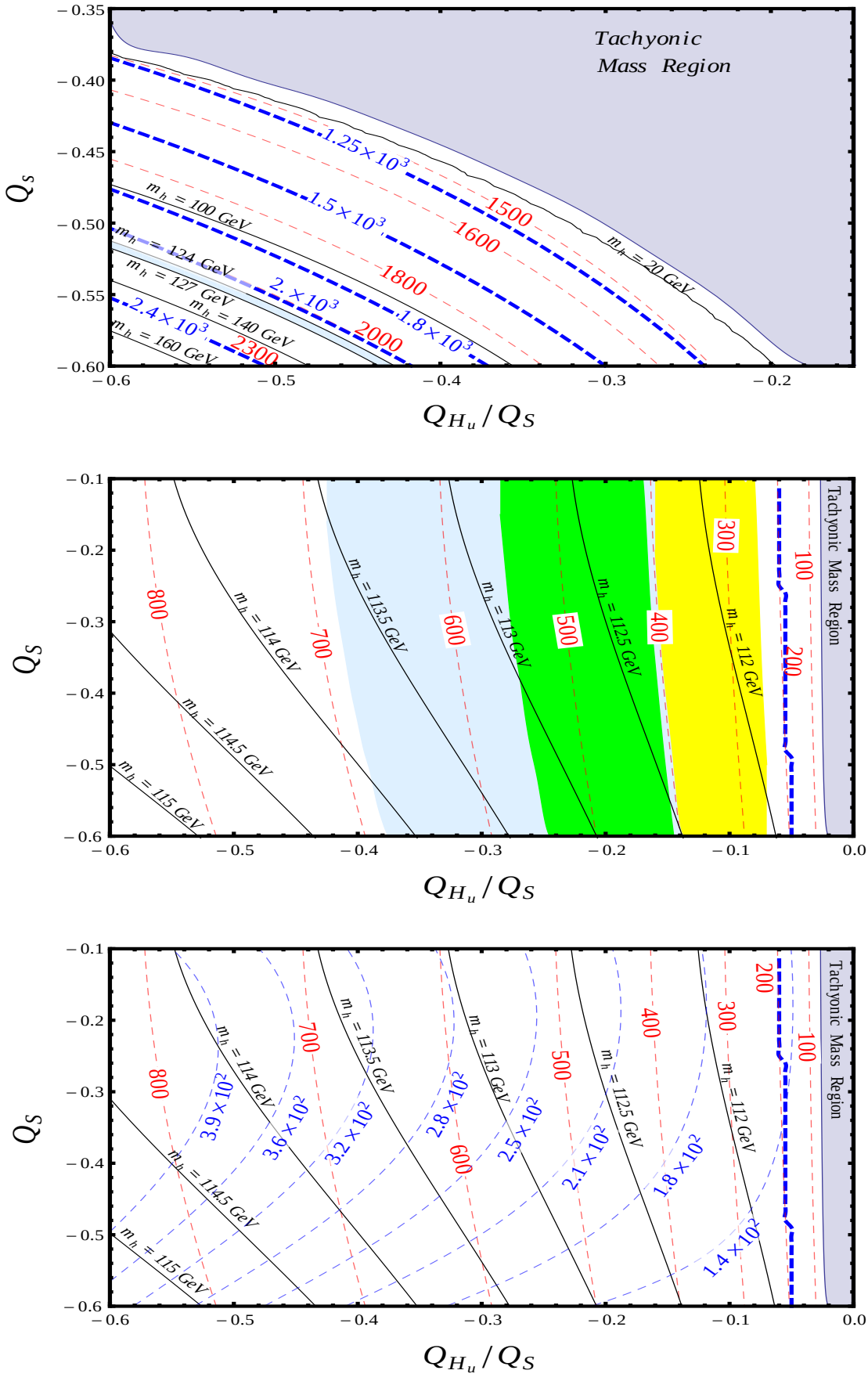

Figure A.17: Plots on page 134. Top: Fig. 5.19a. Middle: Fig. 5.20a. Bottom: Fig. 5.20b